

**Investigation of structural and functional properties of
the betaine transporter **BetP** from *Corynebacterium
glutamicum* by using infrared spectroscopy**

Dissertation

zur Erlangung des Doktorgrades der Naturwissenschaften

vorgelegt beim Fachbereich Physik
der Johann Wolfgang Goethe-Universität
in Frankfurt am Main

von

Günnur Güler

geboren in Gießen, Deutschland

Frankfurt, December 2013

(D 30)

vom Fachbereich Physik der

Johann Wolfgang Goethe-Universität als Dissertation angenommen.

Dekan: Prof. Dr. Joachim Stroth

Gutachter: Prof. Dr. Werner Mäntele

Prof. Dr. Christine Ziegler

Datum der Disputation:.....

Dedicated to my family

PUBLICATIONS

PEER REVIEWED JOURNAL PUBLICATIONS

Güler, G., Gärtner, R., Ziegler, C., Mänteles, W. “Lipid-protein interactions in the regulated betaine symporter BetP probed by Infrared spectroscopy”, *submitted*.

Kaudeer, J., Hartmann, J., Herrmann, J., Schreiber, C., Beyer, S., **Güler, G.**, Vogel, V., Tumulka, F., Abele, R., Mänteles, W., Koch, J. (2013). “A soluble fragment of the tumor antigen BCL2-associated athanogene 6 (BAG-6) is essential and sufficient for inhibition of NKp30-dependent cytotoxicity of natural killer cells”. *Journal of Biological Chemistry*, 10/2013; DOI:10.1074/jbc.M113.483602, *in press*.

Güler, G., Dzafic, E., Vorob'ev, M. M., Vogel, V., Mänteles, W. (2011). “Real time observation of proteolysis with Fourier transform infrared (FT-IR) and UV-circular dichroism spectroscopy: Watching a protease eat a protein”. *Spectrochimica Acta Part A* 79, 104–111.

Vorob'ev, M. M., Vogel, V., **Güler, G.**, and Mänteles W. (2011). “Monitoring of Demasking of Peptide Bonds during Proteolysis by Analysis of the Apparent Spectral Shift of Intrinsic Protein Fluorescence”. *Food Biophysics* 6 (4): 519-26.

PEER REVIEWED CONFERENCE PUBLICATIONS

Güler, G., Gärtner, R., Ziegler, C. and Mänteles W. “Na⁺-coupled betaine symporter BetP from *Corynebacterium glutamicum* studied by Fourier transform infrared spectroscopy”. Proceeding of the Annual Meeting of the German Biophysical Society, Goettingen, Germany (09/2012), **poster number: 236**.

Güler, G., Gärtner, R., Ziegler, C. and Mäntele W. “*Analysis of the molecular mechanisms of the activation of the betaine transporter BetP from Corynebacterium glutamicum by FT-IR spectroscopy*”. Book of abstract of the 31st European Congress on Molecular Spectroscopy (EUCMOS), Cluj Napoca, Romania (08/2012), **oral talk, ISBN: 978-973-647-912-0**.

Güler, G. and Mäntele W. “*Real time observation of proteolysis with Fourier transform infrared (FT-IR) and UV-circular dichroism spectroscopy: Watching a protease eat a protein*”. Proceedings of the 14th European Conference on the Spectroscopy of Biological Molecules (ECSBM), Coimbra, Portugal (08/2011), **oral talk**.

MANUSCRIPTS IN PREPERATION

Güler, G., Gärtner, R., Ziegler, C., Mäntele, W. “Analysis of the molecular mechanisms of the activation of the betaine transporter BetP from *Corynebacterium glutamicum* by FT-IR spectroscopy”, *in preparation*.

Camilo Perez, **Günnur Güler**, Werner Mäntele, Stanislav Masimov, Reinhard Krämer, Ahmadreza Mehdipour, Lucy Forrest and Christine Ziegler. "Structural evidence for an intratrimeric K⁺-induced activation mechanism in BetP upon osmotic stress", *in preparation*.

LIST OF CONTENTS

Abbreviations	iii
Glossary	v
1. INTRODUCTION	1
1.1 PROTEINS	1
1.1.1 Structure and Properties of Amino acids, Peptides and Proteins	1
1.1.2 Structure and Properties of the Plasma Membrane	5
1.1.3 Transport <i>via</i> Membrane and Transport Proteins	7
1.1.4 Challenge of a Cell against Osmotic Stress	9
1.1.5 Na ⁺ /Betaine Symporter BetP from <i>Corynebacterium Glutamicum</i>	12
1.2 INFRARED SPECTROSCOPY IN PROTEIN RESEARCH	20
1.2.1 Absorption of Infrared Light and Molecular Vibrations	20
1.2.2 FTIR Spectrometer	23
1.2.3 Infrared Signatures of Proteins and Amide Bands	25
1.3 GOAL OF THIS STUDY	27
2. MATERIAL AND METHODS	29
2.1 CHEMICALS	29
2.2 PROTEIN SAMPLES: BetP from <i>Corynebacterium glutamicum</i>	29
2.3 LIPID-PROTEIN SYSTEMS: Proteoliposomes and Two-Dimensional Crystals	30
2.4 INFRARED SIGNATURES OF LIPIDS	32
2.5 INFRARED SPECTROMETERS AND SAMPLING TECHNIQUES	34
2.5.1 FTIR Spectroscopy in Transmission Mode	34
2.5.2 ATR-FTIR Spectroscopy and ATR-Perfusion Cell	36
2.6 DESIGN OF EXPERIMENTS	39
2.6.1 <i>In Situ</i> Activation of BetP with Increasing Potassium Concentration	39
2.6.2 Hydrogen/Deuterium Exchange	41
2.6.3 Reaction-Induced Infrared Difference Spectrum	44
2.6.4 pH-Titration Experiments	46
2.6.5 Temperature Excursion Experiments	47

2.7	SECONDARY STRUCTURE ANALYSIS FROM THE INFRARED SPECTRUM.....	51
2.8	SPECTRAL CONTRIBUTIONS OF AMINO ACID SIDE CHAINS.....	57
2.9	SPECTRAL CONTRIBUTIONS OF ATMOSPHERIC WATER VAPOR.....	58
2.10	SPECTRAL CONTRIBUTIONS OF H ₂ O/D ₂ O BUFFERS AND BUFFER SUBTRACTION	60
2.11	CALCULATION OF LIPID-TO-PROTEIN RATIO FROM THE INFRARED SPECTRUM	62
3.	RESULTS AND DISCUSSION	65
3.1	FUNCTIONALLY INTACT BetP SAMPLES FOR IR SPECTROSCOPY.....	65
3.2	SECONDARY STRUCTURE ANALYSIS OF BetP.....	67
3.3	<i>IN SITU</i> ACTIVATION OF BetP WITH INCREASING K ⁺ CONCENTRATION.....	70
3.4	ACTIVATION-INDUCED INFRARED DIFFERENCE SPECTRUM	80
3.4.1	BetP wild type 2D crystals	80
3.4.2	C-terminal truncated BetP (BetP ΔC45) reconstituted in 2D crystals:.....	90
3.4.3	BetP WT proteoliposomes.....	91
3.5	pH TITRATION OF BetP	95
3.6	LIPID-PROTEIN INTERACTIONS OF BetP.....	99
3.6.1	C-H stretching modes from the hydrophobic tails of lipids.....	101
3.6.2	PO ₂ ⁻ stretching modes from the phospholipid headgroups	105
3.6.3	C=O stretching modes from the phospholipid carbonyl groups	112
3.7	¹ H/ ² H EXCHANGE OF BetP	119
3.8	THERMAL STABILITY OF BetP	123
4.	SUMMARY.....	135
5.	ZUSAMMENFASSUNG.....	141
6.	REFERENCES.....	149
7.	ACKNOWLEDGEMENTS	159

ABBREVIATIONS

δ	Bending vibrations
A. U.	Arbitrary unit
ATR	Attenuated total reflection
CaF ₂	Calcium Fluoride
<i>C.G.</i>	<i>Corynebacterium glutamicum</i>
Cg-liposomes	<i>Corynebacterium glutamicum</i> liposomes
cm ⁻¹	Unit of wavenumber
CO	Carbon Monoxide
D ₂ O, ² H ₂ O	Deuterium Oxide
DTGS	Deuterated Triglycine Sulphate
<i>E. coli</i>	<i>Escherichia Coli</i>
HCl	Hydrogen Chloride
HeNe	Helium Neon
H ₂ O	Water
FTIR	Fourier transform infrared
IR	Infrared
K ⁺	Potassium Ion
KCl	Potassium Chloride
kDa	Kilo Daltons
LPR	Lipid-to-protein ratio
MCT	Mercury-Cadmium-Tellurium
Na ⁺	Sodium Ion
NaCl	Sodium Chloride
OD	Optical density
PDB	Protein data bank
PO ₂ ⁻	Phosphate
POPG	1-palmitoyl-2-oleoyl-glycero-3-phosphoglycerol
rpm	Rotations per minute
Rb ⁺	Rubidium Ion
SNR, S/N	Signal-to-noise ratio
T _m	Temperature of melting
TMH	Transmembrane helices
ν	Stretching vibrations (Frequency)
w/w	Weight/weight

GLOSSARY

Active transport: It is the movement of molecules/ions through a membrane against the concentration gradient; that is, from the region of lower concentration to the region of higher concentration, using electrochemical energy.

Amide band: The infrared spectrum of polypeptides gives rise to a number of amide bands that exhibit different vibrational modes of peptide bonds.

Beer-Lambert law: It states the linear relationship of the optical absorbance of a material with both sample cell pathlength and the concentration of this absorbing material.

BetP: It is one of the osmoregulatory uptake systems which sense the osmotic stress in the *Corynebacterium glutamicum*. Secondary active transporter protein BetP counteracts hyperosmotic stress by uptaking one betaine molecule coupled to symport of 2 Na⁺ ions into the cytoplasm.

Carrier proteins: They produce an opening in the lipid bilayer by undergoing a conformational change upon binding of a molecule (or a few) to the receptor such that only the bound substrate molecules are transported across the membrane (i.e. BetP).

Channel proteins: They form hydrophilic pores across the lipid bilayer which can be opened or closed in response to specific signals, allowing water or specific molecules (polar molecules and charged ions) to pass through (i.e. ion channels or pores).

***Corynebacterium glutamicum*:** A rod shaped Gram-positive soil bacterium which is commonly used as an amino acid producer.

Cytoplasm: The inner space within the cell termed as cytoplasm that comprises a gelatinous, semi-transparent fluid in which many organelles are found.

Deprotonation/Protonation: Removal of a proton (H⁺) from a molecule depending on the pK_a value is called **deprotonation** whereas **protonation** refers to addition of a proton (H⁺) to a molecule. Both states alter the chemical and optical properties, hydrophilicity and redox potential of the molecule.

Deuterium: It is one of two stable isotopes of hydrogen atom with mass number of 2, and therefore, it is also called **heavy hydrogen** denoted by **D** or **²H** that involves one proton and one neutron.

Diffusion: A spontaneous movement of the molecules along a concentration gradient, from the higher to the lower concentrated region.

Escherichia coli: A rod-shaped Gram-negative bacterium which is commonly found in the lower intestine of warm-blooded organisms.

Evanescent wave: It exists when electromagnetic wave travelling in a medium totally internal reflected off an interface between two media at an angle greater than the critical angle and its intensity decays exponentially with distance from the interface creating an evanescent field.

Frequency: It is defined as a number of cycles per unit time. Frequency has a unit of hertz (Hz) and in physics it is denoted by f or ν .

Glycine betaine: It serves as organic osmolytes which exists in zwitterionic form at neutral pH with a positively charged quaternary ammonium group and with a negatively charged carboxylate group (N,N,N-trimethylglycine). It is synthesized or taken up from the environment by cells for protection against osmotic stress.

Infrared (IR) radiation: It is a type of electromagnetic radiation which exists between visible light and radio waves. Infrared radiation, which has a longer wavelength than the visible light, is subdivided into the far-IR (1 mm-10 μm), mid-IR (10-2.5 μm) and near-IR (2500-750 nm).

Interference: In optics, it refers to the superimposition of more two waves to generate a new wave pattern. When the phase difference between these waves is a multiple of 2π **constructive interference** exists that creates a new wave whereas when the difference is an odd multiple of π **destructive interference** occurs that the waves cancel each other.

Lipid bilayer: A membrane formed by two layers of the lipid molecules.

Liposome: A liposome is a small vesicle which is made up of lipid bilayer. Liposomes are prepared to be used as model for artificial cells, such as to investigate the membrane proteins embedded into these liposomes, termed as **proteoliposomes**.

Membrane protein: They are associated with or attached to the membrane (lipid bilayer) of a cell by means of hydrophobic, electrostatic and other non-covalent interactions. For instance, **peripheral membrane proteins** are bound to the cytosolic or extracellular site of the membrane and interact with integral proteins and hydrophilic head groups of membrane lipids electrostatically and through

H-bonding while *integral membrane proteins* span the membrane and are firmly attached to hydrocarbon chains of membrane lipids *via* hydrophobic interactions.

Morse potential: The molecules connected by real bonds behave as an anharmonic oscillator which is described by Morse potential. These molecules can break and dissociate if their bonds stretch beyond a limiting distance. According to the Morse potential energy curve, the spacing between the vibrational levels decreases and the interatomic distance increases while the energy reaches to maximum limited value approaching to the dissociation energy of molecules.

Oligomer: It is a non-covalent bonded macromolecular complex that consists of few macromolecules (*monomer* units) such as proteins or nucleic acids. *Dimers* and *trimers* are oligomers respectively made up of two and three monomers.

Osmotic Stress: Osmotic shock is a sudden major change in the external solute concentration of a cell, resulting in a rapid change in the movement of water across its plasma membrane through osmosis. A rapid increase in the external salt/solute concentration of a cell (high external osmolarity) due to drought/frost (*hyperosmotic stress*) causes instant water efflux followed by dehydration/shrinkage of the cell whereas a sudden decrease in the external salt/solute concentration of a cell (low external osmolarity) due to a sudden rain (*hypoosmotic stress*) leads to a water influx followed by swelling/bursting of the cell.

Osmolarity: It is the number of osmoles of solute per liter of solvent that is expressed in terms of osmol/L (or Osm/L) whereas *osmolality* is the number of osmoles of solute per kilogram of solvent which has a unit of osmol/kg (or Osm/kg). Osmolarity and osmolality terms are frequently used to define the osmotic pressure in the fluid systems.

Passive transport (facilitated diffusion): In contrast to active transport, passive transport is the movement of molecules/ions through a plasma membrane along the concentration gradient, from the higher concentrated region to the lower concentrated region, without using energy (i.e. channels).

Penetration depth: It defines the decay of an electromagnetic wave into a medium.

Peptide bond: A peptide bond is formed when the carboxyl group of one molecule reacts with the amino group of the other molecule, leading to the release of a molecule of water.

Periplasm: The outside of the plasma membrane of a cell is called as periplasm.

Plasma membrane: It is the outer cell boundary, which consists of the lipid bilayer and embedded proteins, encloses the cytoplasm so that it separates the interior of the cells from the outside environment for protection.

Polarization: In physics, it is defined as being a property of an electromagnetic wave that oscillates in more than one orientation. Polarization, which describes the direction of electric field vector, is classified as linear, circular and elliptical.

Protomer: In structural biology, it refers to the smallest structural unit of an oligomer, such as protein subunits.

Refractive index: It is described as the ratio of speed of light in vacuum to the speed of light in a medium ($n = c/v$). The refractive index (n) of the medium express how electromagnetic radiation or light travels through this medium such as in air ($n_1=1$) or in water ($n_2=1.33$).

Standing wave: It is the sum of two sinusoidal waves of equal amplitude (peak magnitude of the oscillation) and of same frequency which travel in opposite directions and interfere with each other. A standing wave often exists when they are reflected off a boundary.

Symporter (co-transporter): It is an integral membrane protein which transports the molecules/ions across the plasma membrane in the same direction (i.e. Na^+ /betaine symporter BetP).

Wavelength: It is the distance between the crests or peaks of the repetitions of wave. The wavelength is inversely proportional to the frequency.

Wavenumber: It is the number of waves in a space. Wavenumber (cm^{-1}) is used as the unit of energy in spectroscopy since it is proportional to frequency and to photon energy for electromagnetic radiation ($1 \text{ cm}^{-1} = 1.23984 \times 10^{-4} \text{ eV}$).

1. INTRODUCTION

1.1 PROTEINS

1.1.1 Structure and Properties of Amino acids, Peptides and Proteins

Proteins are the most crucial biochemical compounds within the living cells and used for many purposes for the life; for instance, they have structural, defense and regulatory functions, and are involved in reaction catalysis, transport and storage of nutrients and other molecules in and out of cells as well within cells. Proteins are made up of chains of amino acids that harbour an amino group (-NH₂), a carboxylic acid group (-COOH), a hydrogen atom (H) and a variable side chain (R) bound to the same carbon atom (C_α) (Fig. 1.1).

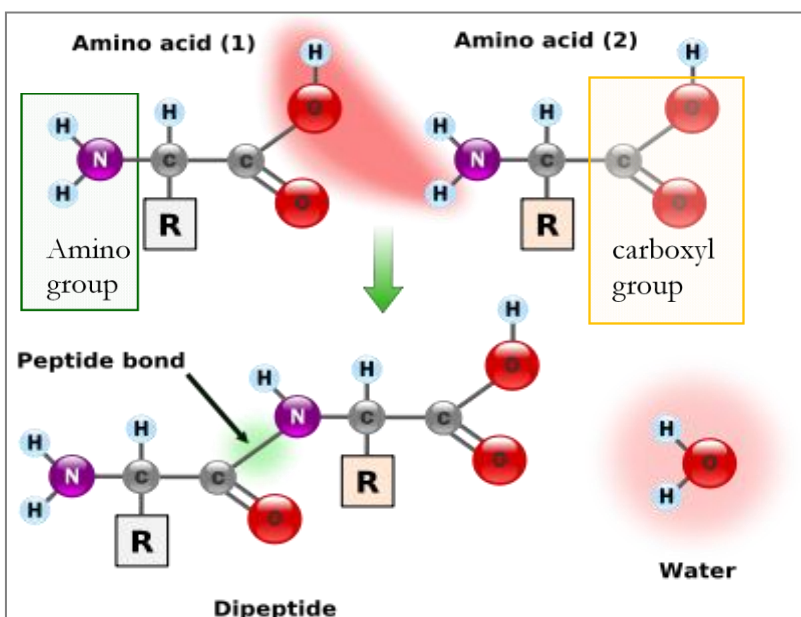


Figure 1.1: Condensation of two amino acids to form a peptide linkage (Figure reproduced from <http://en.wikibooks.org>).

Amino acids in a polypeptide chain are covalently linked by *peptide bonds* which are generated when the carboxyl group of one molecule reacts with the amino group of the other molecule, causing the release of a molecule of water¹⁻⁴. Proteins are synthesized by the ribosome from N-terminus to C-terminus using information encoded in the genes. By convention, peptides and proteins are always

written starting from the left with the N-terminal amino acid (free H_2N group) towards the right side of the peptide with the C-terminal amino acid (free COOH group) (Fig. 1.2 Top).

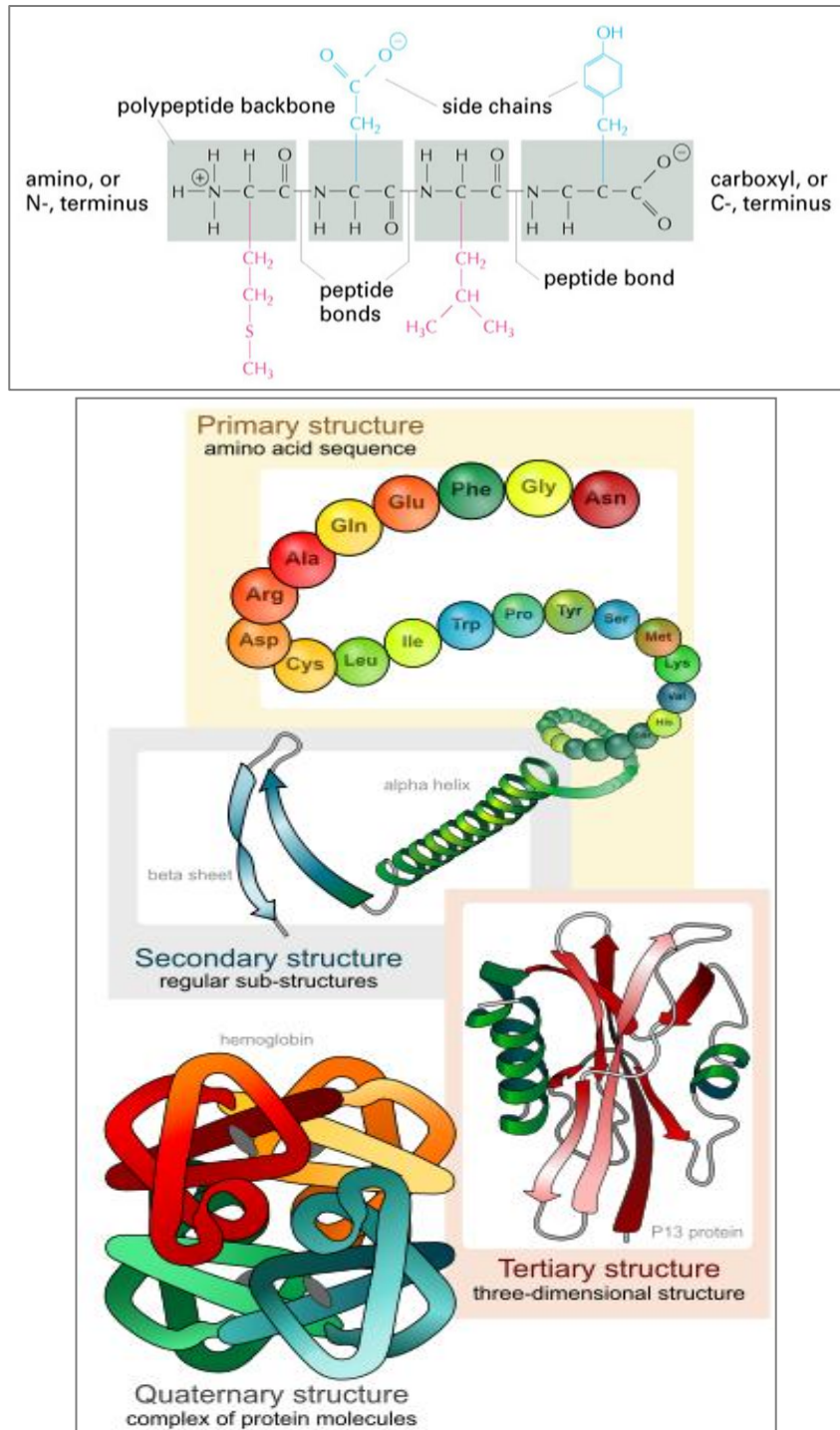


Figure 1.2: (Top) Proteins are made up of a regularly repeating backbone and variable side chains (Figure reproduced from *Essential Cell Biology*, 2nd ed., 2004, Garland Science[®] and from <http://forums.studentdoctor.net>). **(Bottom)** The four distinct levels of structure in the proteins. (http://en.wikipedia.org/wiki/Protein_structure).

Proteins are described by four different levels of structure (Fig. 1.2 Bottom). The most fundamental structure is the **primary structure** of a protein that consists of a linear sequence of amino acids linked together by peptide bonds. The **secondary structure** refers to particularly stable spatial arrangements of amino acid residues that are oriented into a regular pattern by means of H-bonds such as the α -helix, β -pleated sheets and turns/loops. The **tertiary structure** is the specific three-dimensional folding of the entire protein molecule. The **quaternary structure** refers to the spatial arrangement of subunits and the nature of their contacts when a protein has two or more separate polypeptide chains or subunits.

Since the polypeptide chain can only rotate about the Φ (about C_α -N bond) and Ψ (about C_α -C bond) angles, these bonds provide the flexibility of the protein molecule and allow it to fold into regular structures such as α -helix and β -sheet structures which are the most common secondary structures in proteins (Fig. 1.3).

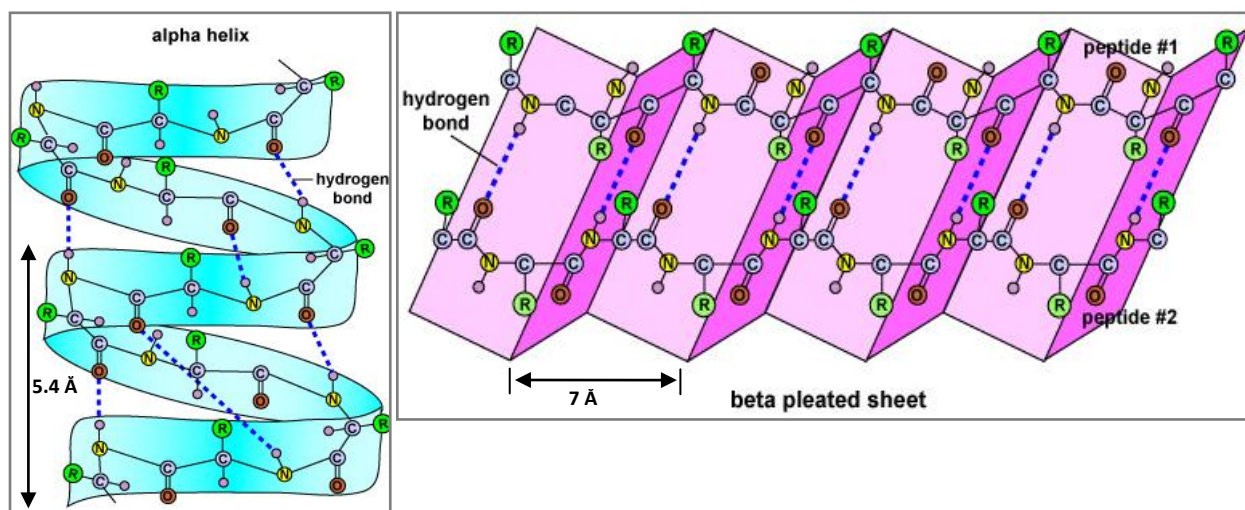


Figure 1.3: (Left) In a right-handed α -helix, the C=O group of residue n (R_1) is H-bonded to the N-H group of residue $(n+4)$ (R_5). Each turn of the helix has a repeat distance that spans 3.6 amino acid residues with a distance of 5.4 Å between the coils (Figure reproduced from <http://www.astrobio.net/>).

(Right) In a β -sheet, adjacent polypeptide chains can run either in the same direction (*parallel β -sheet*) or in the opposite direction (*antiparallel β -sheet*). Antiparallel β -sheet is significantly more stable due to the well aligned H-bonds. (Figure reproduced from <http://faculty.ccbcmd.edu/courses/bio141>).

In an **α -helix**, the side chains point out from the helical backbone while the main polypeptide chain forms the inner part of helical coil. It is stabilized by the interchain H-bonding in the same polypeptide chains (Fig. 1.3 Left).

On the other hand, a **β -sheet** is an almost fully extended polypeptide chain and is stabilized by the interchain H-bonds between the amide N-H and C=O groups in the different polypeptide chains. The side chains in a β -sheet protrude above and below the plane of the sheet and alternate along the chain (Fig. 1.3 Right).

Secondary structural elements are folded into a compact form, shaping the unique conformations of the proteins. Protein folding and overall stability of its conformation are controlled and driven by the combined energy of weak and strong interactions which minimize the entropy lost in protein folding. These favorable intermolecular or intramolecular interactions are formed to tackle with the inevitable reduction of conformational entropy, resulting in a spontaneously protein folding into a well defined native structure⁵. Weak interactions, termed *non-covalent bonds*, are H-bonds, ionic interactions, van der Waals forces and non-specific hydrophobic interactions. ***H-bonds*** are generated when two partially electronegatively charged atoms (e.g. N and O) interact with the same positively charged H-atom which is covalently attached to one atom (donor) but interacts electrostatically with the other atom (acceptor). A H-bond can occur in the secondary structural elements, between the side chains, and occur between the backbone groups and side chain groups. Particularly, atoms located on polar amino acid side chains and on backbone atoms can form interactions *via* H-bonds with water molecules at the protein surface (Fig. 1.4 Left). ***Ionic interactions (salt bridges)*** result from the transfer of electrons between the oppositely charged amino acid side chains that are usually buried in the hydrophobic core (Fig. 1.4 Left). ***Van der Waals interactions*** are very weak but have a crucial role in folding and stabilizing the structure of proteins, influencing side chain packing in the core. ***Hydrophobic interactions*** of non-polar side chains, which exist in the core of the globular proteins

away from water, are the major driving forces in protein folding and in stabilizing the conformation and tertiary structure of the proteins. The non-polar amino acid residues tend to cluster in the water, being excluded from the water molecules (desolvation), due to the unfavorable entropy decrease. Proteins are stabilized also by **disulfide bonds** formed between cysteine residues. Disulfide bridges provide strong covalent interactions that can contribute to tertiary and quaternary structure of proteins after their folding. In addition to these common interactions, another potential interaction which contributes to stability and structure of a protein is the **cation- π interaction** (Fig. 1.4 Right). It is a strong, non-covalent binding between the cationic group of Arg/Lys and the aromatic rings of Phe/Trp/Tyr residues (π -component) predominantly through electrostatic interaction⁶⁻⁸.

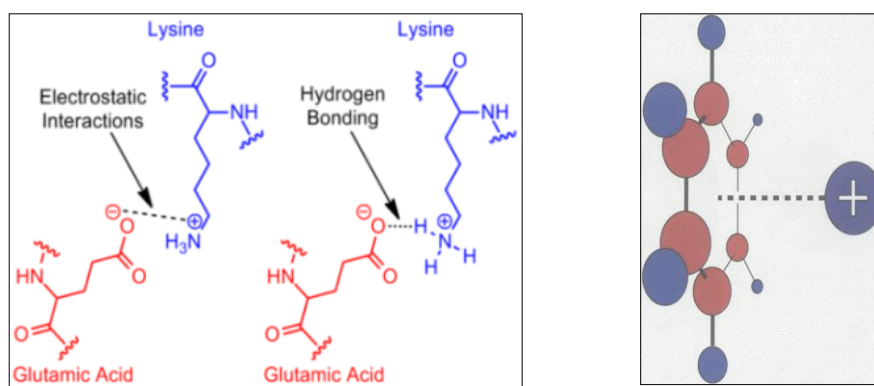


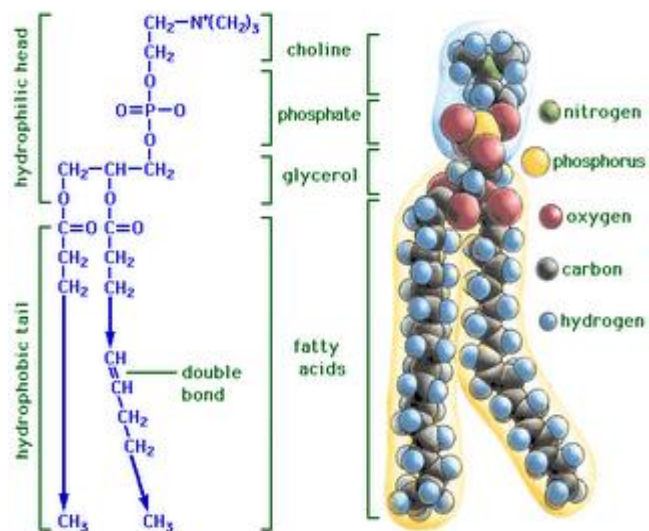
Figure 1.4: (Left) Examples for H-bonding and salt bridge between the Glu and Lys amino acids. (Figure from <http://en.wikipedia.org/>). (Right) The cation- π interaction, showing a generic positive charge interacting with benzene (H is blue, C is red) (Figure adapted from, Dougherty, 1996 *Science*)⁷.

1.1.2 Structure and Properties of the Plasma Membrane

Biological membranes are the external boundaries of the cells that control the molecular traffic and communication between the inside and the outside of the cell. Membranes, highly selective permeability barriers, are made up mainly of lipids with some proteins embedded. These lipids and proteins are held together by non-covalent interactions. Membrane lipids are classified as phospholipids, glycolipids and cholesterol. **Phospholipids**, whose molecules consist of two fatty

acid chains having an ester bond with hydrophilic head groups, are abundant in all biological membranes (Fig. 1.5). Phospholipids derived from glycerol having three-carbon alcohol (*phosphoglycerides*) or from *sphingosine* harbouring a more complex amino alcohol (*sphingomyelin*). The most important phospholipids in the cell membrane are *phosphatidyl choline* (PC or *lecithine*), *phosphatidyl serine* (PS), *phosphatidyl ethanolamine* (PE), *phosphatidyl inositol* (PI) and *diphosphatidyl glycerol* (*cardiolipin*) whose names come from their hydrophilic head groups.

Figure 1.5: Structure of a phospholipid molecule (Figure from <http://knowledgeclass.blogspot.de/>). Usually even numbered (14-24) C-atoms are involved in fatty acid chains (mostly C₁₆ and C₁₈). They can be unsaturated with one double bonded C=C (*oleic acid*) or be saturated (*palmitic acid*). The *cis* double bond in *oleate* (ionized oleic acid) creates a kink in the hydrocarbon chain, affecting the membrane fluidity.



Lipid molecules are self-organized as lipid bilayers, micelles and vesicles (liposomes) if lipids are mixed with water. In the lipid bilayer assembly of biological membranes (Fig. 1.6), the non-polar parts (hydrophobic tails) of lipid molecules in each layer self-associate into a bilayer by means of hydrophobic and van der Waals interactions while their polar head groups face outward interacting with aqueous solution *via* electrostatic interactions and H-bonding. As shown in Fig. 1.6, membrane proteins are classified into two groups, peripheral and integral membrane proteins that carry out many membrane processes. *Peripheral membrane proteins* are bound to the cytosolic or extracellular site of the membrane and interact with integral proteins and hydrophilic head groups of membrane lipids electrostatically and through H-bonding. *Integral proteins* span the membrane (*transmembrane proteins*)

and are firmly attached to hydrocarbon chains of membrane lipids *via* hydrophobic interactions. In some cases, lipids are covalently attached to proteins such as lipoproteins.

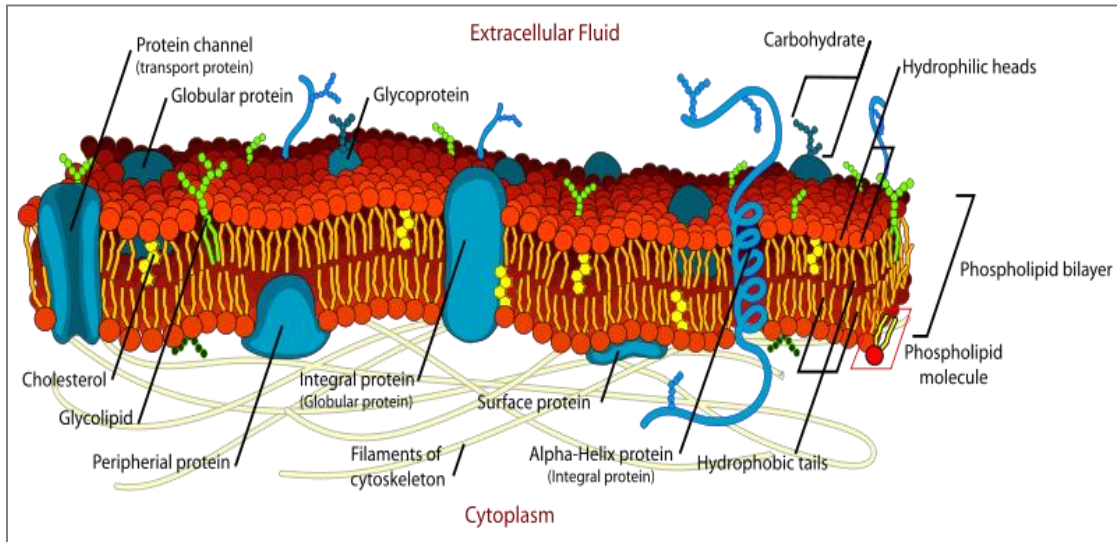


Figure 1.6: Plasma membrane structural components (Figure: <http://cellbiology.med.unsw.edu.au>). Phospholipids aggregate to make up the cell walls, termed as lipid bilayer about 50 Å.

1.1.3 Transport *via* Membrane and Transport Proteins

Membrane transport proteins provide distribution of ions and molecules which determine membrane potentials and gradients inside and outside of the cells. Transport proteins which span the plasma membrane are classified as channels and carriers of the small molecules as well as pumps, antiporters and symporters (Fig. 1.7 Left). These integral membrane proteins exhibit a high degree of specificity for the substance transported. For instance, *channel proteins* (i.e. ion channels or pores) form hydrophilic pores across the lipid bilayer which can be opened or closed in response to specific signals, allowing water or specific molecules (polar molecules and charged ions) to pass through. On the other hand, *carrier proteins* (i.e. a secondary active transporter BetP) produce an opening in the lipid bilayer by undergoing a conformational change upon binding of a molecule (or a few) to the receptor such that only the bound substrate molecules are transported across the membrane as shown in Fig. 1.7 Right. Thereby, different membrane proteins, involved in the biological plasma

membranes, control the movement of various substances into and out of the cell by means of *passive* (also called facilitated diffusion) and *active transport*, depending on the change in the free energy of the transported substances (Fig. 1.7 Right).

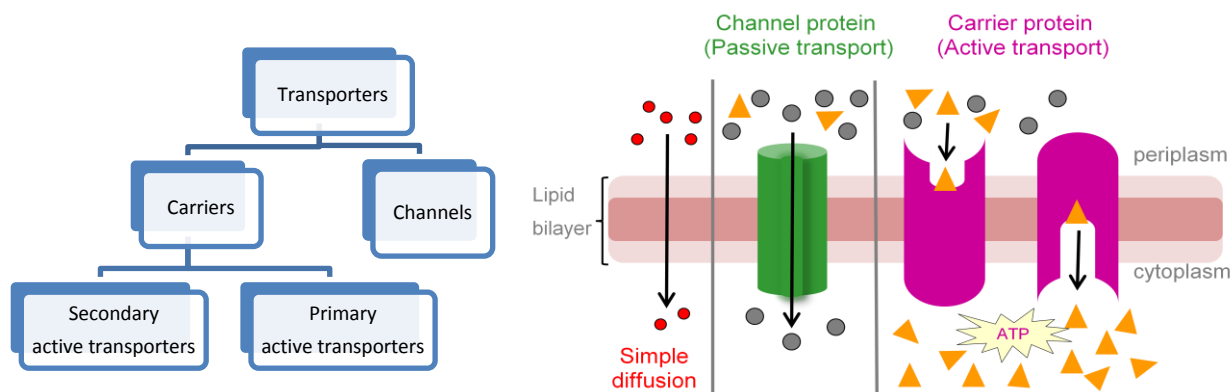
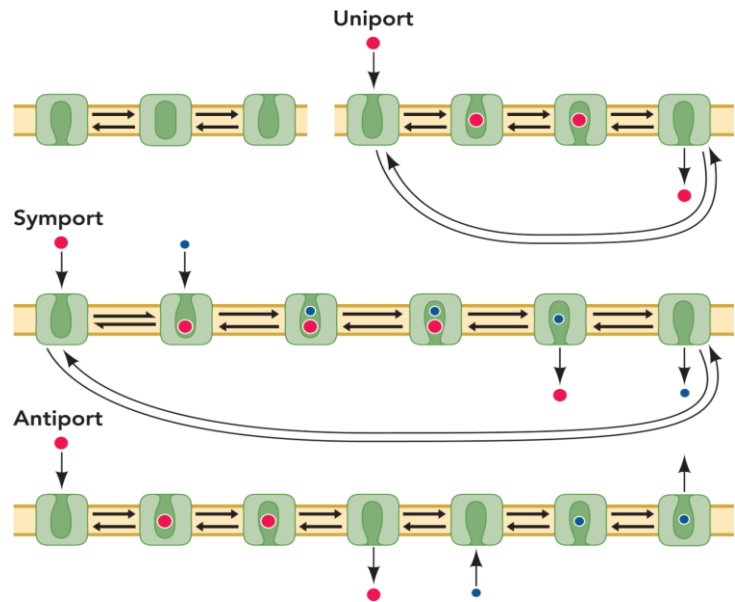


Figure 1.7: (Left) Classification of membrane transport proteins. (Right) A schematic representation of active and passive transport proteins. A carrier protein transports particles from the low concentrated to the high concentrated side of the membrane. Mostly, carrier proteins mediate active transport while channel proteins mediate passive transport.

The lipid bilayer is highly impermeable to ions and charged molecules while permeable to small hydrophobic (i.e. O_2 , CO_2 and N_2) and to small uncharged molecules (i.e. H_2O , glycerol and ethanol). The lipid-insoluble substances and large uncharged polar molecules (i.e. glucose, amino acids), biological effector molecules and inorganic ions (i.e. Na^+ , K^+ , Cl^- , Mg^{2+} , Ca^{2+} and H^+) can not pass through the membrane *via* simple diffusion; therefore, transporter proteins are needed (Fig. 1.7 Right). Some molecules can diffuse passively through the pores or channels along their concentration gradient without using energy while some molecules are transported actively through energy-dependent pumps or transporters (carriers) against their concentration gradient (from low to high ion concentration) using energy. Active transport can be classified according to the source of energy used. *Primary active transport* directly uses chemical energy derived from the hydrolysis of adenosine triphosphate (ATP) to transport molecules through a membrane against their concentration gradient. On the other hand, *secondary active transport* or *co-transport* involves moving of

small molecules across a membrane as the direct result of the diffusion of another substance, and thereby, uses the free energy stored in the form of ionic concentration difference between the two sides of the membrane.

Figure 1.8: Alternating access mechanism for membrane transport proteins. In this mechanism, a substrate binding site is exposed to either side of the membrane *via* conformational changes that involves interconversion of outward- and inward-facing conformations. (Figure from Forrest, L.R. and Rudnick, G., *Physiology*, 2009)⁹.



Secondary active transporters can be either symporter or antiporter proteins. A *symporter* or *coporter* proteins allow a chemical (substrate) to move in the direction of the electrochemical gradient coupled with an ion in the same direction while *antiporters* transport a solute in the opposite direction of the electrochemical gradient by exchanging an ion across a membrane (Fig. 1.8). The transported solute binding site is exposed to either side of the membrane with conformational changes that involves interconversion of outward- and inward-facing conformations of the transporter, termed as *alternating access mechanism*⁹. For instance, the BetP protein used in this study is a symporter that transports one glycine betaine molecule through the cell membrane with co-transport of two Na^+ ions.

1.1.4 Challenge of a Cell against Osmotic Stress

It is indispensable that many bacteria encounter often considerable variations in the solute and ion concentration in their environment. Since the cell membrane is impermeable to solutes, ions and polar organic molecules but permeable to water, rapid major changes in the external solute concentration of a cell induce water flux into or out of the cell. Therefore, microorganisms are

frequently subjected to *osmotic stress* which may result in deleterious effects to survive and growth of the cells or to the vital cellular processes.

As it is represented in Fig. 1.9, an increase in the external salt/solute concentration of a cell (high external osmolality) due to drought or frost, so-called **hyperosmotic stress**, causes instant water efflux followed by dehydration, shrinkage and subsequent collapse of the cell. On the other hand, a decrease in the external salt/solute concentration of a cell (low external osmolality) due to a sudden rain, namely **hypoosmotic stress**, leads to a water influx followed by swelling and even bursting of the cell^{10,11}.

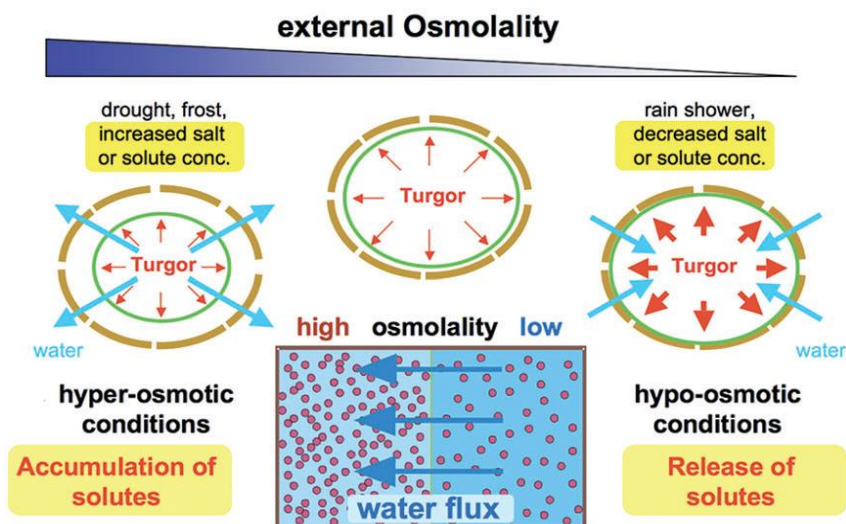


Figure 1.9: A microbial cell can be frequently exposed to hyper- or hypo-osmotic stress in the result of osmotically driven water fluxes across the cytoplasmic membrane (Ziegler et al., *Molecular Microbiology*, 2010)¹¹. Both osmolality and osmolarity, which are the units of solute concentration in solvent, are frequently used where the osmotic pressure is important such as body fluids. However, osmolality of a solution is pretty less than its osmolarity, since the total solution weight excludes the weight of any solutes, whereas the total solution volume includes solute content.

However, microorganisms deal with osmotic stress arising from osmolality changes in their habitat by using a variety of efflux or influx mechanisms. These mechanisms are the transporter proteins which ensure the restoration and maintenance of physiologically normal hydration and turgor pressure within the cell. Therefore, the transporter proteins found in the cell facilitates the cellular osmoregulation and osmoadaptation in response to osmotic stress. For instance, a gram-positive soil

bacterium *Corynebacterium glutamicum*, which is extensively used in amino acid production, frequently experiences osmotic stress in its natural habitat due to dryness or rainfall. As shown schematically in Fig. 1.10 Left, *C. glutamicum* harbours mechanosensitive channels which flux small solutes out of the cell in order to counteract hypoosmotic stress. Besides, *C. glutamicum* counteracts hyperosmotic stress by accumulating the compatible solutes into the cytoplasm, so-called osmoprotectants (proline, betaine and ectoine), by biosynthesis and uptake from outside via membrane transport proteins^{12,13}.

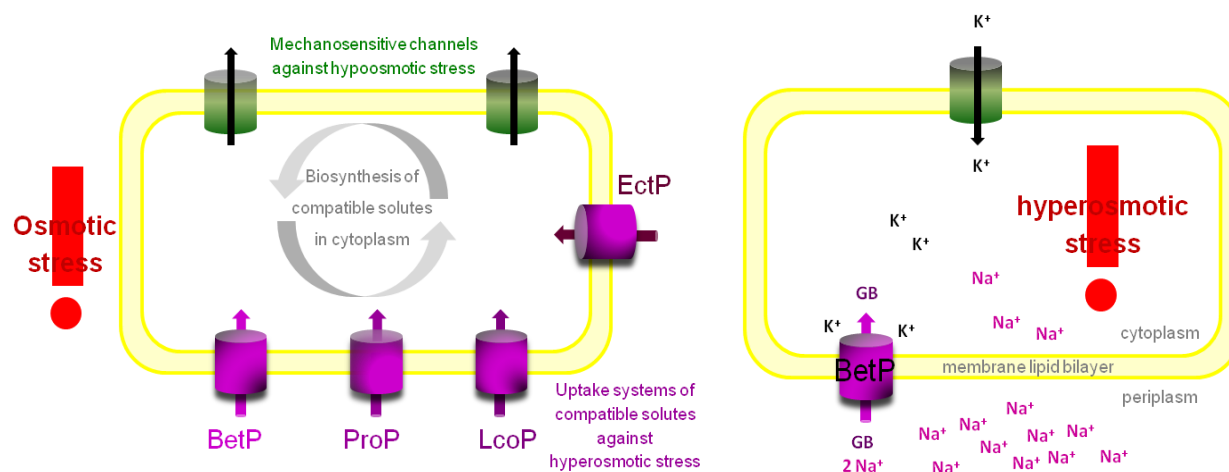


Figure 1.10: (Left) Osmotic stress response systems of *C. glutamicum* that harbors mechanosensitive channels and four osmoregulated uptake systems (BetP, ProP, LcoP and EctP). Glycine betaine (GB) and ectoine (amino acid derivatives) are imported only by uptake while proline is accumulated both by biosynthesis and uptake. **(Right)** The Na⁺/Betaine symporter BetP is activated upon an increase in the cytoplasmic K⁺ concentration in response to hyperosmotic stress.

More precisely, in response to hyperosmotic stress, the concentration of potassium (K⁺) in the cytoplasm increases instantly by means of ion channels in order to counterbalance the solute concentration inside and outside of the *C. glutamicum* cell. **BetP**, which is one of the secondary active transporters found in *C. glutamicum* and used in this study, is subsequently activated by sensing the cytoplasmic K⁺ concentration in order to take up an organic osmolyte, the glycine betaine molecule, into the cytoplasm, a process that is energetically coupled to the electrochemical Na⁺ potential by co-transport with two Na⁺ ions (Fig. 1.10 Right). BetP is so far one of the best characterized

osmoregulated transporter proteins in terms of transport and regulation since its X-ray crystallographic structures with different transport states have been recently resolved [Protein Data Bank (PDB) entries 2WIT, 4AIN, 4DOJ and 3P03]¹⁴⁻¹⁶.

1.1.5 Na⁺/Betaine Symporter BetP from *Corynebacterium Glutamicum*

A secondary active transporter BetP from the soil bacterium *C. glutamicum* belongs to the betaine/choline/carnitine transporter (BCCT) type family. BetP has functions both as an osmosensor and osmoregulator, performing catalytic activity by glycine betaine transport^{11,13}. BetP is activated by high external osmolality, cytoplasmic K⁺, rubidium (Rb⁺) and cesium (Cs⁺) concentration but not ammonium(NH₄⁺), sodium (Na⁺), choline, or glycerol concentration^{17,18}. However, BetP is inactive under the low osmolarity conditions. It is also activated at low temperatures (~10-15 °C), so-called chill stress, independent of osmotic stress but most probably depending on membrane lipid composition. Therefore, a third function of BetP is referred to the chill sensing¹⁹⁻²¹.

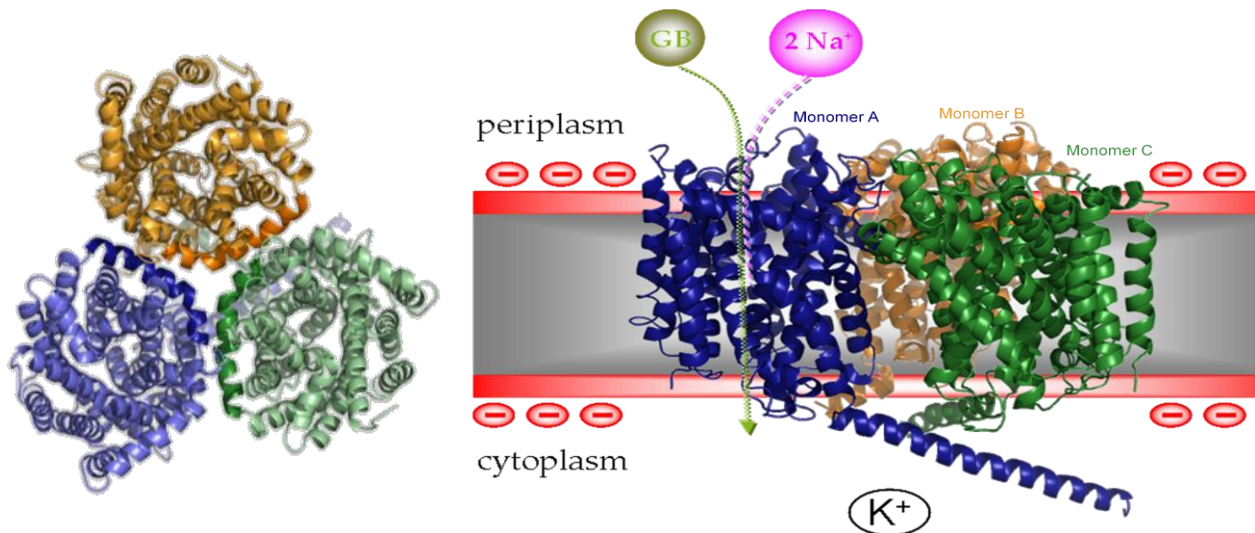


Figure 1.11: (Right) 3-D structure of BetP was drawn with PyMOL software (PDB ID: 2WIT). **(Left)** Periplasmic view of trimeric BetP. Monomers of trimeric BetP form a central conical cavity which is most probably filled with lipids. The amphipathic helix 7 of each monomer on the periplasmic side was highlighted. It is rich in asparagine and leucines residues, and thus, can be a non-specific lipid interaction site to stabilize the trimeric assembly^{11,14}.

An instant increase in the cytoplasmic K^+ concentration is a stimulus to activate the cation specific protein BetP in response to hyperosmotic stress (Fig. 1.11). This is subsequently pursued by importing of a specific compatible solute betaine into the cytoplasm in less than 1 second with co-transport of two Na^+ ions^{12,22–25}. The internal threshold concentration of K^+ necessary for the half-maximal activation of BetP was reported to be 220 mM when the protein was reconstituted in proteoliposomes of *Escherichia coli* phospholipids¹⁸.

The Na^+ /betaine symporter BetP is an integral membrane protein that has been extensively studied to date. Each monomer within the trimeric assembly of BetP activates its neighbouring subunit¹⁴. A trimeric form of BetP was found to be essential for its function because a presence of several intratrimeric interactions ensures the communications between the individual subunits²⁶. Trimeric BetP plays a functional role in both transport and regulation while its monomeric state has only the ability for the activation of betaine transport without regulation. It was also reported that the C-terminal domain of each protomer interacts with cytoplasmic loops of the adjacent protomers *via* ionic interactions solely in the trimeric assembly of BetP^{26,27}. The relevance of the Arg residues located in the C-terminal domain in terms of trimer contacts was also suggested^{11,14}.

According to the X-ray structure of BetP¹⁴, each monomer consists of 595 amino acids comprising 12 transmembrane helices (TMH) that span the membrane as well as a curved α -helix (helix h7) at the periplasmic membrane surface (Figs. 1.11 and 12). BetP has a negatively charged N-terminal domain and a positively charged C-terminal domain that both protrude into the cytoplasm, where they are interacting with adjacent monomers. The atomic structure revealed that BetP contains a LeuT-like fold of two inverted structurally related repeats of 5 TMHs. The first repeat contains TMs 3-7 and the second repeat forms TMs 8-12. An iris-shaped 4-TMH bundle (TM3, TM4, TM8 and TM9) formed by the first two helices of each repeat is the key part for the transport of substrate and co-substrate.

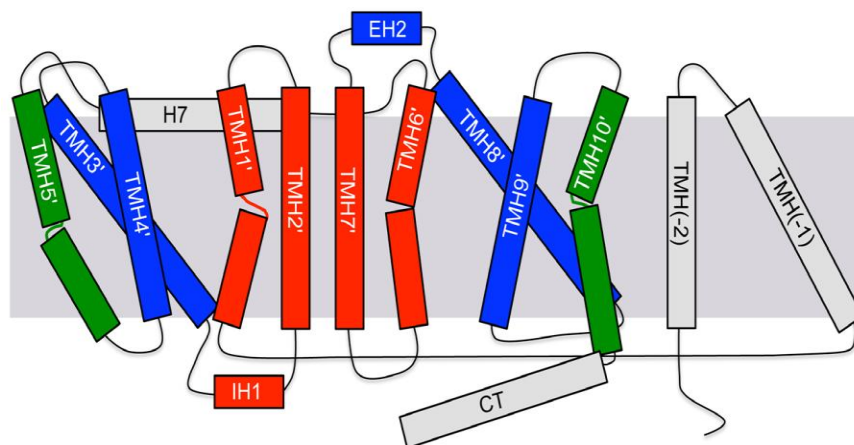


Figure 1.12: BetP topology with LeuT numbering. Bundle domain is shown in red (TMHs 1', 2', 6' and 7'), hash motif in blue (TMHs 3', 4', 8' and 9'), thin gates in green (TMHs 5' and 10'), helix 7 (H7) and the C-terminal domain (CT) in grey (Figure adapted from Perez et al., *Nature*, 2012)¹⁵.

A variety of mutations of the hydrophilic terminal domains of BetP have been extensively studied by biochemical methods. It has been revealed with transport assay experiments that BetP regulates transport activity to the extent of hyperosmotic stress by sensing the cytoplasmic K^+ concentration *via* its osmosensor associated with the C-terminal domain^{13,18,21,23,28}. Integrity and fine structure of both N- and C- termini of BetP play an important role in the regulation of activity^{28,29}. Precisely, deletion of 12 amino acids from the C-terminal domain of BetP between positions 571 and 583 (denoted as BetP Δ 12) partially deregulated BetP, remaining yet sensitive to changes in internal $[K^+]$. However, almost full deletion of the C-terminus (BetP Δ 45) is insensitive to hyperosmotic stress and K^+ sensing. That is, BetP Δ 45 is deregulated in terms of osmoregulation but it is active in the transport regardless of the internal K^+ concentration and in the absence of osmotic stress. Therefore, it was demonstrated that the C-terminal domain of BetP is directly involved in K^+ sensing or K^+ -dependent activation of BetP as a sensor domain²⁸. In comparison to the entire loss of osmoregulation in the C-terminus truncated form of BetP, deletion of the N-terminus of BetP resulted in a less dramatic effect because only the optimum activation profile was shifted to higher osmolarity in terms of regulation (from 1.3 to \sim 2.6 osmol/kg) although it was still an active protein²³.

Osmostress-dependent regulation of BetP has been also studied by using various membrane lipid derivatives. The lipid composition of the surrounding membrane, in which BetP is embedded, has an impact on the transport activity of BetP. Therefore, the activation profile of BetP is plotted to show the betaine uptake rate as a function of the extent of osmotic stress (Fig. 1.13). This indicates that the activity regulation of BetP against osmotic stress is related to the charge of the surrounding membrane^{29–31}. Precisely, Fig. 1.13 demonstrates the modulated activation profile of BetP inserted in different microorganisms which have different membrane lipid head group compositions^{11,30,31}. The optimum external osmolality to activate BetP was found around 1.3 osmol/kg for BetP in the *C. glutamicum* cells whereas it was downshifted around 0.5 osmol/kg in *E. coli* cells³². This is explained by the fact that the plasma membrane of *C. glutamicum* consists mainly of phosphatidylglycerol (87%) which is negatively charged at neutral pH whereas membrane lipids of *E. coli* involve only 20% of anionic phospholipids, demonstrating different distribution of anionic phospholipids. As a result, BetP regulates rapidly its transport activity in response to hyperosmotic stress.

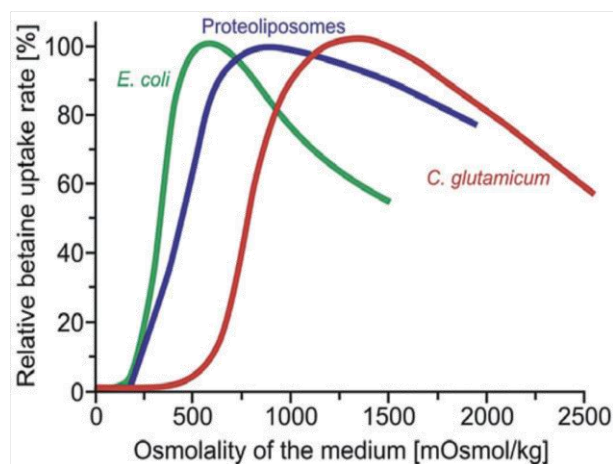


Figure 1.13: Activation profile of BetP embedded in the different membrane lipid systems, namely BetP in the native membrane of *C. glutamicum* (—), heterologously expressed *betP* gene in *E. coli* (—) and reconstitution of purified BetP protein in proteoliposomes (—). The latter two (— and —) are the artificial membrane surroundings for BetP. The plasma membrane of *C. glutamicum* consists mainly of phosphatidylglycerol (87%) whereas *E. coli* has only 20% of anionic phospholipids in its plasma membrane (Figure adapted from Ziegler et al., *Mol. Mic.*, 2010)¹¹.

The activation mechanism of BetP involves internal K^+ concentration, the regulatory C-terminus and negative membrane surface charges^{12,29}. Interactions of the C-terminal domain with the N-terminal domain and cytoplasmic loops were found to be functionally important in terms of osmosensing

and/or osmoregulation. Particularly, the membrane-interacting state of the C-terminus in the presence of anionic lipids refers to the inactive state of BetP whereas interaction of the C-terminal domain with the parts and domains of BetP (i.e. cytosolic loops) are suggested if the protein is in the active state²⁹. As recently reported, interactions of the protomers in the vicinity of the C-terminus and conformational changes which involves distinct displacements of the C-terminus upon activation are significant for activity regulation of BetP³³. This observed dynamic behaviour of the C-terminal domain is in line with the proposed activation model of BetP explained above.

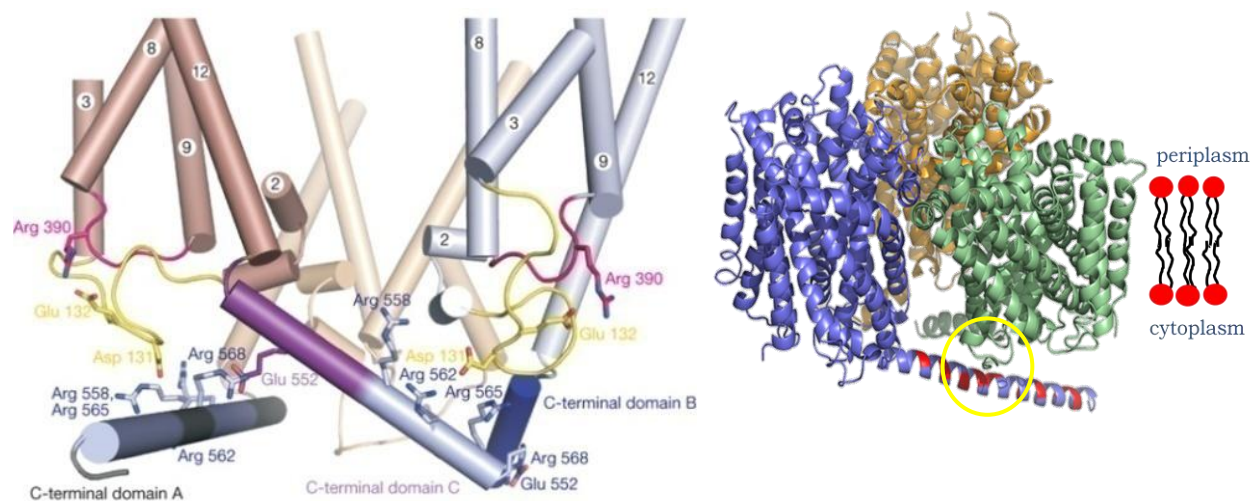


Figure 1.14: (Right) 3-D structure of BetP drawn with PyMOL software (PDB ID: 2WIT). Arginines in the C-terminal domain are shown in red. The Asp/Glu residues in loop 2 are very close to the C-terminus, shown within the yellow circle. **(Left)** Regulatory interactions mediated by the C-terminus (Figure from Ressler et al., *Nature*, 2009)¹⁴.

The regulatory ionic interactions mediated by the C-terminal domain are suggested to include a variety of charged residues (Arg, Asp and Glu) found in the loop2, loop8 and C-terminus (Fig. 1.14 Left)^{11,14}. Particularly, the C-terminal domain of BetP, which protrudes into the cytoplasm, involves a number of positively charged arginine residues (shown with red color in Fig. 1.14 Right) which could be a possible interaction partner with anionic lipid head groups and with negatively charged side chains (Asp131 and Glu132 residues in cytoplasmic loop 2) from the protein environment^{11,14}.

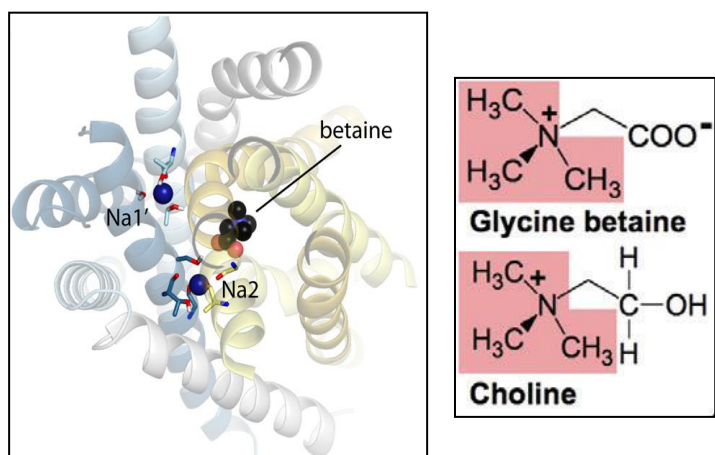
However, a conclusive contribution of lipids to the activation cycle is still under debate. Taken this knowledge into account, one of the aims of this study is to figure out the protein-lipid interactions involved in the activation/regulation mechanism of BetP.

The betaine binding site of BetP is alternately accessible both from the periplasmic and cytoplasmic site, namely the outward- and inward-facing states of BetP. According to its crystal structures, BetP is an asymmetric trimer that undergoes different conformational changes for different transport states *via* individual flexing of symmetry-related helices and rigid body movements which involve a 13° tilting of the scaffold motif (TM5 & TM6). The conformational changes during the ***alternating-access cycle*** of BetP involve outward-inward open or occluded states, and closed transition states with and without betaine. Recently, the 10 conformational states of BetP in the alternating-access cycle mechanism have been demonstrated³⁴. These altogether reveal opening and closing of the periplasmic and cytoplasmic gates, supporting the molecular transport mechanism¹⁴⁻¹⁶. The recently identified two regulatory ionic interaction networks located on the periplasm and cytoplasm side maintain a crosstalk among subunits within the trimer *via* cation- π interactions and link the bundle helices together, limiting their conformational flexibility which might be relevant for substrate specificity^{15,27}. Therefore, both the ***rocking bundle*** of scaffold helices and the ***gating*** movements are a prerequisite to open the pathways in BetP³⁴.

Glycine betaine is an exclusively specific substrate for wild type BetP with highest affinity and highest transport activity³². However, its mutation BetP G153D (exchange of glycine against aspartate) has the ability to transport H⁺-coupled choline with an increased affinity for sodium¹⁶, although both compatible solutes betaine and choline have a trimethylammonium group [R-N⁺(CH₃)₃] (Fig. 1.15 Right). This is explained by the fact that the glycine stretch in TMH3 facilitates the binding of the substrate carboxyl group having an important role in substrate specificity and ion coupling in BetP¹⁶. The binding site for betaine (S1) is found in a tryptophan box formed by

a 4-TM helix bundle close to the centre of BetP, and the aromatic residues from TM4 and TM8 (Trp374, Trp194 and Tyr197) coordinate the trimethylammonium group of betaine by cation- π interactions when BetP is in an inward occluded state with betaine ($C_{10c}S$)¹⁴. However, the location of betaine differs with respect to the type of transition state explained by the observation of side chain rotations in the substrate pathway. For instance, Trp373, Trp374 and Trp377 residues from TM8 contribute to the coordination of the betaine molecule, if BetP is in a closed-substrate bound state (C_cS), in which betaine fits adequately, and only the mutation of Trp377 inactivates BetP along the substrate pathway, suggesting a contribution of periplasmic aromatic residues to the betaine binding site¹⁵.

Figure 1.15: (Left) The glycine betaine and sodium binding sites (Na1 and Na2 sites) in BetP (Figure from Khafizov et al., *PNAS*, 2012)³⁵. **(Right)** Molecular structure of glycine betaine and choline (Figure from Ziegler et al., *Molecular Microbiology*, 2010)¹¹.



The two sodium binding sites were initially proposed by Ressler et al.¹⁴. However, the exact locations of the Na1 and Na2 binding sites in BetP have been recently identified^{15,35}. As shown in Fig. 1.15 Left, both sodium ions locate at the interface between the scaffold (TM5, TM6, TM10 and TM11) and bundle (TM3, TM4, TM8 and TM9) helices that undergo conformational changes during the distinct transport states. More precisely, in the Na2 site, sodium is coordinated by carbonyls from the backbone of the residues Ala147 and Met150 found in an unfolded stretch of TM3 which is an important helix during the alternating-access cycle and by the hydroxyl groups of the Thr467 and

Ser468 residues from TM10. The Na¹ site is formed by Phe380 from TM8, a water molecule and by a backbone carbonyl as well as side chains of residues Thr246 and Thr250 from TM5^{15,35}.

Using single-molecule force spectroscopy which is an another application of atomic force microscopy, it was demonstrated that interaction networks between external helix2, TM12 and C-terminal domain were reinforced in the presence of elevated K⁺ concentration (400 mM KCl), increasing the mechanical rigidity of the symporter upon K⁺- and betaine-binding³⁶. In this study, interactions of the C-terminal domain with the N-terminal domain, loop2 and loop4 on the cytoplasmic site were indicated as well.

Before the structure of BetP has been resolved by X-ray crystallography¹⁴, the secondary structure estimation of BetP was done by our group (Korkmaz, Filiz, Ph. D. Thesis, 2009). Detergent solubilised and some 2D crystals of BetP have been studied by IR spectroscopy. In this study, it was revealed that the N-terminus of BetP has a partial helical structure and the lipid environment is crucial for the stability of BetP shown by temperature excursion experiments with rising temperature. ¹H/²H exchange kinetics and *in situ* activation/deactivation of detergent solubilised wild type, the N- and C-terminal truncated BetP were also performed to determine the structural and functional properties of BetP. Recently, the influence of K⁺-activation on the conformational states of distinct secondary structural elements of BetP and formation of salt bridges between Arg and Asp/Glu residues have been pointed out³⁷.

1.2 INFRARED SPECTROSCOPY IN PROTEIN RESEARCH

Infrared (IR) spectroscopy based on the interaction of infrared radiation with an oscillating electric dipole moment of the molecules is a biophysical method for the study of macromolecules. IR spectroscopy is a very powerful technique for the interdisciplinary research area, including probing of structure-function relationship of proteins which are complex macromolecules composed of thousands of atoms. In this respect, IR spectroscopy shed light on the molecular biophysics of life sciences, particularly by investigation of membrane proteins, lipids, individual amino acids, nucleic acids (DNA and RNA), lipid-protein interactions, protein-ligand interactions, protein-nucleic acid interactions and enzymatic reactions on the molecular level³⁸⁻⁴⁵.

1.2.1 Absorption of Infrared Light and Molecular Vibrations

Energy can be detected in many forms from the highest to lowest energy by means of spectroscopic methods. For instance, IR spectroscopy is an absorption spectroscopic technique which uses the IR radiation of the electromagnetic spectrum that can excite the molecular vibrations. The IR region covers the range of 0.7-500 μm ($14000\text{-}20\text{ cm}^{-1}$) and is divided into three parts as being near-IR (0.78-2.5 μm), mid-IR (2.5-50 μm) and far-IR (50-500 μm) radiation. The most interesting region for the analysis of proteins and chemicals is the mid-IR range ($4000\text{-}400\text{ cm}^{-1}$ or $10^{13}\text{-}10^{14}$ Hz) while the low vibrational frequencies in the far-IR range ($400\text{-}20\text{ cm}^{-1}$) is rather suitable for weak bonds, such as coordination binding as well as for the analysis of molecules containing heavy atoms (i.e. inorganic compounds) which needs specialized sampling techniques.

In principle, the electric field of the electromagnetic wave enhances the movement of the atoms. Thereby, absorption of IR light causes excitation of the molecules among the vibrational energy levels. If the frequency of light coincides with the frequency of vibration and if stretching of bonds between the atoms creates a dipole moment change along with the vibration (IR-active), the incident IR radiation is absorbed by a molecular vibration, generating an IR spectrum (Fig. 1.19) which is a

plot of absorbed radiation *versus* wavenumber (reciprocal of wavelength, $1/\lambda$). This wavenumber unit in cm^{-1} has the advantage of being linear with energy (wavenumber = $1/\lambda = \nu/c$ and Energy = $h\nu$ where h is Planck constant, ν is the frequency and c is the speed of light). Vibrational modes which do not generate a dipole moment change in the molecule are called IR-inactive such as symmetric stretching modes of CO_2 and homonuclear diatomic molecules (H_2 , N_2 and O_2) while heteronuclear diatomic molecules (CO and HCl) are IR active (Dipole moment = Charge \times Distance).

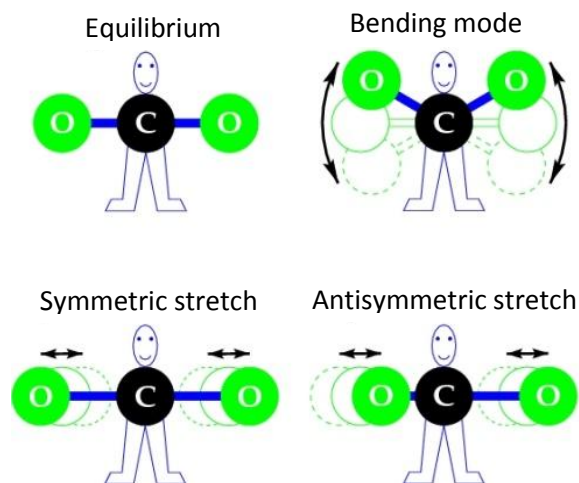


Figure 1.16: Examples of main vibrational modes of the CO_2 molecule. (Figure from <http://www.astro.uwo.ca/~jcami>).

Translations, rotations and vibrations are motions of a molecule. A molecule with N atoms has $3N$ degrees of freedom. A nonlinear molecule has a total of $3N-6$ degrees of freedom while a linear molecule has $3N-5$ normal modes of vibration. Molecules vibrate always at room temperature due to nucleic motion, creating the stretching and bending vibrations of their bonds (Fig. 1.16). Bending (δ) and stretching vibrations are the main types of vibrations. The latter can be symmetric (ν_s) and antisymmetric (ν_{as}) while bending vibrations can be scissoring, rocking, twisting and wagging. Each vibrational mode has a specific frequency in an IR spectrum, which is sensitive to any changes in its molecular environment. Atoms within a molecule oscillate with a frequency of $\nu = \frac{1}{2\pi} \sqrt{\frac{k}{\mu}}$, where μ

is the reduced mass of the atoms within a diatomic molecule ($\mu = \frac{m_1 \cdot m_2}{m_1 + m_2}$), behaving as an anharmonic oscillator and obeying to a realistic Morse potential curve³⁸.

The exact frequency (ν) of the vibrating molecules is dependent on the stiffness of the bond (force constant k) and on the masses (m_1, m_2) of the vibrating atoms (i.e. $^1\text{H}/^2\text{H}$ isotope exchange, see Section 2.6.2). The polarity and type of the vibrating bonds (single, double, triple) affects the vibrational frequency of the molecules in an infrared spectrum as well. For instance, an increment in the polarity of the vibrating bonds increases the strength of absorption in the IR spectrum. As shown clearly in Fig. 1.17, the stretching bonds have higher energy than corresponding bending frequencies, and the H-bonded atoms have higher stretching frequencies than those to heavier atoms due to the reduced mass μ . Therefore, in an IR spectrum we can obtain information regarding the bond length, bond strength, protonation/deprotonation state, H-bonding properties, conformational freedom, charge distributions, electrostatic interactions, redox state, dynamics and kinetics of the molecules^{41,46}.

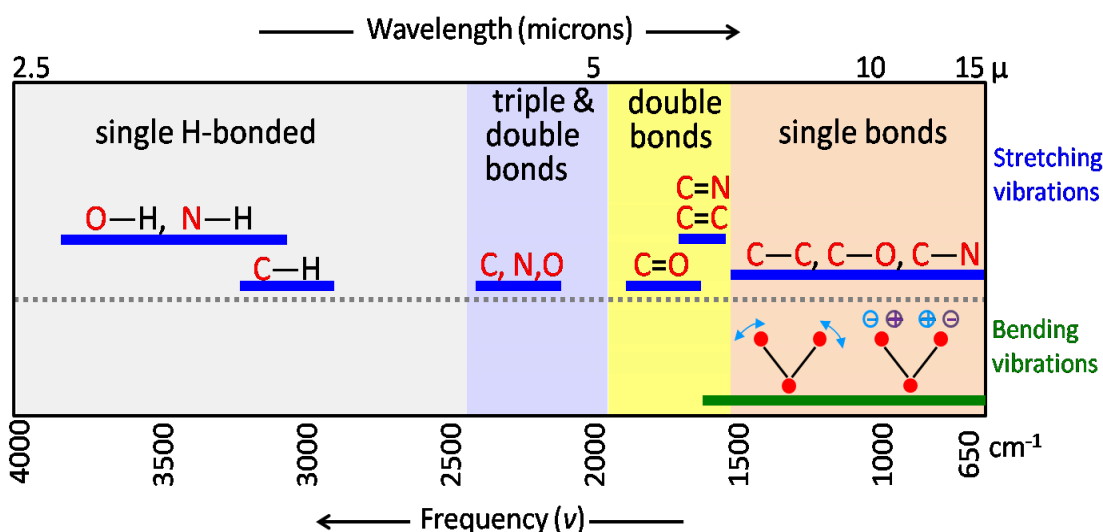


Figure 1.17: Vibrational frequencies of some molecules in an IR spectrum. Stretching vibrations can be classified as single bonds to H (3700-2500 cm^{-1}); triple bonds (2300-2000 cm^{-1}); double bonds (1900-1500 cm^{-1}) and single bonds other than hydrogen (1400-650 cm^{-1}). Bending vibrations exist in the region 1650-650 cm^{-1} in an IR spectrum as well.

1.2.2 FTIR Spectrometer

In the 1940's the dispersive IR spectrometers using a grating monochromator came up for characterization of the organic compounds as an analytical technique. However, since the late 1970's Fourier transform IR spectrometers (FTIR) have been used for advanced researches. These modern FTIR spectrometers have many advantages in the performance over dispersive instruments. One advantage is that FTIR collects the data faster than the dispersive instrument due to simultaneous scanning at all wavelengths, termed as **multiplex advantage**. Other advantages of FTIR are high signal-to-noise ratio, high resolution, spectral quality and sensitivity to weak peaks due to high light intensity at the detector (**throughput advantage**). Besides, a high accuracy in the FTIR spectra was obtained due to usage of a laser (HeNe laser at 633 nm) to calibrate the wavenumber. This internal laser also controls the absolute position of the movable mirror and adjusts the time for collection of data points for each scan (**precision advantage**).

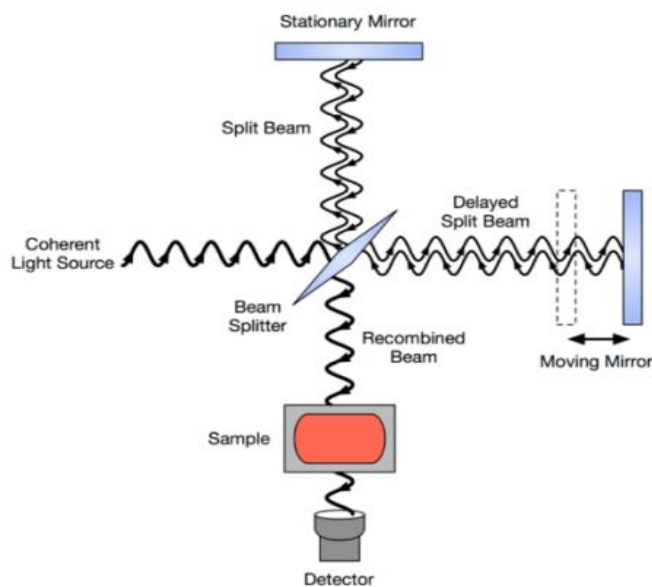


Figure 1.18: Michelson interferometer.
(Figure from <http://en.wikipedia.org/>).

A Michelson interferometer, which is the heart of the FTIR spectrometer to collect a spectrum, harbors a source, beam splitter, two plane mirrors (one fixed and one movable), a laser and a detector (Fig. 1.18)^{38,46}. The IR beam is collimated and passed through the interferometer where it is split into two beams by the beam splitter. The beam splitter recombines them and creates an

interference pattern (constructive or destructive), directing the combined beam to output. The output beam passes through the sample where some energy is absorbed and some is transmitted, and subsequently, the transmitted light is focused towards the detector. The optical path length of a beam varies with a movable mirror. Briefly, the incident IR radiation is absorbed by the sample and reaches to the detector that measures the intensity of the incident beam. The detector signal, the output collected as an *interferogram* is Fourier transformed to obtain an IR spectrum (Fig. 1.19).

To monitor a change in the IR radiation intensity, *thermal detectors* which are made from thermocouples or pyroelectric materials (Deuterated Triglycine Sulphate or DTGS) and *photon detectors* (semiconductor detectors) are available for the spectrometers. Mercury-Cadmium-Tellurium (MCT) detectors are the photon detectors that operate at liquid nitrogen temperature about 77 Kelvin while DTGS detectors work at room temperature.

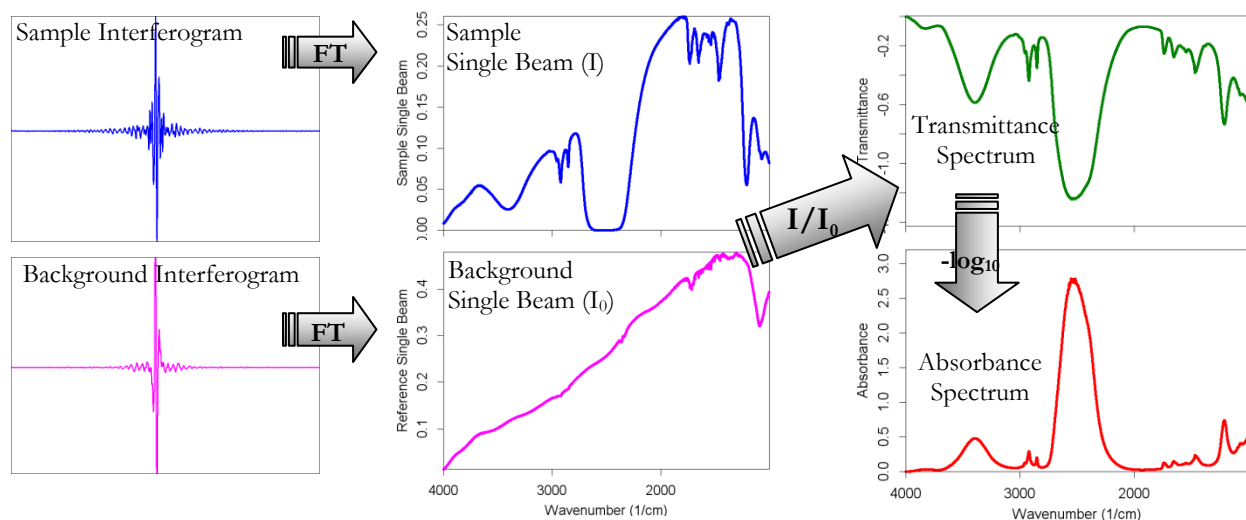


Figure 1.19: The process of formation of a Fourier transform (FT) infrared spectrum drawn by OPUS software.

For an interferogram, the intensity of absorbed light at the detector is described by $I(x) = \int_{-\infty}^{+\infty} I(\nu) \cos(2\pi x\nu) d\nu$ as a function of mirror position x which is the optical path difference. This interferogram is transformed from the space (x) to the frequency (ν) domain by a

computer using the mathematical operation called Fourier-transformation at discrete points to display the IR single beam spectrum. Thereby, the spectral intensity as a function of wavenumber for single beam spectrum is represented by $I(\nu) = \int_{-\infty}^{+\infty} I(x) \cos(2\pi x\nu) dx$. In order to produce “*absorbance or transmittance spectrum*”, the “*sample single beam spectrum*” is collected taking the reference as “*background single beam spectrum*” (Fig. 1.19). This reference spectrum is recorded in the absence of a sample. The final spectrum (transmittance spectrum) can be converted to one another (absorbance spectrum) by calculating the negative logarithm ($A = -\log_{10} T$) of the data points. The absorbed infrared radiation (A) by a sample can be directly calculated by the ***Beer-Lambert equation***, $A = -\log\left(\frac{I}{I_0}\right)$ where I and I_0 are the intensities of the single beam spectrum of the sample and reference, respectively.

An absorption spectrum can be recorded by FTIR spectrometers combined with *attenuated total reflection unit* (ATR-FTIR) or in the *transmission mode*. A brief theoretical background and sampling techniques of those will be explained in Section 2.5.

1.2.3 Infrared Signatures of Proteins and Amide Bands

IR spectroscopy has been widely used for the determination of conformational changes and functional features of proteins. It is a non-destructive and fast technique and requires small sample volume for the study of membrane proteins. Since secondary structural elements, individual amino acids and lipids have distinct absorbance in an IR spectrum, an analysis of the IR spectrum yields information regarding the protein structure and inter- and intra-molecular interactions of proteins with their environment. The structural repeat unit of proteins, a peptide group (Fig. 1.20 Right), leads to nine characteristic amide bands (amide A, amide B and amides I-VII) that harbour different vibrations in an IR spectrum, in the order of decreasing frequency⁴⁵⁻⁴⁷. The IR signals and composition of amide bands of the peptide backbone are summarized in Table 1.1.

Table 1.1 : Characteristics IR bands of the peptide backbone (ν_s : stretching vibration; δ : bending vibration)^{47,45}.

Amide bands	Wavenumber (cm ⁻¹)	Composition and energy fraction located in bond
Amide A	~ 3300	$\nu_s(\text{NH})$ 100%
Amide B	~ 3100	$\nu_s(\text{NH})$ 100%
Amide I	~ 1610-1695	$\nu_s(\text{CO})$ ~80%; out-of-phase $\nu_s(\text{CN})$; in-plane $\delta(\text{NH})$
Amide II	~ 1480-1575	in-plane $\delta(\text{NH})$ ~40-60%; $\nu_s(\text{CN})$ ~18-40%; $\nu_s(\text{CC})$ ~10%
Amide III	~ 1220-1320	$\nu_s(\text{CN})$ ~40%; $\delta(\text{NH})$ ~30%; $\nu_s(\text{CC})$ ~30%
Amide IV	~ 625-765	$\delta(\text{NH})$; $\text{tors.}(\text{CN})$
Amide V	~ 640-800	$\delta(\text{CO})$ ~40%; $\nu_s(\text{CC})$ ~30%; $\delta(\text{CNC})$; $\delta(\text{NH})$
Amide VI	~ 535-605	$\delta(\text{CO})$; $\text{tors.}(\text{CN})$
Amide VII	~ 200	$\delta(\text{NH})$; $\text{tors.}(\text{CN})$; $\delta(\text{CO})$

The amide A ($\sim 3300 \text{ cm}^{-1}$) and amide B bands ($\sim 3100 \text{ cm}^{-1}$), characterized by the N-H stretching vibrations, are originated from a Fermi resonance with the first amide II overtone. The **amide I** band observed in the $1600\text{-}1700 \text{ cm}^{-1}$ region is composed primarily of C=O stretching vibrations of the amide groups with smaller contributions from the out-of-phase C-N stretching vibrations and N-H in-plane bending vibrations which are very sensitive to H-bonding (Fig. 1.20 Left). Since secondary structures (α -helix, β -sheet, turn, loop, 3_{-10} -helix) are stabilized by the interchain H-bonds between the amide N-H and C=O groups, the amide I band is most useful in the IR spectrum for the analysis of protein secondary structures (see Section 2.7). The frequency of the amide I band is influenced by the strength of the H-bond to the C=O groups. For instance, a strong H-bond to the C=O group weakens the strength of the double bonding of the C=O group and thereby lowers the vibrational frequency.

The **amide II** band observed in the $1500\text{-}1600 \text{ cm}^{-1}$ region arises mainly from the in-plane N-H bending vibrations of the amide groups with minor contributions from the C-N stretching and C-C stretching vibrations. This band is $\sim 100 \text{ cm}^{-1}$ downshifted towards $\sim 1490\text{-}1460 \text{ cm}^{-1}$ (named amide II' mode) upon $^1\text{H}/^2\text{H}$ exchange (see Section 2.6.2) which is a useful experimental method to obtain information about the protein accessibility and flexibility.

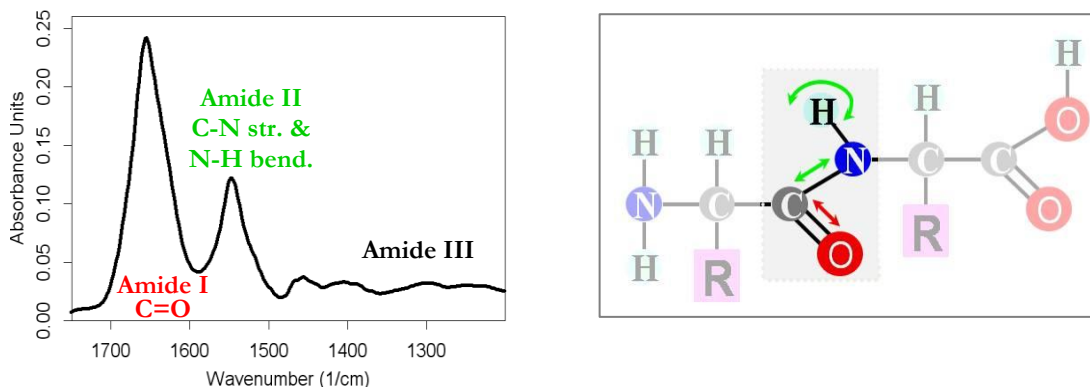


Figure 1.20: (Left) The IR absorption spectrum of the α -helical protein BetP that shows typical amide I and amide II bands. **(Right)** Molecular motions of a peptide group observed as amide I (\leftrightarrow) and amide II vibrations (\leftrightarrow).

1.3 GOAL OF THIS STUDY

The Na^+ /Betaine symporter BetP from *C. glutamicum* is the subject of the present study. BetP has been extensively studied by using a large number of methods to date. Although its atomic structure and the K^+ -binding sites are known in detail, the contributions of the membrane lipids to activate the transport cycle and molecular mechanisms of activation and of regulatory response of BetP are partially known. Therefore, the aim of this study is to investigate the structural and functional properties of BetP on the molecular level upon K^+ -induced activation using Fourier transform infrared spectroscopy. In this study, activation of BetP selectively induced by K^+ ions will be introduced. The structural changes of BetP between the active (K^+ -stimulated) and inactive state conditions will be investigated by using the wild type and mutant BetP which are reconstituted into proteoliposomes and 2D crystals. Particularly, one of the aims of this study is to analyse the infrared lipid signals in order to determine the lipid-protein interactions and the role of lipids upon K^+ -stimulated activation. For this purpose, *in situ* titration of BetP with increasing K^+ concentration and with changing pH will be performed experimentally. Hydrogen/deuterium exchange as well as temperature dependent experiments are going to be performed in the active and inactive states of

BetP to obtain more information regarding the solvent accessibility and thermal stability in its open and closed states. Thereby, in this project, new insights into the structure-function relationship of BetP upon K^+ -induced activation are expected to be revealed on the molecular level by using IR spectroscopic methods.

2. MATERIAL AND METHODS

2.1 CHEMICALS

The chemicals which were used in the present study are listed in Table 2.1 below. In order to prepare the 10 mM sodium phosphate (NaP_i) buffer at the desired pH, proper amounts of acid and base salts (NaH_2PO_4 and Na_2HPO_4) were mixed in distilled water (pH 7.5) or in deuterium oxide (p^2H 7.5) calculating by $\text{p}^2\text{H}=\text{p}^1\text{H}+0.4$ units^{48,49}. If necessary, the amounts of sodium (inactivate buffer conditions) and potassium (activate buffer conditions) salts were directly added to NaP_i buffer at the desired concentration. The final pH value was controlled with a pH-meter.

Table 2.1: The list of chemicals used in this study.

Chemicals	Source
Deuterium oxide (99.9%)	Aldrich
<i>E.coli</i> lipids	Avanti Polar Lipids, Alabaster, USA
KCl	Roth
NaCl	Roth
Na_2HPO_4	Roth
NaH_2PO_4	Roth
n-Dodecyl-b-D-Maltosid (DDM)	Fluka

2.2 PROTEIN SAMPLES: BetP from *Corynebacterium glutamicum*

BetP WT (wild type) and its mutants used in this study are listed in Table 2.2. The protein samples and corresponding blank lipids were kindly provided by Prof. Dr. Christine Ziegler, Department of Structural Biology, Max Planck Institute of Biophysics, Frankfurt, Germany. The aliquots of 2D crystals reconstituted in *C. glutamicum* lipids (~ 2.5 mg/ml in ~ 800 μl) were kept at room temperature due to the high stability of the samples at that temperature while the stocks of proteoliposomes (~ 5 mg/ml in ~ 100 μl), which represents BetP reconstituted in liposomes prepared from *E. coli*

phospholipids (20 mg phospholipid/ml) were divided into 30 μ l fractions and stored at -80 °C for long term stability.

Table 2.2: BetP samples and their stocks were provided to be investigated in the present study. Δ C45 stands for the deletion of amino acids at positions 551-595 from the C-terminus of BetP. *C.G.* is the abbreviation of *Corynebacterium glutamicum* and LPR represents the lipid-to-protein ratio (weight/weight).

Name of sample	Properties	Provided stocks	LPR (w/w)	Concentration
BetP WT	Wild type	Proteoliposomes (in <i>E.coli</i> lipids)	10:1	~5 mg/ml
BetP WT	Wild type	2D crystals (in <i>C.G.</i> lipids)	0.2	~2.5 mg/ml
BetP ΔC45	Mutation	Proteoliposomes (in <i>E.coli</i> lipids)	10:1	~5 mg/ml
BetP ΔC45	Mutation	2D crystals (in <i>C.G.</i> lipids)	0.2	~2.5 mg/ml
<i>C.G.</i> phospholipids	Blank	Lipid bilayer in buffer	-	4 mg/ml
<i>E.coli</i> phospholipids	Blank	Liposomes in buffer	-	20 mg/ml

The buffer of the protein samples was exchanged to the desired sodium phosphate buffer at pH 7.5 either by using ultracentrifugation (6000 rpm for ~30 min, at $+4$ °C) in an eppendorf tube or samples of the protein were directly placed on the ATR diamond. In the latter case, the buffer exchange was achieved by means of a continuous-flow perfusion technique overnight at $+4$ °C (see Section 2.5.2).

2.3 LIPID-PROTEIN SYSTEMS: Proteoliposomes and Two-Dimensional Crystals

If amphipathic lipids are mixed with water, the lipid aggregates (so-called micelle, bilayer and liposome) exist spontaneously, depending on the conditions and the nature of the lipids². Their hydrophobic regions are excluded from water interacting with each other while their hydrophilic head groups at the surface are in contact with water (Fig. 2.1). Accordingly, the extracted and purified specific transport protein is incorporated into phospholipids such as lipid bilayer or liposomes which are the experimental systems to investigate the functional-structural properties of the various membrane proteins. Membrane proteins are embedded into the lipid bilayer with a certain lipid-to-protein ratio (LPR) to ensure the structural and functional integrity. As depicted in Fig. 2.1, two-dimensional (2D) crystals and proteoliposomes are the most commonly used lipid-

protein systems which contain a single type of detergent-solubilized protein reconstituted into pure lipids without loss of function⁵⁰. The 2D crystals have a less LPR in comparison to proteoliposomes because the 2D crystals consist of protein-associated lipids whose molecules bind tightly to the specific binding site of the protein as well as a smaller amount of bulk bilayer lipids whose molecules do not bind directly to the protein.

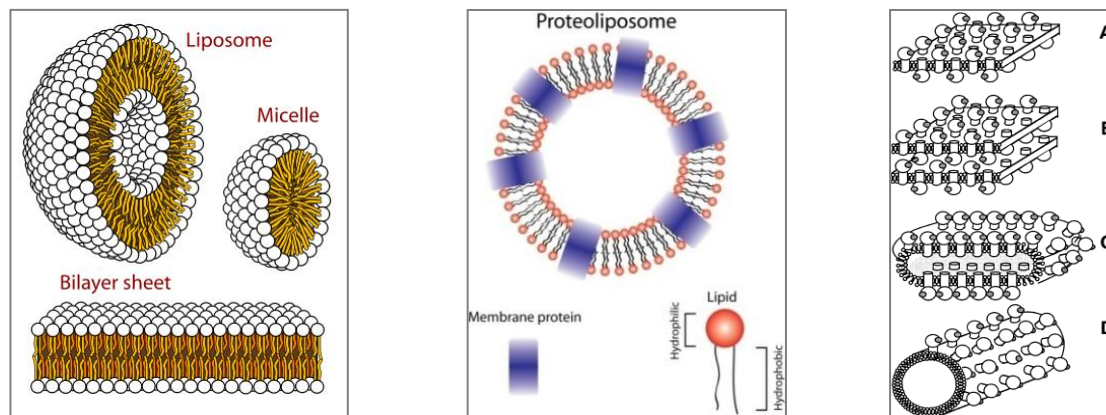


Figure 2.1: (Left) Three types of lipid aggregates (Figure from <http://en.wikipedia.org/>).

(Middle) A proteoliposome is a lipid vesicle with incorporated membrane proteins (Figure from Kaufman, Y. and Freger, V., Ch. 28, DOI: 10.5772/19770).

(Right) Formation of different types of 2D crystals after removal of detergent from a lipid-protein-detergent micellar solution: **(A)** Planar 2D crystals; **(B)** stack of planar 2D crystals; **(C)** vesicular crystals and **(D)** tubular crystals. (Figure reproduced from Rigaud, J.L., 2002, Brazilian Journal of Medical and Biological Research)⁵⁰.

The quality of the crystallization depends on the LPR, the choice of the detergent, pH, the dialysis temperature and on the salt concentration. The provided 2D crystals of BetP were formed by detergent (n-dodecyl- β -D-maltoside or DDM) dialysis for three weeks^{51–53}. The dialysis was performed at 37°C using *E. coli* polar lipids extract/cardiolipin, at 30°C using native *C. glutamicum* lipid extract and at 30°C synthetic phosphatidyl glycerol (PG) 16:0-18:1⁵². Well-ordered crystals were formed only at a pH 7.5 as large crystalline monolayers and round vesicles while at pH 5.5 as small crystal stacks⁵¹. The type of the lipid also effects crystal packing and order. For instance, BetP has preference for fatty acid moieties 16:0-18:1⁵². Lipids extracted from the *C. glutamicum* cell, which is

the natural environment of BetP with a high proportion of PG (87%), provide formation of large well-ordered crystals with the LPR of 0.1-0.2 (weight/weight)⁵².

BetP samples prepared as (1) BetP solubilised in detergent (DDM), (2) BetP reconstituted in POPG (1-palmitoyl-2-oleoyl-glycero-3-phosphoglycerol) lipids as proteoliposomes and (3) 2D crystals of BetP are ideal to study with IR spectroscopy. Among them, only 2D crystals (Fig. 2.2) and proteoliposomes of BetP have been used in the present study. The advantages of 2D crystals of BetP are to obtain stable absorbance spectra in long-term measurements because they are fixed and well oriented on the ATR diamond during perfusion of buffer (see Section 2.5.2) and the 2D crystals have a smaller amount of lipid molecules per monomer in comparison to proteoliposomes.

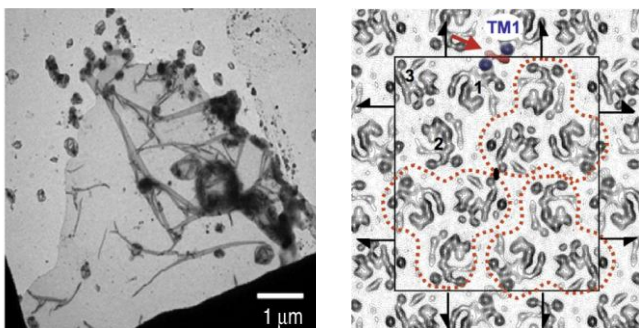


Figure 2.2: (Left) Electronmicrograph and (Right) projection structure of 2D crystals of BetPΔC45. In symmetry-related trimers, two protomers (1 and 2) have similar conformations while protomer 3 appears to be in a different state. (Figures from Tsai et al., 2011, Journal of Molecular Biology)⁹¹.

2.4 INFRARED SIGNATURES OF LIPIDS

Besides IR signatures of proteins and individual amino acids, vibrational modes of lipids are present in the IR spectrum as well. Therefore, membrane proteins can be investigated with IR spectroscopy in their native lipid bilayer environment. Membrane lipids are made up of polar headgroups in the hydrophilic region and of nonpolar acyl chains in the hydrophobic region of the membrane. These different depths of the lipid bilayer are crucial for the study of physical properties of membrane lipids. Phospholipid molecules give rise to distinct positions in a wide range of the mid-IR spectrum as shown explicitly in Fig. 2.3. More precisely, these infrared signatures of the phospholipids arise from the antisymmetric and symmetric stretching vibrations of the phosphate moiety (PO_2^-) in the polar

headgroups that make hydrophilic interactions with the protein *via* H-bonding as well as from the carbon-hydrogen antisymmetric and symmetric stretching vibrations (CH_3 and CH_2) that are sensitive to static order and dynamics of the acyl chains in the hydrophobic region of the membrane. Additionally, the $\text{C}=\text{O}$ stretching modes of the ester carbonyl groups in the interfacial region of the membrane cause a broad band between 1760 and 1700 cm^{-1} and are sensitive to H-bonding and polarity changes in their environment⁵⁴⁻⁵⁶.

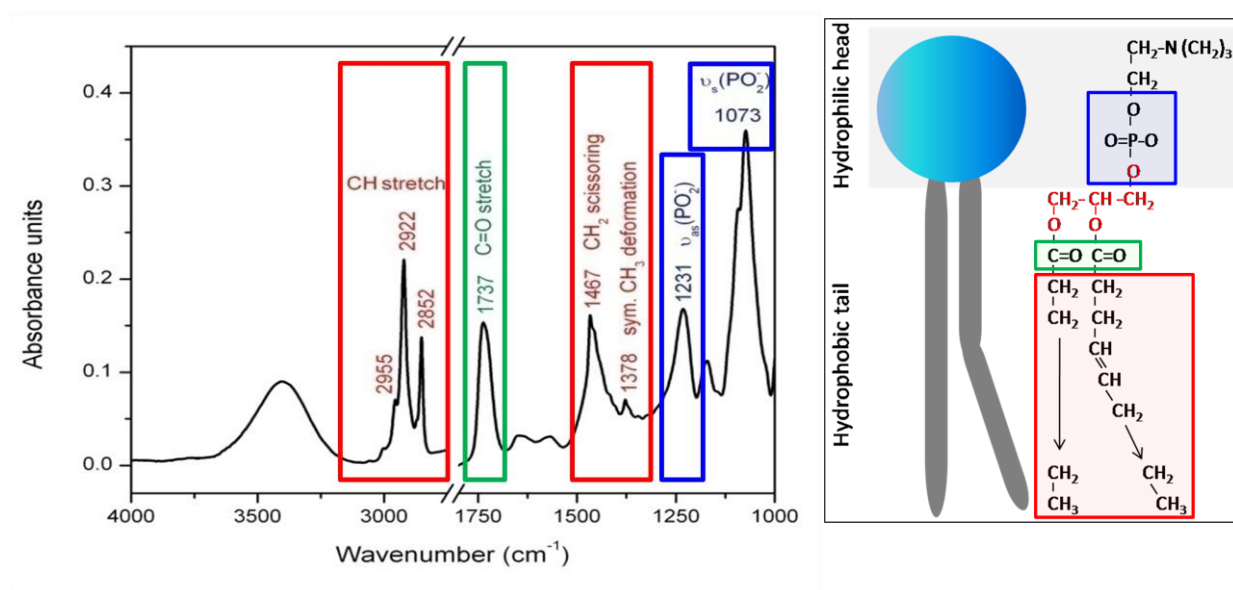


Figure 2.3: (Right) The different depths of a phospholipid molecule and (Left) their corresponding color coded band positions in the IR spectrum (*E. coli* phospholipids).

Membrane proteins that span the plasma membrane perturb actually the order of the membrane lipids but interactions of membrane proteins with the membrane lipids stabilize the conformation of the protein to keep the protein functionally intact. In this respect, infrared spectroscopy is a powerful technique to selectively probe the perturbations by the membrane proteins on the hydrophobic lipid tails, interfacial region or even on the polar headgroups of lipids^{57,58}. Therefore, lipid signals can be followed in width and position to yield information about the lipid-protein interactions as an external parameter. Besides, observation of accompanying spectral alterations in the individual amino acid

side chains from the protein environment as well as in the amide modes from the protein backbone can help to reveal the interactions of the lipids with specific sites of the proteins^{59–61}.

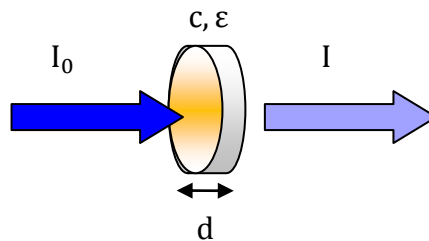
2.5 INFRARED SPECTROMETERS AND SAMPLING TECHNIQUES

A wide variety of infrared spectroscopic methods are used to monitor the conformational changes of a protein upon a perturbation as well as dynamic studies, protein-protein and lipid-protein interactions, characterization of enzyme-substrate reactions, folding-unfolding studies, analysis of secondary structure of proteins and even structural-functional properties of membrane proteins on the molecular level^{41,43–46,60,62}, as already mentioned in Section 1.2. The design of the experiments performed in this study by using FTIR spectroscopy will be addressed below.

2.5.1 FTIR Spectroscopy in Transmission Mode

One of the most frequently applied experimental methods to probe proteins is the FTIR transmission mode. In transmission measurements, the IR beam is passed through a cuvette before it reaches the detector, as shown in Fig. 2.4. The absorbance, $A = -\log\left(\frac{I}{I_0}\right) = c \epsilon(\bar{\nu})d$, is calculated from the *Beer-Lambert's law* (see Section 1.2.2), where I_0 and I are the intensities of incident and transmitted light, respectively, c the concentration of the absorbing molecules, $\epsilon(\bar{\nu})$ the molar extinction coefficient or molar absorption index and d the pathlength of the measuring cuvette.

Figure 2.4: A schematic representation of an absorption measurement.



Several materials that are transparent in the mid-IR range can be used for the FTIR transmission experiments. These are for example ZnSe, AgCl, KRS-5, KBr, CsBr, CsI, KCl, NaCl, CaF₂ and BaF₂.

These materials have different stability against aqueous solution, different refractive indices and other properties, as listed in Table 2.3.

One of the most commonly used IR window is the CaF_2 window to study aqueous solutions of proteins due to its insolubility in water and low refractive index. These windows are composed either of one flat window and a deepened window or of two plane windows separated via a spacer that determines the optical path length (3,5-20 μm). A drop of the liquid sample (0.1-1 mM for proteins) is placed between two windows to produce a thin film, and subsequently, windows are mounted in a cell holder that is placed into the IR chamber for measurement. In the present study, thermal stability experiments have been performed with this method which will be explained in detail in Section 2.6.5.

Table 2.3: Different kinds of optical materials used in transmission IR spectroscopy. (From Stuart, B. H., 2004, Infrared Spectroscopy: Fundamental and Applications, ISBN: 9780470011140, ANTS series, Wiley ⁶³ , from http://www.internationalcrystal.net/ti_sec1.htm ; http://www.photonics.com ; and from Bruker optics).			
Window Material	Useful Range (cm^{-1})	Refractive Index	Properties
CaF_2	77,000-1200	1.4	Insoluble in water; resisting most acid and bases; does not fog; useful for high-pressure work.
BaF_2	50,000-900	1.45	Insoluble in water; soluble in acids and NH_4Cl ; does not fog; sensitive to thermal and mechanical shock.
ZnS	22,000-750	2.2	Insoluble in water, slightly soluble in acids, HNO_3 , H_2SO_4 , and KOH ; reacts to strong oxidizing agents; good resistance to thermal and mechanical shock.
ZnSe	20,000-500	2.43	Insoluble in water and bases; slightly soluble in acids; high resistance to thermal shock and chemical attack; soft material; not recommended in harsh environments; toxic.
Ge	5,000-600	4	Insoluble in water; chemically inert, hard and brittle; handled with extreme care, tends to fracture.
Diamond	45,000-10	2.4	Insoluble in water, acids, and bases; strong IR absorbance between 2700-1800 cm^{-1} .

IR spectroscopy of aqueous solutions has certain difficulties^{42,45,46} because water has a very intense absorbance due to O-H bending mode near 1645 cm^{-1} in the mid-IR range⁶⁴ which overlaps strongly

with the protein amide I band and some side chain signals. This problem can be overcome by using deuterium oxide (D₂O) instead of H₂O because the water band in the amide I region is downshifted to 1210 cm⁻¹ due to the heavier mass of ²H. Besides, the vibrational extinction coefficients are relatively low for aqueous solutions of proteins, resulting in low intensity IR bands. To solve these problems and to achieve a high signal-to-noise ratio, short path lengths (6-12 μm) and relatively high protein concentrations (20-50 mg/ml) should be used for FTIR spectroscopy when using H₂O as a solvent. Alternatively, low protein concentrations (5-10 mg/ml) with higher path lengths (up to 50 μm) can be used when using D₂O.

2.5.2 ATR-FTIR Spectroscopy and ATR-Perfusion Cell

Attenuated total reflection Fourier transform infrared spectroscopy (ATR-FTIR) is an absorption spectroscopic technique widely used to record IR spectra of biological materials^{42,44-46,65}. ATR-FTIR spectroscopy is implemented to yield information regarding the conformational changes of proteins in a changing environment *in situ*, structural and functional relationship of proteins as well as orientation of the molecular groups or secondary structural elements. Since this technique requires a small amount of sample (~5 μl) to produce a strong IR signal, it is well-suited particularly for the study of membrane-associated proteins both solubilised in detergent and reconstituted in lipids.

As represented in Fig. 2.5, the IR beam is directed to a trapezoidal-shaped IR-transparent crystal which is a high refractive index medium, n_1 (i. e. diamond, zinc selenide, zinc sulfide or germanium). Above a critical angle, (depicted by $\theta_c = \sin^{-1} n_2/n_1$, where n_1 and n_2 are the refractive indices of internal reflection element, IRE and of the sample, respectively), several total reflections occur at the surface of the IRE on which the protein sample is placed. Superimpositions of these incoming and reflected waves create a ***standing wave*** within the IRE, and subsequently, extension of IR light beyond the reflecting interface produces an electromagnetic disturbance, namely ***evanescent field*** that protrudes a few μm (0.5-5) into the less optically dense sample medium containing air, protein,

buffer, solid, etc. IR radiation is partially absorbed by the sample deposited on the surface of the ATR crystal, attenuating the main beam and resulting in an IR spectrum.

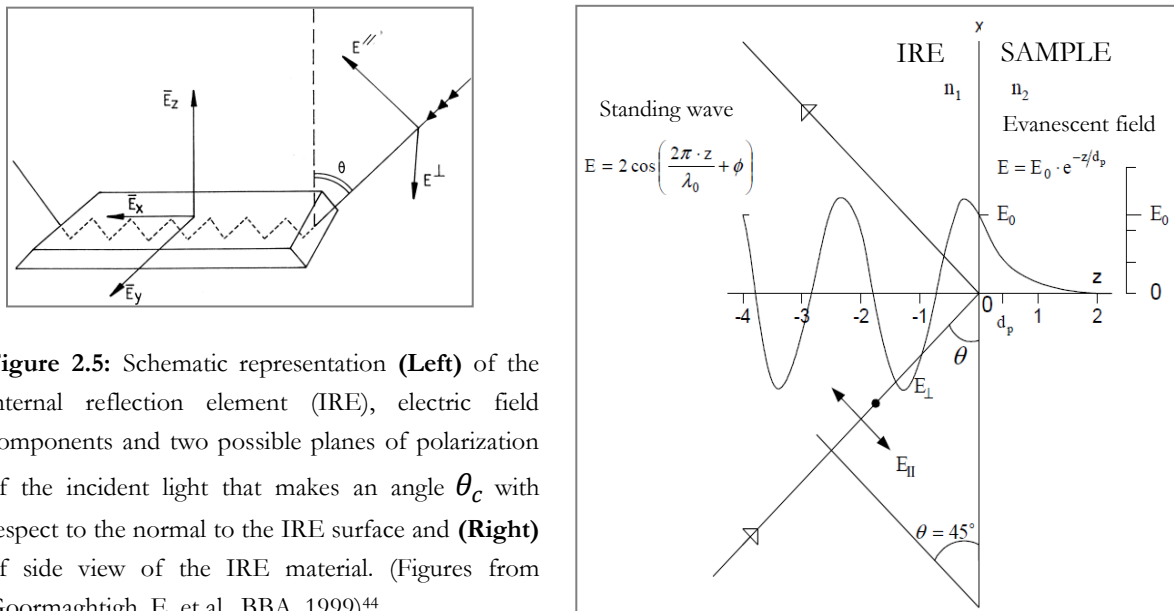


Figure 2.5: Schematic representation (**Left**) of the internal reflection element (IRE), electric field components and two possible planes of polarization of the incident light that makes an angle θ_c with respect to the normal to the IRE surface and (**Right**) of side view of the IRE material. (Figures from Goormaghtigh, E. et al., BBA, 1999)⁴⁴.

The amplitude of the electric field of the standing wave decays exponentially within the absorbing sample in the sample medium represented by $E = E_0 \cdot e^{-z/d_p}$, where E_0 is the electric field intensity at the interface between the IRE and less dense medium, z the distance from the interface in the rare medium and d_p the penetration depth of the evanescent field as given by

$$d_p = \frac{\lambda/n_1}{2\pi\sqrt{\sin^2\theta - (n_2/n_1)^2}}.$$

In this equation, λ is the wavelength of the light within the IRE and θ is the incidence angle of the IR beam. The number of reflections within the IRE material, depth of penetration, wavelength of the IR light, angle of the incident IR beam, refractive indices of IRE and of the sample as well as immobilization of the sample onto the ATR crystal influence significantly the absorbed intensity in the spectrum. Therefore, the IR absorbing sample has to be in a good and intimate contact with the crystal to obtain a stable absorbance spectrum. Particularly, since the

penetration depth of the evanescent wave depends on the refractive index of the IRE (n_1), the choice of the IRE material is essential. In order to obtain a high intensity in the spectrum, the refractive index of the crystal has to be greater than the one of the sample, ($n_{crystal} = \sim 2.4 > n_{sample} = \sim 1.5$). In this respect, some appropriate IRE materials are commercially available such as diamond ($n = 2.4$), ZnSe ($n = 2.42$), germanium ($n = 4$), silicon ($n = 3.42$) and KRS-5 ($n = 2.35$).

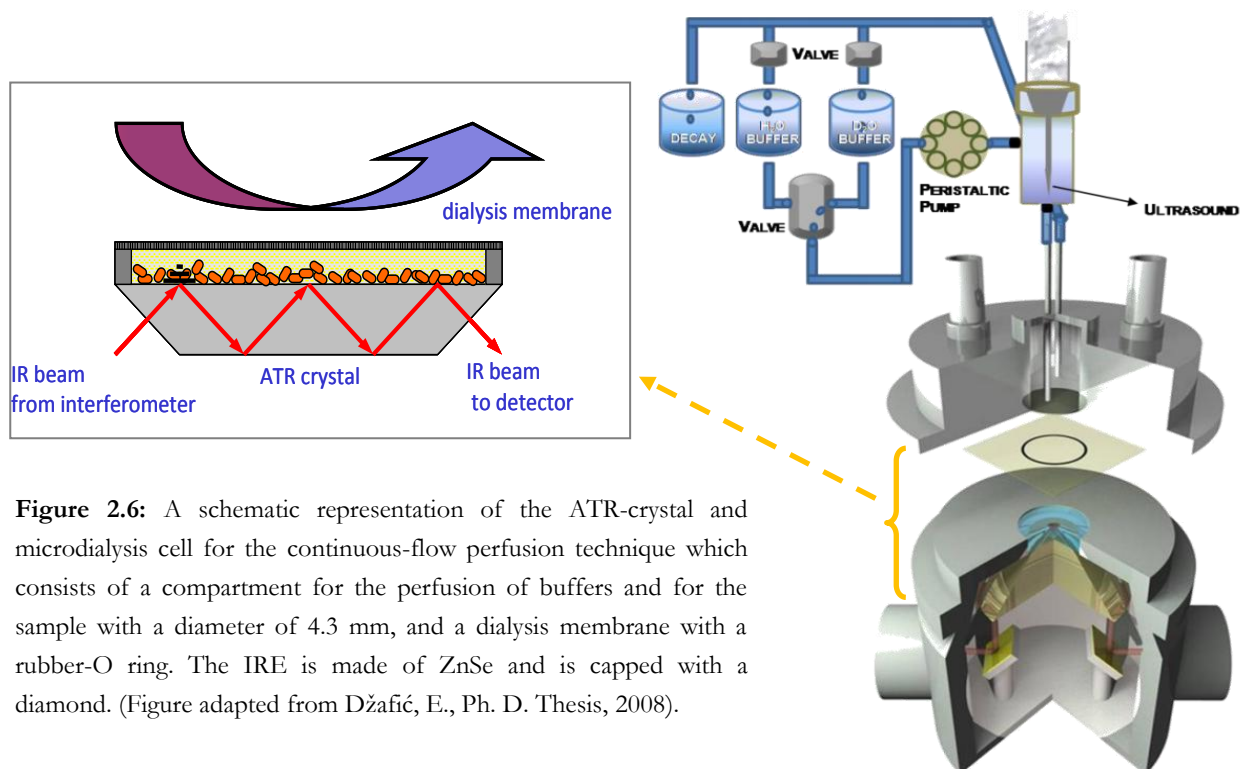


Figure 2.6: A schematic representation of the ATR-crystal and microdialysis cell for the continuous-flow perfusion technique which consists of a compartment for the perfusion of buffers and for the sample with a diameter of 4.3 mm, and a dialysis membrane with a rubber-O ring. The IRE is made of ZnSe and is capped with a diamond. (Figure adapted from Džafić, E., Ph. D. Thesis, 2008).

As schematically indicated in Fig. 2.6, a home-built **ATR micro-dialysis cell**⁶⁶ has been used in this study to perfuse the protein sample continuously with various buffer conditions. The ATR-unit has a diamond as IRE material which produces 7 reflections and harbors a ZnSe-optic in order to direct the IR beam into the diamond. The perfusion unit mounted on the ATR unit allows flowing of the effector molecules towards the sample ($\sim 5 \mu\text{l}$) placed on top of the crystal. Here, the sample is covered with a dialysis membrane whose cut-off has to be selected smaller than the size of the protein sample (i.e. a 25 kDa pore size was selected for a 65 kDa-BetP protein in the present study).

Subsequently, the system is completely closed with a compartment which has inlet and outlet tubes that enable perfusion of the buffer of interest towards the protein sample continuously. The amount and speed of the flowing buffer are adjusted *via* a pulse-free peristaltic pump which was set as 0.32 ml/min in this study. In this way, any *in situ* changes in the protein can be tracked diligently during IR scan by using only small amount of the sample. In this continuous flow-perfusion technique, protein adhesion is very crucial. Particularly, stable protein films which cover the ATR crystal allow reversible exchange of buffers to investigate structural alterations in protein samples induced by changes of ionic strength, pH and by addition of effector/inhibitor molecules, etc. Thereby, this technique is an elegant way to perform the experiments reversibly such as hydrogen/deuterium exchange, pH titration, salt (i.e. K^+ , Na^+) titration, activation/deactivation of a protein, which are introduced in this study (for details see Section 2.6).

2.6 DESIGN OF EXPERIMENTS

2.6.1 *In Situ* Activation of BetP with Increasing Potassium Concentration

The Na^+ -coupled betaine symporter BetP has a cation specific activation mechanism. It was already reported that an increase in the cytoplasmic K^+ (and Rb^+ or Cs^+) concentration is a trigger mechanism to activate BetP. However, BetP is not significantly activated in response to an increased in the cytoplasmic Na^+ concentration compared to activation by K^+ ions¹⁷. Therefore, in the present study, BetP was activated with the buffer which contains K^+ ions while the buffer which involves Na^+ ions was used as inactive buffer conditions in order to investigate molecular mechanisms of K^+ -dependent activation and of osmoregulation of BetP. In this work, 2D crystals of wild type or C-terminal truncated BetP reconstituted in *C. glutamicum* lipids have been used without further process. As a solvent, 10 mM sodium phosphate (NaP_i) buffer in H_2O and in deuterium oxide (99.9%) at pH/p²H 7.5 were utilized. Desired buffer conditions were adjusted by adding the salts of KCl and NaCl into the 10mM NaP_i buffer.

In this study, a FTIR spectrometer (Bruker, Germany) equipped with an ATR accessory and a MCT detector was used in order to record the IR spectra. Combination of a home-built microdialysis cell system (see Section 2.5.2)⁶⁶ with ATR-FTIR spectroscopy allows us to perfuse the BetP sample continuously with the buffer of interest. Thereby, titration experiments with increasing K^+ concentration and *in situ* activation/deactivation of BetP samples have been performed by using this microdialysis perfusion method. A 5 μ l sample of protein (\sim 2.5 mg/ml) was placed on top of the ATR diamond and was dried by monitoring the O-H stretching band (3000 - 4000 cm^{-1}) in the spectrum. This was repeated until reaching a desired absorbance in order to obtain a concentrated, semi-dried sample (\sim 25 mg/ml final concentration). Afterwards, the sample was closed *via* a dialysis membrane (25 kDa cut-off) and the BetP sample was equilibrated by continuous flow of inactive- H_2O buffer (10mM NaP_i , pH 7.5, 500 mM NaCl) with the help of the inlet and outlet tubing system. After stable IR absorbance spectra were obtained, the sample was subsequently titrated with increasing $[K^+]$ by keeping the total ionic strength constant in H_2O buffer. Since Na^+ ions do not activate the BetP protein, the final concentration of ionic strength was adjusted to totally 500 mM by replacing NaCl with KCl. The concentration of K^+ was increased from 0 mM (1st cycle of inactive state) to 500 mM (active state) with 50 mM K^+ intervals, and then switched again to 0 mM K^+ (2nd cycle of inactive state) so that a stepwise activation of BetP is provided. Totally 14 various buffers with different ionic strength of K^+ were perfused towards the protein sample at a constant speed (0.32 ml/min) provided by a non-pulsating peristaltic pump. Each buffer was perfused for 100 min to change the buffer of the sample on the ATR crystal. The spectra were recorded every 2,5 min at a resolution of 4 cm^{-1} . A total of 256 scans were averaged before Fourier transformation, taking the spectrum of the empty ATR cell as background. The temperature of the sample was adjusted to $+4^\circ C$ *via* a circulated water bath and was controlled routinely with a thermocouple. Additionally, the

buffer to be perfused through the protein sample was kept always in ice during perfusion in order to ensure the temperature of the sample on ATR diamond as +4°C.

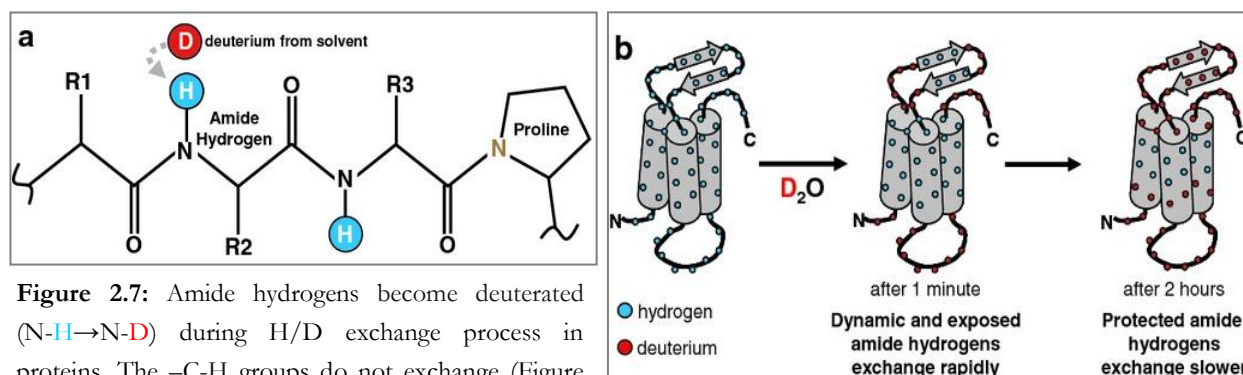
In the absence of protein, the blank lipid samples and the buffers were titrated as well with increasing $[K^+]$ to compare the spectral alterations. K^+ -titration of BetP in 2H_2O has been performed after the sample was equilibrated 24 hours in the activating 2H_2O buffer (in the presence of K^+) to ensure an equilibrated sample in D_2O so that the alterations in the spectra due to deuteration effects can be eliminated. Subsequent, the buffer was again switched from 0 mM K^+ to 10 → 500 mM K^+ to study activation/deactivation of BetP in 2H_2O .

Spectra processing and visualization were carried out using the spectrometer OPUS software 4.2 (Bruker, Germany). The last 5 spectra recorded for each buffer condition were averaged and used for the data processing. Since atmospheric water vapour absorption is inevitable in the long-term experiments and superimposed on the protein spectra⁶⁷⁻⁶⁹, the contribution of atmospheric water vapour was subtracted from the spectra of protein sample as described in Section 2.9. After the atmospheric water vapour had been removed, the corresponding buffer spectrum was subtracted from the each spectrum by taking the O-H stretching band centred around 3400 cm^{-1} as reference as described in Section 2.10.

2.6.2 Hydrogen/Deuterium Exchange

Hydrogen isotope exchange ($^1H/^2H$ or H/D) is an extensively applied experimental method to investigate the protein structure, accessibility, flexibility and dynamics^{44,45}. The rate and extent of exchange of protons (1H) with deuterons (2H or D) of the protein over time allows us to identify fast and slow exchanging parts of the protein. This quantitative result is directly related to protein flexibility and site accessibility. The amide protons found on the surface of the protein and involved in the solvent-exposed flexible loop/turn or in the irregular structures exchange rapidly (milliseconds to seconds) while amide protons buried in the core of the protein and contribute to some secondary

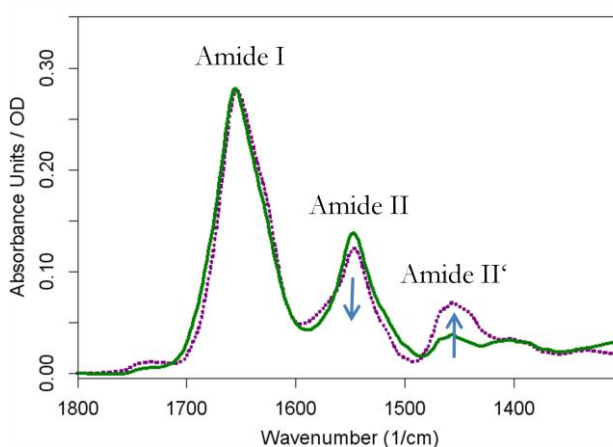
structures such as regular α -helices or β -sheets exchange slowly (minutes to days) (see the schematic representation in Fig. 2.7 adapted from Ref.⁷⁰). Additionally, amino acid clusters in the hydrophobic region of the folded protein either exchange very slowly or are not at all accessible to the solvent. Therefore, it is feasible to assign the type of secondary structure by determining the exchanging protons over the time. In this respect, H-bonded secondary structures are resistant to exchange, depending on their stability. For instance, dissolving the protein in D_2O (heavy water) enables to discriminate α -helix and unordered structure. In addition to the strength of the H-bonding and stability of the protein, the rate of the exchange depends strongly on the pH of the solvent as well as on temperature. The higher the pH or temperature, the faster the exchange; therefore, controlling of pH and temperature is very crucial during the H/D exchange experiments.



The exchangeable hydrogens of proteins include the peptide backbone N-H group and the side chain protons bound to the N, O and S atoms of polar groups. Substitution of protons with deuterons (H \rightarrow D) does not perturb the protein secondary structure but it shifts the IR band positions towards lower wavenumbers due to heavier mass of 2H . From this point of view, spectral intensity changes are observed particularly for the amide II band which originates mainly from peptide N-H bending vibrations coupled with C-N stretching modes. As represented in Fig. 2.8, the intensity at the amide II region ($\sim 1545\text{ cm}^{-1}$) decreases substantially concomitant with an increase in the intensity of amide

II' band ($\sim 1450\text{ cm}^{-1}$) upon exposure of the protein to $^2\text{H}_2\text{O}$. Thereby, the frequency of the amide II band is shifted by $\sim 100\text{ cm}^{-1}$ towards lower wavenumbers, disclosing the CN stretching vibrations from the peptide backbone and amino acid side chain modes (Arg, Tyr, Asp and Glu) in the range $1615\text{-}1490\text{ cm}^{-1}$. However, the frequency shift in the amide I band is relatively small ($5\text{-}10\text{ cm}^{-1}$) upon deuteration of the peptide backbone hydrogens in comparison to the amide II band. Besides amide vibrational modes, band positions of the amino acid side chain modes, which have exchangeable protons, also shift upon H/D exchange (see Section 2.8). Since side chain absorption overlaps with the amide I and II bands complicating the spectrum to analyze, hydrogen isotope exchange is routinely implemented to distinguish the vibrational modes and to assign them.

Figure 2.8: The IR spectra of BetP before (—) and after (...) the $^1\text{H}/^2\text{H}$ exchange.



In order to perform the H/D exchange experiment, the protein sample was first flushed with inactivating/activating H_2O buffer (10 mM NaP_i , pH 7.5, 500 mM NaCl/KCl) with the help of the ATR perfusion cell technique until stable spectra over time were obtained (usually runs overnight). In order to start $^1\text{H}/^2\text{H}$ exchange, the inactivating/activating $^2\text{H}_2\text{O}$ buffer (10 mM NaP_i , pD 7.5, 500 mM NaCl/KCl) was switched and flowed continuously for 24 hours. Temperature was set to $+4^\circ\text{C}$. Each IR spectrum was recorded at a resolution of 4 cm^{-1} . 64 scans were averaged every 40 seconds in the first 60 min of H/D exchange to catch the fast exchanging parts of BetP (It was counted that recording of one spectrum with 64 scans at 4 cm^{-1} resolution takes 32 sec). 128 scans were averaged

every 80 sec during the 2nd hour of the exchange and subsequent, 256 scans were used every 5 min until the 24 hour-H/D exchange process was completed. It is also noteworthy to mention that each buffer used for ¹H/²H exchange and for K⁺-titration experiments in ²H₂O was 15 ml, from which 13 ml is discarded to ensure that the buffer in the closed compartment and in the tubing systems is completely exchanged to other buffer. Later on, the remaining 2 ml buffer was used for the closed circulation towards the protein sample.

For the data processing, contribution of buffer was first subtracted from the IR spectra by observing the ¹H₂O (~3400 or ~1645 cm⁻¹), HOD (~1450 cm⁻¹) and ²H₂O (~1210 cm⁻¹) bands, as precisely described in Džafić et al., 2009⁶⁶. After buffer subtraction, in order to calculate the degree and kinetics of the H/D exchange, the lipid ν(C=O) band (1750-1730 cm⁻¹) which is not affected by the H/D exchange and the amide II band (1530-1560 cm⁻¹) were integrated from the absorbance spectra. The area of the amide II band was divided by the area of the lipid CO band (amide II/lipid CO). The ratio was taken as 0% for the sample spectrum in ¹H₂O buffer (0% exchanged) while the entire shifting of the amide II band refers to 100% exchanged with ²H₂O^{44,68,71}.

2.6.3 Reaction-Induced Infrared Difference Spectrum

Since an IR absorbance spectrum involves many overlapping bands arising from the parts of the protein (i.e. secondary structural elements or side chains), it is not possible to observe small spectral alterations in an absorbance spectrum such as shift of band position or changes of band intensity, all of them related to the reaction induced. Therefore, the absorbance difference between two spectra has to be recorded by means of the ATR-perfusion cell technique because the difference spectrum shows only the functional important parts of the protein upon any perturbation. Since IR difference spectroscopy is a very sensitive method to observe the spectral changes in the spectrum clearly, it is particularly used to investigate any conformational alterations of a protein induced by a reaction. This reaction can be triggered by changing the environment of the protein such as binding of

effector/inhibitor molecules or substrates into the solvent, a change in pH value or a change in the type/amount of salts in the solvent, etc.

As shown in Fig. 2.9, the reaction-induced IR-difference spectrum represents any tiny changes in the protein backbone or even alterations in the individual amino acids side chains upon any perturbation. Ideally, the environment of the protein must be changed within the measurement cell to obtain a high sensitivity so that inactive-to-active switching of BetP can be reversibly induced and *in situ* monitored while the protein is periodically scanned. In this study, while studying with $^2\text{H}_2\text{O}$ buffer, first, $^1\text{H}/^2\text{H}$ exchange of the sample was performed for 24 hours to eliminate the effects of isotopic exchange on the protein. Afterwards, the IR difference spectrum was recorded as active-*minus*-inactive state or inactive-*minus*-active state of BetP as briefly indicated in Table 2.4.

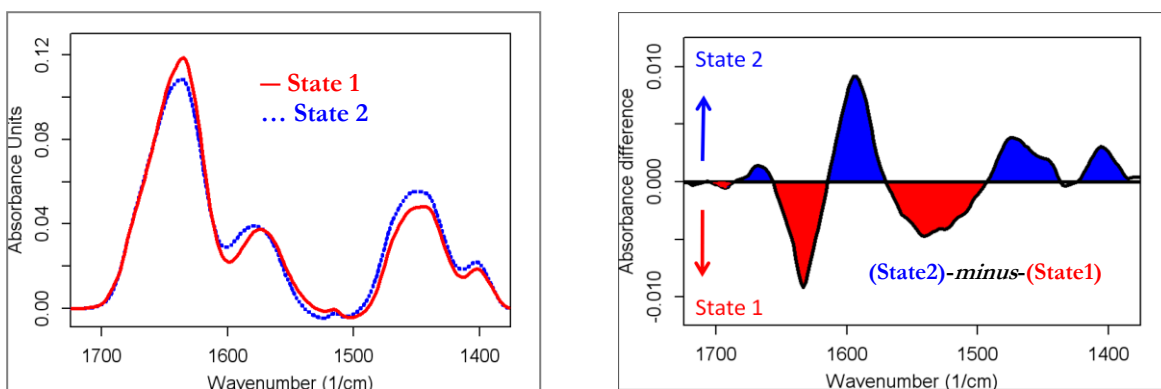


Figure 2.9: (Left) IR absorbance and (Right) difference spectrum shows increased and decreased parts of the protein absorbance due to a perturbation such as due to an enzymatic digestion. (Data was adapted from Güler, G., M.Sc. Thesis, 2010).

In the present study, BetP in 10 mM NaP_i, pH/p²H 7.5, 500 mM KCl (active state of the protein) was recorded as a sample spectrum and the difference spectra were recorded taking the reference as protein in 10 mM NaP_i, pH/p²H 7.5, 500 mM NaCl (inactive state) at +4 °C so that the resultant absorbance difference corresponds to the difference spectrum of active-*minus*-inactive state. The IR-difference spectrum has many signals in the mOD absorbance range (10^{-3} - to 10^{-4} -fold less

intensity than the absorbance spectrum), whose positive difference signals represent the final state (State 2 or active state) of the sample while the negative ones of the initial state (State 1 or inactive state), as being produced and reduced part of the protein, respectively. Alternatively, after the corresponding buffer was subtracted from each sample spectrum, the difference spectrum can also be mathematically calculated. If necessary, atmospheric water vapor subtraction must be applied before calculation of the difference spectrum.

Table 2.4: *In situ* recording of a sample spectrum and its corresponding reference spectrum by using ATR-FTIR spectroscopy combined with a continuous-flow perfusion technique.

Sample Spectrum	Reference Spectrum	Resultant Spectrum
BetP in activating buffer	air or activating buffer	active BetP (State 2)
BetP in inactivating buffer	air or inactivating buffer	inactive BetP (State 1)
BetP in activating buffer	BetP in inactivating buffer	active- <i>minus</i> -inactive
BetP in inactivating buffer	BetP in activating buffer	inactive- <i>minus</i> -active

2.6.4 pH-Titration Experiments

Amino acids are significant clues for determining the structural and functional properties of the proteins since they can vary in their acid-base characteristics (protonated or deprotonated) depending on the pH value of the solvent and the pK_a value of the side chain group. As definition, the pH of a solution is a measure of its concentration of H^+ while the pK_a of an acid is the pH at which it is half dissociated. Therefore, the higher the pH value ($pH \gg pK_a$), the more likely a molecule will lose a proton, being deprotonated, depending on the temperature, ionic strength, microenvironment of the ionizable group and structure of the amino acid¹⁻³. Starting from this fact, pH titration of a protein can be initiated by perfusing the buffers which involve various pH values. Thereby, pH-induced structural changes and the protonated/deprotonated forms of amino acid groups, if they exist in a protein, can be detected in an IR spectrum.

In this study, pH titration of BetP was performed *in situ* to determine the pH-dependent behaviour of BetP in the active and inactive states, to access the protonated/deprotonated amino acid groups (i.e. Asp and Glu) at a certain pH range and to find out the attainable functional amino acid groups determining their locations within the protein (hydrophobic/hydrophilic regions). The pH value of BetP was varied from 8.5 to 5.0 at a constant salt concentration by using ATR-FTIR spectroscopy combined with a continuous flow-perfusion technique. Each buffer was perfused towards the sample for 2 hours. IR difference spectra were obtained from successively recorded spectra (i.e protein in pH 7.5-*minus*-protein in pH 5.0). The temperature was set to +4 °C. Buffers to be perfused through the sample were prepared 1 day before the experiment and the exact pH value of the buffer was controlled with a pH-meter before and after the experiment. Additionally, if necessary, D₂O buffer (pD=pH+0.4) at a certain pH value was used instead of H₂O in order to verify the band assignments and to eliminate the water signals in the amide range.

2.6.5 Temperature Excursion Experiments

With the help of the infrared spectroscopic techniques, the temperature-induced conformational changes, thermal stability and folding/unfolding/misfolding of proteins can be analyzed^{45,59,72}. In this study, the temperature-dependent structural stability of BetP both in proteoliposomes and in 2D crystals has been investigated in order to compare the stability of the secondary structural elements between the active and inactive states of BetP.

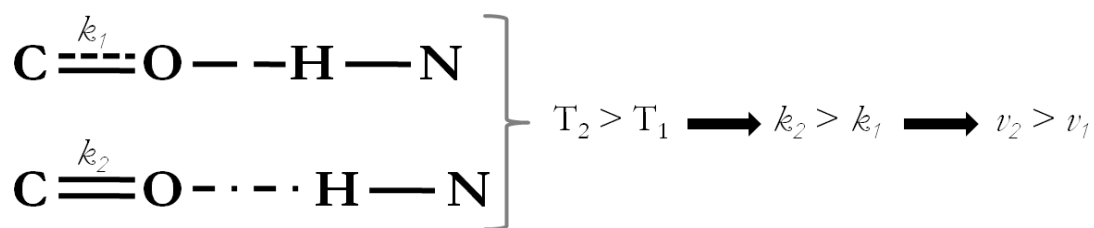


Figure 2.10: Temperature dependent behavior of the molecules involved in the amide I band. T: temperature, k : force constant between the two atoms; v : frequency ($v \sim k/\mu$, where μ is reduced mass of the atoms involved in the stretch).

IR signatures of functional groups that are involved in H-bonding exhibit characteristic spectral shifts with temperature excursion experiments. Since the amide I band from the polypeptide backbone is composed of predominantly peptide C=O bonds and its absorbance is fine-tuned by its H-bonding interaction, the temperature dependent behavior of the amide I band is an indicator for the protein stability. As it is indicated in Fig. 2.10, the hydrogen atom (H) behaves as an exerting outward force on the oxygen atom (O), weakening the quasi-harmonic intramolecular CO force constant (k_c) as well as increasing the length of the C=O bond. However, if the temperature of the protein increases from T_1 to T_2 , the IR stretching frequencies (C=O) shift to higher wavenumbers (ν) and even bending frequencies of coupled groups move towards lower band positions as well while the amide group H-bonds (O... H) to other amide residues weaken⁷³.

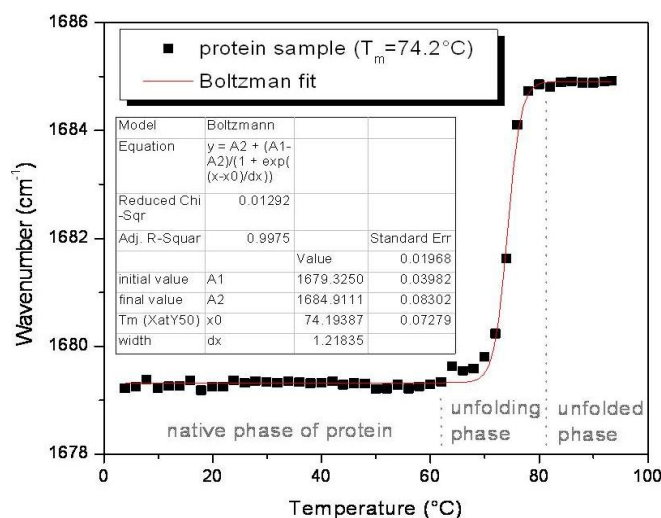
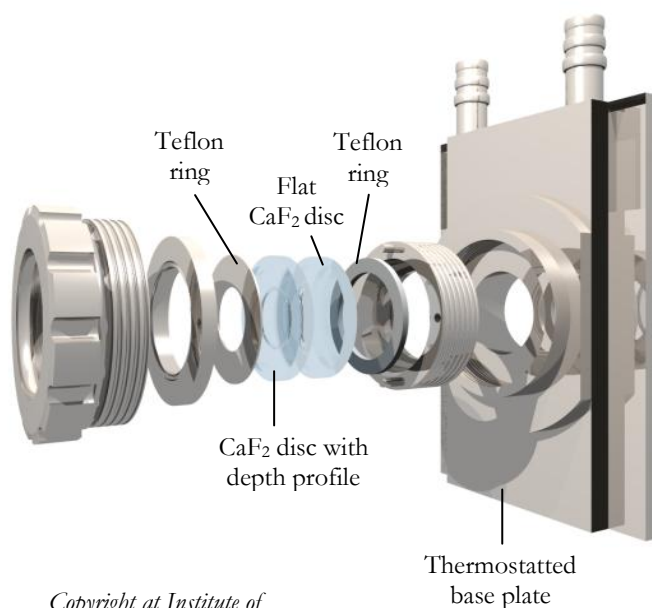


Figure 2.11: The wavenumber shifting profile of the amide I component with respect to rising temperature (Origin 8.5). The transition temperature (T_m) between the folded and unfolded states was calculated from a Boltzmann function, $y = (A_1 - A_2) / (1 + e^{(x-x_0)/dx}) + A_2$, where A_1 is the initial value (left horizontal asymptote), A_2 is the final value (right horizontal asymptote), x_0 is the center (point of inflection) and dx is the width (the change in X corresponding to the most significant change in Y values).

Consequently, rising of the temperature within the protein sample induces a change in the strength of the H-bonds, and thereby, structural alterations occur in the secondary structural elements. These are observed in an infrared spectrum as a change in the amplitude or a shifting of the band positions of the individual amide I components. Therefore, the peak positions from the second derivative spectrum or from the maxima of the absorbance spectrum can be followed to plot the thermal

stability profile of secondary structures (α -helix, β -sheet and turn/loop) and even of lipids (CH_2 , CH_3 , CO , PO_2) as a function of temperature. Fig. 2.11 was plotted as an example to show the shift in peak positions with respect to increasing temperature that demonstrates three different phases (native, unfolding and unfolded) of a protein as the temperature increased.

In the present study, the measurements were carried out by using a Vector-22 FTIR Spectrometer equipped with a DGTS detector (Bruker, Germany). In order to study temperature-induced conformational changes in the protein, temperature-controlled calcium-fluoride (CaF_2) cells are needed which are ideal for higher temperature applications and are transparent in the mid-IR range. The IR-spectra were recorded in a transmission mode by using a demountable cell with CaF_2 windows developed at our institute (Fig. 2.12)⁴⁵. These consist of a flat and a trough window with an optical path length of $\sim 8 \mu\text{m}$ that allows IR radiation to transmit through the sample, as shown in Fig. 2.12. A small amount of sample, less than $2 \mu\text{l}$, is enough to probe the sample solution by means of these circular CaF_2 windows (for properties of the windows see Table 2.3 in Section 2.5.1).



*Copyright at Institute of
Biophysics, Frankfurt*

Figure 2.12: The deepened and flat calcium-fluoride windows used for the FTIR transmission spectroscopy. The deepened window has a cavity that separates the center of the window from the outer ring so that contamination of the sample with oil or PTFE paste can be avoided.

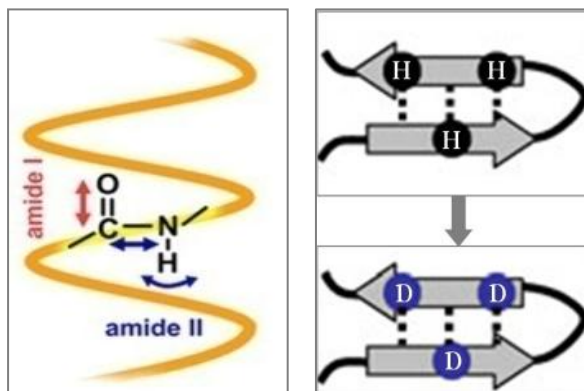
The buffer of the protein samples was exchanged to 10 mM NaP_i buffer (pH or pD7.5), which includes various amounts of Na⁺ (inactivation condition) and K⁺ (activation condition) ions, by ultrafiltration (6000 rpm for ~30 min at +4°C) in an eppendorf. The samples were subsequently equilibrated for 3 days in ²H₂O buffer at +4°C. Afterwards, 1.7 µl of BetP samples in 2D crystals and in proteoliposomes were loaded in the center of a demountable CaF₂ microcell (~8 µm pathlength). The cuvette was diligently sealed with PTFE paste (Carl Roth, Karlsruhe, Germany) in order to avoid drying of the sample upon heating, and subsequently mounted into a thermostated sample holder. This sample holder was placed in a motor driven slide which was developed at our institute. The reference spectrum was recorded as air spectrum just before recording of each sample spectrum so that the sample chamber is continuously purged with a dry air, preventing contributions of water vapor in the spectra. After the sample was equilibrated at +4°C, the temperature was increased stepwise from +4°C to +96°C (heating) and then was cooled down to +4°C (cooling), in 2°C intervals using a cell holder thermostatically circulating water. The temperature was controlled by the spectroscopy software. 128 interferometer scans were averaged at 4 cm⁻¹ spectral resolution for both sample and reference spectra. The buffer solutions and blank lipid samples in the absence of protein were measured under the same conditions.

The buffer absorption was subtracted from the protein and blank lipid absorption, as described in Section 2.10. The peak positions of each amide I component and of lipid signals obtained from the second derivative spectra was plotted as a function of temperature in order to characterize the structural differences between the inactive and active states of BetP as well as to yield information about the lipid-protein interactions of BetP.

2.7 SECONDARY STRUCTURE ANALYSIS FROM THE INFRARED SPECTRUM

As briefly mentioned in Section 1.2.3, the amide I band (1700-1600 cm^{-1}), which is the most intense peptide absorption band in the IR spectrum, consists mainly of the peptide C=O stretching modes (80%), and therefore, is directly associated with the backbone conformation (Fig. 2.13 Left from Ref.⁷⁴). The full-width at half-maximum and frequency of the amide I band allow digging out the intermolecular interactions of the peptide carbonyl groups. Hence, among the nine characteristic amide bands (amide A, amide B and amides I-VII), the amide I band, which is sensitive to the strength of a H-bond, dipole-dipole interaction and to geometry of the peptide backbone, is frequently used for determination of protein secondary structural elements as well as for estimation of their percentages by analyzing the IR spectra^{45,46,75,76}.

Figure 2.13: (Left) Amide I and II vibrational modes of the polypeptide backbone (Figure from Jiang, X. et al., PNAS, 2008)⁷³. **(Right)** Schematic representation of H→D substitution in β -sheets (C=O-N-D) (Figure reproduced from Marcsisin et al., 2010)⁶⁹.



It is clear in Fig 2.14 that the shape of the amide I band is typical for the secondary protein structures. Globular proteins which are composed mainly of α -helices (i.e. BetP) have a maximum position at around 1654 cm^{-1} in the amide I region while β -stranded proteins (i.e β -lactoglobulin) have a strong absorption position near 1633 cm^{-1} and a weak band around 1685 cm^{-1} . In contrast to the folded protein which has a sharp amide I band, the unfolded protein possess a broad amide I band centered near 1650 cm^{-1} that stem from the unordered structure while an aggregated protein

represents two characteristics bands at around 1620 and 1685 cm^{-1} attributed to intermolecular β -sheet structures.

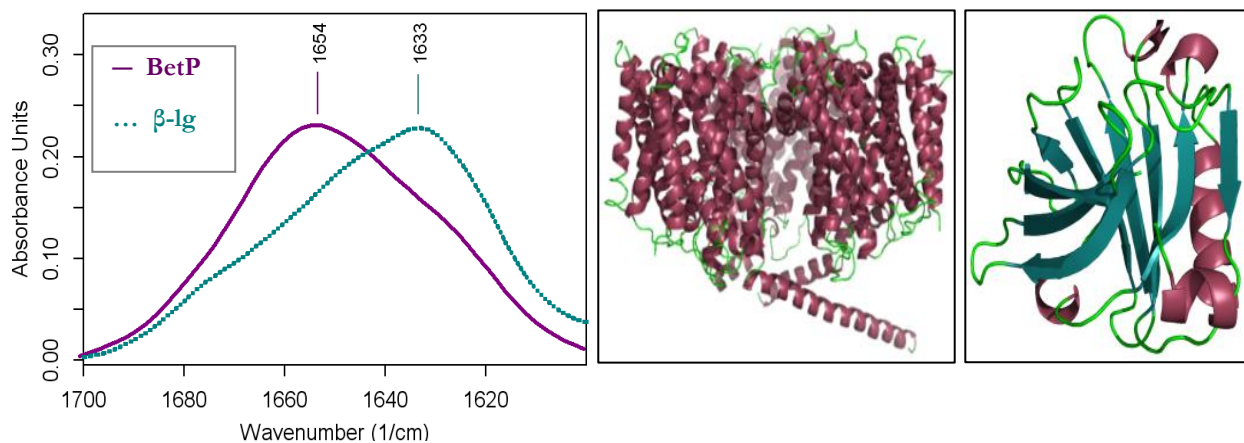


Figure 2.14: A typical amide I profile (**Left**) for α -helical BetP (**middle**) and for β -stranded β -lactoglobulin (β -lg) (**Right**). The 3D-structures were rendered with PyMOL. α -helices are shown in maroon color, β -sheet in bluish green color and loops in green.

The amide I band harbors a series of overlapping components such as from α -helix, β -sheet, turn, loop and irregular structures. The characteristic band positions for individual secondary structures are given in Table 2.5. However, their exact positions depend on the environmental variations. One of them is the strength of H-bonding which directly or indirectly alters the electron density around the C=O bond of a peptide group (see Fig 2.10). Subsequently, an alteration in the force constant of C=O vibrations induces a change in the vibrational frequency of the C=O bond. For instance, an α -helix consists of long and weak H-bonds whereas a β -sheet has relatively short and strong H-bonds in its structure, and hence, the C=O groups of β -sheets vibrate at lower frequencies in comparison to the C=O groups of α -helices. Additionally, the frequency of the secondary structures depends also on their length, namely the number of residues involved in the structure. In this regard, short α -helices have C=O peaks at higher wavenumbers around 1660 cm^{-1} in H_2O buffer while the peak position of α -helix shifts down near 1654 cm^{-1} with increasing helical length.

Table 2.5: Assignments and frequencies of protein secondary structures in the amide I band region when H₂O and D₂O are used as solvents^{45,46,76}.

Secondary structure	Band position in H ₂ O (cm ⁻¹)		Band position in D ₂ O (cm ⁻¹)	
	Range	Average	Range	Average
α -helix	1657-1648	1654	1660-1642	1652
β -sheet (strong)	1641-1623	1633	1638-1615	1630
β -sheet (weak)	1695-1674	1684	1694-1672	1679
turn/loop	1686-1662	1672	1691-1653	1671
unordered	1657-1642	1654	1654-1639	1645

The H→D substitution affects the band positions of protein secondary structures as well. The peptide backbone (-C=O...H-N) becomes (-C=O...²H-N) upon deuteration as schematically represented in Fig. 2.13 Right, and the frequency of these components shift towards lower wavenumber by less than 20 cm⁻¹. For instance, short α -helices shift down from 1660 cm⁻¹ to near 1640 cm⁻¹ upon deuteration. Similarly, since α -helix and unordered structures overlap at around 1654 cm⁻¹ in the amide I region, it is plausible to discriminate both structures if D₂O is used as a solvent. Particularly, unordered structures shift ~10 cm⁻¹ towards lower positions (1645 cm⁻¹) in the first couple of minutes of the H/D exchange while regular α -helices downshift only a few wavenumbers (1652 cm⁻¹) and need long time-exposure to D₂O because of the fact that unordered structures are located in the hydrophilic region of the protein and their protons are more attainable in comparison to helical structures. Therefore, both H₂O and D₂O buffers have to be used as a solvent so as to authenticate the band assignments of the secondary structural elements.

Amide I band is the broad absorption envelope of overlapping protein secondary structures. Therefore, further spectral processing is definitely a prerequisite to resolve these overlapping features in the complex protein spectrum. After the contribution of water is subtracted from the IR spectra, band narrowing techniques such as Fourier self-deconvolution (FSD) and differentiation are

commonly applied to resolve the peak positions almost completely in the spectrum⁷⁷⁻⁷⁹. These mathematical operations yield narrower spectral bands without raising the instrumental resolution. After the peak positions in the amide I band have been determined by performing either FSD or derivatives from the raw spectrum, curve fitting programs are implemented for the analysis of protein secondary structures, as explicitly explained below^{45,77-79}.

The infrared derivative spectrum, which is the most ordinarily used mathematical procedure to resolve the overlapping components and to yield line shapes with narrower width, is calculated from the raw absorbance spectrum by using OPUS software. The 2nd derivative gives rise to a negative peak for each band or shoulder in the original spectrum (Fig. 2.15 Right). The spectrum is multiplied by $-(2\pi x)^2$ for the 2nd derivative and by $(2\pi x)^4$ for the 4th derivative (x is the variable associated to the frequency)^{71,75}. Both derivatives can be introduced to detect minor components in the spectrum. The 4th derivative can be occasionally used as well to reveal strongly overlapping features because it yields better resolved bands than the 2nd derivative. The derivative spectrum has to be smoothed simultaneously to minimize noise or artifacts. Minima from the 2nd derivative spectrum or maxima from the 4th derivative spectrum refer to positions of the secondary structure components.

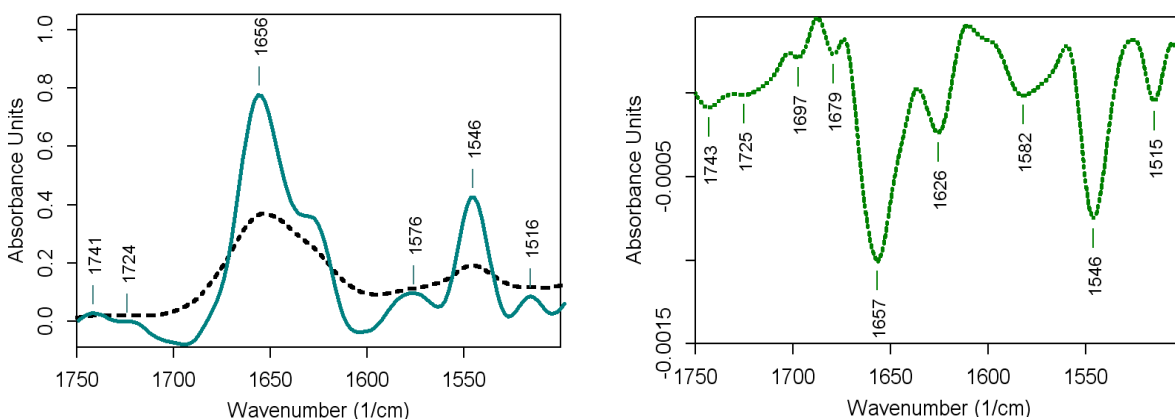
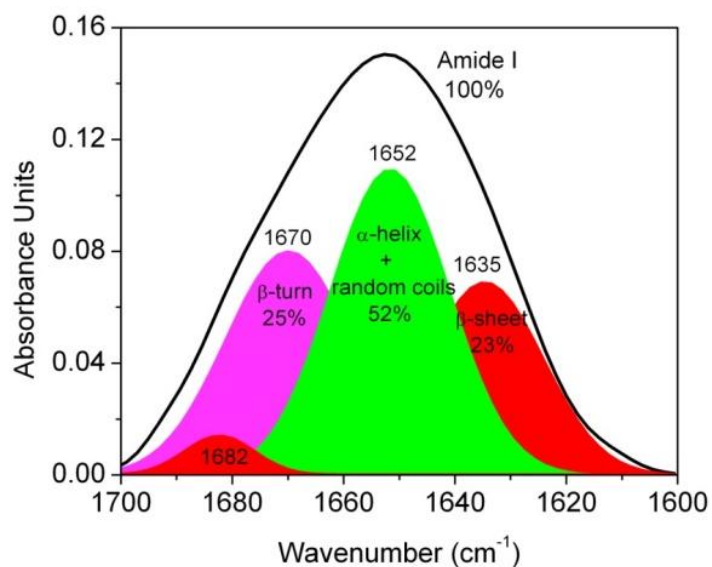


Figure 2.15: (Left) The raw (---) and deconvoluted (—) spectra for amide I and II. To deconvolve the overlapping bands in the raw spectrum, Fourier self-deconvolution was used selecting a Lorentzian line-shape with 28 cm^{-1} bandwidth by using a built-in macro in OPUS 4.2. (Right) The infrared 2nd derivative spectrum (...) was calculated from the raw spectrum (---) using the Savitzky-Golay algorithm involved in the OPUS software.

Fourier self-deconvolution (FSD) is another mathematical technique allows to identify peak frequencies of the overlapping components which contribute to the composite amide I band as shown in Fig. 2.15 Left. After deconvolution, the spectral bands become narrower but their relative ratios do not change. However, the correct choice of parameters is essential to distinguish the band components from the artifacts in the protein spectrum. Line shape (Gaussian or Lorentzian function), band width and resolution enhancement factor are three independent parameters to perform FSD with the OPUS software. Finally, the positions and numbers of the resolved individual components from a broad envelope amide I band, which are plainly revealed in the deconvoluted or derivative spectrum, are introduced for the estimation of secondary structures by performing a curve fitting analysis.

Curve fitting is used here to reconstruct a measured spectrum so as to predict the content of protein secondary structures, as demonstrated in Fig. 2.16. In order to set out the curve fitting, first of all, the amide I region is baseline corrected between 1600 and 1700 cm^{-1} . After the amide I band is decomposed into its components by means of band narrowing techniques, the number and peak position of bands as well as the band shape are introduced as input parameters in the curve fitting program involved in the OPUS software.

Figure 2.16: Model spectra for secondary structural elements were obtained from the curve fitting process by using the Levenberg-Marquardt method with OPUS 4.2. This method allows the curve or peak fitting based on the algorithm of non-linear peak fitting (Marquardt, D.W., 1963)⁸⁰.



The band shape of the spectrum can be selected as either Gaussian or Lorentzian function, or a mixture of both, which are characterized by three parameters: location (frequency), height (intensity) and line width. A *Lorentz function* is defined as,

$$L(x; \gamma) = \frac{1}{\pi\gamma[1+(\frac{x-x_0}{\gamma})^2]} \quad \text{Eq. 2.1}$$

where, x_0 refers to the location of the peak and γ is the half-width at half-maximum (HWHM) while a *Gaussian function* is depicted as,

$$G(x; \sigma) = \frac{1}{\sigma\sqrt{2\pi}} e^{-\frac{(x-\mu)^2}{2\sigma^2}} \quad \text{Eq. 2.2}$$

where, μ is the location of the peak and σ corresponds to the standard deviation. Subsequently, herein the band width and intensity are iteratively varied until the difference between the fitted and original spectra is minimal so that their envelopes coincide with lowest possible error. The second derivative spectra of fitted and measured amide I profiles can be also compared in order to vindicate the accuracy of the curve fitting analysis. Both derivatives should be exactly overlapping for a successful analysis. At last, the fractional areas under the curve of the fitted components are used to determine the percentages of each component bands in the amide I region. Afterwards, the proportion of each secondary structural element, which is assigned with respect to Table 2.5, can be estimated by dividing the area of each by the total area of amide I, as represented in the model spectrum in Fig. 2.16, obtained from the curve fitting process by using the Levenberg-Marquardt method⁸¹.

2.8 SPECTRAL CONTRIBUTIONS OF AMINO ACID SIDE CHAINS

Since proteins are made of variable side chains as indicated in Fig. 1.1, amino acid side chains carry a lot of valuable information regarding the structure and function of the proteins, and therefore, they are crucial to pursue the molecular reaction mechanisms. The environmental and structural alterations of side chains, i.e. protonation states, electrostatic interactions or H-bonding properties, give rise to distinct spectral alterations. Therefore, it is feasible to detect a subtle change around an individual side chain with infrared spectroscopy by using either band narrowing techniques or difference spectroscopy. The pK_a of acidic residues (Asp, Glu) in proteins might also be affected from the environmental conditions. Particularly, deuteration discriminates the side chain absorption from that of the protein backbone or from the other side chains because most side chains exhibit large shifts upon H/D exchange. For instance, Arg residues (1635 & 1673 cm^{-1}) downshift by 50 - 70 cm^{-1} and Asn/Gln residues observed entirely in the amide I region downshift by 30 - 400 cm^{-1} while ionized Asp/Glu residues (1550 - 1580 cm^{-1}) shift 2 - 9 cm^{-1} towards higher wavenumbers with rising intensity upon deuteration. On the other hand, secondary structures shift up to solely 10 cm^{-1} within the amide I band upon deuteration^{41,45,68,82}.

Some side chains have significant absorbance in the range 1750 - 1480 cm^{-1} , as given in Table 2.6. Absorption of side chains in an IR spectrum overlaps with other side chain absorptions or with the polypeptide backbone, particularly with the amide I and II bands of proteins. Therefore, the contribution of the amino acid side chains on the protein amide I band influences the estimation of the proportion of the secondary structures up to 10% of the total amide I area^{41,68,83}. Hence, several methods can be used to subtract the contribution of side chains in the spectrum, which take an internal reference as either the Tyr signal at 1515 cm^{-1} or a shoulder at 1583 cm^{-1} arising from both ionized Asp/Glu signals and Arg residues^{44,68,84-88}. In this study, the side chain contributions in the IR spectrum was required to be subtracted prior to curve fitting analysis according to the method

described previously^{44,68}, using the software Kinetics (provided by Prof. Dr. Erik Goormaghtigh from Université Libre de Bruxelles, Belgium) running under MATLAB.

Table 2.6: Band positions for some amino acid side chain modes in the range 1750-1450 cm^{-1} in H_2O and D_2O (Fabian and Măntele, 2002)⁴⁵. ν_s and ν_{as} are the symmetric and antisymmetric stretching frequencies, respectively while δ_s and δ_{as} are the symmetric and antisymmetric bending frequencies, respectively.

Side Chain/Assignment	Band Position in $^1\text{H}_2\text{O}$ (cm^{-1})	Band Position in $^2\text{H}_2\text{O}$ (cm^{-1})
Asn (C=O) (ν)	1678	1646
Asn (NH ₂) (δ)	1622	-
Asp (COOH/COOD) (ν)	1716	1710
Asp (COO ⁻) (ν_{as})	1574	1585
Arg (CN ₃ H ₅ ⁺) (ν_{as})	1673	1605
Arg (CN ₃ H ₅ ⁺) (ν_s)	1633	1586
Glu (COOH/COOD) (ν)	1712	1706
Glu (COO ⁻) (ν_{as})	1560	1570
Gln (C=O) (ν)	1670	1635
Gln (NH ₂) (δ)	1610	-
Lys (NH ₃) (δ_{as})	1629	-
Lys (NH ₃) (δ_s)	1526	-
Phe (C-C Ring)	1494	1498
Tyr (C-C Ring)	1614	1614
Tyr (C-C Ring)	1518	1515

2.9 SPECTRAL CONTRIBUTIONS OF ATMOSPHERIC WATER VAPOR

The atmosphere involves CO_2 and H_2O in its content, which have rigorous signatures in the mid infrared spectral region (Fig. 2.17 Left). The antisymmetric stretching vibration of CO_2 gives rise to a strong absorption at around 2350 cm^{-1} , which fortunately remains outside the regions for the study of proteins. On the other hand, the pronounced IR signals of the atmospheric water vapor are involved in the entire IR spectral region, importantly, in the amide I and II regions of proteins. Water vapor signals are observed at 1733, 1717, 1684, 1653, 1647, 1636, 1559, 1541, 1521 and 1507 cm^{-1} in the region of $1800\text{-}1500 \text{ cm}^{-1}$ which is the most important part of the IR spectrum for

probing of the membrane proteins. These IR signatures can be confused with individual components of proteins. One can discriminate the contribution of atmospheric water vapor from the protein signals by comparing the intrinsic bandwidth. Water vapor has sharp signals whereas a protein has quite broad bands. Interestingly, the selected nominal resolution influences the bandwidth of the water vapor. The higher the nominal resolution (i.e. 2 cm^{-1}), the narrower the water vapor is recorded in the spectra^{44,67,68}. In order to compete with this problem and to record a high quality spectrum as given for BetP in Fig. 2.17 Right, the spectrophotometer has to be purged extensively with dry air or nitrogen gas.

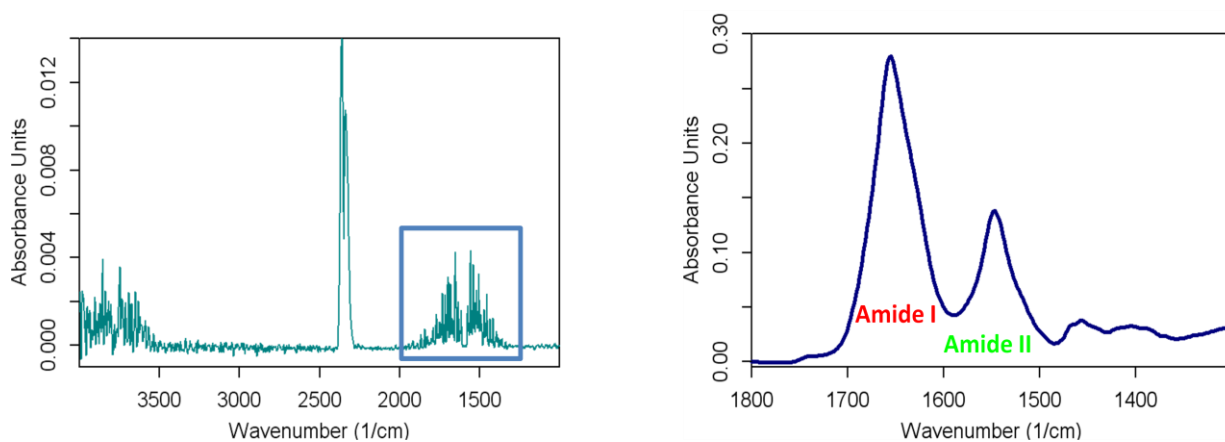


Figure 2.17: (Right) The IR spectrum of α -helical BetP was obtained during continuously purging of the spectrometer. **(Left)** The IR spectrum of atmospheric water vapor was obtained when the lid of the sample chamber of the interferometer was left open during recording of the spectrum.

It is inevitable that, during long-term experiments with the ATR FT-IR technique, water vapor bands are obtained. Subtraction of water in the amide I band is not enough to remove all artifacts. In such cases, removal of the atmospheric water contribution is required prior to elaborate interpretation of the individual components of the amide bands or of side chains. Particularly subtraction is essential for interpretation of a difference spectrum or for analyzing of the secondary structure content because water vapor signals can be confused with the weak protein signals in the spectrum and might result in misinterpretation. There are several methods available to subtract the water vapor

contribution adequately. One of them is that the second derivative of the water vapor spectrum can be subtracted from the second derivative of raw sample spectrum, and thereby, it possible to calculate the subtraction coefficient^{89,90}. Another method uses the intrinsic bandwidth difference between the sample and water vapor bands^{44,67,68}. In this study, if necessary, atmospheric water contribution was subtracted by using the Kinetics software⁶⁹ for Matlab developed by Erik Goormaghtigh from the Université Libre de Bruxelles, Belgium. This software program determines the subtraction coefficient using the integrated area between 1565 and 1551 cm^{-1} on the sample spectrum and on the reference atmospheric water spectrum.

2.10 SPECTRAL CONTRIBUTIONS OF $\text{H}_2\text{O}/\text{D}_2\text{O}$ BUFFERS AND BUFFER SUBTRACTION

In the present study, the FTIR experiments of the liquid sample of BetP have been executed both in $^1\text{H}_2\text{O}$ and $^2\text{H}_2\text{O}$ buffers which include various salts and pH conditions. As explicitly indicated in Fig. 2.18 Left, $^1\text{H}_2\text{O}$, $^2\text{H}_2\text{O}$ and mixture of them have several strong absorption bands in the mid-IR spectrum which coincidence with protein backbone and amino acid side chain bands. Water has its strongest band around 3400 cm^{-1} arising from O-H stretching vibrations. The combination of the O-H bending mode with the vibrations of associated water molecules gives rise to a shoulder at around 2200 cm^{-1} . Since water has a pronounced absorption at around 1645 cm^{-1} in the amide I band due to the O-H bending vibration, the infrared study of proteins in $^1\text{H}_2\text{O}$ buffer is more sophisticated than that of in $^2\text{H}_2\text{O}$ solution. Therefore, it is advantage to use $^2\text{H}_2\text{O}$ as a solvent in order to eliminate the water contributions to the amide I region which is the most profitable band for the secondary structure estimation. As mentioned in detail in Section 2.6.2, water bands are downshifted upon deuteration so that particularly the protein amide I band gets rid of the water contribution, allowing observation of even weak IR signals of proteins and of side chains in the range 1800-1400 cm^{-1} .

The large contribution of water to the spectrum can not be neglected. Hence, absorption of water is subtracted from the sample spectrum, taking either the 1900–2400 cm^{-1} region or the O-H stretching region at $\sim 3400 \text{ cm}^{-1}$ as reference when water is used as a solvent. In principle, the region 1900–2400 cm^{-1} has to be a flat baseline in the case of a proper subtraction (Fig. 2.18 Right). If the sample is in the D_2O environment, the O-D stretching ($\sim 2500 \text{ cm}^{-1}$) or bending ($\sim 1200 \text{ cm}^{-1}$) regions should be taken as reference for the subtraction^{44,45,68}. In order to subtract the $^1\text{H}_2\text{O}$ or $^2\text{H}_2\text{O}$ contribution adequately, the spectrum of the buffer have to be recorded under identical conditions as those of the sample spectrum, such as nominal resolution, number of scans, temperature, pH/pD and ionic strength. A proper H_2O buffer correction with respect to the 1900–2400 cm^{-1} region was demonstrated in Fig. 2.18 Right. In the present study, the buffer absorption was subtracted from the protein and blank lipid absorption, taking the region with respect to the kind of solvent as reference, as described above.

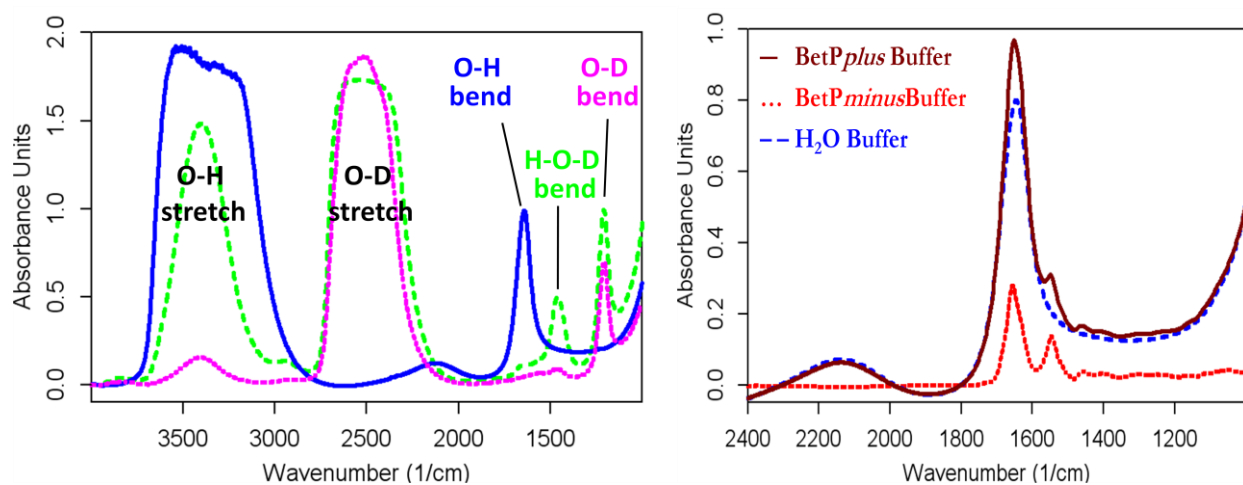


Figure 2.18: (Left) The IR spectra of $^1\text{H}_2\text{O}$ (blue), $^2\text{H}_2\text{O}$ (pink) and mixture of $^1\text{H}_2\text{O}$ and $^2\text{H}_2\text{O}$ (green). (Right) The FTIR absorbance spectra of BetP before and after H_2O -buffer subtraction.

2.11 CALCULATION OF LIPID-TO-PROTEIN RATIO FROM THE INFRARED SPECTRUM

IR spectroscopy is also used to calculate the lipid-to-protein ratio (LPR) and to quantify the content of the protein as well as the amount of the lipids unambiguously by means of the amide I band (1600-1700 cm^{-1}) and the ester C=O band (near 1740 cm^{-1}), respectively^{44,68,88,91}.

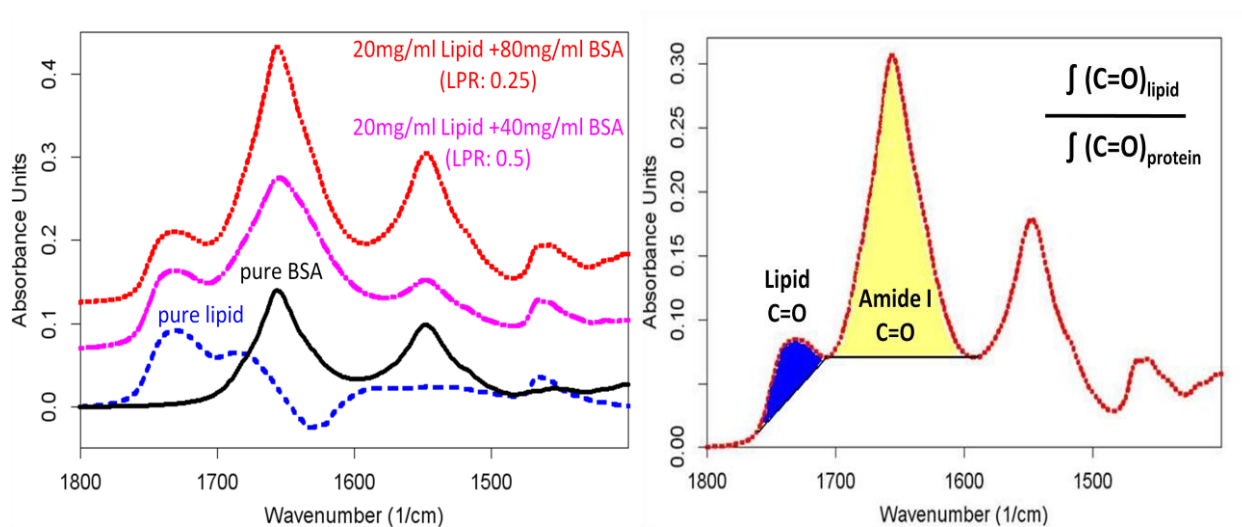


Figure 2.19: (Left) The IR spectra for BSA (—), lipid (---) and for the lipid-BSA mixture with a LPR of 0.25 (...) and 0.5 (- · -). For instance, a 80 mg/ml of BSA was mixed with a 20 mg/ml of lipid to obtain LPR as 0.25 (w/w). **(Right)** The shaded areas in the spectrum refer to the integrated intensities of the $\nu(\text{C=O})$ modes for lipid and protein amide I used to ascertain the LPR.

The amide I band of the IR spectrum provides direct information regarding the number of the peptide bonds in the protein, since it involves mainly the peptide C=O stretching modes. Similarly, the lipid C=O modes are directly associated with the number of lipid molecules. This lipid signal is absent in the pure protein spectrum and does not overlap with the protein components in the amide I region (Fig. 2.19 Left). Therefore, the association between the number of the C=O bonds of both lipid and protein can be further analyzed. The ratio of the integrated intensities of the lipid C=O band around 1740 cm^{-1} to the amide I band around 1650 cm^{-1} gives information to the ratio of

lipid-to-protein. If the LPR of the lipid-protein mixture is known, the protein content can be straightforwardly calculated from the spectrum of the mixture with the help of number of C=O bonds of peptide and lipid.

The LPR is crucial for the study of lipid-protein mixtures, particularly for the membrane-associating proteins because the concentration of an unknown protein can be accurately calculated from LPR or vice versa. An example of LPR (weight/weight) determination from the known ratios of the lipid-protein mixture is represented in Fig. 2.19. A constant concentration (20 mg/ml) of *E. coli* lipids was mixed with various concentrations (80 or 40 mg/ml) of bovine serum albumin (BSA) by dissolving in H₂O buffer. Subsequently, the IR spectra of pure BSA, pure lipid and the lipid-BSA mixture were measured with FTIR spectroscopy. First, the buffer absorption was subtracted from each spectrum. As represented in Fig. 2.19 Right, after the spectra were base line corrected for the region of 1770-1708 cm⁻¹ and 1708-1600 cm⁻¹, the intensities of the lipid C=O region (near 1740 cm⁻¹) and of the protein associated amide I region (near 1650 cm⁻¹) were integrated, assuming that all the C=O modes absorb equally. As shown in Table 2.7, the ratio of integrated areas of the lipid absorption to the protein absorption was divided by the ratio of the respective number of carbonyl groups per molecule in order to estimate LPR⁸⁸. The number of carbonyl groups was taken 1 for each protein residue (totally 583 residues per molecule) and 2 for one lipid molecule.

Table 2.7: Estimation of LPR for the lipid-BSA mixture. “A” stands for the ratio of integrated intensities of the carbonyl groups for the lipid and BSA. Molecular weight was taken as 500 Dalton for the lipid and 66500 Dalton for BSA.			
Known values before experiment	Calculations from the IR spectra		
LPR (w/w)	$A = \frac{\int \nu(C=O)_{lipid}}{\int \nu(C=O)_{protein}}$	$\frac{A}{(2/583)}$	Estimated LPR (w/w)
0.25	0.115	34	$34 * (500/66500) = 0.26$
0.5	0.212	62	$62 * (500/66500) = 0.47$

The estimated results for the LPR of lipid-BSA mixture are quite close to the known values of LPR in Table 2.7. The known value of 0.25 and 0.5 for the LPR were calculated as 0.26 and 0.47, respectively. In the present study, the samples of the lipid-BetP mixture were provided with known concentrations and LPR. However, their LPRs were controlled with the method expressed above so as to be sure about the LPR of the BetP samples, if necessary, as represented in Table 2.8 and Fig 2.20. Accordingly, BetP harbors 26 lipids molecules per monomer and 78 lipids per trimer when its LPR is 0.2.

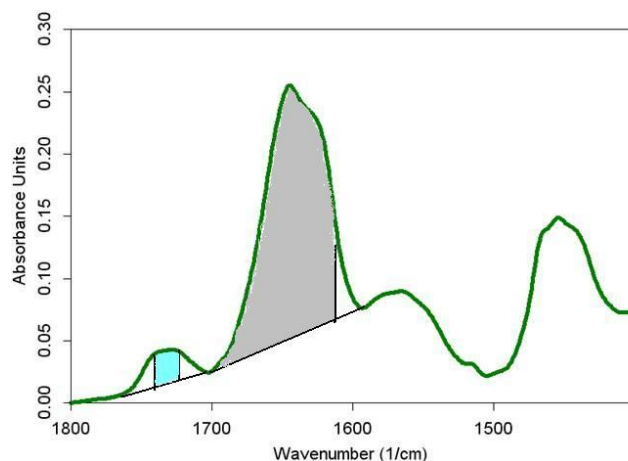


Figure 2.20: The IR spectrum of BetP 2D crystals reconstituted in *C. glutamicum* lipids. The lipid $\nu(\text{C}=\text{O})$ modes in the region 1753-1720 cm^{-1} (cyan) and protein $\nu(\text{C}=\text{O})$ modes for the region 1700-1618 cm^{-1} (gray) were integrated to calculate the LPR due to intense side chain absorption of BetP above 1700 cm^{-1} and below 1618 cm^{-1} . The LPR can be also calculated from the side chain subtracted spectrum.

Table 2.8: Estimation of LPR for BetP 2D crystals reconstituted in <i>C. glutamicum</i> lipids. Molecular weight was taken as 500 Dalton for the lipid and 65000 Dalton for BetP.			
Provided BetP with known LPR (w/w)	Calculations from the IR spectra		
0.2	$\frac{\int \nu(\text{C}=\text{O})_{lipid}}{\int \nu(\text{C}=\text{O})_{BetP}} = 0.09$	$\frac{0.09}{(2/595)} = 26$	Estimated LPR (w/w) $26*(500/65000) = 0.2$

3. RESULTS AND DISCUSSION

3.1 FUNCTIONALLY INTACT BetP SAMPLES FOR IR SPECTROSCOPY

It has been previously shown that when BetP is in the native membrane (*C. glutamicum* lipids), the maximum transport activity for the uptake of betaine is achieved at the highest external osmolarity (1.3 osmol kg⁻¹) in comparison to artificial membrane surroundings¹¹ which is explained by different contribution of negatively charged phospholipids in the membrane³¹. Thereby, the secondary transporter BetP is highly regulated depending on the membrane composition. It was previously also studied that BetP is a stable trimer in the 2D⁹² and 3D¹⁴ crystals, in the presence of membrane and detergent, respectively. Therefore, functionally intact BetP samples prepared as BetP solubilised in detergent (n-dodecyl- β -D-maltoside), BetP reconstituted in POPG (1-palmitoyl-2-oleoyl-glycerol-3-phosphoglycerol) lipids as proteoliposomes and two-dimensional crystals of BetP (in *C. glutamicum* lipids) were used for IR spectroscopy. The infrared spectra of those are shown in Fig. 3.1. It is noticeable that we observe not only signals arising from protein backbone (amide I and amide II) but also lipid molecules possessing distinct positions in an IR spectrum. The latter is due to (1) molecular vibrations of phosphate head groups that correspond to the hydrophilic part of the lipid which gives signals around 1250 cm⁻¹ (ν_{as}) and 1085 cm⁻¹ (ν_{as}); (2) lipid C=O stretching mode around 1735 cm⁻¹ attributed to the interfacial region of lipid assemblies (ester carbonyl group) and (3) lipid CH₂ and CH₃ modes that correspond to the hydrocarbon tails of lipids in the hydrophobic part⁵⁵. Therefore, lipid signals in width and position can be followed to get information about the lipid-protein interactions as an external parameter. On the basis of the IR spectra (Fig. 3.1), various forms of membrane proteins are ideal to study with IR spectroscopy. In particular, a continuous buffer-perfusion technique based on evanescent wave spectroscopy (ATR-FITIR spectroscopy) is used for the selective analysis of the reaction of interest and for activation/deactivation control of the protein. This experimental method hereby allows structural-functional analysis of membrane proteins. For

instance, inactive-to-active switching can be reversibly induced and *in situ* monitored by IR spectroscopy.

In the present study, samples of BetP 2D crystals reconstituted in *C. glutamicum* lipids were titrated with increasing $[K^+]$. In comparison to other forms of BetP, the 2D crystals are fixed and well oriented on the ATR diamond during perfusion of buffer. If the protein sample does not properly settle down on the ATR crystal, then any unavoidable changes in the absorbance of the spectra due to instability of the protein on the ATR diamond can result in misinterpretations of the results. Therefore, one advantage of BetP 2D crystals is to record stable absorbance spectra in the long-term measurements. Additionally, BetP 2D crystals reconstituted into 100% negatively charged *C. glutamicum* lipids have a lower lipid-to-protein ratio in comparison to proteoliposomes so that any small change in the lipid signals due to activation can be followed accurately in the natural environment of BetP.

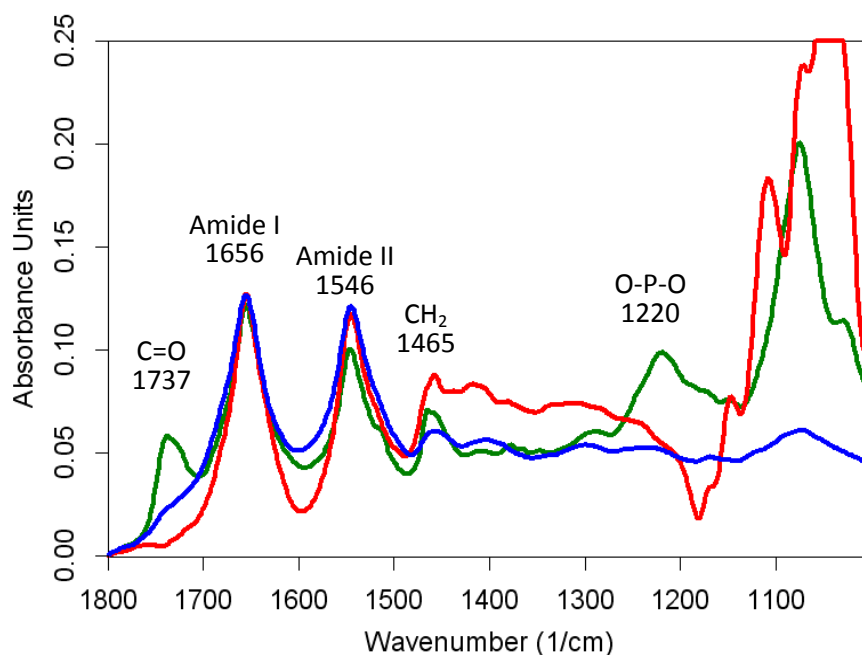


Figure 3.1: The IR absorbance spectra in H₂O buffer for functionally intact BetP samples in detergent (—), reconstituted in liposomes (—) and reconstituted in 2D crystals (—).

3.2 SECONDARY STRUCTURE ANALYSIS OF BetP

As demonstrated above in Fig 3.1, the amide I band of BetP is centered around 1656 cm^{-1} , which is representative for the C=O stretching vibrational mode of α -helical protein. Both BetP solubilized in detergent, prepared as proteoliposomes, and arranged in 2-D crystals have a maximum position at around 1656 cm^{-1} in H_2O buffer (1654 cm^{-1} in D_2O). This indicates that all forms of BetP are more or less identical and predominantly α -helical.

To calculate the relative proportion of each secondary structural element of BetP, curve fitting procedures (see Section 2.7) have been performed in the presence and absence of K^+ ions both in H_2O and D_2O buffers. The contributions of corresponding buffers and of side chains to the protein spectra were subtracted (see Sections 2.8 and 2.10) prior to curve fitting analysis.

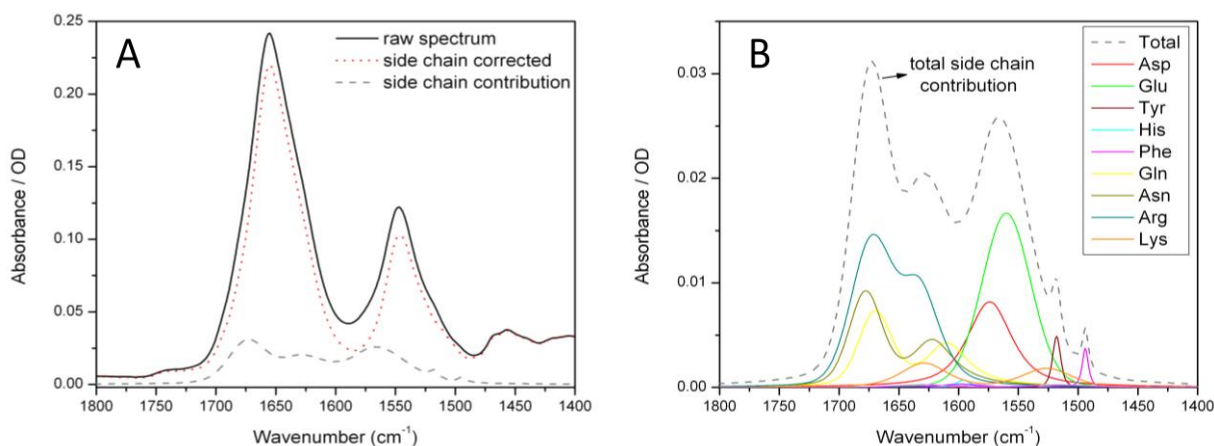


Figure 3.2: (A) The IR absorbance spectra of BetP WT 2D crystals (pH 7.5, 200 mM KCl) before (—) and after (...) side chain subtraction. (B) The total side chain contribution (---) subtracted from the absorbance spectrum.

Fig. 3.2 demonstrates the IR spectra obtained before and after side chain subtraction, revealing significant absorbance of side chains in the amide I band ($1700\text{-}1600\text{ cm}^{-1}$). The side chain subtracted absorbance spectra were used for the curve fitting analysis so that only contributions of protein secondary structures were analyzed. The generated envelope of amide I band by curve fitting exhibited the subbands lying under the curve, which allude to individual secondary structural

elements (Fig. 3.3A). The matched second derivative profiles (Fig. 3.3B) of both raw and fitted spectra confirm the accuracy of the curve fitting.

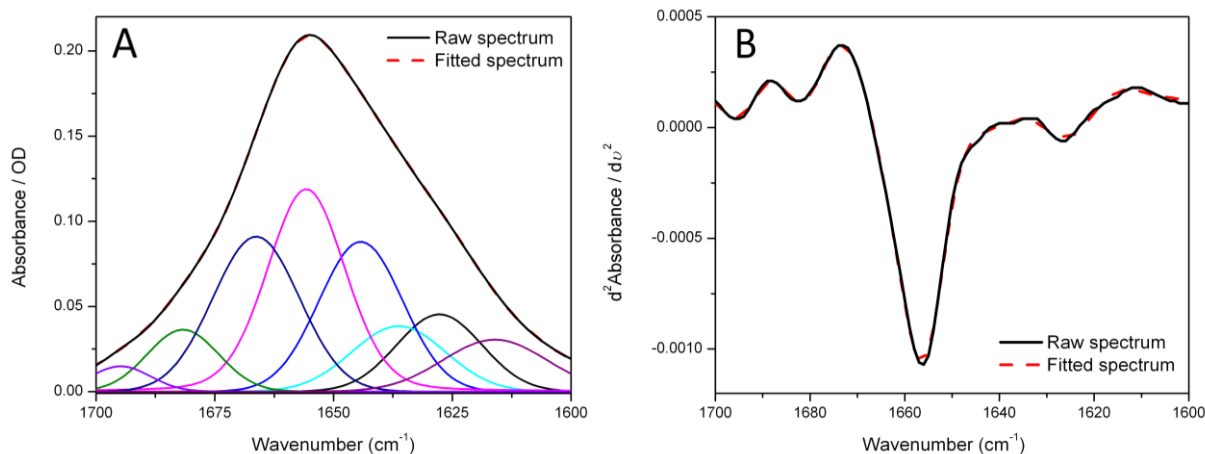


Figure 3.3: Curve fit analysis of BetP 2D crystals for the amide I band at pH7.5, 200 mM K⁺. **(A)** The IR absorbance and **(B)** 2nd derivative spectra. The envelope band formed by fitted bands is shown in red (---) and the original spectrum in black (—). The 2nd derivatives of the original and fitted spectrum are shown to compare the success of the curve fit.

BetP WT in D ₂ O buffer						BetP WT in H ₂ O buffer			
0 mM K ⁺		200 mM K ⁺		500 mM K ⁺		Band Assignments	200 mM K ⁺		
Position (cm ⁻¹)	Area (%)	Position (cm ⁻¹)	Area (%)	Position (cm ⁻¹)	Area (%)		Position (cm ⁻¹)	Area (%)	Band Assignments
1626	-	1624	-	1626	-	non-native contacts	1627	-	non-native contacts
-	-	1635	16.3	-	-	short/3 ₁₀ -helix; solvated loop	1636	11.5	short helix
1640	11.8	1642	2.4	1640	14.0	short/3 ₁₀ -helix; solvated loop	1644	23.4	short helix
1654	74.9	1654	69.0	1654	68.4	α-helix	1656	31.9	α-helix
1665	7.2	1668	6.5	1665	10.8	turn/loop	1666	25.0	solvated loop; short helix
-	-	1676	2.7	-	-	turn/loop	-	-	
1679	6.1	1682	3.0	1679	6.9	turn/loop	1682	8.2	turn/loop
1693	-	1694	-	1693	-	non-native contacts	1695	-	non-native contacts

Table 3.1: Tentative assignment of amide I components and percentages of secondary structure elements of BetP 2D crystals in H₂O and D₂O buffers. The area of the band positions at around 1626 and 1694 cm⁻¹ were not included for calculation of the fractions of other bands.

In the presence of 200 mM K⁺ in deuterated buffer, the peaks obtained from the 2nd and 4th derivative spectra are positioned at 1654, 1635/1642 and 1668/1676/1682 cm⁻¹ (Table 3.1) and are attributed to α -helices, solvated secondary structures (i.e. unordered structures, solvated loops/short helices and/or 3_{10} -helices) and to turn/loops buried in the hydrophobic region which are not affected by deuteration, respectively (for band assignments see Refs.^{42,43,45,46}). The bands at 1624 and 1694 cm⁻¹ can be assigned to non-native contacts and are proposed to arise from BetP units in crystal contact. These signals observed also for the detergent solubilized BetP³⁷ have also been attributed to intermolecular β -sheet structures and/or inter-monomer contacts.

Protein Secondary Structures	BetP WT 2D crystals		
	0 mM K ⁺ (%)	200 mM K ⁺ (%)	500 mM K ⁺ (%)
unordered; solvated loop; short helix; 3_{10} -helix	12	19	14
α -helix	75	69	68
turn/loop	13	12	18

Table 3.2: The total fractions of secondary structures of BetP 2D crystals at pD7.5, calculated from Table 3.1.

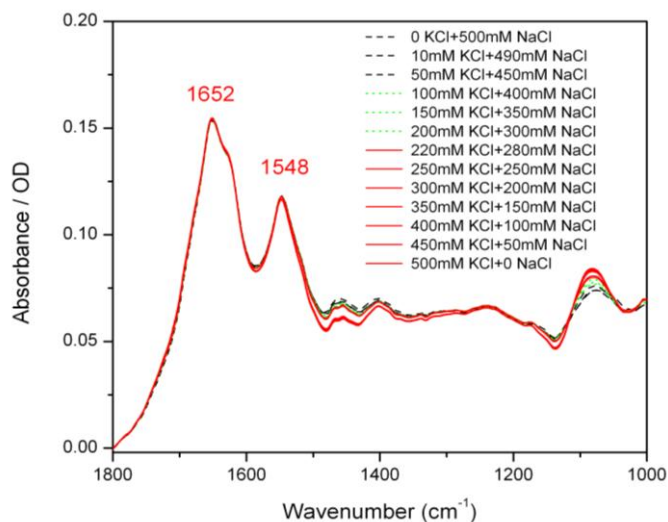
The fraction of each component was calculated with respect to the total amide I area, as described in detail in Section 2.7, and listed in Table 3.1. In the absence of K⁺, BetP exhibits 75% α -helical content, 12% solvated loops/short helices, 3_{10} -helix and/or unordered structure, and 13% restricted turns/loops, as summarized in Table 3.2. The content of α -helices decreases by 6% while solvated/short secondary structures increase by 7% at 200 mM K⁺. Under activating buffer conditions (500 mM K⁺), the amount of α -helices diminishes by 7% while the proportion of restricted turn/loops and solvated/short structures increases by 5% and 2%, respectively. In comparison to inactive BetP (0 mM K⁺), the population of restricted turn/loops significantly increases with high K⁺ (500 mM), which is not the case also for 200 mM K⁺. These alterations in the population can arise from either rearrangement of the secondary structural elements or a change in

their solvation status due to a conformational change during K^+ -induced activation. The relative content of the secondary structures of BetP 2D crystals determined by FTIR is slightly different from its X-ray structures (65% α -helix for N-terminus lacking BetP, PDB ID: 2WIT) and detergent solubilized FTIR data (71.5% α -helix for wild type BetP)^{14,37}.

3.3 *IN SITU* ACTIVATION OF BetP WITH INCREASING K^+ CONCENTRATION

A stepwise activation of BetP was carried out by using ATR-FTIR spectroscopy. In this experiment (for details see Section 2.6.1), the protein sample was titrated with increasing K^+ from 0 to 500 mM to activate the protein by keeping the total salt concentration constant. The final concentration of the buffer to be perfused towards the sample was adjusted to 500 mM by replacing the NaCl with KCl so that the total ionic strength stays constant, avoiding unspecific conformational changes which could arise from electrostatic ion shielding and ionic strength effects. Fig. 3.4 demonstrates the IR spectra of wild type BetP in the 2D crystal form recorded in H_2O buffer. If peak positions are followed, the positions of the maxima (1652 and 1548 cm^{-1}) in the absorbance spectra do not show any striking changes in the presence of various amount of K^+ . For this reason, these spectra should be further processed by calculating second derivative and difference spectra to obtain subtle changes in the IR spectra.

Figure 3.4: The buffer corrected IR spectra for BetP WT 2D crystals in H_2O buffer. The color coded spectra are for 0→50 mM K^+ (—), 100→200 mM K^+ (···) and for 220→500 mM K^+ (—). The buffer conditions used during the titration experiment are shown as inset.

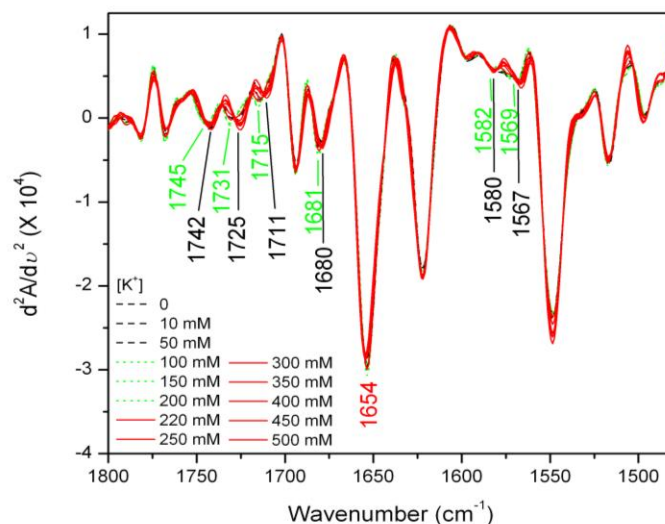


The 2nd derivative IR spectra (Fig. 3.5) were obtained from the absorbance spectra recorded during a stepwise activation of BetP. It is obvious that there are no band shifts for the major amide I band components (α -helix, turn and loop) in the 1700 and 1600 cm^{-1} interval. However, the positions of the minima in the second derivative spectra exhibit several distinct band shifts, particularly above 1700 cm^{-1} . It is clearly seen that there are many sub positions above 1700 cm^{-1} which can be attributed to C=O stretching modes of carboxylate groups of protonated Asp/Glu residues and/or with a possible overlap of lipid-C=O modes. Since the lipid-to-protein ratio (0.2) is very low for BetP 2D crystals, the protein C=O modes overweigh the lipid signals above 1700 cm^{-1} . Moreover, a band position at 1711 cm^{-1} is too low for a lipid C=O signal^{54,55,58,82}. In this respect, signals at 1711, 1725 and 1742 cm^{-1} can arise from the protonated Asp/Glu residues making strong (closer the surface), middle and weak H-bonding interactions with the protein itself, respectively. Significantly, these bands are upshifted by 4-5 cm^{-1} upon increasing K^+ (0 \rightarrow 200 mM); afterwards, these signals return again to the same position in the presence of 500 mM K^+ . In addition to these signals, a band absorbing at 1767 cm^{-1} shows a small change in position and intensity upon activation. This band can arise from some non-bonded or weakly H-bonded Asp/Glu residues which are well hidden inside the protein; thereby, suggesting environmental changes around these residues upon activation. Moreover, a signal detected at 1567 cm^{-1} which corresponds to deprotonated Asp/Glu acid residues shows a spectral shift in a similar manner but the change in the wavenumber position is only 1-2 cm^{-1} in comparison to protonated groups of those. This suggest that deprotonated Asp/Glu residues play a different role as compared to protonated Asp/Glu residues in the K^+ -induced activation of BetP.

In the 2nd derivative spectrum, we also observed two distinct band positions located at 1622 and 1693 cm^{-1} which cannot be attributed to side chain and/or regular secondary structures because these signals did not show shifting upon exposure of the protein to 2H^+ in deuterated buffer. Since intermolecular β -sheet structures are generated *via* H-bonding between molecules, i.e non-native

contacts, contacts among ordered secondary structural elements, protomer-protomer contacts and/or inter-monomer contacts, these band positions are very likely to become additional crystal contacts between the protomers. Such a crystal contact has been previously proposed for the X-ray structure of 2D crystals of BetP⁹². Additionally, in Fig. 3.11D in the next section, it is also clearly seen that a positive signal located at 1627 cm^{-1} and a negative signal at 1621 cm^{-1} are also a clue for the formation of intermolecular β -sheet structure because these signals are too low for ordered secondary structures and too high for the side chains in deuterated buffer. It is therefore conceivable that an increase in the intensity of 1627 cm^{-1} suggests that contacts between possible interaction partners weaken upon K^+ -induced activation of BetP, which is also the case observed in the FTIR data of detergent solubilized BetP³⁷.

Figure 3.5: The IR second derivative spectra calculated from the absorbance spectra shown in Fig. 3.4. The peaks are for the protein in the presence of 0 mM K^+ (—), 200 mM K^+ (....) and 500 mM K^+ (—).



In order to elucidate the spectral alterations deduced from the 2nd derivative spectra shown in Fig. 3.5, the shift of the peak position was plotted for the C=O modes of protonated Asp/Glu residues with respect to increasing K^+ concentration applied during a titration experiment (Fig. 3.6). Obviously, the C=O modes of carbonyl groups of protonated Asp/Glu side chains are upshifted indicating weakening or loss of H-bonds of those residues upon activation. Shifts are complete at 100 mM K^+ for the strongly and medium H-bonded Asp/Glu residues located at 1711 and 1725 cm^{-1} . However, weakly H-bonded Asp/Glu residues which are located deeper inside the protein

and centred at 1742 cm^{-1} , the upshifting still proceeds at 100 mM K^+ and lags in terms of $[\text{K}^+]$ completing the ascent at 200 mM K^+ . Afterwards, shifts are reversed for $[\text{K}^+]$ above $\sim 250\text{ mM}$ for all three groups of protonated Asp and Glu residues in a similar manner. When BetP is gradually activated switching from 0 mM to 500 mM K^+ , surprisingly the entire process is fully reversible, most likely as a consequence of occupied K^+ -binding sites. The reversibility of this process has been also proven that the peak positions returned almost to the initial positions when the BetP sample was perfused again with the potassium-free buffer (2nd cycle of inactivation). These results are also compatible with the IR-difference spectra shown in Fig. 3.11. From this point of view, we can propose that protonated Asp/Glu side chains are directly involved in the regulation of activity of osmoregulated BetP upon K^+ binding.

Figure 3.6: The shift of the peak position for BetP WT 2D crystals at around (\blacktriangle) 1711 , (\bullet) 1725 and (\blacksquare) 1742 cm^{-1} versus K^+ concentration in the course of K^+ titration experiment. Open signs in blue color represent the 2nd cycle of the inactive state without K^+ ions.

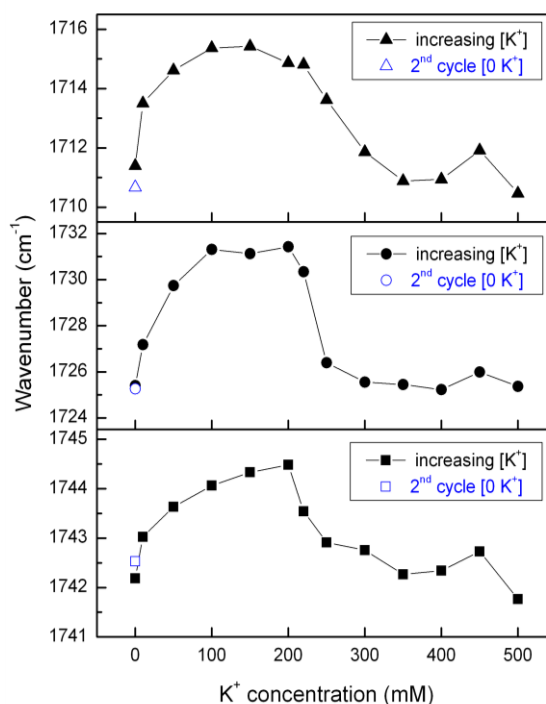
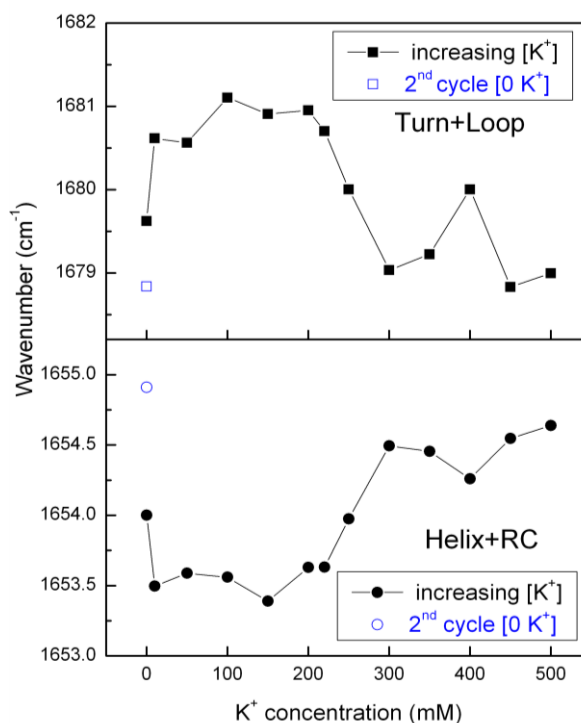


Fig. 3.7 demonstrates that band shifts are much smaller in the amide I range ($1700\text{-}1600\text{ cm}^{-1}$), where protein absorbs, in comparison to distinct shifts for protonated Asp/Glu side chains as mentioned above. In H_2O buffer, an Amide I signal located around 1680 cm^{-1} (turns/loops and contributions from Arg, Gln and Asn) is shifted $\sim 2\text{ cm}^{-1}$ while a band position around 1654 cm^{-1} (combination of

both α -helix and unordered structure) is shifted by 1 cm^{-1} . This indicates that small conformational changes occur in the secondary structural elements of BetP and their hydration status are altered upon K^+ -stimulated activation. This result matches also with the difference spectra of active BetP shown in Fig. 3.11. More precisely, a signal absorbing at 1654 cm^{-1} is downshifted to 1653.5 cm^{-1} for $[\text{K}^+]$ below $\sim 250\text{ mM}$ indicating stronger H-bonding characteristics of α -helices because possible H-bonds to the C=O group lower its frequency. Since an α -helix with a high number of residues absorbs around 1653 cm^{-1} in H_2O buffer⁷⁴, the flexibility of long-helices which absorb around 1654 cm^{-1} can be restricted for $0 < [\text{K}^+] < 250\text{ mM}$. On the other hand, the same signal is upshifted towards 1654.5 cm^{-1} for $[\text{K}^+]$ above $\sim 250\text{ mM}$ suggesting weakening or loss of H-bonding to helices that become relatively flexible. This result is in good agreement with the previous study which has revealed the threshold of K^+ concentration as $\sim 220\text{ mM}$ to activate the BetP reconstituted in *E. coli* lipids⁹³. *C. glutamicum* has very high content of anionic lipids (87% are phosphatidyl glycerol) in comparison to *E. coli* lipids; therefore, the higher concentration of K^+ is required to activate the BetP transporter. Apart from these quantitative results, since positively charged C-terminal domain acts as an osmosensor sensing the cytoplasmic K^+ concentration, it can be suggested that one or more helical structure can undergo conformational changes individually or in a common concerted mechanism upon exposure of BetP to cytoplasmic K^+ ions. It has been already studied that the osmosensor C-terminal domain and the unresolved N-terminal domain, both facing to the cytoplasm, has a crucial role in the regulatory mechanism of activity of BetP^{28,29}. Therefore, a change in the H-bonding properties of helices can be explained in such a way that elevated internal K^+ concentration can modify the orientation of the osmosensor and the osmoregulator C-terminal domain resulting in further possible concerted conformational changes of TM helices and/or the negatively charged N-terminal domain. If this is true, one scenario could be that sensing of K^+ concentration by the C-terminal domain alters the stabilization and orientation of TM12 (a flexible helix within the

inverted repeat 2) making reinforced interactions *via* stronger H-bonds up to 250 mM K^+ . As a result, TM12 might be a communication bridge between the periplasmic and cytoplasmic sites of BetP providing signal transduction. This is also in line with the results reported recently by single-molecule force spectroscopy showing strengthened cooperative interaction between the C terminal domain, TM12 and the external helix 2 located at the periplasmic site of BetP³⁶. On the basis of data in Fig. 3.7, another scenario could be that the C-terminal domain has at least three different orientations as weak (1654.5 cm^{-1}), medium (1654 cm^{-1}), and strong (1653.5 cm^{-1}) H-bonded upon perturbation with rising intracellular K^+ concentration up to 500 mM K^+ . In this respect, different orientations of the C terminal domain have been already proposed by means of EPR spectroscopy³³.

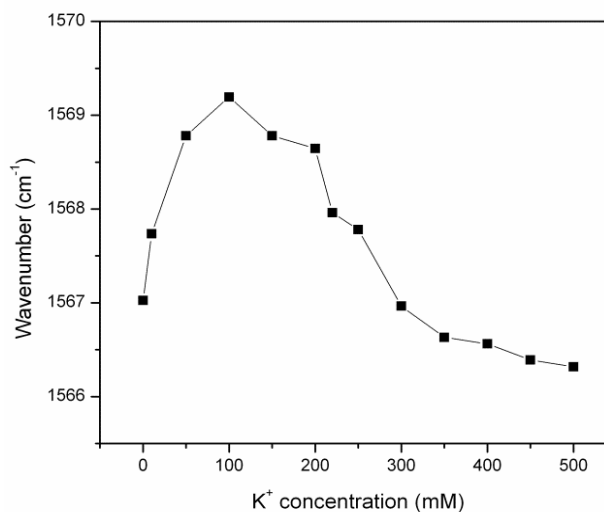
Figure 3.7: The shift in the wavenumber for BetP WT 2D crystals at around (■) 1680 and (●) 1654 cm^{-1} versus K^+ concentration in the course of K^+ -titration experiment. The blue colored (□) and (○) signs (1680 and 1654 cm^{-1} , respectively) represent the 2nd cycle of inactive state of BetP without K^+ ions.



Band positions located between 1550 and 1590 cm^{-1} ascribed to antisymmetric stretching modes of carboxylate groups (COO^-) of ionized Asp/Glu undergo drastic spectral alterations in position and in intensity that are observable in the 2nd derivative IR spectra. Therefore, the shift in the wavenumber was plotted at 1567 cm^{-1} for deprotonated Asp/Glu residues, as shown in Fig. 3.8. The

signal at 1567 cm^{-1} is upshifted to 1569 cm^{-1} completing the shifting at 100 mM K^+ , and then, downshifts gradually towards 1566 cm^{-1} . Therefore, ionized forms of Asp and Glu residues exhibit a different response to K^+ increase which does not resemble to protonated Asp and Glu residues, indicating different role of deprotonated Asp and Glu residues in regulation of K^+ -triggered activity of BetP. It can be suggested that some detectable changes take place around 100 mM K^+ at the inflection point of the curve that can be sensed as a change in the microenvironment of those residues. As a result, we propose that deprotonated Asp and Glu residues might also serve for communication sites in terms of osmoregulation of BetP.

Figure 3.8: The shift in the wavenumber for BetP WT 2D crystals at around (■) 1567 cm^{-1} versus K^+ concentration during K^+ -titration experiment.



Response of tyrosines to K^+ increase:

The C-C ring mode of tyrosine (Tyr) residues, which are mainly involved in K^+ coordination, exhibits also a clear response to K^+ titration, which provides dynamic information on changes in the interaction network of BetP during regulation (Perez C., Güler G. et al., to be published). This mode is a strong absorber in the mid-IR range and sensitive to protonation/deprotonation states; therefore, a Tyr residue within the protein senses the changes in its microenvironment when the protein is perturbed. In the 2nd derivative spectra (Fig. 3.9A) for BetP WT 2D crystals, we observe two strong bands located at 1517 and 1497 cm^{-1} which are attributed to the C-C ring stretching vibrations of protonated and deprotonated Tyr residues, respectively⁸². These signals exhibit small

spectral alterations, namely a change in the intensity and a shift in the peak position ($\sim 1 \text{ cm}^{-1}$), in the course of increasing K^+ concentration. This points out that the strength of H-bonding formed between the tyrosine oxygen and hydrogen is fine-tuned. The electron density and the strength of the bonds between the carbons of the Tyr aromatic ring are subsequently affected, giving rise to a shift in the band position of Tyr, which is an unequivocal indicator for the movement of the BetP backbone upon K^+ -induced activation. This result is also in line with the IR-difference spectrum of active BetP that harbors multiple positive and negative peak positions of Tyr between the region 1500 and 1524 cm^{-1} (Fig. 3.11, see next section). Additionally, the protonated Tyr signals exhibit a broad band in the difference spectrum (active-*minus*-inactive) at around 1524 cm^{-1} . According to these changes, we can conclude that a few Tyr residues are involved in the K^+ -induced activation of BetP as being reporter and/or actor.

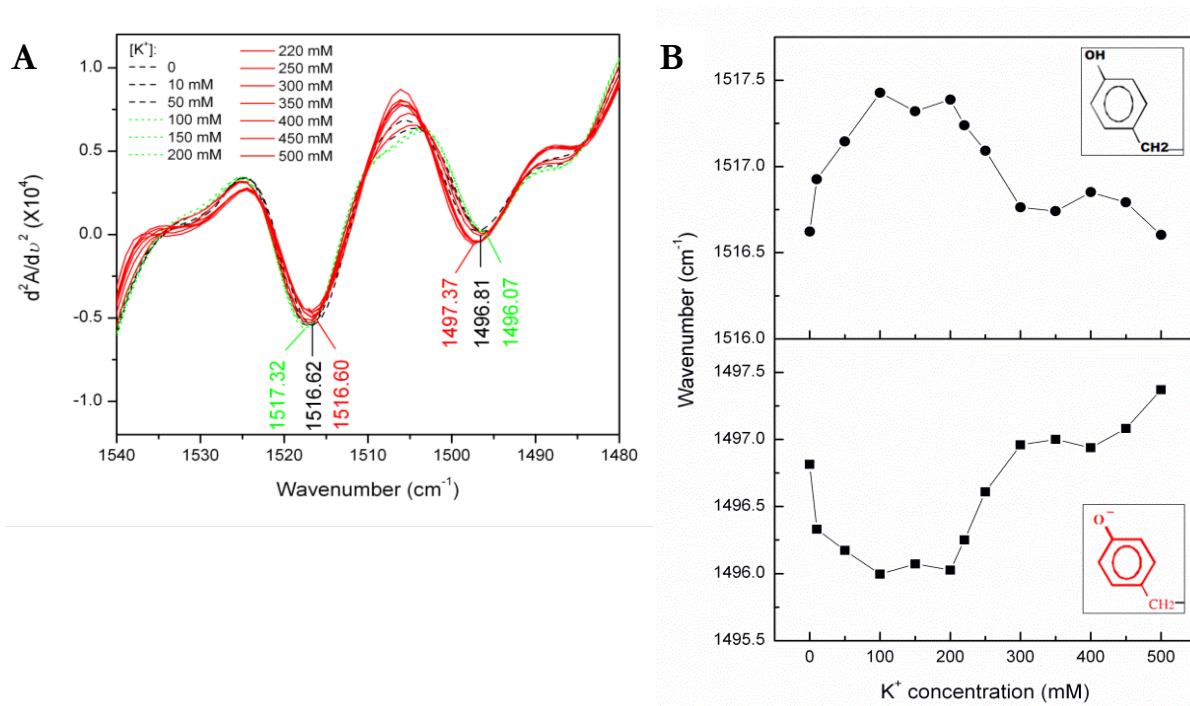


Figure 3.9: (A) The IR 2nd derivative spectra of the BetP WT 2D crystals in H₂O buffer was zoomed in Fig 3.5. The peak positions are for the protein perfused with 0 mM K⁺ (—), 150 mM K⁺ (···) and 500 mM K⁺ (—). (B) The shifts in the peak positions of protonated (●) and deprotonated (■) forms of tyrosines *versus* increasing K⁺.

The shift of the peaks for the C-C ring modes of Tyr obtained from the 2nd derivative spectra was drawn with respect to increasing K⁺ (Fig. 3.9B). There are two populations of Tyr residues in BetP, protonated and deprotonated tyrosines that both undergo opposite spectral changes upon elevated K⁺. Obviously the C-C ring stretching vibrations for protonated Tyr residues (1517 cm⁻¹) are upshifted under low, non-physiological K⁺ concentrations and above a threshold around 150-250 mM KCl, which is in the range of the apparent K_m value calculated for the activation of BetP by K⁺ (Perez, C. et al., to be published) the wavenumbers are decreasing again. An increase in the wavenumber signifies a weakening or loss of H-bonding upon K⁺ increment. In an opposite way, these modes for deprotonated Tyr residues absorbing at 1497 cm⁻¹ are downshifted below the threshold, reflecting the additional interactions of the Tyr residues of BetP *via* H-bonding, and afterwards, the peaks are increasing again above the threshold. Although it is not possible to assign specific residues to the observed IR spectral changes, it is plausible to speculate that residues involved in Rb⁺ binding, such as Asp131, Arg568, Glu552, Asp547, Tyr206 and Tyr553, or in formation of the periplasmic betaine-binding site, such as Tyr157, might contribute to the observed IR shifts. Recently, the K⁺ dependent interaction network in BetP (Perez, C. et al., to be published) and formation of the S2 site for betaine under up-regulating conditions as well as stabilization of TM12 by the C-terminal domain³⁶ were pointed out. According to these studies, the K⁺-dependent formation of the S2 site occurs through conformational changes in TM12, establishing an additional salt bridge between Tyr206 of TM4 and Aps547 in the cytoplasmic tip of TM12 when the K⁺ interaction sites at the cytoplasmic side are occupied (Fig. 3.10 from Perez, C. et al., to be published).

Moreover, in the IR-difference spectrum (Fig. 3.11) we observe also multiple positive and negative peaks that are assigned to tryptophanes in BetP. These Trp signals are located in the spectral region 1330-1365 cm⁻¹, 1420-1470 cm⁻¹ and 1509-1511 cm⁻¹ and undergo minute spectral changes with increasing K⁺. In fact, it is also expected to see small changes for Trp due to its non-polar character,

and thus, it is a weak absorber in the mid-infrared range⁸². Therefore, monitoring of a change in the intensity and the shifts of the peak positions of the Trp residues reflect the environmental changes around those residues upon K^+ -stimulated activation of BetP. Finally, observation of the spectral changes for Tyr residues accompanied by environmental changes around the Trp residues suggest that these residues are directly or indirectly involved in the K^+ -induced activation mechanism of BetP. These findings collected by means of IR spectroscopy can contribute to understanding of activity regulation of BetP. Recently, the significance of cation- π interactions of Trp and Arg residues in stabilization of regulatory ionic networks, and thus, correlation of reorientations of Trp residues with activation of BetP was suggested for the detergent solubilized BetP³⁷.

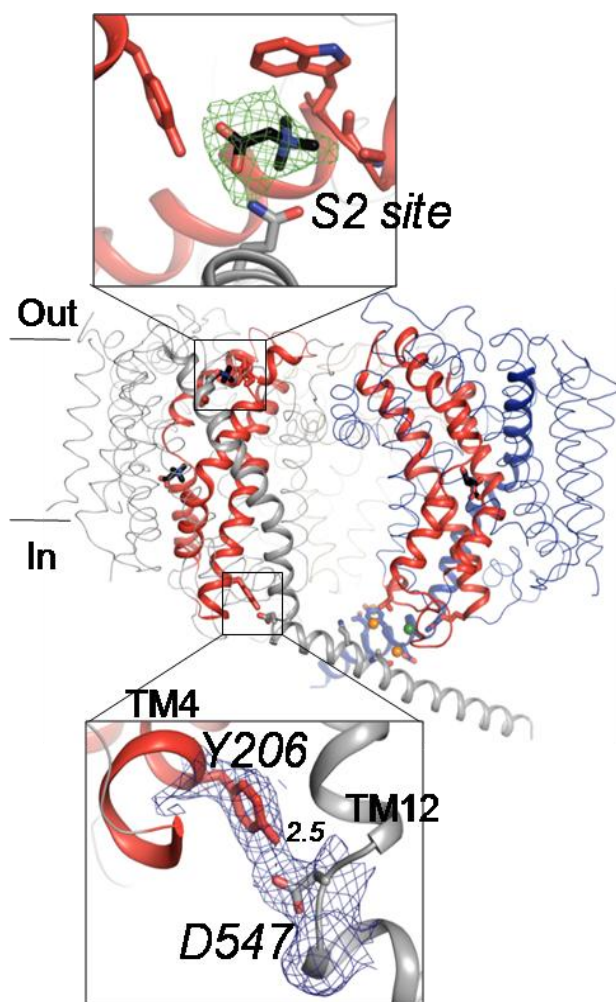


Figure 3.10: Connection between cytoplasmic and periplasmic site and the K^+ dependent ionic interaction networks. Formation of the S2 site occurs through conformational changes in TM12 moving Gln519 to a position ideal to coordinate the carboxyl group of betaine. Importantly, it was observed that individual mutations of Tyr206 and Aps547 against alanine abolish regulation completely (Figure reproduced from Perez C., Güler G. et al., to be published).

3.4 ACTIVATION-INDUCED INFRARED DIFFERENCE SPECTRUM

3.4.1 BetP wild type 2D crystals

Fig. 3.11 represents the IR-difference spectra between the region of 1800 and 1300 cm^{-1} performed in H_2O and in D_2O buffers. Here, the color coded spectra correspond to the active state of BetP with various concentrations of K^+ (10, 50, 100, 150 and 200 mM), taking the background as inactive state of BetP without K^+ ions. The positive sign represents the appearing parts while the negative sign corresponds to disappearing parts of the protein upon K^+ -induced activation. The difference spectrum taken at great sensitivity reveals many tiny alterations within the protein backbone and amino acid side chains induced by K^+ activation. The signals between 1770 and 1700 cm^{-1} arising from C=O stretching modes (COOH) of protonated Asp/Glu residues show a spectral shift reflecting a change in the H-bonding properties of those, namely H-bonds to Asp/Glu residues are strengthened or weakened/lost upon activation (Fig. 3.11A). Since intensities of bands absorbing at 1765, 1748, 1731 and 1716 cm^{-1} increase, population of these residues are also very likely to increase in the K^+ -induced active state of BetP. Interestingly, signals located at 1582(+) (shoulder), 1576(-), 1563(+) and 1560(-) cm^{-1} attributed to the antisymmetric stretching mode of deprotonated carboxylate groups [$\nu_{\text{as}}(\text{COO}^-)$] for Asp/Glu exhibit also wavenumber shifting in the presence of K^+ . Particularly, a negative absorbance between 1600 and 1550 cm^{-1} centred at 1576 is a prominent indicator manifesting a decrease in the population of deprotonated Asp/Glu residues. Besides, difference signals located at 1416(+), 1414(-), 1396(+), 1382(-) attributed to symmetric stretching modes [$\nu_{\text{s}}(\text{COO}^-)$] of Asp/Glu residues are also shifted (for band assignments see Refs.^{41,82}). Therefore, we can conclude that a H-bonded network of Asp/Glu residues in BetP is perturbed by elevated K^+ . Altogether this suggests that eventually a protonation/deprotonation of those residues may be involved in the activation state of BetP.

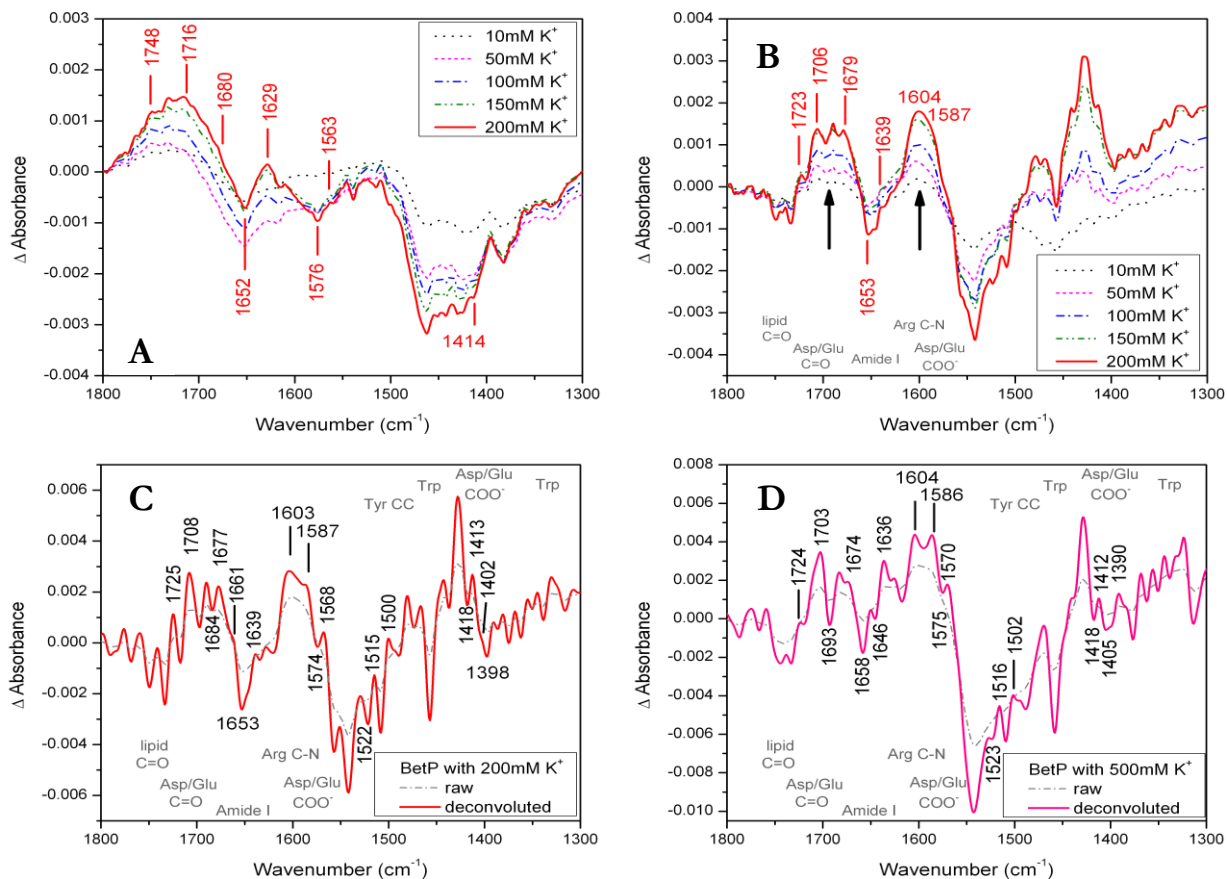


Figure 3.11: The IR-difference spectra (active-*minus*-inactive) of BetP WT 2D crystals at (A) pH7.5 and (B) pD7.5. The deconvoluted difference spectrum (calculated with a Lorentzian band shape with a bandwidth of 23 cm^{-1}) of active BetP in D_2O in the presence of (C) 200 mM and (D) 500 mM K^+ . All difference spectra represent the active state of BetP with various concentration of K^+ taking the background as 0 mM K^+ (inactive state).

Surprisingly, in the IR-difference signals at the lower end of the C=O range towards 1705-1690 cm^{-1} , we can identify two signals (1704 and 1692 cm^{-1}) that are too low for Asp/Glu C=O groups and too high for the amide I bands in H_2O buffer (Fig. 3.11A). Since the C=O modes of asparagine and glutamine residues are observed up to 1704 cm^{-1} and 1696 cm^{-1} , respectively, and the C-N mode (ν_{as}) of arginine has a signal between 1672 and 1695 cm^{-1} ,⁸² these groups are very likely candidates for Asn/Gln and/or arginine residues (for band assignments see Refs.^{41,82}). Since the $\nu_{\text{s}}(\text{CN}_3\text{H}_5^+)$ mode for Arg is observed between 1614 and 1663 cm^{-1} , a positive signal around 1629 cm^{-1} detected in the IR-difference spectra is attributable to the symmetric stretching C-N mode of Arg residues that

intensifies dramatically upon activation as well. Absorbance differences which appear at 1614(-) and 1611(+) cm^{-1} (Fig. 3.11A) are absent in $^2\text{H}_2\text{O}$ buffer (Fig. 3.11B). Thus, these signals can be assigned to NH_2 bending modes of Asn residues that undergo a change in the H-bonding pattern as well upon activation. These results are in good agreement with the insights regarding the ionic networks on the periplasmic side of BetP²⁷ which harbor leucine and asparagine riched amphipathic helix¹⁴. Hence, it can be suggested that ionized Asp/Glu residues can interact with Arg residues and this probably leads to conformational alterations around the Asn/Gln residues on the periplasmic side. These findings collected by means of FTIR spectroscopy are in accord with the structural studies of BetP. One of those was carried out by dynamic simulations²⁶ that shows inter-protomer H-bonds between Thr351 (L7 preceding TM8) and Asn331 (h7) or Asn339 (h7) as a polar interaction in the most important interfacial region of BetP.

Absorption of amino acid side chains between 1800 and 1300 cm^{-1} and absorption of the H–O–H bending vibration around 1643 cm^{-1} superimpose with the amide modes⁴¹. In this respect, the experiment performed in H_2O buffer was repeated also in $^2\text{H}_2\text{O}$ buffer with the same conditions so that the overlapped signals of side chains can be distinguished from the secondary structural elements in the spectrum. Difference spectra recorded in both H_2O and $^2\text{H}_2\text{O}$ buffers showed very small changes for the signals arising from secondary structural elements (helix, turn and loop) during perturbation of BetP with rising K^+ . In Fig. 3.11B, the signals located around 1653(-), 1648(+) cm^{-1} are assigned to α -helix, while the bands at 1646(-), 1639(+) are attributed to solvated short helices, 3_{10} helices, unordered structure and/or open loops^{42,43,45,46,76,94}. These band shifts suggest that regular secondary structural elements undergo a change in their H-bonding strengths. H-bonding properties of two types of α -helical structure (membrane buried and solvated) strengthen due to exposition to solvent with K^+ -induced activation; thus, the frequency shifts towards lower signals. This FTIR data indicates that there are definitely minute conformational changes in the protein backbone indicated

by small amide I difference signals upon upregulation of BetP. This agrees well with secondary structure analysis of detergent solubilized BetP³⁷.

In order to make a definite band ascription Figures 3.11A and B were compared which show the shifting of absorbance maxima for amino acid side chains due to deuteration. Band positions located between 1765 and 1716 cm^{-1} in H_2O buffer (Fig. 3.11A) are downshifted in $^2\text{H}_2\text{O}$ buffer towards 1723 and 1706 cm^{-1} (Fig. 3.11B) which are attributed to H-bonded protonated Asp/Glu residues. It is clearer in the deconvoluted difference spectrum that these residues undergo a change in the H-bonding properties giving rise to the signals absorbing at 1725(+), 1718(-), 1708(+), 1698(-) cm^{-1} with perfusion of 200 mM K^+ (Fig. 3.11C). These positive peaks detected at 1725 and 1708 cm^{-1} are downshifted towards 1724 and 1703 with perfusion of 500 mM K^+ (Fig. 3.11D), indicating an increased population of the stronger H-bonded protonated Asp/Glu residues under high K^+ . Since Arg signals overlap with amide I band in H_2O buffer (Fig. 3.11A), the deconvoluted IR-difference spectrum of active BetP in the presence of 200 mM and 500 mM K^+ , recorded in $^2\text{H}_2\text{O}$ buffer, was used as a proof to resolve the Arg signals (Fig. 3.11C-D). The intensity of the signals absorbing at 1604 and 1587 cm^{-1} attributed to the antisymmetric and symmetric stretching C-N mode of Arg residues^{41,82}, respectively, increases dramatically with increasing K^+ pointing out an increment in the interactions of Arg residues during activation of BetP. In the deconvoluted difference spectrum, signals absorbing at 1587(+), 1574(-), 1568(+), 1556(-) and 1551(-) cm^{-1} are assigned to deprotonated Asp/Glu residues. Since a shoulder is detected around 1582(+) in H_2O buffer (Fig. 3.11A), the ionized Asp residues can overlap with Arg at 1586 cm^{-1} in D_2O buffer (Fig. 3.11C-D) Therefore, activation-induced vivid alterations in the H-bonding properties of both $\nu_{\text{as}}(\text{COO}^-)$ (1551-1590 cm^{-1}) and $\nu_{\text{s}}(\text{COO}^-)$ (1390-1420 cm^{-1}) modes of Asp/Glu residues were detected in the difference spectra. Altogether this proves that activation is initiated by a H-bonded network with Asp/Glu and Arg residues. Finally, it can be concluded that Arg and Asp/Glu residues can unzip with tiny

conformational alterations of the protein backbone in the active state of BetP. Hereby, these residues might contribute to communication sites in terms of signal transduction among the protomers.

In the difference spectra (Fig. 3.11C-D), two positive signals are also absorbing at 1517 and \sim 1502 cm^{-1} attributed to the C-C ring stretching vibrations of protonated and deprotonated Tyr residues⁸², respectively, reflecting additional H-bonding interactions of Tyr residues of BetP upon K^+ -induced activation. As commented in detail in Section 3.3, the IR shifts suggest that Tyr residues sense the movement of the BetP backbone due to conformational changes in the result of K^+ binding and/or play a role in the regulation of BetP activation.

Moreover, upon K^+ binding positive signals absorbing at 1467 and 1329 cm^{-1} and negative signals absorbing at 1473 and 1339 cm^{-1} are observed in $^2\text{H}_2\text{O}$ (Fig. 3.11B-D) together with detection of pronounced peaks located at 1455(+) and 1462(-) cm^{-1} in H_2O (Fig. 3.11A). These bands are assigned to tryptophan residues⁸². This reflects that Trp residues undergo reorientation and/or are affected from environmental changes upon K^+ -stimulated activation of BetP. Taken together, our results are in line with a recent structural study that presents linkages between particular loops and transmembrane helix (TM3) *via* cation- π interactions of Trp and Arg residues on the cytoplasmic and periplasmic side of BetP²⁷.

As recently reported, the activation mechanism of BetP involves internal K^+ concentration, the regulatory C-terminal domain and negative membrane surface charges¹². The osmosensor C terminal domain detects the intracellular K^+ concentration⁹ undergoing different orientations. This is followed by conformational changes of loops (L2 and L8) and of TM helices during activity regulation of BetP^{11,25,33}. Moreover, two ionic networks existing on cytoplasmic and periplasmic sides of BetP have been identified recently²⁷. These ionic networks involve mainly arginine, aspartic acid and glutamic acid residues. Precisely, ionic interactions on the periplasmic side contribute to the stability of

amphipathic helix h7¹⁴. On the cytoplasmic side, ionic interactions exist not only between positively charged residues in the C-terminal domain (Arg552-Arg568) and negatively charged Asp131 located in loop2 (L2) of the adjacent protomer but also between L2 (Glu132) and L8 (Arg390)¹⁴. Furthermore, reorientation of the three C-terminal domains in the BetP trimer points out that this domain involves lipid-protein and protein-protein interactions during osmoregulation²⁵. This study reveals first FTIR spectroscopic evidence on the molecular level for the K⁺-induced regulatory activation mechanism of BetP. In the current study, the threshold for most band shifts is 150-200 mM K⁺ which is adequate to activate the BetP. Here, we conclude that the observation of band shifting for K⁺ below 200 mM is the upregulation of BetP while the reverse process for K⁺ above 250 mM accounts for the relaxation of the protein in which BetP turns back into relatively stable state but still in the active state. Our findings manifest dramatic alterations in the H-bonding pattern of aspartic and glutamic acid residues deduced from IR-difference spectra and 2nd derivative profiles; we confirm that activation of BetP is initiated by a H-bonded network with Asp/Glu and Arg residues as a consequence of perturbation *via* a rise in cytoplasmic K⁺ concentration. Taking FTIR and structural data into consideration which are mentioned above, we have a view of the scenario of “unzipping” of Arg and Asp/Glu residues between particular loops and C-terminal domain which could well represent the activation of BetP. This is accompanied by a tiny conformational change of the protein backbone indicated by characteristic amide I band shifts. Additionally, one or more tyrosine residue(s) act(s) as reporter group(s) which sense(s) the modifications in its/their microenvironment upon K⁺-induced activation.

Further activation/deactivation experiments:

BetP WT 2D crystals in H₂O buffer — The effect of K⁺ ions on BetP was analyzed in H₂O buffer again with perfusion of 200 mM and 500 mM KCl to compare the results described above. In the difference spectra (Fig. 3.12A), the intensity of the C=O vibrations of protonated Asp/Glu modes absorbing above 1700 cm⁻¹ increases with K⁺. Precisely, we observed positive difference signals for those modes absorbing at 1720 and 1701 cm⁻¹ concomitant with minute spectral alterations in the amide I region (1679(-), 1670(+), 1661(-) and 1648(+) cm⁻¹) in the presence of 200 mM KCl. However, perfusion of 500 mM KCl causes a shifting of protonated Asp/Glu modes absorbing at 1731(+) and 1705(+) cm⁻¹ and reversing of some amide I signals absorbing at 1682(+), 1670(-), 1661(+) and 1646(-) cm⁻¹. This implies a different response of protonated Asp/Glu residues and of secondary structural elements (loops and helices) to the mechanism of regulation and K⁺-induced activation of BetP. Additionally, both antisymmetric and symmetric stretching vibrations of ionized form of Asp/Glu residues absorbing at 1589, 1564/1569 and 1409 cm⁻¹ exhibit spectral shifts with increasing K⁺ but these spectral alterations are less pronounced compared to the protonated groups. Particularly, observation of the multiple negative peaks around 1589, 1564/1569 and 1409 cm⁻¹ concomitant with positive peaks above 1700 cm⁻¹ can be interpreted as having a change in the protonation state and/or environment of Asp/Glu residues under high K⁺. These spectral changes agree with the results described above in Fig 3.11. A clear band absorbing at 1627 and 1614 cm⁻¹ in the difference spectra can arise from combination of Arg ($\nu_s\text{CN}_3\text{H}_5^+$) and Lys ($\delta_{as}\text{NH}_3^+$) residues with contributions also from Asn (δNH_2). Therefore, the FTIR data suggest that both COOH (protonated) and COO⁻ (deprotonated) groups of Asp/Glu side chains interact most likely with Arg/Lys residues *via* salt bridge, being involved in K⁺-dependent activation of BetP, and the strength of these interactions is also influenced with elevated K⁺.

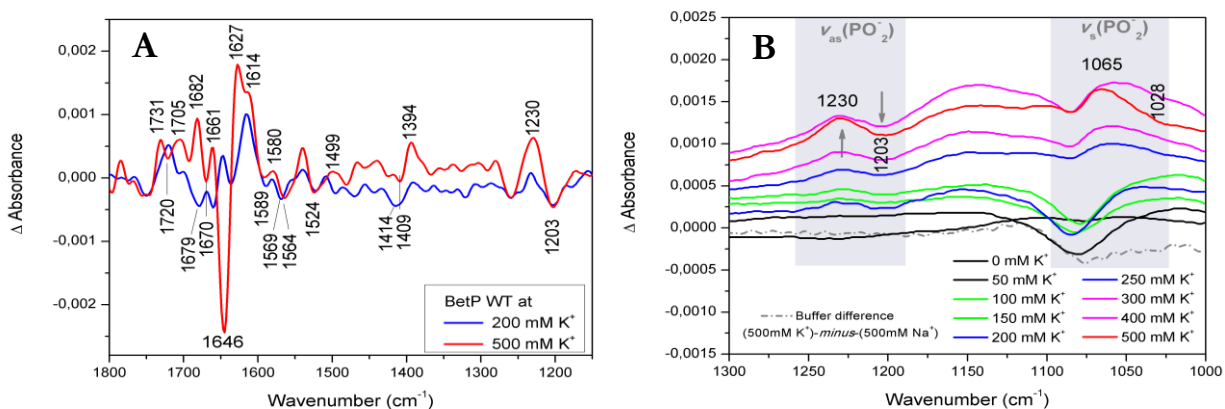


Figure 3.12: The IR difference spectra (active-*minus*-inactive) of BetP WT 2D crystals at pH7.5. **(A)** Deconvoluted difference spectra with 200 and 500 mM K⁺ in the region 1800-1100 cm⁻¹. **(B)** Difference spectra which represent the lipid PO₂⁻ modes. Background spectrum is recorded with perfusion of the K⁺ free buffer (inactive state conditions).

The impact of K⁺ ions on the hydrophilic region of lipid bilayer is also monitored in Fig. 3.12B. Upon K⁺ increment, there is an apparent intensity increase of the signals absorbed at 1230 and 1065 cm⁻¹, attributed to the antisymmetric and symmetric stretching vibrations of PO₂⁻ modes from phospholipid headgroups, respectively. However, the lower frequencies of those modes (1203 and 1028 cm⁻¹) exhibit negative signals in the difference spectra. Briefly, this means that the hydration status of the phosphate moiety found in the hydrophilic region of the membrane is remarkably perturbed upon K⁺-induced activation of BetP. The lipid-protein interactions will be discussed in detail in Section 3.6.

BetP WT 2D crystals after 24h-deuteration with perfusion of potassium-free buffer — The samples of BetP WT 2D crystals were incubated 24 hours in D₂O buffer which does not contain potassium ions. Afterwards, the spectra were recorded for two hours during perfusion of the buffer, which involves 500 mM K⁺ taking the reference as inactive state of BetP without K⁺ ions. These spectra refer to active-*minus*-inactive state of BetP, which exhibits the effects of both deuteration and K⁺-induced activation (red lines, Fig. 3.13A,B). Afterwards, the spectra of the BetP sample perfused with again potassium-free buffer were recorded (inactive-*minus*-active) for the next two hours taking the reference as active state of BetP with K⁺ (black lines, Fig. 3.13A,B).

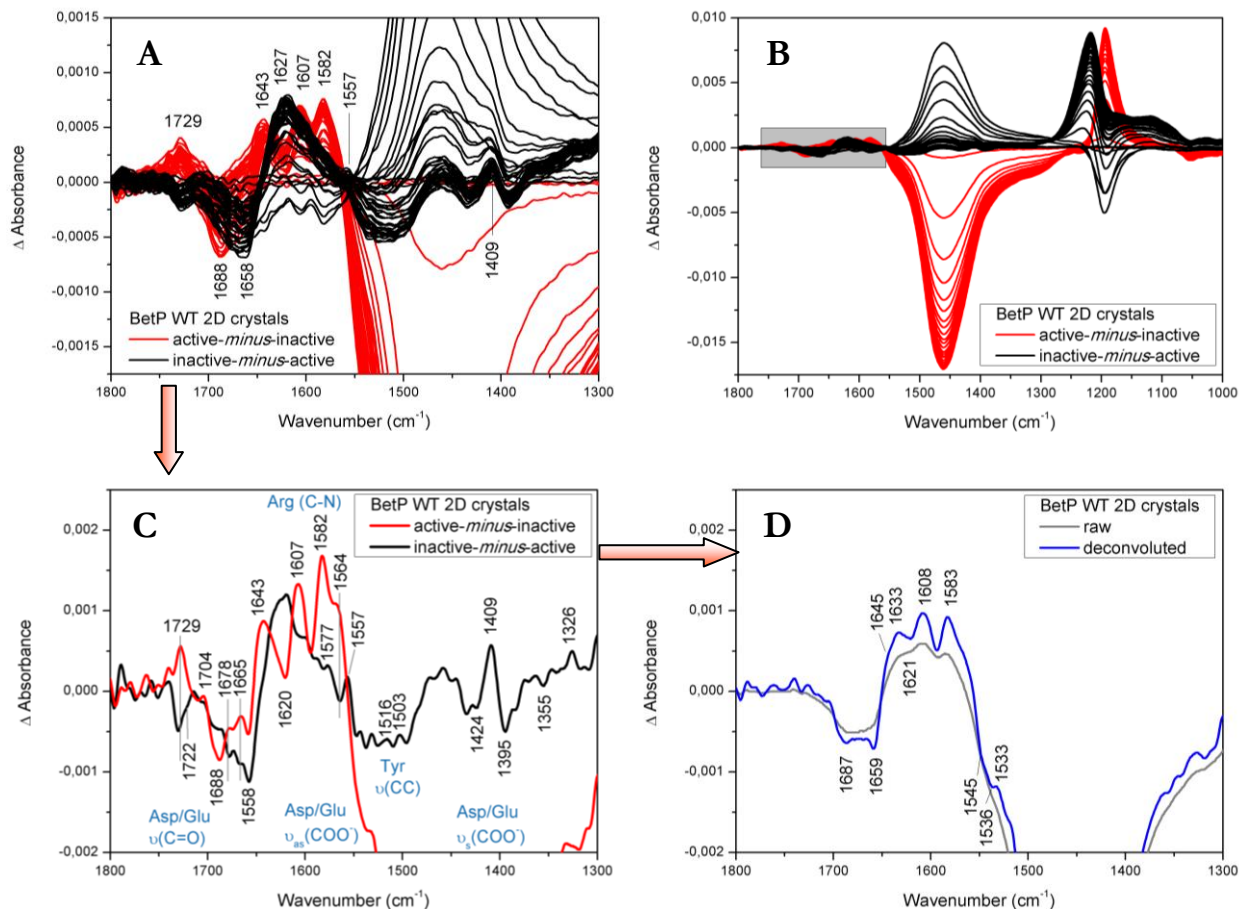


Figure 3.13: (A) The IR difference spectra of BetP at pD7.5 with 0 mM and 500 mM K⁺ after 24h deuteration. (B) Zoom of (A) for the range 1800-1300 cm⁻¹. (C) Deconvoluted difference spectrum was calculated using the last spectrum recorded at t=2h shown in (B). Background spectrum is recorded with perfusion of the K⁺ free buffer (active-*minus*-inactive) or perfusion of 500 mM K⁺ (inactive-*minus*-active). (D) Addition of two difference spectra in (C).

For the case of active-*minus*-inactive state of BetP (Fig. 3.13C, red line), we observed distinct wavenumber shiftings and intensity changes in the amide I region as well as amino acid side chains. The intensity of the bands absorbing at 1671/1688 (broad), 1658 and 1620 cm⁻¹ decreases while the intensity of the bands absorbing at 1729/1704, 1678, 1665, 1643 (broad), 1607/1582 and 1564 cm⁻¹ increases. This reflects that secondary structural elements (helices and loops) as well as Arg, Asp, Glu, Asn and Gln residues show a clear response to deuteration and/or K⁺-induced activation.

However, for the case of inactive-*minus*-active state of BetP (Fig. 3.13C, black line), some wavenumber positions are reversed partially or completely. Here, we expect only the effects of inactivation not that of deuteration since this is the second perfusion of potassium free buffer. Upon inactivation, the C=O vibrations of protonated Asp and Glu residues absorbing at 1729 cm⁻¹ disappear, splitting up into two negative bands (1730 cm⁻¹ and shoulder at 1722 cm⁻¹) and the signal at 1704 cm⁻¹ downshifts towards 1701 cm⁻¹. Additionally, both antisymmetric and symmetric stretching vibrations of ionized Asp and/or Glu residues undergo upshifting and intensity changes (1564→1577 and 1395→1409 cm⁻¹) without K⁺ ions. Moreover, the small positive difference signals monitored at 1678/1665 cm⁻¹ and 1643 cm⁻¹, attributed to turns/loops and solvated helices, respectively, have opposite signs with inactivation. Small difference signals of Arg residues in the range 1608-1586 cm⁻¹ in D₂O are also reversed being negative bands with inactivation.

These spectral alterations coincide with the FTIR data described above in Fig 3.11D. Briefly, the FTIR data here indicate that loops as well as solvated helices (C-terminal domain and/or short helices) in the hydrophilic part of the protein, which contain Asp/Glu and Arg residues are involved in the K⁺-induced activation of BetP. Observation of tiny difference signals for the C-C bonds in the ring of protonated and deprotonated tyrosines (around 1600 cm⁻¹ and at 1516/1503 cm⁻¹) as well as for Trp residues (~1326 cm⁻¹) is indicative for reorientations of these residues in response to K⁺-stimulated activation of BetP.

Fig. 3.13D represents the IR spectrum which is the addition of two difference spectra shown in Fig. 3.13C, namely (active-*minus*-inactive state of BetP) + (inactive-*minus*-active state of BetP). In this resultant spectrum, the spectral alterations due to K⁺-induced activation are cancelled but only the effects of deuteration with K⁺ on solvated helices/unordered structures (1659→1645 cm⁻¹), solvated/open loops (1659→1633 cm⁻¹) and on Arg residues (1687/1621→1608/ 1583 cm⁻¹) remain. The C=O region of protonated Asp/Glu residues exhibits small signals above 1700 cm⁻¹ while the

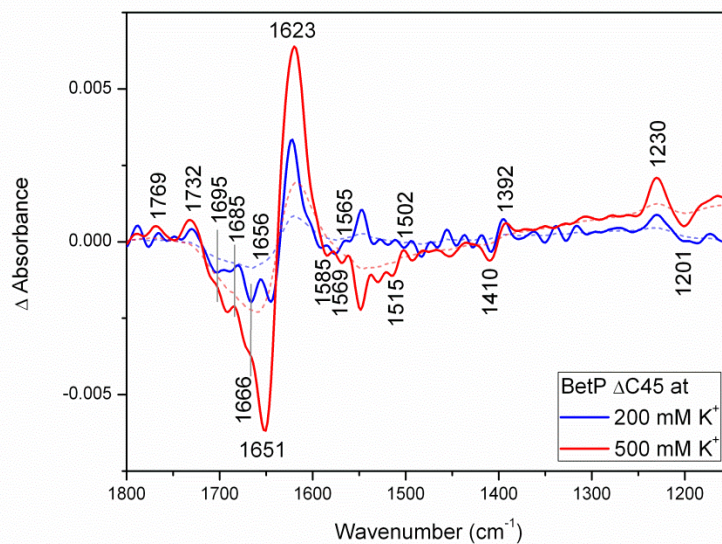
deprotonated state of Asp/Glu residues has only a shoulder around 1560 cm^{-1} which is hardly detected due to overlapping of the strong Arg signals. Hence only a few Asp/Glu residues should be further deuterated with K^+ ions. We assume that the osmosensor C-terminal domain which contains 14 Arg residues found in the cytoplasmic side of BetP is a strong candidate to be deuterated with the addition of K^+ ions into the buffer. With K^+ ions, this domain might reorient its conformation losing some interactions with the membrane surface/protein environment concomitant with exposition of some Arg residues to the solvent. This might cause also a change in the conformation of some open loops which harbor negatively charged Asp/Glu residues in the periplasmic and/or cytoplasmic sides of BetP.

3.4.2 C-terminal truncated BetP (BetP ΔC45) reconstituted in 2D crystals:

Upon deletion of the last 45 amino acids from the C-terminal domain of BetP, BetP (termed BetP ΔC45) is not sensitive to hyperosmotic stress and K^+ sensing. This mutant is less active and not regulated anymore. The difference spectra of BetP ΔC45 2D crystals were recorded with perfusion of 200 and 500 mM K^+ , taking the K^+ -free buffer as background in H_2O buffer (Fig. 3.14). The mutant exhibits minor amide I changes together with tiny spectral alterations in the region for the protonated (above 1700 cm^{-1}) and deprotonated ($1600\text{-}1550\text{ cm}^{-1}$) form of Asp/Glu residues, compared to the IR-difference spectra of wild type BetP (Fig. 3.11A and 3.12A). Wild type BetP has strong positive signals at 1731 and 1705 cm^{-1} while the mutant has only a small difference band at 1732 cm^{-1} . Disappearing of the band positions for protonated Asp/Glu (1731 and 1705 cm^{-1}) and Arg/Lys ($\sim 1614\text{ cm}^{-1}$) residues in the case of mutant suggests that these charged residues respond to K^+ increment for the wild type of BetP, indicating an important role of the C-terminal domain in activation and regulation of BetP. Then, the C-terminal domain is involved in the ionic interaction network on the cytoplasmic side of BetP (i.e. between Arg558 from C-terminal domain and Asp131 from loop2 of the adjacent monomer)^{27,37}.

Moreover, tyrosine residues absorbing at 1515(+)/1502(-) (for 500 mM K^+) as well as deprotonated carboxylate groups of Asp/Glu residues absorbing in the region 1600-1550 cm^{-1} and 1410(-)/1392(+) cm^{-1} (for 200-500 mM K^+) also represent small spectral shifts in the K^+ -induced difference spectra. Moreover, the hydration status of the phosphate moiety from the membrane surface is also affected by K^+ ions, which is indicated by IR difference signals absorbing at 1230(+) and 1201(-) cm^{-1} .

Figure 3.14: The IR difference spectra of BetP Δ C45 2D crystals at pH7.5 with 200 and 500 mM K^+ . Deconvoluted spectra are shown in solid lines and raw spectra in short-dashed lines. Background spectrum is recorded with perfusion of the K^+ -free buffer (inactive state conditions).



3.4.3 BetP WT proteoliposomes

Proteoliposomes of wild type BetP reconstituted into *E. coli* lipids in a lipid-to-protein ratio of 10:1 (w/w) have a higher LPR as compared to 2D crystals of BetP. As described in detail in Section 2.3, these lipids include both protein-associated lipids whose molecules bind tightly to the specific binding site of the protein and a larger amount of bulk bilayer lipids whose molecules do not bind directly to the protein environment. Activation/deactivation of proteoliposomes of BetP WT was performed to compare the results obtained for 2D crystals. According to the ATR-IR absorbance spectra of BetP recorded both in H_2O and D_2O buffers (Fig. 3.15A,B), the maxima of the spectra do not change significantly in the active (500 mM K^+) and inactive state (0 mM K^+) conditions. We observed only a small shoulder at around 1580 cm^{-1} for the deuterated sample, which is indicative for the antisymmetric stretching vibrations of carboxylate groups of Asp/Glu.

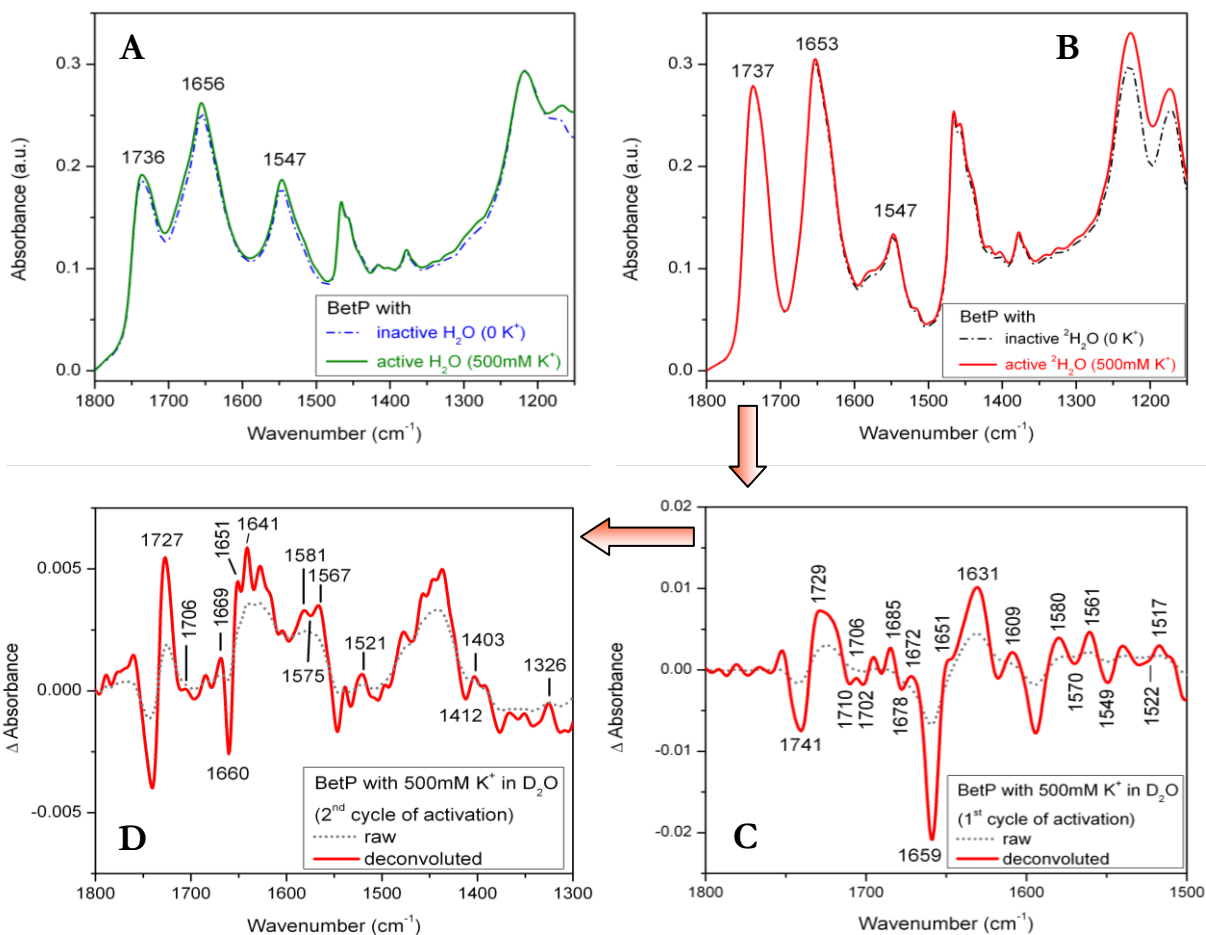


Figure 3.15: IR absorbance spectra of BetP WT proteoliposomes at **(A)** pH7.5 and **(B)** pD7.5 in the inactive (0 mM K⁺) and active (500 mM K⁺) state. **(C)** 1st cycle of activation: ATR-IR difference spectrum was recorded with perfusion of 500 mM K⁺ at pD7.5 for the first time after 24h-¹H/²H exchange with potassium-free buffer has been performed. **(D)** 2nd cycle of activation: Difference spectrum was recorded again with 500 mM K⁺ at pD7.5 for the second time. In both cases, the background spectrum was recorded with perfusion of the K⁺ free buffer (active-*minus*-inactive).

After the 24h-¹H/²H exchange of BetP without K⁺ ions was performed, the IR difference spectrum (active-*minus*-inactive) was recorded with perfusion of 500 mM K⁺ at pD7.5 for the first time. This is termed as the “1st cycle of activation” (Fig. 3.15C). Afterwards, the sample was again perfused with the inactivating D₂O buffer for 2 hours, which does not contain K⁺ ions. After this step, a difference spectrum of active-*minus*-inactive state was recorded for the second time again by switching 500 mM K⁺ at pD7.5, namely 2nd cycle of activation (Fig. 3.15D). In both cases, the background spectrum was recorded with perfusion of the K⁺ free buffer (active-*minus*-inactive) so that positive signs in the

difference spectrum refer to the final state of BetP (active state) while negative ones correspond to the initial state of BetP (inactive state).

In the 1st cycle of activation (Fig. 3.15C), we observed the effects of both deuteration and high K⁺; therefore, it is not possible to discriminate the spectral changes due to K⁺-induced activation. On the basis of the difference spectrum, negative and positive peaks at 1741/1729 (broad), 1710/1706 and 1702/1697 cm⁻¹ can be attributed to the carboxylic acid residues because it has been reported that the COOH modes of Asp/Glu residues downshift 5-10 cm⁻¹ upon deuteration⁸². This suggests that some Asp/Glu residues are exposed to solution with replacement of NaCl by KCl in the buffer, and thus, being further deuterated. The C=O modes of the lipids contribute most likely to the band detected at 1741 cm⁻¹ but the lipid signals were not significantly affected from deuteration. The most pronounced change in the difference spectrum is the observation of a negative peak at 1659 cm⁻¹ and positive peaks at 1651/1631 cm⁻¹. This kind of spectrum shows unmasking of some secondary structural elements. A downshift of the peak at 1659 cm⁻¹ towards a broad band at 1631 cm⁻¹ implies that short helices, 3₁₀ helix and/or open loops are deuterated under high K⁺. This shifting agrees well with the secondary structure analysis that fraction of the signal detected at 1666 cm⁻¹ in H₂O decreases after deuteration concomitant with an increased fraction of the band absorbed at 1635 cm⁻¹ (Table 3.1). Particularly, a decreased intensity at 1678 cm⁻¹ accompanied by increased bands absorbing at 1609 and 1580 cm⁻¹ is an unequivocal indicator for the deuterated Arg residues which are exposed to solvent. Therefore, it is conceiving that Arg residues are masked in the inactive state without K⁺ ions but are accessible to the solvent with K⁺-induced activation of BetP. Moreover, we observed a series of positive and negative difference signals located at 1580, 1570 and 1561 cm⁻¹ upon K⁺-induced deuteration, which are assigned to antisymmetric stretching vibrational modes of the deprotonated carboxylic groups. In the lower range of the amide II band, a signal absorbing at 1522(-) cm⁻¹ downshifts towards 1517(+) cm⁻¹ upon activation-induced deuteration, which arises

from the C-C ring stretching vibrational modes of protonated Tyr residues. This Tyr signal might be associated to changes in the environment of some Tyr residues occurring under high K^+ .

In the case of 2nd cycle of activation (Fig. 3.15D), we observe only the spectral changes due to K^+ -induced activation. The majority of bands shift upon activation in the deconvoluted difference spectrum, revealing minute conformational changes in the BetP backbone. Precisely, detection of subtle difference signals in the amide I region provides evidence for minor rearrangement of the protein secondary structures occurring upon K^+ -induced activation of BetP. A clear downshift from 1660(-) to 1651(+) cm^{-1} and from 1648(-) to 1641(+) cm^{-1} provides evidence that hydration of helices is altered with K^+ . Therefore, the H-bonding networks of both hydrophobic and solvated helices change upon activation, forming additional H-bonds with the solvent. This result is consistent with detergent solubilized BetP³⁷. Moreover, open loops/ 3_{10} helices absorbing at 1634(-)/1628(+) cm^{-1} as well as turns located at 1678(-)/1669(+) cm^{-1} become stronger H-bonded upon activation. We also observed changes in the absorbance and several distinct band shifts for Asp/Glu, Arg, Tyr and Trp residues in the ATR-IR difference spectrum. These K^+ -induced perturbations on amino acid side chains of BetP are resolved after deconvolution. The most dramatic change is detected above 1700 cm^{-1} , which is the region of carboxylic acid groups of protonated Asp/Glu residues. A number of negative and positive peaks are located at 1740(-), 1727(+), 1710(-) and 1706(+) cm^{-1} , indicating a change in the H-bonding pattern of these residues together with an increase in their population upon K^+ -induced activation. Moreover, minute difference signals of deprotonated Asp/Glu residues located at 1567(+), 1575(-) and 1581(+) cm^{-1} (antisymmetric stretching of COO^- groups), and at 1412(-)/1403(+) cm^{-1} (symmetric stretching of COO^- groups) as well as for arginines absorbing at 1608(-), 1604(+), 1598(-) and 1581(+) cm^{-1} are observed in the deconvoluted spectrum. We observe also perturbations of K^+ ions on Tyr residues. An intense and broad positive signal located at 1521 cm^{-1} suggests that a few tyrosines are involved in the K^+ -induced activation of BetP.

The FTIR results of proteoliposomes of BetP are in agreement with its 2D crystals described above. Taking everything into consideration, the alterations in the protonation states and in the environment of Asp/Glu and Arg residues suggest the formation of salt bridges between Asp/Glu and Arg residues in the presence of K^+ ions as an activation condition for BetP. This might be related to regulatory ionic interaction networks of charged residues both on the periplasmic and cytoplasmic sides of BetP, which was recently identified (i.e. between Arg558 from C-terminal domain and Asp131 from loop2 of the adjacent monomer)^{27,37}. A salt bridge interaction between Glu132 from loop2 and Arg390 from loop8 is also reported to be important for the alternating-access mechanism of BetP^{15,27}.

3.5 pH TITRATION OF BetP

To investigate further the activation-induced alterations in the population and H-bonding properties of protonated Asp/Glu residues under elevated K^+ concentration, pH titration of BetP was performed *in situ* at various pH values. By means of this experiment, we can prove one important step in the regulatory activation mechanism of BetP, which involves the ionic interaction of terminal domains with cytoplasmic loops *via* charged residues, as discussed in the previous section and recently reported³⁷. It is also possible to determine the protonation/deprotonation states of amino acid residues (i.e. Asp/Glu), their locations within the protein as well as the pH-induced conformational changes in BetP, as explicitly mentioned in Section 2.6.4.

The pH titration experiment of BetP WT 2D crystals was performed at +4°C using 10 mM NaP_i , 500 mM KCl for the pH range 5-8. Each buffer was perfused 2 hours towards the sample. The pH of the each buffer was controlled before and after the experiment. The ATR-IR difference spectra were recorded as pH5-*minus*-pH5.5; pH5.5-*minus*-pH6; pH6-*minus*-pH6.5; pH6.5-*minus*-pH7; pH7-*minus*-pH7.5 and pH7.5-*minus*-pH8 (Fig. 3.16A). On the basis of the IR difference spectra, the most pronounced spectral changes are observed for pH5.5-*minus*-pH6, pH6-*minus*-pH6.5, pH6.5-*minus*-

pH7 and for pH7-*minus*-pH7.5, namely in the pH range of 5.5-7.5. In this pH range, the intensity of the C=O stretching vibrational modes of protonated Asp/Glu residues increases (1700-1750 cm^{-1}) while population of the antisymmetric (1550-1590 cm^{-1}) and symmetric (~ 1405 cm^{-1}) stretching vibrational modes of deprotonated Asp/Glu residues diminishes (for band assignments see Refs.^{45,82}). This means that the associated pK_a value of Asp/Glu residues exists in a wide range between pH5.5 and pH7.5 which is remarkably high for a carboxylic acid, and thus, protonation/deprotonation states of those residues change in this pH range. Such spectral alterations are not observed in the difference spectra of pH5-*minus*-pH5.5 and pH7.5-*minus*-pH8. The buffer difference spectrum recorded in the absence of the protein (pH6.5-*minus*-pH7) was added for comparison, which does not exhibit spectral alterations between 1800 and 1300 cm^{-1} upon pH changes. However, the O-P-O modes of phosphate groups have multiple peaks in the spectrum below 1100 cm^{-1} . The buffer difference spectrum (Fig. 3.16A) has multiple negative bands observed at 1090(-) and 1067(-) cm^{-1} due to the fact that the absorption of phosphate groups at pH/pD5 is smaller than those of at pH/pD8.

To prove the spectral changes detected in H_2O buffer environment for protonated/deprotonated Asp/Glu residues (Fig. 3.16A), the IR-difference spectrum was also recorded in D_2O buffer as pD6.5-*minus*-pD7.5 and compared with pH6.5-*minus*-pH7.5 (Fig. 3.16B). The carboxylate signals of both protonated and deprotonated Asp/Glu residues shift upon deuteration, i.e., 1714 \rightarrow 1701 cm^{-1} for $\nu(\text{COOH})$ and 1558 \rightarrow 1560 cm^{-1} for $\nu_{\text{as}}(\text{COO}^-)$ and 1405 \rightarrow 1407 cm^{-1} for $\nu_{\text{s}}(\text{COO}^-)$, which backs up the band assignments and responds also to the pH titration experiment if the D_2O buffer is used as a solvent. Again the protonated Asp/Glu signals intensify above 1700 cm^{-1} while deprotonated ones are reduced in intensity at pH/pD6.5 once the reference was taken as pH/pD7.5, indicating a change in the acid-base characteristics of Asp/Glu residues in BetP. To resolve the band positions better, the difference spectrum recorded as pD6.5-*minus*-pD7.5 was deconvoluted, which represents

signals at 1678(+) and 1515(+)/1505(-) cm^{-1} well (Fig. 3.16C). The latter corresponds to the tyrosine residues while the peak position at around 1678 cm^{-1} can be attributed to turns/loops in D_2O buffer environment. This suggests that protonation/deprotonation states of Asp/Glu residues are altered concomitant with conformational changes of turn/loops as well as with microenvironmental changes around tyrosines in BetP. However, we do not observe significant conformational changes for helices.

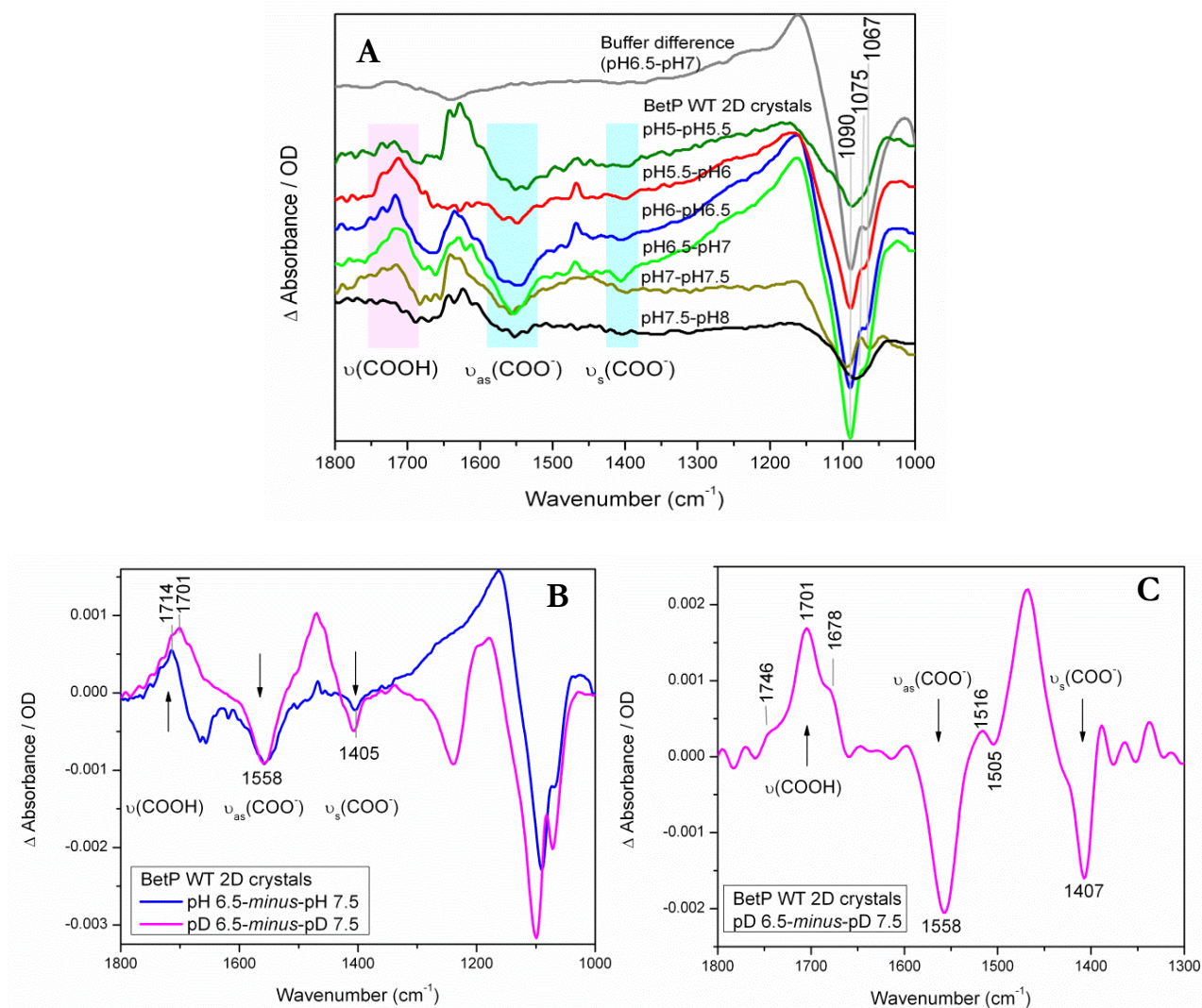
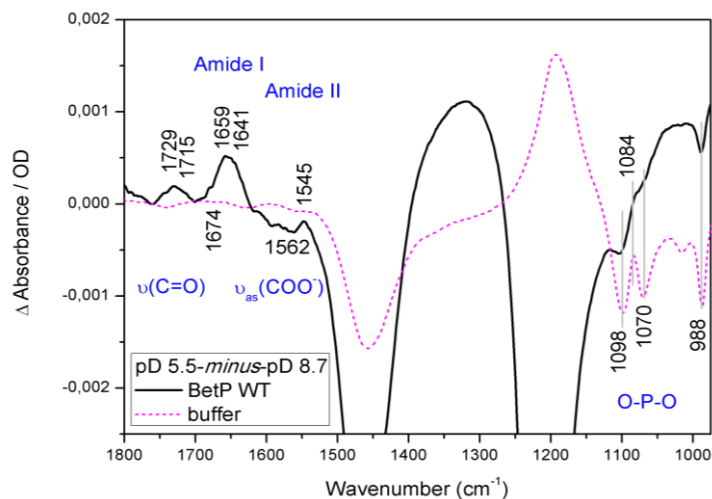


Figure 3.16: (A) The ATR-IR difference spectra of BetP WT 2D crystals recorded as pH5-minus-pH5.5 (—); pH5.5-minus-pH6 (—); pH6-minus-pH6.5 (—); pH6.5-minus-pH7 (—); pH7-minus-pH7.5 (—); pH7.5-minus-pH8 (—) and buffer difference (—). (B) IR-difference spectra recorded as (pH/pD 6.5)-minus-(pH/pD 7.5) in H_2O and D_2O buffered environment. (C) Deconvoluted difference spectrum for pD6.5-minus-pD7.5 from (B).

Here, the FTIR data indicate that the pK_a value of most Asp/Glu residues in BetP is determined in the range pH 5.5-7.5. This suggests that protonation/deprotonation states of those residues are altered around this wide pH range. As already discussed in Section 3.4 (Figs. 3.11 and 3.13), protonated and deprotonated Asp/Glu residues undergo H-bonding changes upon K^+ -induced activation of BetP. Particularly, the population of protonated Asp/Glu residues was observed to be increased under high K^+ concentration. On the basis of FTIR data obtained with the pH titration experiment, some Asp/Glu residues are protonated if pH of the solvent is low. So, it is conceiving that the same groups of Asp and/or Glu residues may be involved in the K^+ -induced activation of BetP. The clusters of Asp/Glu residues of BetP could be located away from the solvent because the pK_a is quite high even up to 7.5 and/or these groups make electrostatic interactions with the environment, most likely with some positively charged residues (i.e. Arg/Lys) with K^+ -induced activation.

Figure 3.17: The ATR-FTIR difference spectrum of BetP WT proteoliposomes recorded as pD5.5-*minus*-pD8.7 (—). The buffer difference (···) was added for comparison.



The ATR-FTIR difference spectrum of BetP WT proteoliposomes was recorded as pD5.5-*minus*-pD8.7 (Fig. 3.17). The buffer difference spectrum was also added for comparison. Observation of a clear increase in the population of protonated Asp/Glu residues absorbing above 1700 cm^{-1} and a reduced intensity of deprotonated Asp/Glu residues absorbing in the range $1560\text{-}1590\text{ cm}^{-1}$ is a strong indication for a change in the protonation/deprotonation characteristics of those residues. This result is in line with the results obtained for 2D crystals of BetP (Fig. 3.16).

3.6 LIPID-PROTEIN INTERACTIONS OF BetP

The latest structure of BetP to 2.7Å reveals specific binding of eight PG lipids to a hydrophobic cavity in the center of the BetP trimer as well as to the outer rim of BetP⁹⁵. These lipids stabilize essential parts of the transporter core and the trimeric interface (Fig. 3.18A). However as the structure represents only a snapshot of a crystallographically selected state of BetP it was not possible to assign the observed tight lipid-protein interactions to a specific activation state of BetP, i.e., the down-regulated (inactive) state.

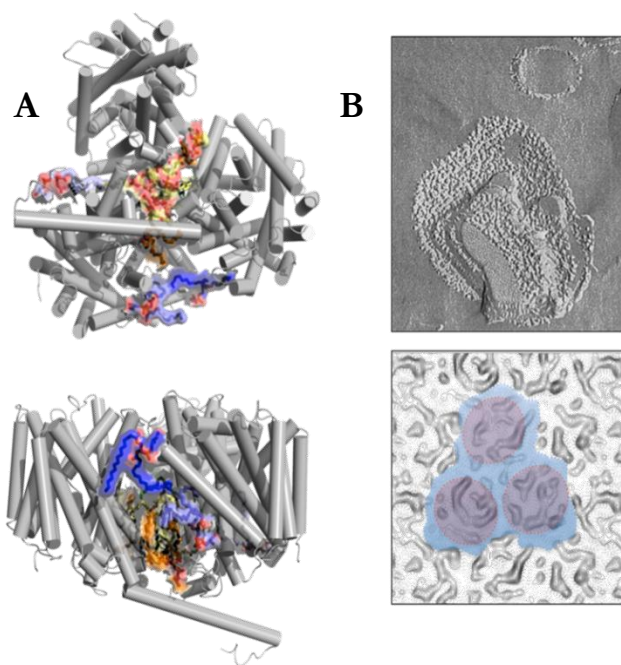
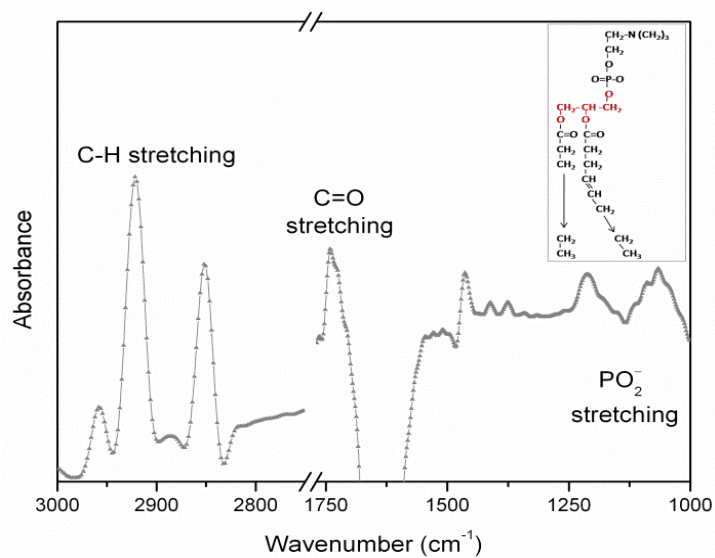


Figure 3.18: Structure of the BetP trimer to a resolution of 2.7 Å in complex with 8 POPG lipids (Koshy, C. et al., 2013). **(A)** The lipids are found in the center (yellow) stabilizing the C-terminal domains, in between two adjacent protomers (orange) and at the perimeter of individual protomers (blue). They span the whole bilayer reaching to the amphiphatic helix h7 (blue) that is plunging in the upper part of at the periplasmic leaflet **(B)** Freeze-Fracture image of closely packed, vesicular BetP 2D crystals and projection map of these crystals. Each protomer (red surface) is surrounded by a large belt of bulk lipids (blue surface), which enables us to use 2D crystals for this study (Fig. from Güler, G. et al., to be published).

The activation threshold of BetP depends crucially on the lipid composition of the surrounding membrane, e.g., BetP reaches its activity optimum at higher osmolalities in more negatively charged lipid environments. Although structural studies revealed lipid interaction sites in BetP, the dynamical role of lipids during transport regulation is still not clear. In the current study, we investigate the nature of lipid-protein interactions of BetP reconstituted in 2D crystals and probed at the molecular level by using ATR-FTIR spectroscopy to identify specific changes under activating conditions upon K^+ incubation.

Figure 3.19: The ATR-FTIR absorbance spectrum of Cg-liposomes. The inset represents the molecular structure of phospholipids.



C. glutamicum membranes comprise only anionic glycerophospholipid species, phosphatidylglycerol (PG), phosphatidylinositol (PI) and cardiolipin (CL) (each at approx. 1/3)²⁰ (Fig. 3.19, inset). The polar headgroups and non-polar acyl chains of lipid bilayer cause distinct positions in the IR spectrum due to the CH₃, CH₂, C=O and PO₂⁻ stretching modes which serve for analyzing the physical properties of membrane lipids and lipid-protein interactions (Fig. 3.19). The IR spectrum of *C. glutamicum* liposomes, i.e., protein free liposomes prepared from the *C. glutamicum* lipids, which will in the following be denominated as Cg-liposomes and serve as a control, was recorded in H₂O without K⁺. The IR signatures of the phospholipids arise from the antisymmetric and symmetric stretching vibrations of the phosphate moiety (PO₂⁻) in the polar headgroups (1300-1150 cm⁻¹) that make hydrophilic interactions with the protein *via* H-bonding and arise from the carbon-hydrogen (CH₃ and CH₂) antisymmetric and symmetric stretching vibrations (3000-2800 cm⁻¹) that are sensitive to static order and dynamics of the acyl chains in the hydrophobic region of the membrane. Additionally, the C=O stretching modes of the ester carbonyl groups in the interfacial part (1760-1700 cm⁻¹) are sensitive to H-bonding and polarity changes in their environment^{54,55}. The band positions and assignments of phospholipids for Cg-liposomes and of vesicular closely packed 2D crystals (Fig. 3.18B) in which BetP is reconstituted into *C. glutamicum* lipids in a LPR of 0.2 (w/w) are

shown in Table 3.3 (For band assignments see^{54,55,58}). The use of closely packed BetP 2D crystals provides an elevated amount of protein, however, with a minimum of crystal contacts as it can be anticipated from the projection structure of BetP WT in Cg-lipids (Inset, Fig. 3.18B, Ref.⁵²).

Position (cm ⁻¹), Cg-liposomes	Position (cm ⁻¹), BetP WT	Band assignment
2957	2957	CH ₃ stretching (antisymmetric)
2920	2917	CH ₂ stretching (antisymmetric)
2873	2972	CH ₃ stretching (symmetric)
2851	2849	CH ₂ stretching (symmetric)
1741, 1720	1742	C=O stretching (esters)
1466	1469	CH ₂ bending, scissoring
1453 (shoulder)	1454	CH ₂ bending, scissoring
1415	1417 (shoulder)	CH ₃ bending (symmetric)
1378	1386, 1368	CH ₃ bending, deformation (symmetric)
1206	1239	PO ₂ ⁻ stretching, double bond (antisymmetric)
1172	1172	C-O stretching
1148	1150	C-C stretching
1091	1092	PO ₂ ⁻ stretching, double bond (symmetric)
1070	1071	R-O-P-O-R`

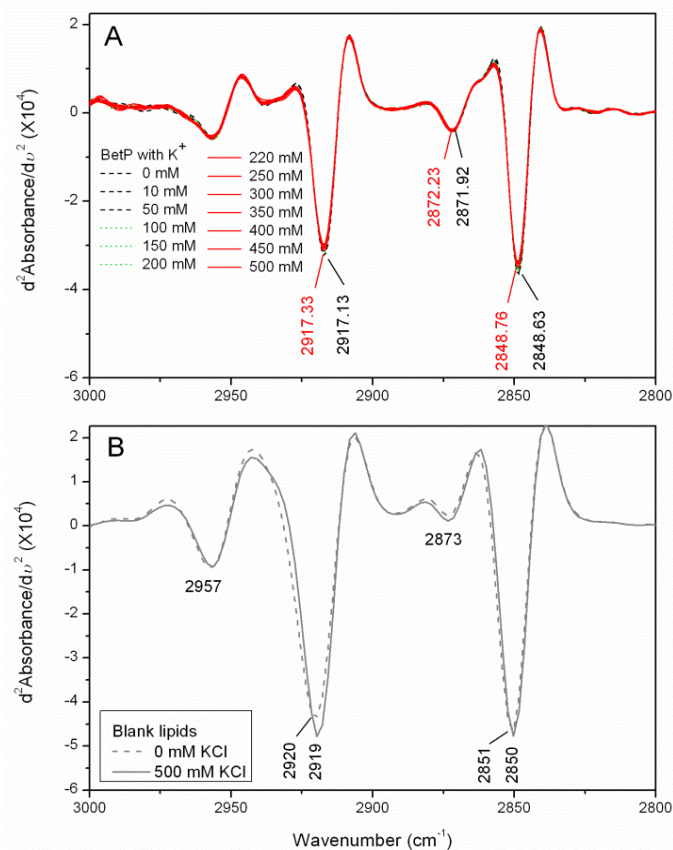
Table 3.3: Band positions and assignments of phospholipids in the IR spectrum for Cg-liposomes and BetP 2D crystals in H₂O. The peak positions were determined from the absorbance spectrum in Fig. 3.19 and 2nd derivative spectra.

3.6.1 C-H stretching modes from the hydrophobic tails of lipids

Fig. 3.20 shows the IR second derivative spectra of Cg-liposomes and BetP 2D crystals, which recorded during increasing K⁺ concentrations (0→500 mM). The carbon-hydrogen stretching modes from the hydrophobic tails of bilayer lipids give rise to the strongest absorbance bands in the spectral region 2800-3100 cm⁻¹ with their position, depending on the acyl chain packing and conformation. However, the bending vibrations (scissoring, wagging) of those molecules give rise to weak signals in the 1350-1500 cm⁻¹ region (as seen from Fig. 3.19) and overlap with a number of side chains of the proteins. Henceforth, one can reveal the potential interactions of hydrophobic part of the lipid bilayer with the protein, by following these signals. In particular, the C-H stretching vibrations are used to obtain information regarding the freedom of motion and fatty acyl order⁵⁶. According to Fig. 3.20B, Cg-liposomes exhibited band positions at 2920 and 2851 cm⁻¹ attributed to the antisymmetric

and symmetric CH_2 stretching vibrations, respectively, and at 2873 and 2957 cm^{-1} arising from the antisymmetric and symmetric CH_3 stretching vibrations, respectively. These peak positions observed for the blank lipid samples (Fig. 3.20B) are downshifted regardless of K^+ concentration when the BetP protein (Fig. 3.20A) is embedded into the lipid bilayer ($2920 \rightarrow 2917\text{ cm}^{-1}$, $2851 \rightarrow 2849\text{ cm}^{-1}$ for the CH_2 modes and $2957 \rightarrow 2956\text{ cm}^{-1}$, $2873 \rightarrow 2872\text{ cm}^{-1}$ for the CH_3 modes). In comparison to the pure lipids, the band positions of both CH_2 and CH_3 modes for 2D crystals of BetP WT are at lower position. This indicates that the orientation of the membrane lipid acyl chains in the hydrophobic region is noticeably ordered in the presence of BetP, resulting in a favorable alteration in the lipid chain packing for the protein-lipid system.

Figure 3.20: The influence of K^+ ions on the hydrophobic lipid tails. The IR second derivative spectra show the C-H stretching modes for (A) BetP 2D crystals and (B) Cg-liposomes in H_2O buffer in the course of increasing K^+ concentration.



Cg-liposomes and 2D crystals of wild type BetP were stepwise titrated with increasing K^+ concentration in H_2O buffer from 0 mM (1^{st} cycle of the inactive state) to 500 mM (active state), afterwards, 0 mM K^+ switched again (2^{nd} cycle of the inactive state). The total ionic strength was kept

constant to prevent non-specific conformational alterations upon changes of ion shielding. According to previous studies, BetP was shown not to be activated by increasing internal Na^+ concentrations¹⁷; therefore, NaCl within the NaP_i buffer was replaced with KCl to adjust the final concentration of ionic strength to totally 500 mM. As shown in Fig. 3.20A, an increase in the K^+ concentration perturbs the fatty acid moieties in the IR spectrum of the reconstituted BetP sample into anionic lipids. Both CH_2 and CH_3 stretching vibrations of the fatty acid chains are slightly upshifted upon K^+ -induced activation of BetP ($2848.6 \rightarrow 2848.7 \text{ cm}^{-1}$ for the $\nu_s(\text{CH}_2)$ modes and $2871.9 \rightarrow 2872.2 \text{ cm}^{-1}$ for the $\nu_s(\text{CH}_3)$ modes) suggesting minor conformational disordering of the acyl chains in the hydrophobic part of the lipid-BetP system. Although these changes are small, they can be reliably measured. When BetP 2D crystals were again perfused with inactivating buffer for the second time which does not involve K^+ ions (2nd cycle of inactivation), these IR signals shift to a slightly lower position again, close to the position recorded during the 1st circulation of inactivating buffer without K^+ ions. On the other hand, the frequency of the CH_2 stretching modes for the blank lipid samples downshifts ($2920 \rightarrow 2919 \text{ cm}^{-1}$ and $2851 \rightarrow 2850 \text{ cm}^{-1}$) while its CH_3 stretching modes located at around 2957 and 2873 cm^{-1} do not change significantly in response to a rise in the K^+ concentration (Fig. 3.20B).

The wavenumber changes determined from the IR second derivative spectra were drawn as a function of increasing K^+ concentration from 0 mM to 500 mM and represented in Fig. 3.21A,B. According to the graphs, the peak positions of the C-H stretching signals for the 2D crystals of BetP sample are slightly but consistently shift upward whereas those signals for the pure lipid sample in the absence of protein exhibits a random behavior, either downshifts (CH_2 signals) or remains constant (CH_3 signals) upon an increment in the K^+ concentration.

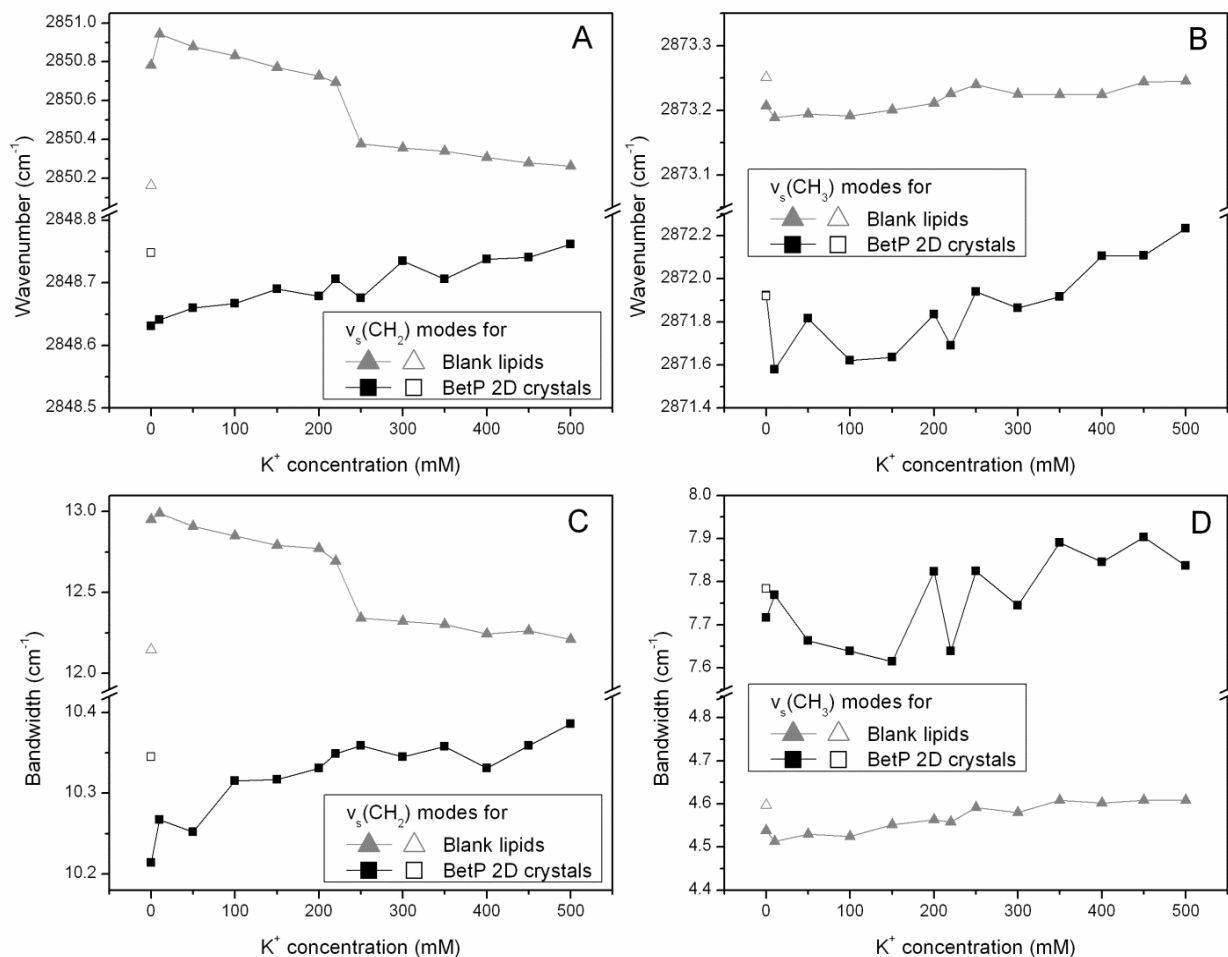


Figure 3.21: The shift of the peak position and full width at half maximum (FWHM). **(A, C)** The CH₂ and **(B, D)** CH₃ symmetric stretching modes for Cg-liposomes (▲) and BetP 2D crystals (■) with respect to increasing K⁺ in H₂O buffer. The peak positions were obtained from the IR 2nd derivative spectra while the FWHM was obtained from the absorbance spectra. Open signs represent the 2nd circulation of the inactivating buffer which does not include K⁺.

In this study, the bandwidths at half-height for the symmetric stretching of CH₂ and CH₃ modes were determined from the absorbance spectra and were also plotted as a function of increasing K⁺ concentration (Fig. 3.21C,D). The plots of the change in the bandwidth are very similar to those of wavenumber shifting. Both antisymmetric (data not shown) and symmetric stretching vibrations of CH₂ and CH₃ modes for the 2D crystals of BetP sample broaden slightly with increasing K⁺ which is not observed for Cg-liposomes. This indicates that K⁺ ions induce to some extent an increment in the dynamics of the fatty acyl chains. The frequencies of the C-H stretching modes have a tendency

to upshift and to become broad bands in the presence of K^+ ions even though a minute change is monitored in the FTIR spectra for those modes of the lipid-protein system. This is usual case due to the fact that the non-polar C-H molecules of the lipid acyl chains do not make H-bonds with the solvent, and thus, found in the hydrophobic part of the lipid bilayer excluding from water. Particularly, the position and bandwidth of the CH_3 stretching modes for the BetP-lipid system are exactly the same during perfusion of the 1st and 2nd cycle of inactivating buffer without K^+ ions, becoming a narrower band and having a lower frequency as compared to the recorded spectra under high $[K^+]$. Altogether the FTIR data strongly suggest that the hydrophobic tails of the lipids involved in lipid-protein interactions become more mobile and even disordered upon K^+ -induced activation of BetP.

3.6.2 PO_2^- stretching modes from the phospholipid headgroups

One of the reporter groups for probing the lipid-protein interactions near to the membrane surface is the infrared signatures of the phosphate moiety found in the hydrophilic region of the phospholipids. As represented in Table 3.3, the O-P-O antisymmetric and symmetric stretching vibrations are located in a wide range at about 1190-1265 cm^{-1} and around 1100-1050 cm^{-1} , respectively, and are very sensitive to hydrogen bonding. Therefore, the number of these bands and their exact frequency depends strongly on the hydration state of the lipids. The frequencies of the O-P-O stretching modes are downshifted due to hydration while upshifted upon dehydration of phosphate headgroups^{54,96}.

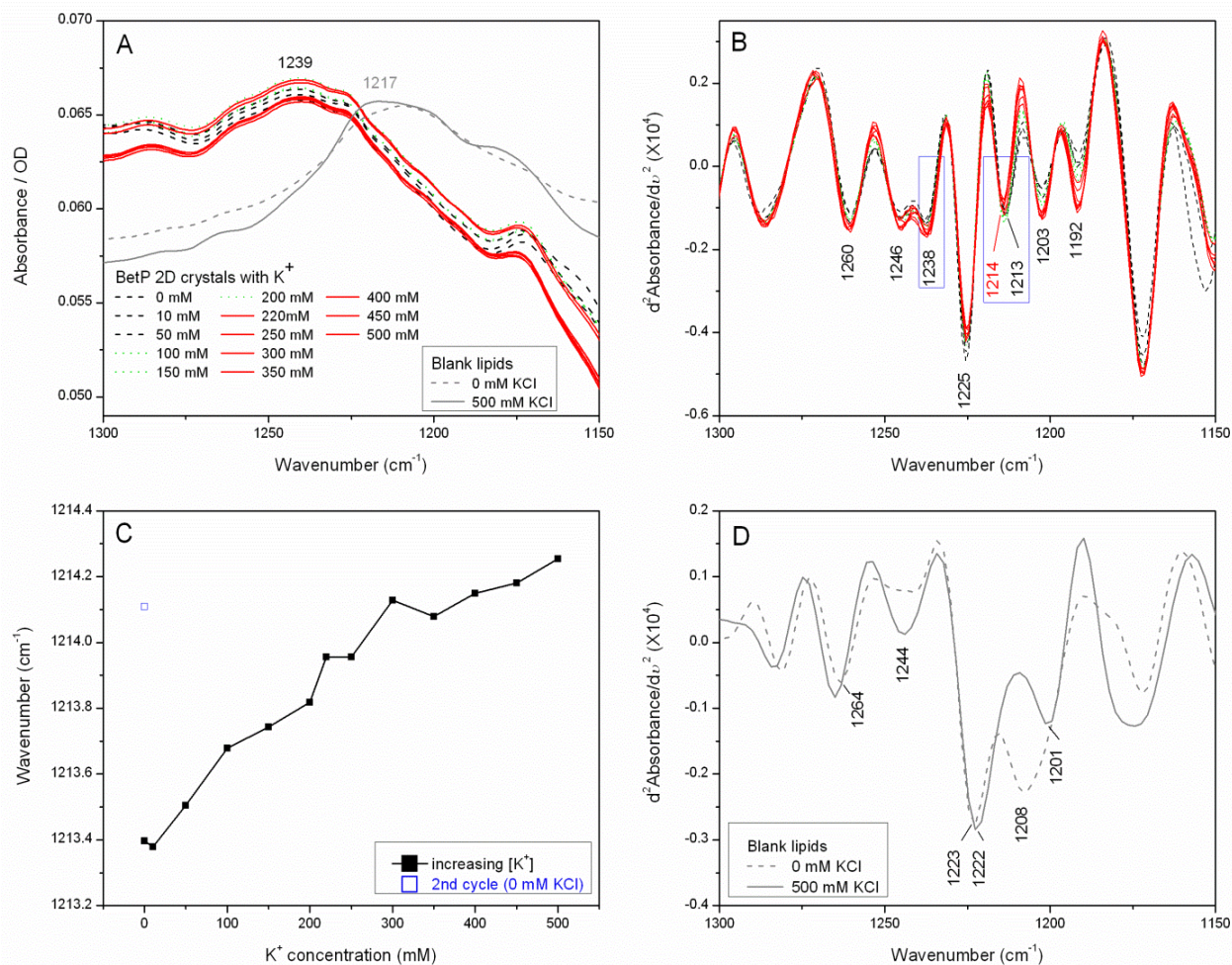


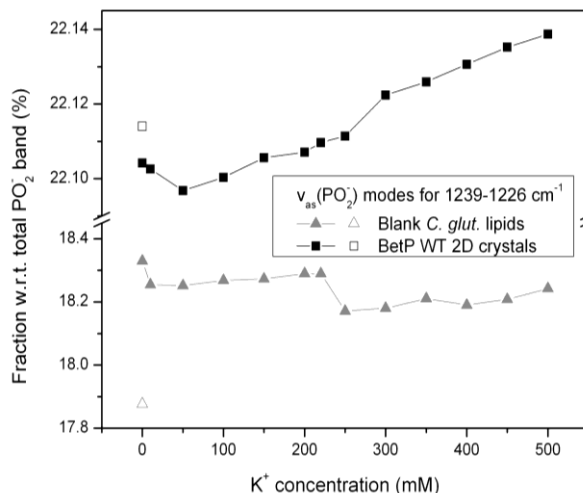
Figure 3.22: The influence of K^+ on the PO_2^- modes of phospholipid headgroups. The $\nu_{as}(PO_2^-)$ modes in the IR absorbance (**A**) and second derivative spectra for (**B**) BetP 2D crystals and (**D**) for Cg-liposomes recorded at pH7.5. (**C**) The shift of the peak position around 1213 cm^{-1} for BetP was drawn from the second derivative spectra shown in (**B**). Open sign in (**C**) represents the 2nd circulation of the inactivating buffer which does not include K^+ .

Fig. 3.22A shows the antisymmetric stretching vibrations of O-P-O modes in the IR absorbance spectra ($1300\text{--}1150\text{ cm}^{-1}$) for pure lipids and BetP WT 2D crystals in the course of increasing K^+ concentration ($0 \rightarrow 500\text{ mM}$). These $\nu_{as}(PO_2^-)$ modes give rise to a broad band at around 1239 cm^{-1} for BetP WT reconstituted in phospholipids (Table 3.3). Since the band position of the pure lipids appearing around 1217 cm^{-1} is strikingly away from the frequency of the protein/lipid system (1239

cm^{-1}); it is conceiving that BetP interacts with the headgroups of the lipids regardless of K^+ concentration, resulting in less stable H-bonding/electrostatic interactions, and thereby altering the electronic microenvironment of the phosphate headgroups. Nevertheless, splitting of these bands into seven positions absorbing at 1260, 1246, 1238, 1225, 1213, 1203 and even 1192 cm^{-1} (inactive state with 0 mM K^+) for the BetP-lipid system is well recognized in the second derivative spectrum which is one of the band narrowing techniques used most (Fig. 3.22B). On the other hand, as shown in Fig. 3.22D the second derivative spectrum of the pure lipids has a different profile as compared to the BetP-lipid system that $\nu_{\text{as}}(\text{PO}_2^-)$ modes have four band positions absorbing at 1264, 1244, 1223 and 1208 cm^{-1} (at 0 mM K^+). Therefore, if the protein is interacting with phospholipids, at least three different forms of PO_2^- groups gain a distinct position due to a change in the H-bonding properties and/or electrostatic interactions, i.e., PO_2^- groups of hydrated phospholipids are in the polar environment and therefore maintain H-bonding interactions with the solvent. The strength of H-bonding to the O-P-O bond alters the electron density around the O-P-O bond of the phosphate headgroups inducing a change in the vibrational frequency of the O-P-O bond. The frequencies of the PO_2^- groups of hydrated phospholipids are observed at a lower frequency in comparison to anhydrous phospholipids. Therefore, the observed 3 different frequencies reflect a different hydration status and H-bonding strength if BetP is reconstituted into the phospholipid bilayer. Particularly, a band located at around 1244 cm^{-1} in the case of pure lipids is split into two bands located at 1246 and 1238 cm^{-1} attributed to the free/weakly H-bonded lipid headgroup molecules if BetP is reconstituted in anionic lipids. This implies that at least one of these bands (1246 or 1238 cm^{-1}) can be an actor group which directly interacts with the hydrophilic part of BetP. This suggests that the lipid-protein interactions substantially influence some PO_2^- groups which are located in the polar environment of the protein (periplasmic and/or cytoplasmic sites), resulting in a

change of the hydration status of the PO_2^- groups and in the H-bonding strength disregarding of K^+ ions.

Figure 3.23: The fraction of the $\nu_{\text{as}}(\text{PO}_2^-)$ modes for Cg-liposomes and BetP WT 2D crystals at pH7.5. The $\nu_{\text{as}}(\text{PO}_2^-)$ bands from the absorbance spectra were integrated for the range 1239-1226 cm^{-1} (free/weakly H-bonded) and 1265-1190 cm^{-1} (total $\nu_{\text{as}}(\text{PO}_2^-)$ band). Afterwards, the relative fraction of each component was calculated with respect to the total band area. Open signs represent the 2nd circulation of the inactivating buffer which does not include K^+ .

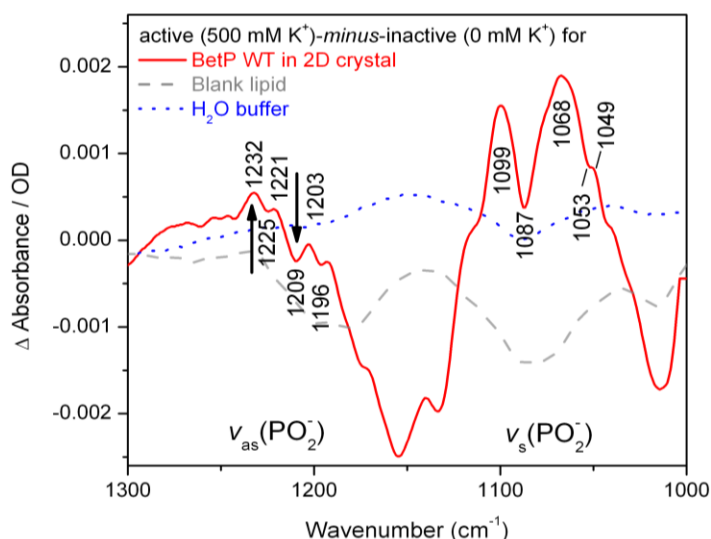


However, upon a rise in the K^+ concentration, the intensity at 1225 and 1213 cm^{-1} attributed to the strongly H-bonded phosphate headgroups decreases concomitant with a shift towards higher wavenumbers (1213 \rightarrow 1214 cm^{-1}) while the intensity at 1260, 1246 and 1238 cm^{-1} ascribed to the free/weakly H-bonded phosphate headgroups increases (for band assignments see^{54,55}). The shift of the peak position around 1213 cm^{-1} determined from the second derivative spectra was plotted with respect to increasing K^+ concentration (Fig. 3.22C). This band undergoes a slight downshift under the second perfusion of 0 mM K^+ (2nd cycle of inactivation). The fraction of the antisymmetric stretching of O-P-O modes, $\nu_{\text{as}}(\text{PO}_2^-)$, around 1238 cm^{-1} was obtained from the absorbance spectra and drawn as a function of increasing K^+ concentration (Fig. 3.23). The relative percentage of this component was calculated by integrating the spectral range 1239-1226 cm^{-1} (free/weakly H-bonded) and 1265-1190 cm^{-1} (total $\nu_{\text{as}}(\text{PO}_2^-)$ band). Afterwards, the integrated intensity around 1238 cm^{-1} was divided by the integration of total band area. The blank lipid samples were also added in the graphs for comparison. According to Fig. 3.23, the population of $\nu_{\text{as}}(\text{PO}_2^-)$ modes around 1239-1226 cm^{-1} does not change significantly below 220 mM K^+ but their fraction increases above 200 mM K^+ concentration. Interestingly, the population in this range decreases and comes almost back to the

initial value when the BetP sample was perfused again with 0 mM K^+ (2nd cycle of inactivation) which is not the case for Cg-liposomes, In the FTIR spectra, we observe an upshifting from 1213 to 1214 cm^{-1} that indicates weakening and/or loss of H-bonds. Consistently, the population of free/weakly H-bonded lipid headgroups ($\sim 1238\text{ cm}^{-1}$) increases upon K^+ -induced activation of BetP. Although the spectral alterations for both antisymmetric and symmetric O-P-O stretching vibrations are relatively small ($\sim 1\text{ cm}^{-1}$), the changes are consistent.

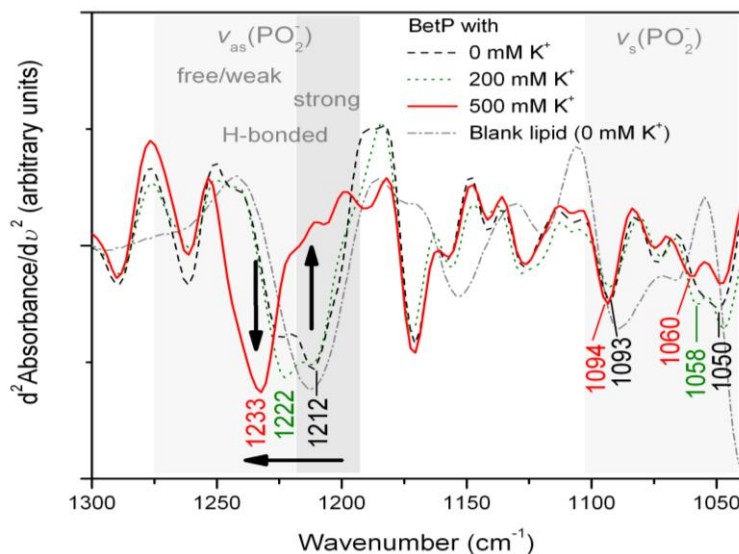
These results were confirmed by the ATR-IR difference spectrum (active-*minus*-inactive) of active (high K^+) and inactive (no K^+) BetP reconstituted in 2D crystals (Fig. 3.24). IR-difference spectra of the blank lipid sample as well as buffer difference were added in the graphs for comparison. The IR buffer difference was recorded as (activating buffer with 500 mM K^+)-*minus*-(inactivating buffer without K^+), taking the reference as potassium-free buffer (inactivating buffer) in the absence of the protein. Again the population of both free/weakly H-bonded $\nu_{as}(PO_2^-)$ and $\nu_s(PO_2^-)$ modes increases at around 1232 cm^{-1} and 1099/1068 cm^{-1} , respectively, concomitant with a decrease in the intensity of stronger H-bonded headgroups absorbing at 1209 cm^{-1} and around 1087/1053 cm^{-1} . Such spectral differences are not observed for blank lipid which provides strong evidence for the liberation of some phospholipid head groups with an elevated K^+ concentration.

Figure 3.24: The IR difference spectrum of BetP WT showing the $\nu_{as}(PO_2^-)$ and $\nu_s(PO_2^-)$ modes at pH7.5. The difference spectrum of BetP (—) was recorded taking the reference as inactive state: (active)-*minus*-(inactive). The blank lipid-difference (---) and H₂O buffer-difference (···) were recorded taking the reference as inactivating buffer condition: (buffer or lipid at 500 mM K^+)-*minus*-(buffer or lipid without K^+).



Deuterated phospholipids headgroups — In order to validate the effect of K^+ ions on the H-bonding properties and hydration state of the membrane lipid headgroups, BetP WT 2D crystals and Cg-liposomes were incubated in D_2O buffer in the absence (0 mM K^+) and presence (200 mM and 500 mM) of K^+ ions and kept 3 days at $+4^\circ C$. Afterwards, they were analyzed with FTIR spectroscopy in the transmission mode at $+4^\circ C$ (Fig. 3.25).

Figure 3.25: The IR second derivative spectra for the $\nu_{as}(PO_2^-)$ and $\nu_s(PO_2^-)$ modes. Cg-liposomes and BetP WT 2D crystals were incubated 3 days at $+4^\circ C$ in D_2O which involves various concentrations of K^+ (0, 200 and 500 mM).



Obviously, the protein-lipid system harbors again three more components for the phospholipids PO_2^- modes (both antisymmetric and symmetric stretching) as compared to pure lipids which have only one component at 1213 cm^{-1} (with 0 mM K^+). Protein reconstitution leads to bands absorbing at 1262 , 1244 and 1224 cm^{-1} (with 0 mM K^+), indicating the presence of both free/weak and strong H-bonds. This determination matches definitely with the spectra recorded in H_2O buffer. These components are significantly perturbed with K^+ ions. BetP WT 2D crystals exhibit a band at 1212 cm^{-1} (strong H-bonded) in the deuterated solution without K^+ ions whereas this band position shifts upward to 1222 cm^{-1} and 1232 cm^{-1} (free/weak H-bonded) in the presence of 200 mM and 500 mM K^+ , respectively (Fig. 3.25). A large upshifting of both antisymmetric and symmetric stretching vibrations of O-P-O modes ($1212 \rightarrow 1222 \rightarrow 1233\text{ cm}^{-1}$ for $0 \rightarrow 200 \rightarrow 500\text{ mM } K^+$ ions, respectively) together with the appearance of a strong band at 1233 cm^{-1} indicative for free/weakly H-bonded

headgroups that proves the release of some of anionic phospholipids headgroups formerly bound to BetP under activating high K^+ conditions.

Thermal stability of anionic phospholipids headgroups — Fig. 3.26A represents the thermal stability of lipid headgroups for the blank lipids and for BetP WT 2D crystals. The peak positions of the phospholipid $\nu_{as}(PO_2^-)$ modes were determined from the second derivative spectra in 2H_2O buffer monitored with FTIR spectroscopy in the transmission mode and were plotted with respect to increasing temperature from $4^\circ C$ to $96^\circ C$ recorded in $2^\circ C$ intervals. The plot clearly indicates that in the presence of $500\text{ mM } K^+$ BetP 2D crystals exhibit a sharp phase transition at $49^\circ C$ which is quite lower value than for pure lipids ($57^\circ C$). On the other hand, the lipid-protein system in the presence of 0 mM and $200\text{ mM } K^+$ does not show a transition state but undergoes a slight instability only in the range $10\text{-}28^\circ C$. This suggests that high K^+ concentration (500 mM) induces a dramatic change in the H-bonding strength of the membrane lipid headgroups for reconstituted BetP and results in a more accessible anionic lipid headgroups exposed to the solvent.

Fig. 3.26B and C present the percentage of the $\nu_{as}(PO_2^-)$ modes for pure lipid and BetP WT reconstituted in 2D crystals in D_2O buffer. The relative fraction of each component was calculated with respect to the total band area from the absorbance spectra and was drawn as a function of increasing temperature. Pure lipids without K^+ displays 49% of lipid headgroups in the high frequency-region ($1275\text{-}1219\text{ cm}^{-1}$) while the lipid-protein system harbors 80% ($500\text{ mM } K^+$), 60% ($200\text{ mM } K^+$) and 50% ($0\text{ mM } K^+$) of those modes. Here, we can conclude that the population of free/weak H-bonded lipid headgroups increases under the high K^+ concentration whereas the amount of the stronger H-bonded lipid headgroups decreases. According to the plots in Fig. 3.26B,C, BetP WT 2D crystals exhibit the most dramatic change with increasing temperature in the presence of high K^+ (500 mM). Its low-frequency fraction in the range $1219\text{-}1184\text{ cm}^{-1}$ increases from 20% to 54% while its high-frequency percentage decreases from 80% to 46% . This indicates

that 34% of lipid headgroups becomes more H-bonded upon increasing temperature from 4 to 94°C due to an increased dynamics of lipid head groups upon K^+ -induced activation of BetP.

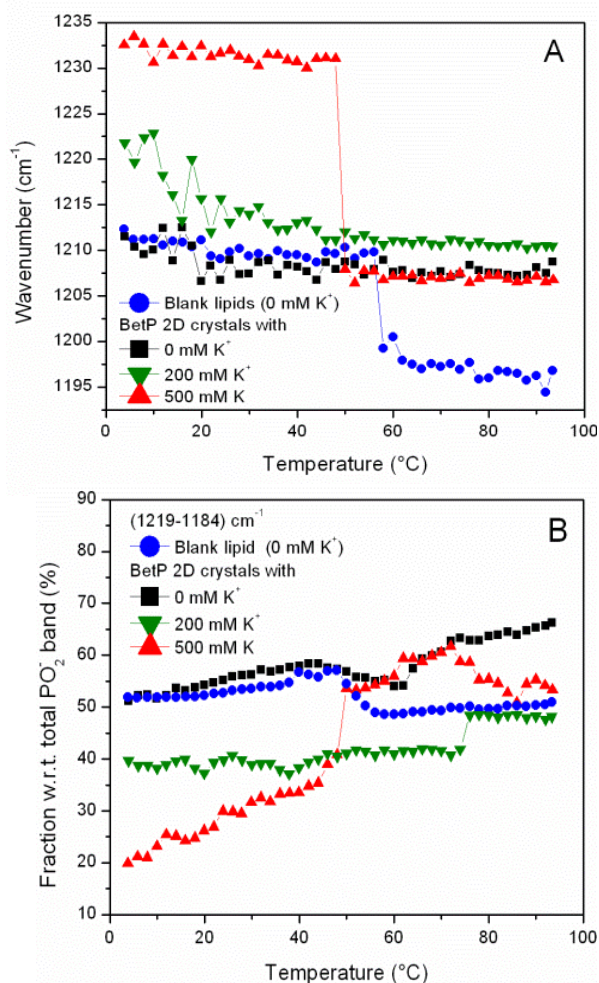


Figure 3.26: (A) The shift of the peak positions for the $\nu_{as}(PO_2^-)$ modes *versus* temperature (4 \rightarrow 94°C) for Cg-liposomes and BetP WT 2D crystals at pD7.5. The fraction of the low-frequency (B) and high-frequency (C) $\nu_{as}(PO_2^-)$ modes. The $\nu_{as}(PO_2^-)$ bands from the absorbance spectra were integrated for the range 1275-1219 cm^{-1} (free/weakly H-bonded), 1219-1184 cm^{-1} (strongly H-bonded) and 1275-1184 cm^{-1} (total $\nu_{as}(PO_2^-)$ band). Afterwards, the relative fraction of each component was calculated with respect to the total band area.

3.6.3 C=O stretching modes from the phospholipid carbonyl groups

The C=O stretching modes from the interfacial part of the membrane give rise to a broad band between 1760 and 1700 cm^{-1} that is influenced by the strong absorption of Asp/Glu residues⁵⁵. The C=O modes from those charged residues are downshifted by a few (5-10) cm^{-1} in 2H_2O while the vibrations arising from the lipid ester carbonyl groups are not affected by the $^1H \rightarrow ^2H$ isotope exchange. Thereby, one can easily distinguish these signals in an infrared spectrum.

In the second derivative spectrum at the higher end of the C=O range (towards 1750-1735 cm^{-1}), we observed minute spectral alterations in the presence of high K^+ concentration (Fig. 3.27A). Since the band positions at this region did not response to hydrogen/deuterium exchange (data not shown) and this range is unusual for Asp/Glu C=O groups in $^2\text{H}_2\text{O}$, these vibrations can be assigned to the ester carbonyl groups. From this point of view, we can conclude that the double bond character of the C=O modes from ester carbonyl groups is slightly perturbed in response to K^+ -stimulated activation of BetP.

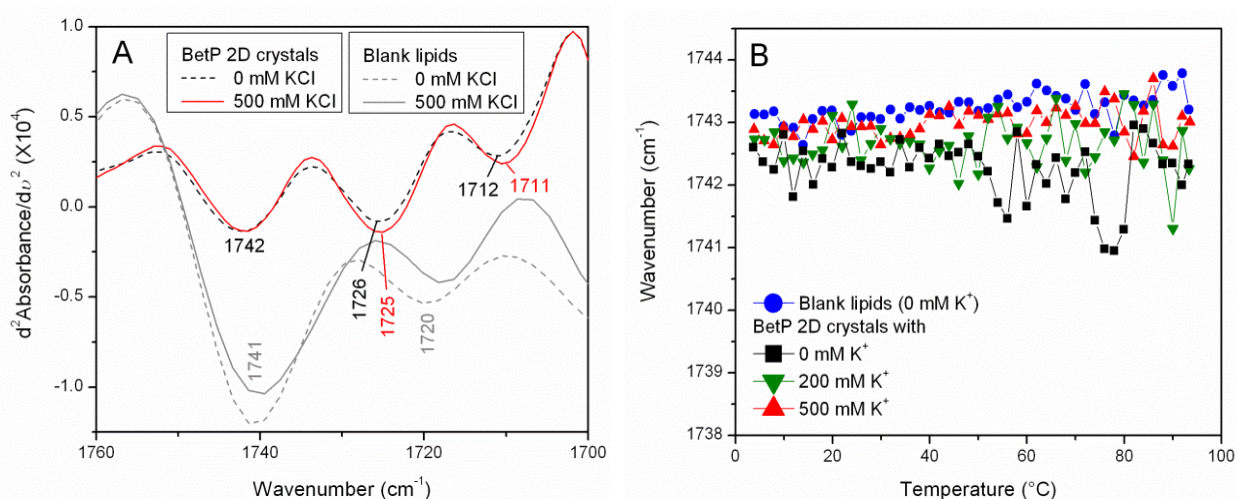


Figure 3.27: (A) The IR 2nd derivative spectra for the C=O stretching region (1760-1700 cm^{-1}) in the absence (Cg-liposomes) and presence of BetP at pH 7.5. (B) Lipid C=O stretching vibrations at around 1743 cm^{-1} versus temperature (4 \rightarrow 94 $^{\circ}\text{C}$) for Cg-liposomes and BetP 2D crystals at pH 7.5.

A broad single C=O band which appears around 1735 cm^{-1} in the absorbance spectrum (Fig. 3.19) is split into two positions in the second derivative spectrum depending on its hydration status (Fig. 3.27A). The second derivative spectra represent the C=O stretching region (1760-1700 cm^{-1}) in H_2O buffer recorded for the inactive (with 0 mM K^+) and active state (500 mM K^+) of BetP WT and for blank lipid. Pure lipids exhibit two components at around 1741 cm^{-1} (not H-bonded) and around 1720 cm^{-1} (H-bonded) due to probably two different forms of carbonyl-water interactions^{55,96-98}.

However, BetP 2D crystals exhibit band positions at 1742, 1726 and 1712 cm^{-1} which overlap with the Asp/Glu C=O groups in H_2O . Overall, insertion of the protein into the membrane lipids decreases the mobility of the ester carbonyl groups located at the membrane-water interface and restricts the accessibility of the membrane surface to water molecules, indicated by narrower and upshifted infrared signals, respectively. This is most probably related to the effect of the protein on the lipid structure and dynamics, but not associated with direct interaction of phospholipid carbonyl groups with the protein itself because this mode (1742 cm^{-1}) did not respond to increasing temperature up to 94°C both in the active and inactive state of BetP recorded in $^2\text{H}_2\text{O}$ (Fig. 3.27B).

Discussion about Lipid-protein interactions of BetP — Probing the lipid-protein interactions on the molecular level represents a key experiment on the way towards an understanding of membrane transport. Here, our FTIR data reveal the effect of activating K^+ ions on lipids accommodating BetP in an artificial bilayer. In this study we have used 2D crystals of native *C. glutamicum* lipids, in which BetP is highly enriched⁹² ensuring a sufficient interaction cross section of lipids with BetP (Fig. 3.18B).

However, interactions will always include both protein-associated lipids whose molecules bind tightly to the specific binding site of the protein and bulk bilayer lipids whose molecules do not bind directly to the protein environment but are influenced from the lipid-lipid interactions. In the case of BetP a recent high-resolution structure has revealed specific lipid-binding sites (Fig. 3.18A) that interact directly with the protein and enable us (at least to some extent) to interpret the wealth of data we could obtain by IR spectroscopy.

Insertion of BetP into the lipid bilayer results in significant conformational ordering of the lipid tails compared to a lipid bilayer without protein (Fig. 3.20). From the crystal structure of BetP⁹⁵ it is obvious that the central lipids (yellow, Fig. 3.18A) and annular lipids show straightened fatty acid tails due to hydrophobic protein interactions with transmembrane helix 2 and the amphiphatic helix h7.

Subsequently, K^+ induces a conformational disordering of the acyl chains, i.e., an increase in dynamics of the hydrophobic lipid tails (Figs. 3.20 and 21). These changes in mobility of fatty acyl chains deep in the membrane leaflet at elevated K^+ concentration might be part in the activation mechanism and reflect an altered interaction between BetP and lipids. Although we can not quantitatively distinguish an effect on bulk lipids or on lipids that are directly associated to BetP, here we assume that especially the fatty acid chains of the central lipids and one of the peripheral lipid (blue, Fig. 3.18A), which are in close contact with the amphiphatic helix h7 contribute to this effect. As these lipids stabilize the trimeric assembly, we assume that activation requires a more flexible trimeric architecture to adopt the active state. Looking at the unsaturated fatty acyl chains resolved in the BetP structure we observe a lower interaction surface compared to the saturated chain. However, functional studies have shown that the unsaturated fatty acid chain is essential for regulation. We can only speculate that the binding of this chain to BetP is not favored and instead a pre-requisite to have certain parts of BetP not restricted to lipid-protein interactions.

The hydrophilic region of the bilayer lipids is also affected by BetP reconstitution, causing a dramatic change in the hydration status of the phosphate moiety (Fig. 3.22). Some of the anionic lipid head groups are hydrated while others are dehydrated upon interaction indicated by down- or upward shifting of the O-P-O stretching IR signals, respectively. Upon a rise in the K^+ -concentration, the FTIR data reveal an increase in intensity of high-frequency region and shifting of O-P-O stretching signals to higher values (Figs. 3.22-26). A high K^+ concentration (500 mM) results in a pronounced change in the H-bonding strength of lipid headgroups of 2D crystals of BetP and renders anionic lipid headgroups more accessible to the solvent (Fig. 3.26). The population of free/weakly H-bonded lipid headgroups absorbing at 1238 cm^{-1} increases significantly with elevated K^+ concentration, reflecting weakening or release of the membrane lipid headgroups from the bound state upon

K⁺-binding. Again, we assume that the FTIR data describe partly the effect of central lipids as they interact with their head groups with the osmo-sensing C-terminal domains.

The C-terminal domain of BetP, which protrudes into the cytoplasm, comprises a number of positively charged arginine residues which could be a possible interaction partner with anionic lipid head groups but also with negatively charged side chains (Asp/Glu) from the protein environment. Such clusters can be found in the N-terminal domain and in loop 2. Recently, the ionic interaction of terminal domains with cytoplasmic loops *via* charged residues has been described³⁷. A change in the intensity of the arginine signals as well as activation-induced alterations in the population and H-bonding properties of C=O stretching modes from the protonated Asp/Glu residues absorbing in the range of 1700-1725 cm⁻¹ (for band assignments see Refs.^{45,82}) were detected in the difference spectra of the deuterated sample (*active-minus-inactive*) for BetP 2D crystals under an elevated K⁺ concentration (Section 3.4 and Fig. 3.27A). Starting from this point we can postulate that negatively charged phosphate lipid headgroups are released from the positively charged Arg residues located at the end of C-terminal domain upon K⁺-binding and might undergo a change in interaction towards loops or the N-terminal domains.

In this context, the FTIR data suggest that due to K⁺ activation the positively charged C-terminal domains switch their interaction partner from lipids (under down-regulating conditions) to protein-interactions, which could also involve intratrimeric interactions between C-terminal domains as suggested by structural studies¹⁴ and the fact that monomeric BetP is down-regulated. The C-terminal domains also comprise negatively charged Glu-residues approximately at a location where C-terminal domains of individual trimers are crossing each other, which can not be mutated without loss in regulation. This interpretation would also be in agreement with the observed lipid dependency of K⁺-activation, which is reflected by a significant shift to higher K⁺ concentration in a negatively charged lipid environment.

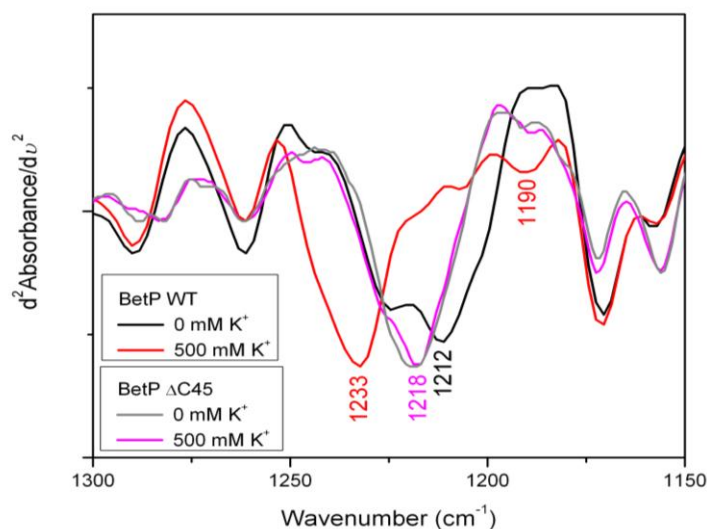
According to the FTIR data, the phospholipid carbonyl groups are affected neither by K^+ nor by temperature suggesting that there is no direct interaction of these groups with BetP. Moreover Cg-liposomes exhibit identical spectra (Fig. 3.27). The lipid C=O double bonding undergoes minute modifications in terms of H-bonding and polarity in response to a change in the lipid/protein environment upon K^+ -induced activation of BetP. Additionally, the lipid molecules provide a more protecting environment for BetP and this lipid environment is crucial for the stability of the protein if BetP is reconstituted into bilayer lipids (see Section 3.8).

In summary, our findings collected by means of FTIR spectroscopy if they are interpreted in the frame of the structural studies of BetP^{14,25,29} suggest that negatively charged *C. glutamicum* lipids are not only stabilizing the whole transporter core, but are modulating some specific interactions by the hydrophobic tails as well as the hydrophilic headgroups, in response of BetP to K^+ increase (e.g. to hyperosmotic stress). Here, K^+ initiates a release of lipid interactions probably in the center of the trimer, and both on the cytoplasmic and periplasmic side. These alterations will most likely affect the rigidity of the trimer assembly, and the FTIR data support here previous speculations⁹² that small changes in the trimer architecture are exploited for transport regulation.

PO₂⁻ stretching modes for BetP ΔC45 2D crystals — A weak interaction of the C-terminal domain either with adjacent domains of BetP or with the lipid bilayer was suggested by EPR studies³³. To clarify this assumption, BetP ΔC45 2D crystals were incubated 3 days at +4°C in D₂O buffer which involves 0 mM and 500 mM K^+ , and afterwards, analyzed with FTIR spectroscopy. In the second derivative spectrum (Fig. 3.28), the C-terminal truncated BetP 2D crystals exhibit a clear signal at around 1218 cm⁻¹ both in the active and inactive states. This low-frequency mode is attributed to the antisymmetric stretching vibrations of O-P-O modes of the phospholipid headgroups, which are strongly H-bonded. The peak positions of the phospholipids $\nu_{as}(PO_2^-)$ modes are not significantly altered with K^+ . This implies that the phospholipid headgroups surrounding BetP ΔC45 2D crystals

do not respond to K^+ -induced activation in the absence of the C-terminus, as compared to BetP WT 2D crystals which exhibit a pronounced change in the electrostatic and H-bonding properties of the phospholipid headgroups (Fig. 3.25 and 3.28). BetP WT 2D crystals harbor free/weakly H-bonded headgroups at high K^+ , indicating the liberation of some of lipid headgroups formerly bound to BetP under activating high K^+ conditions. According to the functional model of BetP, the C-terminal domain is considered to interact with the membrane phospholipid headgroups in the resting state²⁹. The lack of the C-terminal domain in the BetP $\Delta C45$ 2D crystals renders the phospholipid headgroups stronger H-bonded, most likely with the solvent.

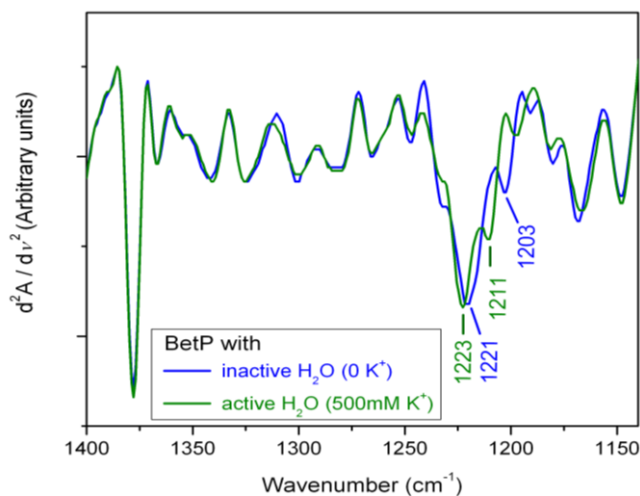
Figure 3.28: The IR second derivative spectra for the $\nu_{as}(PO_2^-)$ modes. BetP $\Delta C45$ 2D crystals were incubated 3 days at $+4^\circ C$ in D_2O which involves 0 mM and 500 mM K^+ . FTIR data of BetP WT 2D crystals were adapted from Fig. 3.25 for comparison.



PO_2^- stretching modes for BetP proteoliposomes — As observed in the IR second derivative spectrum (Fig. 3.29, at pH7.5), the phospholipid $\nu_{as}(PO_2^-)$ modes of BetP WT proteoliposomes exhibit also an apparent shifting towards the high-frequency components ($1203 \rightarrow 1211$ cm^{-1} and $1221 \rightarrow 1223$ cm^{-1}), which is in line with the results obtained for 2D crystals of BetP (see Section 3.6.2). Overall, this argues in favor of a change of the hydration status of the PO_2^- groups under high K^+ , i.e., dehydration of phosphate headgroups results in an upshift of the frequencies of the O-P-O stretching modes. The $\nu_{as}(PO_2^-)$ modes of phospholipid headgroups undergo an upshifting in D_2O as well whereas hydrophobic residues absorbing between 1400 and 1300 cm^{-1} do not change with

deuteration (data not shown). Thereby, the IR spectra recorded both in H₂O and D₂O buffers extremely elicit the effects of K⁺ ions on the membrane lipid headgroups.

Figure 3.29: The IR second derivative spectra for the $\nu_{as}(\text{PO}_2^-)$ modes of BetP WT proteoliposomes in H₂O buffer which involves 0 mM and 500 mM K⁺.



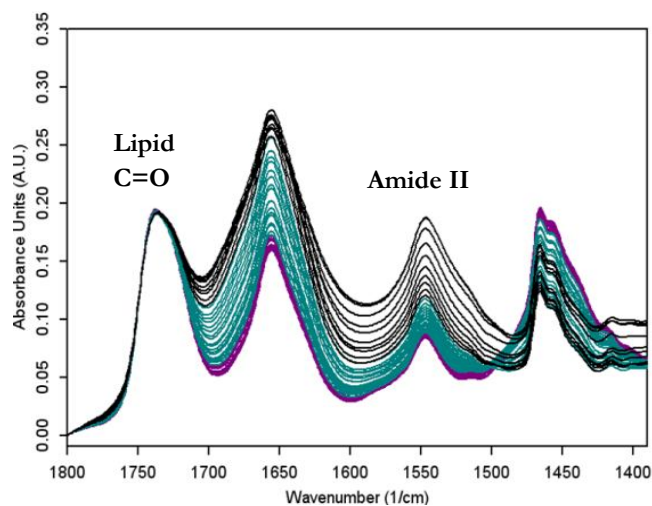
3.7 ¹H/²H EXCHANGE OF BetP

To gain better insight into the activation mechanism of BetP on the molecular level, isotopic ¹H/²H exchange of BetP was performed. ¹H/²H exchange yields information regarding the extent of solvation, i.e., protein flexibility, accessibility and dynamics as well as population between the “closed” and “open” states. Accessible residues to the solvent have exchangeable protons, and thus, act an internal probe within the protein. In the present study, H/D exchange experiments of BetP were performed with ATR-FTIR perfusion cell technique. As explained explicitly in Section 2.6.2, H/D exchange of 2D crystals and proteoliposomes of wild type BetP was performed under activating (with high K⁺) and inactivating (without K⁺) buffer conditions at pH/pD 7.5 to compare the conformational changes, solvent accessibility and fast/slow exchanging parts between the two states of BetP.

Fig. 3.30 represents the IR absorbance spectra of BetP WT proteoliposomes in the course of H/D exchange. Upon deuteration, intensity of the amide II band mainly composed of peptide N-H bending vibrations diminishes and its frequency downshifts 100 cm⁻¹ towards ~1450 cm⁻¹. The N-H bending vibrations are substituted by N-D bending vibrations for the accessible amide modes once

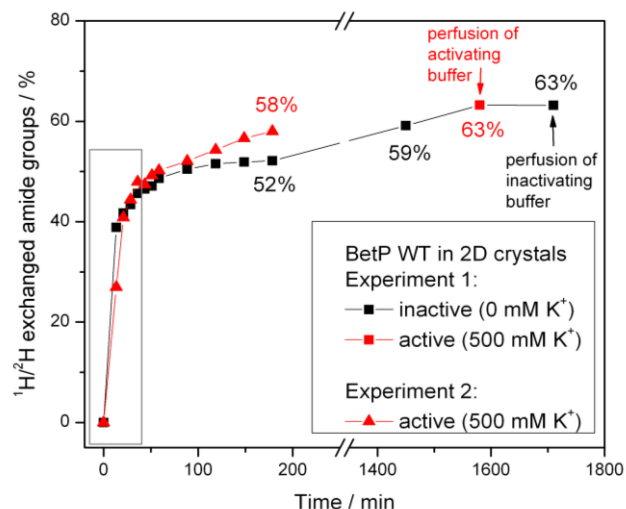
the H₂O buffer was replaced with the D₂O. Thereby, the residual amide II band (~ 1550 cm⁻¹) corresponds to the peptide C-N stretching vibrations which are not affected by deuteration, namely non-exchanged peptide groups. Therefore, to calculate the fraction of the non-exchanged/exchanged protons of the protein during H/D exchange, the integration of the amide II band intensity was divided by the area of the lipid C=O stretching region absorbing at ~ 1737 cm⁻¹ (amide II/lipid CO). The latter is not affected by deuteration.

Figure 3.30: The IR absorbance spectra of BetP WT proteoliposomes during H/D exchange.



H/D exchange extent and kinetics — To analyze the solvent accessibility as well as fast/slow exchanging parts of the BetP protein, the H/D exchange degree and kinetics of 2D crystals and proteoliposomes of BetP was followed in two different experiments for functionally different states, namely in the active (500 mM K⁺) and inactive (no K⁺) state conditions (Figs. 3.31 and 3.32).

Figure 3.31: Hydrogen/deuterium exchange extent and kinetics for BetP WT 2D crystals.



In the first experiment (experiment 1), H/D exchange of BetP was achieved for 24 h without K^+ ions as the inactive state of BetP, afterwards, the activating buffer with 500 mM K^+ was perfused for the next 2 h, and again 0 mM K^+ was switched for the next 2 h as a second time (Fig. 3.31). In the second experiment (experiment 2), H/D exchange was followed with 500 mM K^+ as the active state of BetP. Overall, the accessible fraction of the exchanged amide groups is significantly larger in the active state (58%) of BetP than in the inactive state (52%) at the end of 3 hours, indicating a more open conformation of BetP upon a rise in the K^+ concentration. At the end of the first part in the experiment I (after 24h), the accessible fraction of the polypeptide chain rises from 59% to 63% with perfusion of activating buffer. Then, 4% of BetP which correspond to approx. 24 amino acids (i.e., Asp/Glu and Arg residues located in the solvated loops/helices, suggested with respect to Fig. 3.13D) are exposed to the solvent with K^+ ions. Fraction of exchanged amide groups as well as the number of exchanged amino acids of BetP in the course of H/D exchange was summarized in Table 3.4. In the last part of the experiment I, H/D exchange rate remains constant with the second perfusion of inactivating buffer, indicating that no further conformational changes occur without K^+ ions. Finally, we can conclude that the dynamic fluctuations of BetP result in more accessible parts when the protein in its open state with K^+ -induced activation. In literatures^{15,34}, the *alternating access mechanism* of BetP reveals opening and closing of the periplasmic and cytoplasmic gates, which may result in inward-outward open state or closed state. In this respect, both *rocking bundle* and *gating* movements are also found to be important for opening of the pathways in BetP (Fig. 1.14 Left).

D ₂ O exposure time (t)	Activation state	BetP WT proteoliposomes		BetP WT 2D crystals	
		% of exchanged amide groups	# of exchanged amino acids	% of exchanged amide groups	# of exchanged amino acids
at t=3h	inactive	54 %	321	52 %	309
	active	60 %	357	58 %	345
after t=24h	inactive			59%	351
	active			63%	375

Table 3.4: Fraction (%) of exchanged amide groups and number (#) of exchanged amino acids for 2D crystals and proteoliposomes of BetP WT in the course of H/D exchange. The number of exchanged amino acids was calculated with respect to total amino acids (595) of the BetP monomer.

Interestingly, inactive BetP exhibits faster exchange of amide protons in the first 25 min than the active BetP, reflecting abundance of unordered structures and solvated loops/short helices in the absence of K^+ ions (Fig. 3.31). This implies that some solvated loops and/or short helices located in the hydrophilic region of the protein make additional interactions, hiding somewhere and being away from the solvent upon K^+ -induced activation. According to the structural and functional studies of BetP, interactions of the C-terminal domain with the N-terminal domain and cytoplasmic loops were considered to be functionally significant in osmosensing and/or osmoregulation of BetP²⁹. The regulatory ionic interaction network which includes a variety of charged residues located in loop 2, loop8 and C-terminus (Asp, Glu and Arg) was also pointed out^{11,14}. Moreover, Arg residues of the C-terminal domain are in close contacts with Asp/Glu residues of the loop2 as shown in Fig. 1.14 Right. Then it is plausible to assume that a change in the conformation/orientation of the C-terminal domain of BetP alters these ionic interaction networks upon activation. On the basis of the FTIR data (Fig. 3.13D, Section 3.4.1), Asp/Glu and Arg residues located in loops and the C-terminal domain were suggested to be deuterated with K^+ ions. It is likely that these residues change their interaction partners shielding from the solvent in the result of reorientation of the C-terminal domain as well as solvated loops.

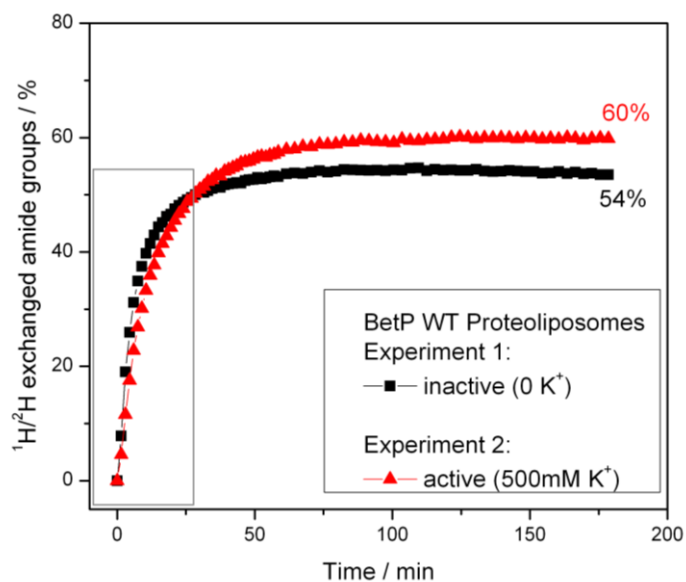


Figure 3.32: H/D exchange extent and kinetics for proteoliposomes of BetP WT for 3 hours.

The H/D exchange extent and kinetics was also analyzed for proteoliposomes of wild type BetP (Fig. 3.32). A similar H/D exchange profile was also observed as in the case of 2D crystals. According to Fig. 3.32, after 3 h-deuteration the accessible fraction of the polypeptide chain of BetP proteoliposomes is larger (60%) in the active state than that of the inactive protein (54%). This indicates that the active state of BetP reveals a structural opening under high K^+ . Moreover, inactive BetP without K^+ ions exhibits a faster H/D exchange in the first 25 min than the active BetP, again suggesting abundance of unordered structures and solvated loops/short helices in the absence of K^+ .

3.8 THERMAL STABILITY OF BetP

As described in detail in Section 2.6.5, temperature of 2D crystals and proteoliposomes of wild type BetP as well as their C-terminal truncated mutants was increased from 4 to 94°C under activating (with 200 or 500 mM K^+) and inactivating (no K^+) buffer conditions at pD 7.5 to yield information regarding the thermal stability in the open and closed states of BetP. A rise in temperature causes a change in the strength of H-bonds to the C=O molecules, and thereby, temperature-induced conformational changes in the secondary structures can be followed in the amide I region. The peak positions obtained from the IR second derivative spectra were drawn as a function of temperature.

BetP WT in 2D crystals: Fig. 3.33A represents the 3-dimensional IR absorbance spectra of BetP WT 2D crystals in the absence of K^+ recorded over a temperature range of 4°C to 94°C. The amide I band centered around 1653 cm^{-1} broadens and downshifts towards 1648 cm^{-1} concomitant with an increase in the intermolecular β -sheet signal as indicated by the appearance of a strong band at 1626 cm^{-1} . This altogether indicates unfolding of the secondary structural elements with rising temperature. Moreover, the amide II band is reduced in intensity, reflecting a loss of tertiary structure of BetP at higher temperatures.

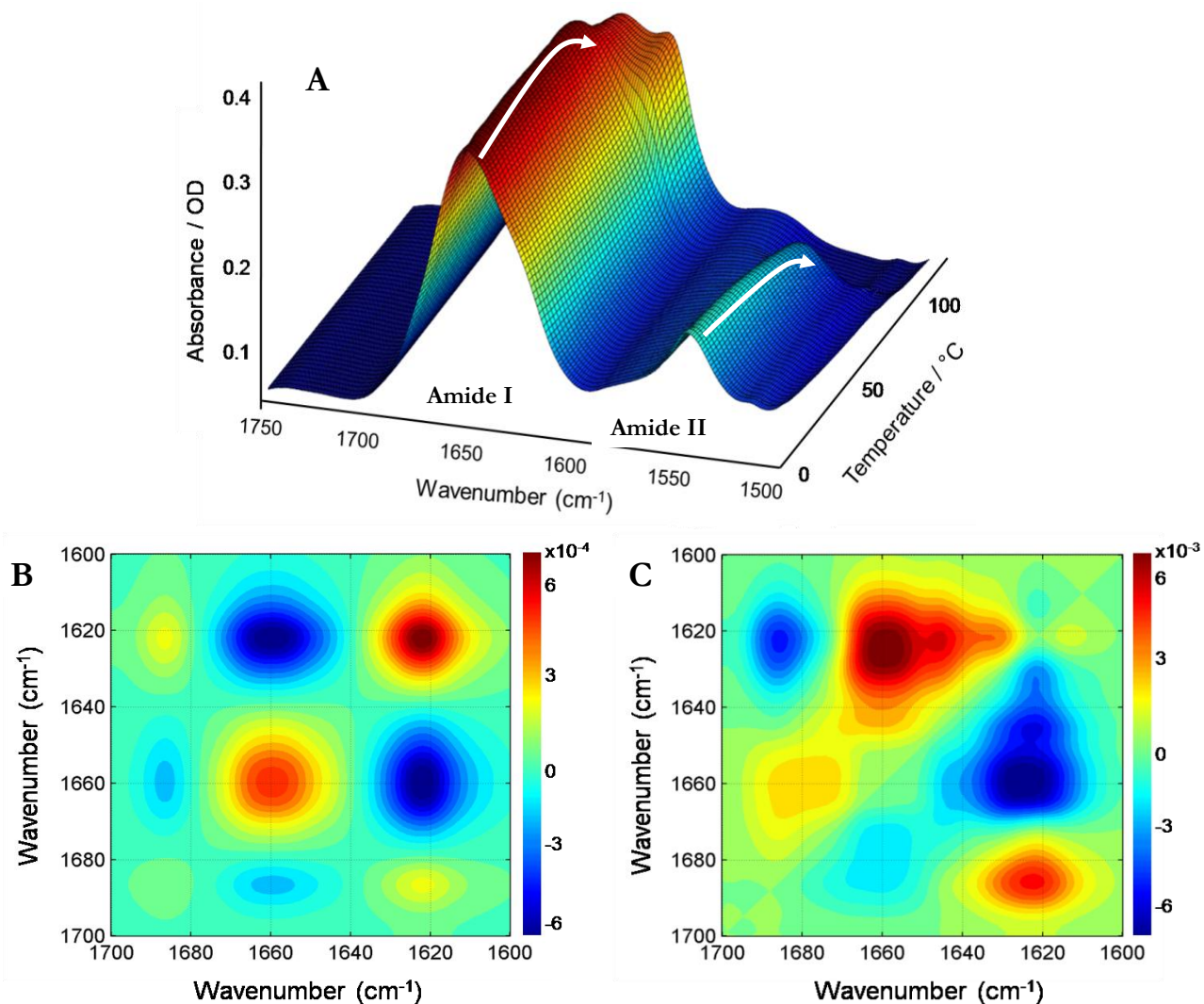


Figure 3.33: (A) A 3-dimensional IR spectra of BetP WT 2D crystals at pD7.5 in the absence of K^+ collected at increasing temperatures. The synchronous (B) and asynchronous (C) 2DCOS maps of inactive BetP in the amide I region perturbed with increasing temperature.

A mathematical analysis of the infrared spectra coupled with two-dimensional correlation spectroscopy (2DCOS)^{99,100} provides a more detailed knowledge regarding the rearrangements of the secondary structures of proteins as well as time-course of the events induced by the external perturbation, i.e., temperature-induced perturbations. In the current study, the 2DCOS maps (synchronous and asynchronous spectra) were drawn by using the Kinetics software for Matlab developed by Erik Goormaghtigh from the Université Libre de Bruxelles⁶⁹. Briefly, the asynchronous spectra, which demonstrate out-of-phase cross-correlation between the bands, yield

information regarding the interaction among bands concomitant with the sequence of the events upon a perturbation. The synchronous spectra, in which the peaks positioned in the diagonal that are always positive, show in-phase cross-correlation between the bands and represent the intensity changes. Therefore, two-dimensional correlation analysis has been frequently used to date^{69,99,101}.

Correlation between bands in the amide I region was shown in the synchronous and asynchronous spectra of BetP (Fig. 3.33 B,C) which refer to the real and imaginary parts of the cross-correlation of intensity at two wavenumbers. The 2DCOS maps reveal that the unfolding process of both active and inactive BetP is very similar (active BetP is not shown). The sequence of the bands during unfolding process with increasing temperature from 4 to 94°C is $1623 \rightarrow 1685/1679 \rightarrow 1660 \text{ cm}^{-1}$. First, we observe a change in the non-native contacts (i.e. intermolecular β -sheets between monomers/trimers) with rising temperature; second, turn structures, and finally, the α -helical structure. The spectral alterations in α -helices (1660 cm^{-1}) and β -sheets ($1623/1685 \text{ cm}^{-1}$) are in the opposite directions. Overall, both in the active and inactive state of BetP the structures which are exposed to the solution (loop/turn/ 3_{10} -helix) unfolds together with appearing of the intermolecular β -sheet signals. This is followed by the unfolding of long α -helices with rising temperature.

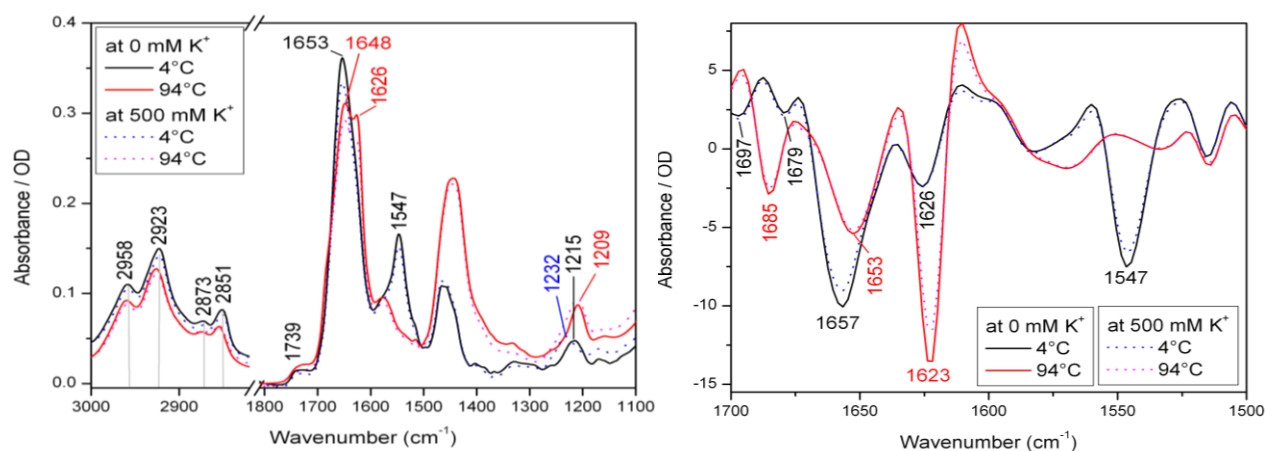


Figure 3.34: Deuterated IR absorbance (Left) and 2nd derivative (Right) spectra of BetP WT 2D crystals.

Fig. 3.34 Left demonstrates the IR absorbance spectra of BetP monitored at +4°C and 94°C in the active and inactive state conditions. The amide bands as well as lipids undergo spectral alterations

with rising temperature. The temperature-induced spectral changes are more obvious in the second derivative spectra (Fig. 3.34 Right). Amide I band decreases in intensity and the frequency downshifts ($1657 \rightarrow 1653 \text{ cm}^{-1}$) concomitant with appearing of two new bands at 1685 and 1623 cm^{-1} (intermolecular β -sheets) with increasing temperature, which is indicative for the partially unfolding of BetP.

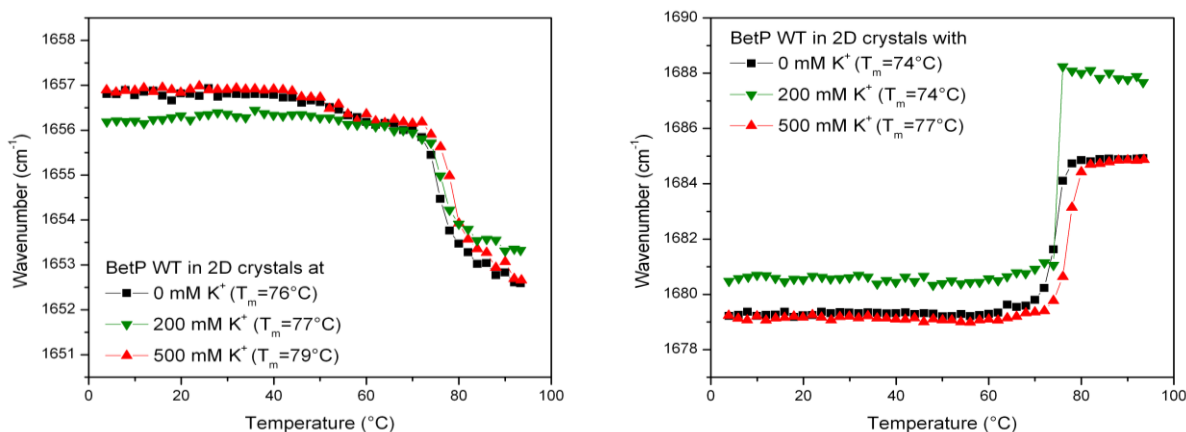


Figure 3.35: The shift of the wavenumber for α -helix ($\sim 1656 \text{ cm}^{-1}$) and turn/loops ($\sim 1679 \text{ cm}^{-1}$) of BetP WT 2D crystals in $^2\text{H}_2\text{O}$ buffer in the absence and presence of K^+ with respect to increasing temperature ($4^\circ\text{C} \rightarrow 94^\circ\text{C}$).

The shift of the wavenumber obtained from the second derivative spectra was drawn with respect to increasing temperature in the absence and presence (200 and 500 mM) of K^+ ions (Fig. 3.35). Turn and helices undergo dynamic fluctuations till $\sim 70^\circ\text{C}$. However, the unfolding state of BetP progresses above 72°C and aggregation begins for the all activation conditions. After undergoing a transition temperature (T_m) between the folded and unfolded state of BetP the spectral changes occur sharply. As summarized in Table 3.5, α -helix and turns/loops of active BetP with 500 mM K^+ exhibit a T_m of 79°C and 77°C , respectively, while they are 76°C and 74°C for inactive BetP without K^+ . As expected, turns/loops of BetP exhibit a lower T_m as compared to helices because turns/loops are the hydrophilic parts of BetP located in the cytoplasmic and periplasmic sides of the membrane, and thus, they are affected by temperature changes prior to α -helices. Moreover, both α -helix and turns/loops exhibit a 3°C higher T_m under high K^+ . Therefore, it is conceiving that active BetP has

more rigid loops and helices in comparison to inactive BetP, reflecting a more stable status of BetP in the active state conditions with K^+ ions. This findings are in perfect agreement with the H/D exchange results, which show interactions of solvated secondary structures located in the hydrophilic part of BetP, i.e., solvated loop/turn and helices represented by a slower exchange rate for active BetP (Figs. 3.31 and 3.32). In this respect, interaction of the C-terminal domain with loop 2 of the adjacent monomer forming the cytoplasmic ionic network has been already shown¹⁴.

Secondary structures	T_m (°C) for BetP WT 2D crystals		
	0 mM K^+	200 mM K^+	500 mM K^+
turn/loop	74 °C	74 °C	77 °C
α -helix	76 °C	77 °C	79 °C

Table 3.5: Melting temperature T_m (°C) for BetP WT 2D crystals was obtained from Fig. 3.35.

Fig 3.36 represents the thermal stability of the hydrophobic lipid tails for the blank lipids in the absence of protein and for wild type BetP reconstituted in 2D crystals. The peak positions of the CH_2 and CH_3 stretching modes were determined from the second derivative spectra in 2H_2O buffer and were plotted as a function of increasing temperature from 4°C to 94°C recorded in 2°C intervals. As argued explicitly in Section 3.6.1, insertion of BetP into the lipid bilayer downshifts the frequency of both CH_2 and CH_3 stretching modes of lipid acyl chains, implying an increase in the ordering of lipid tails (Fig. 3.36 A,B). At the same time the lipid acyl chains exhibit an increased conformational flexibility in the lipid-BetP system, which is represented an increment in the bandwidth (Fig. 3.36C and D). A rise in temperature from 4°C to 94°C does not induce a significant conformational change in the fatty acyl chains of the pure lipids. However, in the case of BetP WT 2D crystals, the band position of CH_2 stretching modes shifts upward till ~60°C while the band width of those decreases, reflecting an increased conformational disordering concomitant with a decreased conformational dynamics in the CH_2 groups of the lipid tails, respectively. Particularly, in Fig. 3.36A, existence of a phase transition for the temperature range ~40-60°C upon heating is not reversible as seen from the

wavenumber shifting profile during decreasing of temperature ($94 \rightarrow 4^\circ\text{C}$). Such a transition is not observed for the blank lipid samples (Fig. 3.36A) as well as for the proteoliposomes of BetP WT (data not shown). These temperature induced alterations in the static order and motion of the CH_2 groups of the lipid acyl chains within the 2D crystals of BetP WT occur regardless of K^+ concentration, which may not be functional related. On the other hand, no significant change is monitored upon rising temperature for the CH_3 groups of lipid tails within the 2D crystals of the BetP-lipid system.

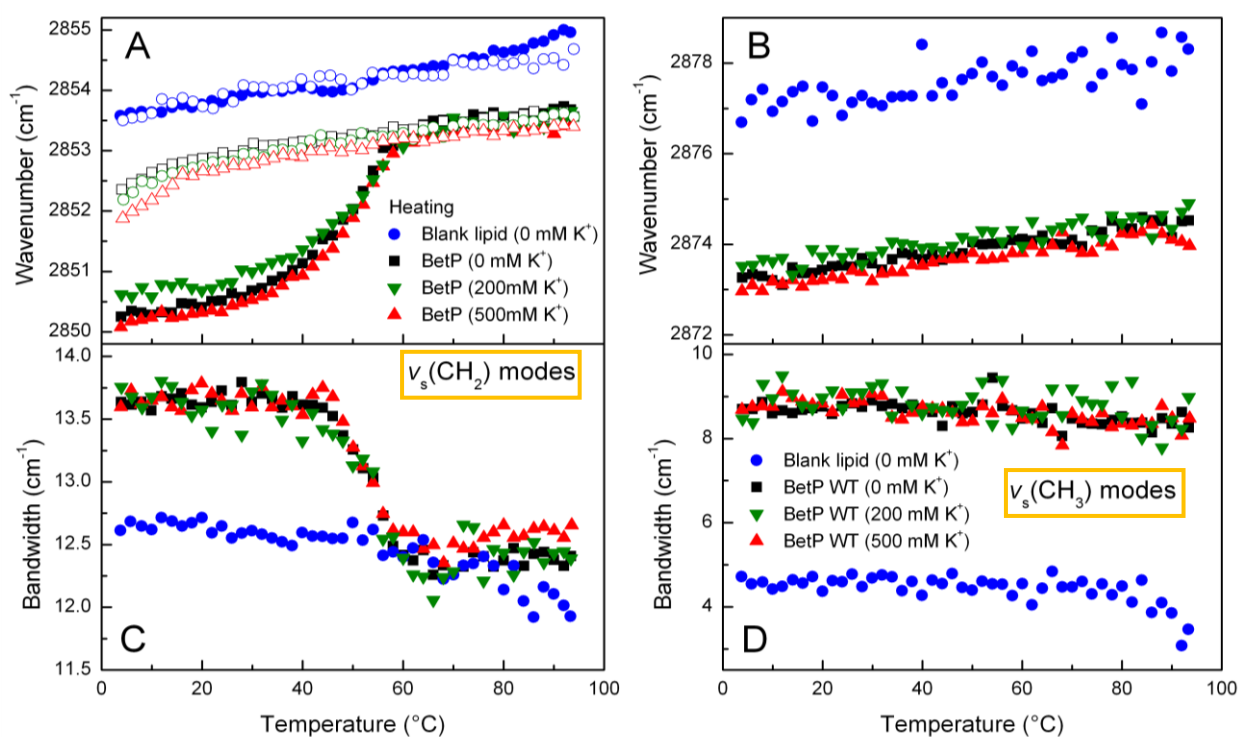


Figure 3.36: The shift of the maximum and full width at half maximum (FWHM) of the CH_2 (A, C) and CH_3 (B, D) symmetric stretching modes with respect to increasing temperature ($4 \rightarrow 94^\circ\text{C}$) for blank *C. glutamicum* lipids and BetP WT 2D crystals in D_2O buffer. The peak positions were obtained from the IR second derivative spectra while the FWHM was obtained from the IR absorbance spectra. Open signs in (A) represent the shift in the wavenumber of the CH_2 symmetric stretching modes recorded during the cooling step ($94 \rightarrow 4^\circ\text{C}$).

Taking these findings into account, we can conclude that the observed pronounced alterations in the CH_2 groups of the lipid tails within the 2D crystals of BetP could arise from the crystal contacts and/or from behavior of the BetP protein in the crystal. This could be associated to asymmetric

binding of the PG lipids to BetP trimer which has been identified recently⁹⁵. Additionally, it was previously reported⁵² that the type of the lipid affects crystal packing and order of BetP that has a preference for fatty acid moieties 16:0-18:1.

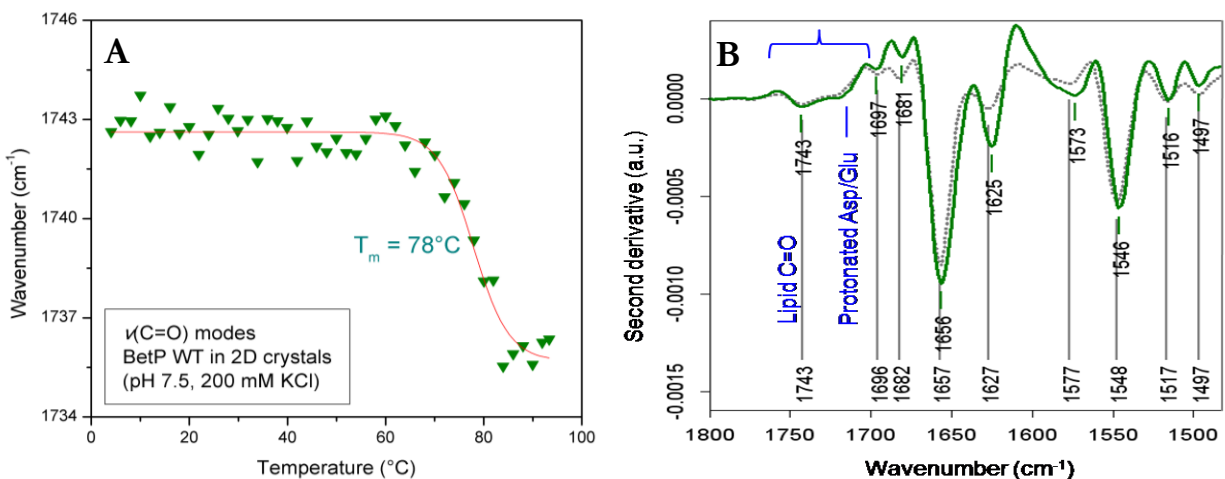


Figure 3.37: (A) The shift of the peak position around 1743 cm^{-1} for BetP WT 2D crystals at pH 7.5 in the presence of 200 mM K^+ respect to increasing temperature (4 \rightarrow 94°C). (B) The IR second derivative spectra of BetP WT 2D crystals at pH/pD 7.5, 200 mM K^+ in the H_2O (...) and D_2O (—) buffer environments.

The shift of the peak position at $\sim 1743 \text{ cm}^{-1}$ which is attributed to the C=O stretching vibrations was obtained from the second derivative spectra for BetP WT 2D crystals at pH 7.5 in the presence of 200 mM K^+ and was plotted with respect to rising temperature (Fig. 3.37A). Since a signal at 1743 cm^{-1} does not response to the H/D exchange (Fig. 3.37B); however, upon increasing temperature it downshifts in H_2O (Fig. 3.37A) but not in D_2O (Fig. 3.27B, Section 3.6.3), this signal is assigned to C=O stretching modes of carboxylate groups of protonated Asp/Glu residues with a possible overlap of the lipid C=O modes in H_2O buffer environment while this band absorbing at 1743 cm^{-1} is attributed only to the lipid C=O modes in D_2O buffer.

BetP ΔC45 in 2D crystals: The C-terminal truncated BetP in 2D crystals was also perturbed with increasing temperature from 4 to 94°C under activating (500 mM K^+) and inactivating (0 mM K^+) buffer conditions at pD 7.5 to compare the thermal stability of the secondary structures with wild type BetP.

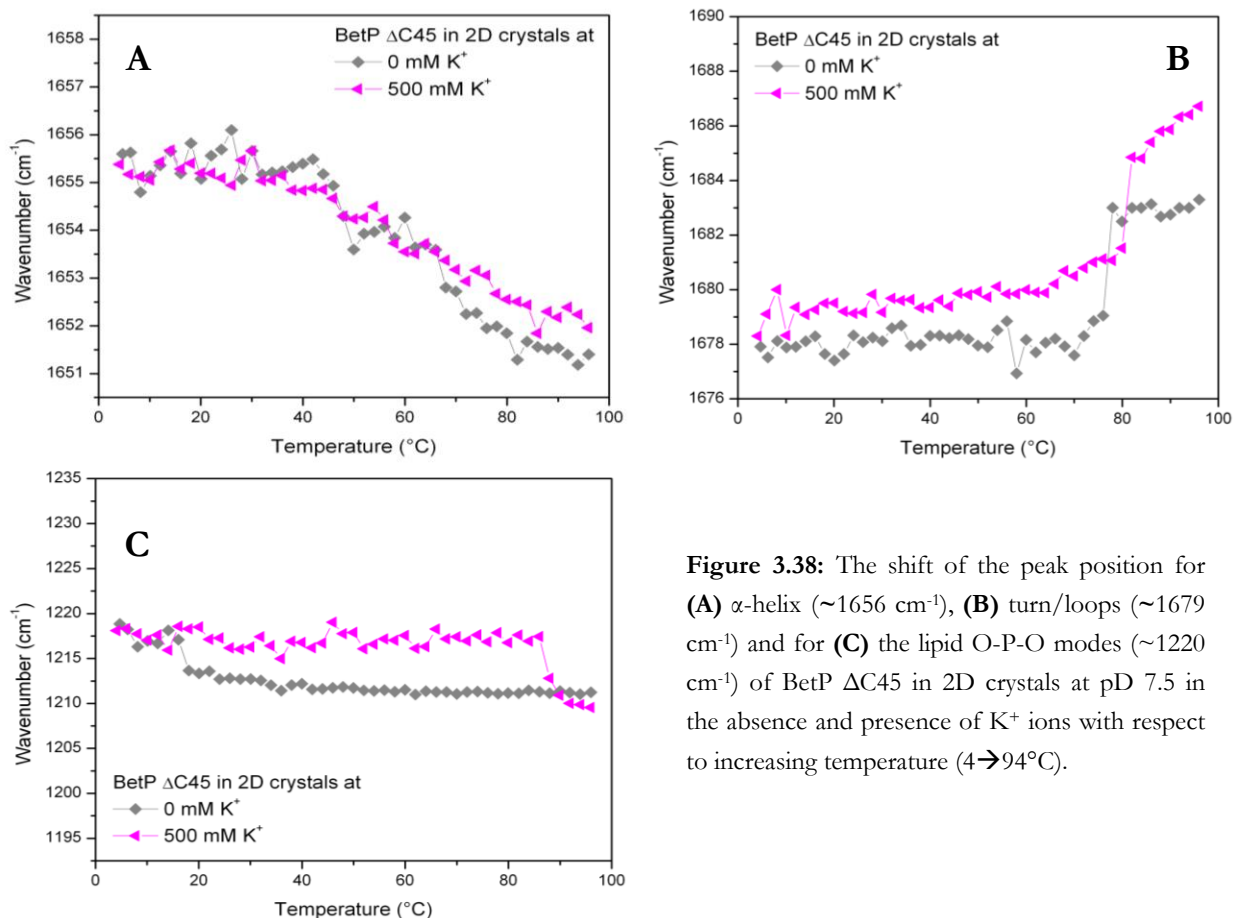


Figure 3.38: The shift of the peak position for (A) α -helix ($\sim 1656 \text{ cm}^{-1}$), (B) turn/loops ($\sim 1679 \text{ cm}^{-1}$) and for (C) the lipid O-P-O modes ($\sim 1220 \text{ cm}^{-1}$) of BetP ΔC45 in 2D crystals at pD 7.5 in the absence and presence of K^+ ions with respect to increasing temperature ($4 \rightarrow 94^{\circ}\text{C}$).

In comparison to BetP WT, the C-terminus lacking BetP does not have a sharp transition for α -helices ($\sim 1656 \text{ cm}^{-1}$) between the folded and unfolded state (Fig. 3.38A). The peak positions obtained from the second derivative spectra downshift gradually from 1656 to 1652 cm^{-1} with rising temperature. Particularly, a steady downshift is observed above $\sim 45^{\circ}\text{C}$ and the shifting of the peak positions exhibits a similar profile both in the active and inactive state of BetP ΔC45 . Then, the C-terminus lacking BetP is affected from the rising temperature in a similar manner and we do not observe significant differences between the both states. On the other hand, wild type BetP exhibits a significant transition temperature in the two states of BetP WT, indicating a different interaction of the C-terminal domain at the active and inactive forms of BetP.

Turns/loops of BetP absorbing at around 1679 cm^{-1} have a sharp transition above 76°C and 80°C in the inactive ($T_m=77^\circ\text{C}$) and active ($T_m=81^\circ\text{C}$) forms of BetP ΔC45 (Fig. 3.38B). The transition temperatures of the two states of BetP ΔC45 have higher values unlike BetP WT. This indicates a different role of turns/loops in the thermal stability as well as K^+ -induced activation of both wild type and the C-terminal lacking protein. It is likely that deletion of the C-terminal domain renders the interactions of turns/loops more strengthened or causes shielding of turns/loops from the solvent.

The peak positions of the phospholipids $\nu_{\text{as}}(\text{PO}_2^-)$ modes for BetP ΔC45 in 2D crystals was shown in Fig. 3.38C. The membrane lipid headgroups are not perturbed with rising temperature in the active and inactive forms of BetP ΔC45 . However, a sharp phase transition was observed in the case of wild type BetP at 500 mM K^+ (Fig. 3.26A, Section 3.6.2). Altogether this indicates a crucial role of the C-terminal domain and lipid headgroups in the K^+ -induced activation of BetP WT.

BetP WT in proteoliposomes: In order to probe the thermal stability of the secondary structures, perturbation of proteoliposomes of BetP reconstituted into *E. coli* lipids by rising temperature was analyzed under activating (500 mM K^+) and inactivating (0 mM K^+) buffer conditions at pH 7.5 and was compared with 2D crystals of BetP reconstituted into *C. glutamicum* lipids. Fig. 3.39A shows the IR absorbance spectra of BetP WT proteoliposomes monitored at $+4$ and 96°C in the inactive state conditions. The spectral alterations induced by rising temperature are clearly observed in the amide I and II bands. The temperature-dependent peak positions are resolved in the second derivative spectra better (Fig. 3.39B). In the absorbance spectrum the amide I band centered around 1655 cm^{-1} broadens and downshifts towards 1650 cm^{-1} while intensity of the amide II band is reduced with rising temperature. These spectral changes occur concomitantly with the appearance of two strong bands absorbing at 1686 and 1626 cm^{-1} , which is an unequivocal indicator for the forming of intermolecular β -sheets due to aggregation. Altogether FTIR data reflects partial unfolding of the secondary structures of BetP and a loss of the tertiary structure with increasing temperature.

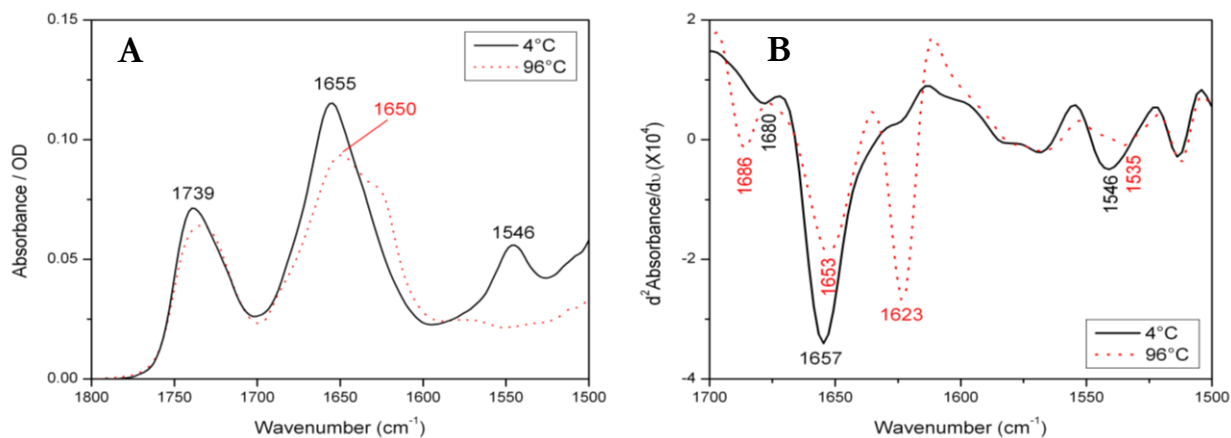


Figure 3.39: Deuterated IR absorbance **(A)** and second derivative **(B)** spectra of BetP WT proteoliposomes in the absence of K^+ with temperature-dependent peak positions at 4°C and 96°C .

The shift of the peak positions obtained from the IR second derivative spectra was drawn *versus* increasing temperature at 0 mM and 500 mM K^+ (Fig. 3.40). Both turns/loops ($\sim 1680\text{ cm}^{-1}$) and α -helices ($\sim 1657\text{ cm}^{-1}$) undergo phase transitions at high temperatures. The α -helical structure has transition temperatures of 71°C (without K^+) and 79°C (with 500 mM K^+) (Fig. 3.40A) while this T_m values of turns/loops are 73°C and 79°C , respectively (Fig. 3.40B). As given in Table 3.6, both α -helix and turns/loops exhibit a $\sim 6^\circ\text{C}$ higher T_m value under high K^+ . Thus, it can be concluded that the active form of BetP has more rigid turns/loops and α -helices having different interactions in comparison to inactive form of BetP. This findings are in line with the H/D exchange results (Figs. 3.31 and 3.32) as well as with 2D crystals of BetP (Fig. 3.35). However, proteoliposomes has considerably high T_m values unlike BetP WT 2D crystals. This is most likely due to a change in the lipid environment of BetP. Proteoliposomes of BetP have a higher LPR value (10:1) while 2D crystals have only LPR of 0.2. This means that proteoliposomes consist of both protein-associated lipids as well as a large amount of bulk bilayer lipids whose molecules do not bind to the protein. It is likely that turns and helices of BetP in proteoliposomes are surrounded by a large amount of bulk bilayer lipids, and thus, protected rather from the external perturbations (i.e. rising temperature) in comparison to 2D crystals.

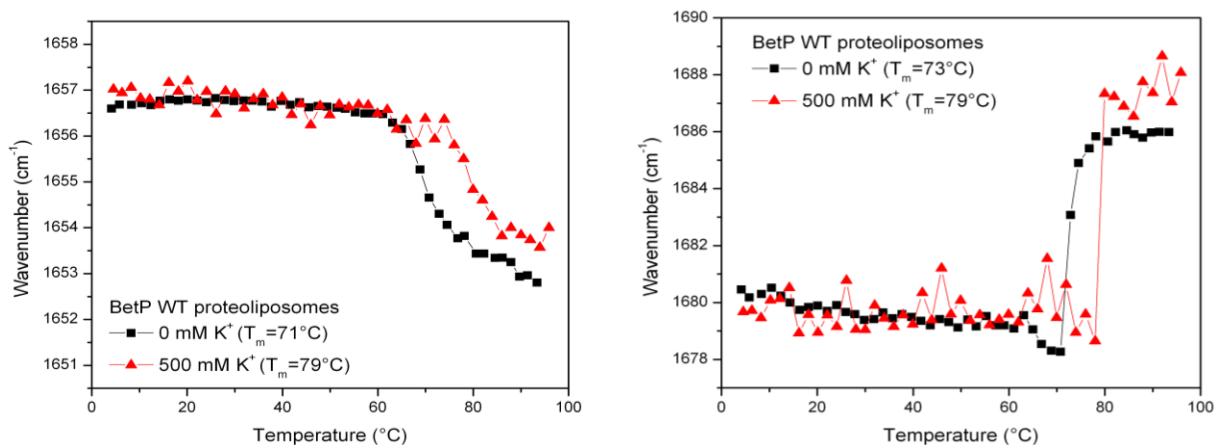


Figure 3.40: The shift of the wavenumber for α -helix ($\sim 1657\text{ cm}^{-1}$) and turns/loops ($\sim 1680\text{ cm}^{-1}$) of BetP WT proteoliposomes in $^2\text{H}_2\text{O}$ buffer in the absence and presence of K^+ with respect to increasing temperature.

Secondary structures	T_m ($^{\circ}\text{C}$) for BetP WT		T_m ($^{\circ}\text{C}$) for BetP ΔC45	
	0 mM K^+	500 mM K^+	0 mM K^+	500 mM K^+
turn/loop	73°C	79°C	73°C	79°C
α -helix	71°C	79°C	73°C	79°C

Table 3.6: Melting temperature T_m ($^{\circ}\text{C}$) for BetP WT proteoliposomes obtained from Figs. 3.40 and 3.42

BetP ΔC45 in proteoliposomes: To compare the thermal stability of the secondary structures with BetP WT, the C-terminal truncated mutant of BetP reconstituted into proteoliposomes was also perturbed with rising temperature under activating (500 mM K^+) and inactivating (0 mM K^+) buffer conditions at pD 7.5. On the basis of the FTIR data (Fig. 3.41), upon increasing temperature BetP ΔC45 loses its tertiary structure represented by a decrease in intensity of the amide II band. The secondary structures of BetP ΔC45 partially unfold as well which is indicated by broadening and downshifting of the amide I band and appearing of the intermolecular β -sheet signals. The shift of the peak positions was drawn with respect to elevated temperature from 4 to 96°C (Fig. 3.42). Upon increasing temperature, the C-terminus lacking BetP undergoes a sharp transition for α -helices ($\sim 1657\text{ cm}^{-1}$) and turns/loops ($\sim 1680\text{ cm}^{-1}$) between the folded and unfolded states, and both secondary structures exhibit a T_m of 73°C (without K^+) and 79°C (with 500 mM K^+). This

implies that α -helices and turns/loops of BetP Δ C45 have similar interactions both in the active and inactive states.

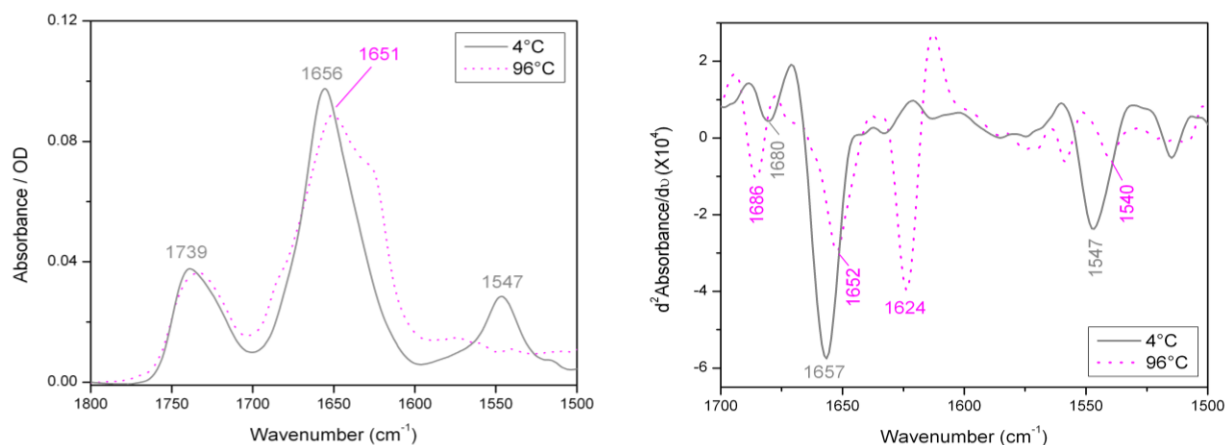


Figure 3.41: Deuterated IR absorbance (**Left**) and second derivative (**Right**) spectra of BetP Δ C45 proteoliposomes in the absence of K^+ with temperature-dependent peak positions at 4°C and 96°C.

Both wild type and the C-terminal lacking BetP are perturbed by rising temperature. However, we do not observe significant spectral differences between the wild type and mutant in terms of turn/loop stability, indicating a similar interaction of turns/loops in the both forms of BetP. However, in the inactive state, both wild type and mutant of BetP exhibit a slight difference ($\Delta 2^\circ\text{C}$) in the transition temperature in terms of α -helix stability (71°C for the wild type and 73°C for the mutant), suggesting a different interaction of the C-terminal domain in the two forms of BetP.

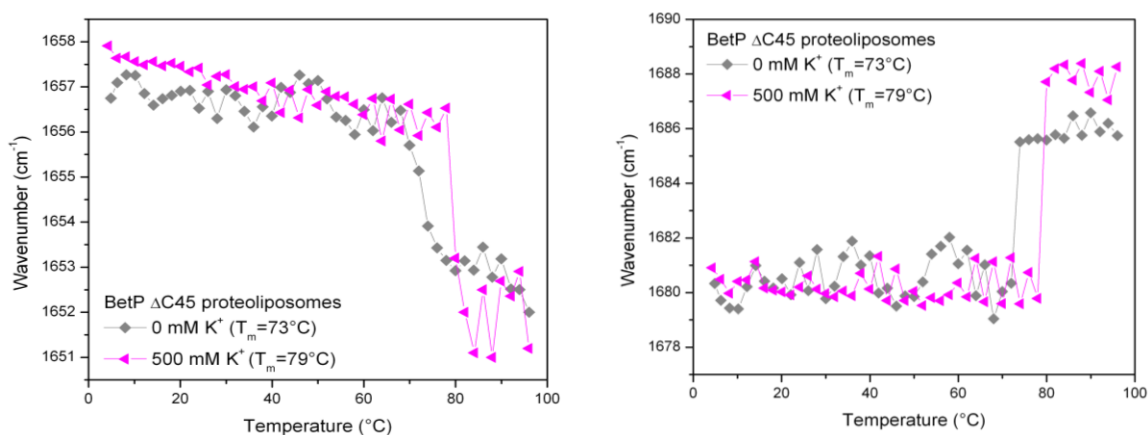


Figure 3.42: The shift of the peak positions obtained from the second derivative spectra for α -helix ($\sim 1657\text{ cm}^{-1}$) and turns ($\sim 1680\text{ cm}^{-1}$) of BetP Δ C45 proteoliposomes in $^2\text{H}_2\text{O}$ in the absence and presence of K^+ *versus* temperature.

4. SUMMARY

In this study, the structural and functional properties of the Na⁺/Betaine symporter BetP were investigated upon K⁺-induced activation. BetP regulates transport activity dependent on the amount of associated anionic lipids and the cytoplasmic K⁺-concentration. For this purpose, FTIR spectroscopy was implemented as a non-perturbing biophysical method which shed light on how the membrane lipids contribute to the molecular mechanisms of activation and regulatory response of BetP.

Secondary structure analysis: The FTIR data showed that all forms of BetP (i.e., detergent solubilized, proteoliposomes and 2D crystals) exhibit more or less identical spectra and are mainly α -helical. BetP exhibits 75% α -helix, 12% solvated loops/short helices, 3_{10} -helix and/or unordered structure, and 13% restricted turns/loops under inactivating buffer conditions (i.e. without K⁺). However, the fraction of α -helices decreases by 7% while the amount of restricted turn/loops and solvated/short structures increases by 5% and 2%, respectively, upon activation (with 500 mM K⁺). These small changes in the fraction of secondary structures of BetP 2D crystals could result from either an alteration in the solvation status of the secondary structures due to a conformational change or from the reorganization of the secondary structures within the protein upon K⁺-induced activation.

K⁺ titration experiments and activation/deactivation of BetP: The IR data revealed *in situ* structural changes of BetP WT 2D crystals upon a stepwise activation with increasing K⁺ ions (0→500 mM). On the basis of the FTIR spectra, we observed only slight band shifts for the major amide I components (α -helix and turn/loops) with increasing K⁺. This suggests that the H-bonding strength of the regular secondary structures is altered under high K⁺. Observation of small amide I difference signals both in H₂O and D₂O buffer environment confirms minute conformational alterations in the protein backbone upon upregulation of BetP.

On the other hand, several distinct band shifts were detected with increasing K^+ above 1700 cm^{-1} which corresponds to the C=O stretching modes of carboxylate groups of protonated Asp/Glu residues. Strongly, intermediately and weakly H-bonded protonated Asp/Glu respond to K^+ increment in a similar manner that the shifts are reversed above $\sim 250\text{ mM } K^+$. Additionally, the signals of protonated Asp/Glu residues intensify upon activation, indicating increase interactions of these residues upon activation. This reflects that the H-bonding properties of protonated Asp/Glu residues are altered; H-bonds are strengthened or weakened/lost upon K^+ -stimulated activation. Moreover, the C=O stretching modes of carboxylate groups of deprotonated Asp/Glu residues undergo clear spectral shifts concomitant with a decrease in their population in the presence of high K^+ concentrations. Thereby, we can conclude that a H-bonded network of both protonated and deprotonated Asp/Glu residues in BetP is disturbed with increasing K^+ concentration both in H_2O and D_2O buffer. Altogether this suggests that eventually a protonation/deprotonation of Asp/Glu residues may be involved in the K^+ -induced activation of BetP.

Unlike wild type BetP, the C-terminal truncated BetP in 2D crystals exhibit only tiny IR-difference signals for protonated Asp/Glu residues above 1700 cm^{-1} under activating conditions. The IR signals of protonated Asp/Glu and of Arg/Lys residues disappear in the case of this mutant. This indicates that these charged residues respond to an increase of the concentration of K^+ only in the case of BetP WT. This clearly proves an important role of the C-terminal domain in the ionic interaction network on the cytoplasmic side of BetP and in the activation/regulation cycle of BetP. It is conceiving that K^+ -induced activation of BetP involves the interactions of Asp/Glu and Arg residues in the cytoplasmic region. In this respect, the intensity of the IR signals of arginine residues increases dramatically with elevated K^+ indicating an increase in the interactions of Arg residues of BetP under activating conditions. Recently, the ionic interaction of terminal domains with cytoplasmic loops *via* charged residues has been described²⁷.

The IR-difference spectra also showed that the C=O modes of Asn and Gln residues intensify significantly concomitant with a shifting of the NH₂ bending modes of Asn residues that undergo a change in the H-bonding pattern upon activation. These results are in line with the fact that formation of inter-protomer H-bonds includes Asn (h7) and Thr (loop 7) residues in the interfacial region of BetP. It is likely that conformational alterations occur around Asn/Gln residues on the periplasmic side of the protein.

A clear response of the C-C ring mode of tyrosine residues to K⁺ titration provided dynamic information on changes in the interaction network of BetP during regulation. This is in good agreement with the fact that some tyrosine residues are involved in K⁺ coordination revealed by structural studies. The IR signals of both protonated and deprotonated Tyr residues exhibit opposite spectral alterations in terms of intensity changes as well as band shifting (a weakening/loss or strengthening of H-bonding) with elevated K⁺. This suggests that some Tyr residues either play a role in the regulation of BetP activation or sense the movement of the backbone due to conformational alterations in the result of K⁺ binding. Particularly, the signals of protonated Tyr exhibit a broad band in the IR-difference spectrum (active-*minus*-inactive), suggesting that a few Tyr residues are involved in the activation of BetP as being reporter and/or actor. It is likely to speculate that residues involved in Rb⁺ binding or in formation of the periplasmic betaine-binding site (S2 site) might contribute to the observed IR shifts. Besides, the K⁺-dependent formation of the S2 site occurs through conformational changes in TM12, establishing an additional salt bridge between Tyr206 and Aps547 in the cytoplasmic tip of TM12.

The FTIR data of BetP proteoliposomes are in good agreement with 2D crystals. Both forms of BetP exhibit identical spectral alterations, particularly in the protonation states and in the environment of Asp/Glu and Arg residues under high K⁺. Overall, the FTIR data indicate that loops and solvated helices (C-terminal domain and/or short helices) in the hydrophilic region of BetP,

which contain Asp/Glu and Arg residues, are involved in the activation. Asp/Glu residues interact most likely with Arg/Lys residues *via* salt bridges, being involved in K⁺-dependent activation of BetP, and the strength of these interactions is also influenced with K⁺. Observation of tiny difference signals for Trp residues is indicative for reorientations of these residues in response to K⁺ increase. Altogether this suggests that K⁺-stimulated activation of BetP is initiated by a H-bonded network of Asp/Glu and Arg residues.

pH titration experiments: *In situ* titration of BetP at various pH values showed the protonation states of Asp/Glu residues with their locations in BetP and the pH-induced conformational changes, shedding light on the ionic interaction networks of terminal domains with cytoplasmic loops *via* charged residues. According to the FTIR data, the most pronounced spectral changes are monitored in the pH range of 5.5-7.5. The IR signals for protonated Asp/Glu intensify while the population of deprotonated Asp/Glu residues decreases. This suggests that protonation/deprotonation states of Asp/Glu residues are altered in this pH range concomitant with conformational changes of turn/loops as well as with microenvironmental changes around Tyr in BetP. Hereby, the pK_a value of Asp/Glu residues lies in a wide range of pH5.5-pH7.5 which is remarkably high for a carboxylic acid. This suggests that Asp/Glu residues influenced by pH changes locate most likely away from the solvent and/or these groups make electrostatic interactions with the environment, most likely with some positively charged residues (i.e. Arg/Lys). It was already argued that upon K⁺-induced activation, both protonated and deprotonated Asp/Glu residues undergo H-bonding changes, and interactions of both Arg and protonated Asp/Glu residues increase under high K⁺. It is likely that the same groups of Asp/Glu residues are involved in the regulatory activation mechanism of BetP.

Lipid-protein interactions: Probing of the lipid signals provided experimental evidence on how BetP dynamically interacts with the bilayer lipids under high K⁺. Phospholipid headgroups undergo K⁺ dependent changes in their electrostatic and H-bonding properties favoring weak/free H-bonds,

while the hydrophobic tails become more mobile and even disordered upon K^+ -induced activation of BetP. FTIR data suggest that the inactive state of BetP is characterized by tight lipid-protein interactions most likely similar to what was observed in the latest structure of BetP⁹⁵. The FTIR data also reveal that K^+ abolishes a tight interaction of BetP especially with the anionic lipid headgroups suggesting that lipid-protein interactions have to soften so that BetP can adopt its active state. Hereby, the hypothesized molecular switch model was confirmed that due to K^+ activation the positively charged C-terminal domains switch their interaction partner from lipids (under down-regulating conditions) to protein-interactions, which could also involve intratrimeric interactions between C-terminal domains as suggested by structural studies and the fact that monomeric BetP is down-regulated.

$^1H/^2H$ exchange: $^1H/^2H$ exchange experiments provided information regarding the solvent accessibility in the open and closed states of BetP. On the basis of the $^1H/^2H$ exchange extent and kinetics, the fraction of the exchanged amide groups is significantly larger in the active state (58%) than in the inactive state (52%) at the end of 3 hours deuteration, indicating a more open conformation of BetP WT 2D crystals upon a rise in the K^+ concentration. Interestingly, inactive BetP exhibits faster exchange of amide protons in the first 25 min than the active BetP, reflecting abundance of unordered structures, loops and solvated helices in the absence of K^+ . A similar H/D exchange profile was observed in the case of proteoliposomes of BetP. This suggests that some solvated loops and/or short helices located in the hydrophilic region of BetP make additional interactions, hiding somewhere and being away from the solvent upon activation. The FTIR data also reveal that Asp/Glu and Arg residues, located in loops and in the C-terminal domain, are deuterated further with increasing K^+ concentration. It is likely that these residues change their interaction partners shielding from the solvent in the result of reorientation of the C-terminal domain as well as solvated loops upon activation.

Thermal stability: Both in the active and inactive states of BetP WT 2D crystals, loops/turns and 3_{10} -helix unfold with appearing of the intermolecular β -sheet signals, being affected by temperature changes prior to α -helices. α -helix and turns/loops of active BetP exhibit a T_m of 79°C and 77°C, respectively, while they are 76°C and 74°C for inactive BetP. Moreover, both α -helix and turns/loops exhibit a 3°C higher T_m under high K^+ . This proves that active BetP has more rigid loops and helices as compared to inactive BetP, reflecting a more stable status of BetP in the active state with K^+ ions. These findings are in perfect agreement with the H/D exchange results as well as with the thermal stability analysis of BetP WT proteoliposomes. Unlike BetP WT 2D crystals, the C-terminal domain truncated BetP 2D crystals is also affected by rising temperature in a similar manner but without significant differences between the both states, indicating different interactions of the C-terminal domain at the active and inactive states of BetP.

In summary, probing of the lipid-protein interactions as well as K^+ -dependent structural changes provided more holistic information on function-related structural properties of BetP. Altogether the FTIR data suggest that secondary structure rearrangements and observation of interactions between charged residues are the 'hot spots' which are involved in the activation cycle of BetP. It can be postulated that negatively charged phosphate lipid headgroups are released from the positively charged Arg residues located at the end of the C-terminal domain upon K^+ -binding and might undergo a change in interaction towards loops or the N-terminal domains. This is followed by reorientation of C-termini/transmembrane helices and by unzipping of interactions of charged residues between the cytoplasmic loops and C-termini, resulting in structural opening in the active state of BetP. Hereby, new insights into the structure-function relationship of BetP upon activation selectively induced by K^+ ions were revealed on the molecular level with IR spectroscopy.

5. ZUSAMMENFASSUNG

Im Rahmen dieser Arbeit wurden die strukturellen und funktionellen Eigenschaften des Na^+ /Betain Symporters BetP auf die K^+ -induzierte Aktivierung hin untersucht. BetP reguliert die Transportaktivität in Abhängigkeit von der Menge an assoziierten anionischen Lipiden und der zytoplasmatischen K^+ -Konzentration. Für diesen Zweck wurde die FTIR Spektroskopie als eine zerstörungsfreie biophysikalische Methode verwendet um herauszufinden, wie die Membranlipide zum molekularen Mechanismus der Aktivierung und Regulation beitragen.

Sekundärstrukturanalyse: Die FTIR Daten zeigen, dass jede Form von BetP (gelöst in Detergens, Proteoliposomen und 2D Kristalle) mehr oder weniger identische Spektren liefern und hauptsächlich α -helikal aufgebaut sind. BetP besteht zu 75% aus α -Helix, aus 12% Lösungsmittel-zugänglichen Schleifen/kurzen Helices, 3_{10} -Helices und/oder Zufallsknäuel und zu 13% eingeschränkten Schleifen unter inaktivierenden Pufferbedingungen (ohne K^+). Durch Aktivierung (mit 500 mM K^+) sinkt jedoch der Anteil an α -Helices um 7% während der Anteil an eingeschränkten Schleifen um 5% beziehungsweise Lösungsmittel-zugänglichen Schleifen/kurzen Helices um 2% steigt. Diese kleinen Änderungen in der Zusammensetzung der Sekundärstruktur von BetP 2D Kristallen könnten das Ergebnis sowohl einer Änderung der Lösungsmittel-Zugänglichkeit der Sekundärstruktur bedingt durch eine Konformationsänderung als auch einer Reorganization der Sekundärstruktur innerhalb des Proteins ausgelöst durch die K^+ -induzierte Aktivierung sein.

K^+ -Titrationsexperimente und Aktivierung/Deaktivierung von BetP: Die IR Daten zeigten eine *in situ* Strukturänderung von BetP WT 2D Kristalle durch eine Aktivierung mittels einer schrittweisen Erhöhung der K^+ -Ionenkonzentration bis auf 500 mM. Auf der Grundlage von FTIR Spektren wurden mit steigender K^+ -Konzentration lediglich leichte Verschiebungen der Hauptkomponenten der Amid I Bande (α -Helix und Schleifen) beobachtet. Dies legt nahe, dass die

Stärke von H-Brücken innerhalb der regulären Sekundärstruktur durch hohe K^+ -Konzentrationen beeinflusst wird. Das Auftreten von kleinen Amid I Differenzsignalen in sowohl H_2O als auch D_2O bestätigt kleine Konformationsänderung im Proteinrückgrat, die durch die Regulation von BetP verursacht werden.

Auf der anderen Seite wurden einige deutliche Bandenverschiebungen bei über 1700 cm^{-1} , bedingt durch eine Erhöhung der K^+ -Konzentration, beobachtet, die der C=O Streckschwingung von Carboxylgruppen in Asp/Glu-Seitenketten zugeordnet werden können. Protonierte Asp/Glu-Seitenketten, die starke bis schwache H-Brücken eingehen, reagieren ähnlich auf eine K^+ Konzentrationserhöhung. Zusätzlich steigt durch die Aktivierung die Intensität der Signale von protonierten Asp/Glu-Seitenketten, was auf eine durch die Aktivierung steigende Wechselwirkung der Seitenketten hindeutet. Dies spiegelt eine Änderung von H-Brückenbindungen von protonierten Asp/Glu-Seitenketten wieder; H-Brücken werden durch K^+ -abhängige Aktivierung gestärkt oder geschwächt/gebrochen. Ferner erfahren die C=O Streckschwingungen der Carboxylgruppen von deprotonierten Asp/Glu-Seitenketten eine deutliche spektrale Verschiebung mit einer gleichzeitigen Depopulation der Schwingungen in Anwesenheit von hohen K^+ -Konzentrationen. Daher können wir zusammenfassend sagen, dass eine Erhöhung der K^+ -Konzentration in sowohl H_2O als auch D_2O Puffer eine Störung des H-Brücken-Netzwerks der sowohl protonierten als auch deprotonierten Asp/Glu-Seitenketten in BetP führt. Alles in allem lässt sich schließlich vermuten, dass die Protonierung/Deprotonierung der Asp/Glu-Seitenketten möglicherweise bei der K^+ -induzierten Aktivierung von BetP beteiligt ist.

Im Gegensatz zum Wildtyp BetP zeigt das C-terminal verkürzte BetP in 2D Kristallen unter aktivierenden Bedingungen bei Wellenzahlen von über 1700 cm^{-1} lediglich schwache IR-Differenzsignale für protonierte Asp/Glu-Seitenketten. Im Falle dieser Mutation verschwinden die IR-Signale von protonierten Asp/Glu- und Arg/Lys-Seitenketten. Dies deutet darauf hin, dass

die geladenen Seitenketten lediglich im BetP WT auf eine K^+ -Erhöhung reagieren. Dies beweist eindeutig die wichtige Rolle der C-terminalen Domäne bei der ionischen Wechselwirkung auf der zytoplasmatischen Seite von BetP und beim Aktivierungs/Regulationszyklus von BetP. Es ist verständlich, dass die Wechselwirkung der Asp/Glu-Seitenketten und Arg-Seitenketten auf der zytoplasmatischen Seite an der K^+ -induzierten Aktivierung von BetP beteiligt ist. In diesem Zusammenhang legt die, mit steigender K^+ -Konzentration zunehmende, Intensität der IR Signale von Arg-Seitenketten, eine erhöhte Wechselwirkung von Arg-Seitenketten in BetP bei aktivierenden Bedingungen nahe. Kürzlich wurden die ionischen Wechselwirkungen von geladenen Seitenketten in terminalen Domänen mit zytoplasmatischen Schleifen beschrieben²⁷.

Die IR-Differenzsignale zeigen auch, dass sich die Intensität von C=O Moden von Asn- und Gln-Seitenketten stark erhöht, und zwar in Abhängigkeit der Verschiebung der NH_2 Biegeschwingung von Asn-Seitenketten, die aufgrund der Aktivierung eine Veränderung der H-Brückenbindungsmuster erfahren. Diese Ergebnisse sind im Einklang mit der Tatsache, dass an der Bildung von Inter-Protomer-H-Brücken an der Schnittstelle von BetP die Seitenketten von Asn (h7) und Thr (Schleife 7) beteiligt sind. Es ist wahrscheinlich, dass die Konformationsänderungen in der Nähe von Asn/Gln-Seitenketten auf der periplasmatischen Seite des Proteins stattfinden.

Eine deutliche Reaktion von C-C-Ringschwingungen von Tyrosin-Seitenketten auf die K^+ -Titration lieferten dynamische Information über die Änderung des Wechselwirkungsnetzwerks während der Regulation von BetP. Das ist in guter Übereinstimmung mit Strukturdaten, die zeigen, dass manche Tyrosin-Seitenketten an der Koordination von K^+ -Ionen beteiligt sind. Die IR-Signale von sowohl protonierten als auch deprotonierten Tyr-Seitenketten liefern durch eine Erhöhung der K^+ -Konzentration entgegengesetzte spektrale Veränderungen in Form von sowohl Intensitätsänderungen als auch Bandenverschiebungen (Schwächung/Bruch oder Stärkung von H-Brücken). Das deutet darauf hin, dass manche Tyrosinreste entweder eine Rolle bei der Regulation

von BetP spielen oder die Bewegung des Proteinrückgrats als Ergebnis der K^+ -bindungsabhängigen Konformationsänderung registrieren. Teilweise liefern protonierte Tyr-Seitenketten eine breite Bande im IR-Differenzspektrum (aktiv-*minus*-inaktiv), was daraus schließen lässt, dass einige wenige Tyr-Seitenketten als Reporter und/oder Akteure an der Aktivierung von BetP beteiligt sind. Es ist wahrscheinlich anzunehmen, dass die Seitenketten, die an der Rb^+ Bindung oder an der Formgebung der periplasmatischen Betain-Bindetasche beteiligt sind, zu den beobachteten Verschiebungen der IR-Banden beitragen. Daneben findet die Ausbildung der K^+ -abhängigen Ausbildung der S2-Einheit durch Konformationsänderungen in TM12 statt, was zu einer Bildung einer zusätzlichen Salzbrücke zwischen Tyr206 und Asp547 an der cytoplasmatischen Spitze von TM12 führt.

Die FTIR Daten von BetP Proteoliposomen sind in guter Übereinstimmung mit den Daten, die von BetP in 2D Kristalle gewonnen wurden. Beide Formen von BetP liefern identische spektrale Veränderungen, teils in den Protonierungszuständen und der Umgebung der Asp/Glu und Arg Seitenketten bei hohen K^+ -Konzentrationen. Alles in allem legen die FTIR Daten nahe, dass Schleifen und Lösungsmittel-exponierte Helices (C-terminale Domäne und/oder kurze Helices) in der hydrophilen Region von BetP, welche Asp/Glu- und Arg-Seitenketten enthält, an der Aktivierung beteiligt sind. Wahrscheinlich wechselwirken Asp/Glu-Seitenketten mit Arg/Lys-Seitenketten über Salzbrücken, die an der K^+ -abhängigen Aktivierung von BetP beteiligt sind, wobei die Stärke dieser Wechselwirkungen ebenfalls K^+ -abhängig ist. Die Beobachtung von schwachen Differenzsignalen für Tyr-Seitenketten ist ein Hinweis für Umorientierungen dieser Seitenketten als Folge einer erhöhten K^+ -Konzentration. Summa summarum lässt sich vermuten, dass die K^+ -stimulierte Aktivierung von BetP durch H-Brückenbindungen von Asp/Glu- und Arg-Seitenketten initiiert wird.

pH-Titrationsexperimente: Die *in situ* Titration von BetP bei verschiedenen pH-Werten zeigte die verschiedenen Protonierungszustände der Asp/Glu-Seitenketten mit ihrer Position in BetP und die

pH-abhängige Konformationsänderung, wodurch die ionischen Wechselwirkungen von cytoplasmatischen Schleifen innerhalb terminaler Domänen über geladene Seitenketten beleuchtet wurden. Basierend auf den FTIR Daten erscheinen die erwähnenswertesten spektralen Änderungen in einem pH-Bereich von 5,5 bis 7,5. Die IR-Signale für protonierte Asp/Glu steigen, während die Population der deprotonierten Asp/Glu-Seitenketten sinkt. Dies legt nahe, dass sich der Protonierungs/Deprotonierungsgrad von Asp/Glu-Seitenketten in diesem pH-Bereich ändert, was in BetP sowohl mit einer Konformationsänderung von Schleifen als auch Veränderungen in der mikroskopischen Umgebung von Tyr einhergeht. Hierbei erstreckt sich der pKa-Wert der Asp/Glu-Seitenketten über einen weiten Bereich von 5,5 bis 7,5, was für eine Carbonsäure bemerkenswert hoch ist. Dies legt wiederum nahe, dass die pH-abhängigen Seitenketten von Asp/Glu wahrscheinlich unzugänglich für das Lösungsmittel sind und/oder diese Seitenketten elektrostatisch mit der Umgebung und dabei sehr wahrscheinlich mit geladenen Seitenketten von z.B. Arg/Lys wechselwirken. Es wurde bereits behauptet, dass sowohl protonierte als auch deprotonierte Seitenketten von Asp/Glu durch K^+ -induzierte Aktivierung Änderungen in ihren H-Brückenbindungen erfahren und dass unter hohen K^+ -Konzentrationen Wechselwirkungen von sowohl Arg- als auch Asp/Glu-Seitenketten zunehmen. Es ist wahrscheinlich, dass die dieselben Gruppen von Asp/Glu-Seitenketten an dem regulatorischen Aktivationsmechanismus beteiligt sind.

Lipid-Protein Wechselwirkung: Das Messen von Lipid-Signalen lieferte experimentelle Hinweis darüber, wie BetP unter hohen K^+ -Konzentrationen dynamisch mit der Lipid-Doppelmembran interagiert. Phospholipid-Kopfgruppen erfahren eine K^+ -abhängige Veränderungen in ihren elektrostatischen Eigenschaften, wobei schwache/frei H-Brücken bevorzugt werden, während die hydrophoben Schwänze durch die K^+ -induzierte Aktivierung von BetP beweglicher und ungeordneter werden. Anhand der FTIR Daten lässt sich vermuten, dass der inaktive Zustand von BetP eher mit engen Lipid-Protein-Wechselwirkungen beschrieben werden kann, vergleichbar mit

den letzten bekannten Strukturen von BetP⁹⁵. Außerdem zeigen die FTIR Daten, dass K⁺ eine enge Wechselwirkung von BetP vor allem mit den anionischen Lipid-Kopfgruppen verhindert, was vermuten lässt, dass sich die Lipid-Protein-Wechselwirkungen lockern müssen, sodass BetP seine aktive Form annehmen kann. Somit wurde die Hypothese des molekularen Schalters bestätigt, worin die positiv geladene C-terminale Domäne durch die K⁺-Aktivierung ihren Wechselwirkungspartner von Lipiden (unter drosselnden Bedingungen) zu Proteinen wechselt, woran außerdem intratrimere Wechselwirkungen zwischen C-terminalen Domänen beteiligt sein könnten, was anhand von Strukturdaten und der Tatsache, dass monomeres BetP in ihrer Aktivität gedrosselt wird, bereits vermutet wurde.

¹H/²H-Austausch: ¹H/²H-Austauschexperimente lieferten Informationen bezüglich der Lösungsmittelzugänglichkeit des BetP Proteins sowohl im offenem als auch im geschlossenem Zustand. Auf der Grundlage der Daten zum Ausmaß und zur Kinetik des ¹H/²H-Austauschs ist nach einer Deuterierung von 3 Stunden der Anteil an ausgetauschten Amid-Protonen im aktiven Zustand (58%) entscheidend größer als im inaktiven Zustand (52%), was für eine, bedingt durch die K⁺-Konzentrationserhöhung, eher offenere Konformation des BetP WT in 2D Kristallen spricht. Interessanterweise liefert inaktives BetP einen schnelleren Austausch von Amid Protonen in den ersten 25 Minuten als das aktive BetP, was die Anwesenheit von ungeordneten Strukturen, Schleifen und Lösungsmittel-exponierten Helices bei Abwesenheit von K⁺ widerspiegelt. Ein ähnliches H/D-Austauschprofil wurde im Falle von BetP in Proteoliposomen beobachtet. Das lässt vermuten, dass manche Lösungsmittel-zugänglichen Schleifen und/oder kurze Helices, die sich in der hydrophilen Region von BetP befinden, zusätzliche Wechselwirkungen eingehen, sich somit verstecken und durch die Aktivierung Lösungsmittel-unzugänglich sind. Die FTIR Daten legen außerdem dar, dass Asp/Glu- und Arg-Seitenketten, die sich in Schleifen und der C-terminalen Domäne befinden, bei Aktivierung durch K⁺ weiter deuteriert werden. Es ist wahrscheinlich, dass diese Seitenketten ihre

Wechselwirkungspartner ändern, was durch Aktivierung zu einer Abschirmung vom Lösungsmittel führt und somit zu einer Umorientierung der C-terminalen Domänen und von Lösungsmittel-zugänglichen Schleifen.

Thermische Stabilität: Sowohl im aktiven als auch im inaktivem Zustand von BetP WT in 2D-Kristallen entfalten sich Schleifen und 3_{10} -Helix, während Signale von intermolekularen β -Faltblättern erscheinen, was durch eine Temperaturänderung beeinflusst wird, wobei Temperaturerhöhungen α -helices begünstigen. α -Helix und Schleifen von BetP liefern eine Schmelztemperatur von 79°C beziehungsweise 77°C , während diese Werte sich für den inaktiven Zustand zu 76°C beziehungsweise 74°C ändern. Das heißt, dass sowohl α -Helices als auch Schleifen unter hohen K^+ -Konzentrationen eine um 3°C höhere Schmelztemperatur aufweisen als bei niedrigen K^+ -Konzentrationen. Das beweist, dass aktives BetP unbeweglichere Schleifen und Helices hat verglichen mit dem inaktiven BetP, was einen stabileren Zustand von BetP bei aktivierenden Bedingungen, also hohen K^+ -Konzentrationen, widerspiegelt. Dieser Befund ist in hervorragender Übereinstimmung sowohl mit den H/D-Austausch-Experimenten als auch mit den Thermostabilitäts-Analysen von BetP WT Proteoliposomen. Im Gegensatz zu BetP WT 2D-Kristallen reagiert C-terminal abgeschnittenes BetP in 2D-Kristalle auf eine ähnliche Art und Weise auf Temperaturerhöhung, aber ohne einen signifikanten Unterschied zwischen den einzelnen Zuständen, was eine anderweitige Wechselwirkung der C-terminalen Domäne im aktiven und inaktiven Zustand nahelegt.

Zusammenfassend lieferten sowohl die Messungen der Lipid-Protein-Wechselwirkung als auch die Messung der K^+ -abhängigen Konformationsänderungen ein vollständigeres Bild über den Zusammenhang zwischen funktionellen und strukturellen Eigenschaften von BetP. Alles in allem lassen die FTIR Daten vermuten, dass Umorientierungen in der Sekundärstruktur und die Beobachtung von Wechselwirkungen zwischen geladenen Seitenketten die entscheidenden Schritte

innerhalb des BetP Aktivationszyklus' sind. Es kann postuliert werden, dass durch K^+ -Bindung negativ geladene Phospholipid-Kopfgruppen von positiv geladenen Arg-Seitenketten am Ende der C-terminalen Domäne gelöst werden und eventuell eine Wechselwirkung mit Schleifen oder der N-terminalen Domäne aufnehmen. Dem folgt eine Umorientierung von C-terminalen/transmembranen Helices und das Lösen mehrerer Wechselwirkungen zwischen geladenen Seitenketten der zytoplasmatischen Schleifen und dem C-Terminus, was in einer Öffnung der Struktur im aktiven Zustand resultiert. Demzufolge wurden mithilfe der IR-Spektroskopie der Zusammenhang zwischen Struktur und Funktion von BetP im Rahmen der selektiven Aktivierung durch K^+ -Ionen auf molekularem Niveau ans Tageslicht gebracht.

6. REFERENCES

1. Stryer, L. *Biochemistry*. (3rd edition, W.H. Freeman and Company: NY, 1988).
2. Nelson, D. L. and Cox, M. M. *Lehninger-Principles of Biochemistry*. (4th edition. W.H. Freeman and Company, NY: 2005).
3. McMurry, J. *Fundamentals of Organic Chemistry*. (3rd edition, Brooks/Cole Publishing Company, Pacific Grove, California: Pacific Grove, California., 1994).
4. Bruce Alberts, Dennis Bray, Karen Hopkin, Alexander Johnson, Julian Lewis, Martin Raff, Keith Roberts, P. W. *Essential Cell Biology*. (New York, NY: Garland Science Pub.: 2004).
5. Brady, G. P. & Sharp, K. A. Entropy in protein folding and in protein—protein interactions. *Current Opinion in Structural Biology* **7**, 215–221 (1997).
6. Dougherty, D. A. Cation- π Interactions Involving Aromatic Amino Acids. *The Journal of Nutrition* **137**, 1504S–1508S (2007).
7. Dougherty, D. A. Cation- π Interactions in Chemistry and Biology: A New View of Benzene, Phe, Tyr, and Trp. *Science* **271**, 163–168 (1996).
8. Gromiha, M. M. & Suwa, M. Structural analysis of residues involving cation- π interactions in different folding types of membrane proteins. *International Journal of Biological Macromolecules* **35**, 55–62 (2005).
9. Forrest, L. R. & Rudnick, G. The Rocking Bundle: A Mechanism for Ion-Coupled Solute Flux by Symmetrical Transporters. *Physiology (Bethesda)* **24**, 377–386 (2009).
10. Bettina Kempf & Erhard Bremer Uptake and synthesis of compatible solutes as microbial stress responses to high-osmolality environments. *Archives of Microbiology* **170**, 319–330 (1998).
11. Ziegler, C., Bremer, E. & Krämer, R. The BCCT family of carriers: from physiology to crystal structure. *Molecular Microbiology* **78**, 13–34 (2010).
12. Krämer, R. Osmosensing and osmosignaling in *Corynebacterium glutamicum*. *Amino Acids* **37**, 487–497 (2009).

13. Krämer, R. & Morbach, S. BetP of *Corynebacterium glutamicum*, a transporter with three different functions: betaine transport, osmosensing, and osmoregulation. *Biochimica et Biophysica Acta* **1658**, 31–36 (2004).
14. Ressler, S., Terwisscha van Scheltinga, A. C., Vorrhein, C., Ott, V. & Ziegler, C. Molecular basis of transport and regulation in the Na⁽⁺⁾/betaine symporter BetP. *Nature* **458**, 47–52 (2009).
15. Perez, C., Koshy, C., Yildiz, O. & Ziegler, C. Alternating-access mechanism in conformationally asymmetric trimers of the betaine transporter BetP. *Nature* **490**, 126–130 (2012).
16. Perez, C. *et al.* Substrate specificity and ion coupling in the Na⁺/betaine symporter BetP. *The EMBO Journal* **30**, 1221–9 (2011).
17. Schiller, D., Krämer, R. & Morbach, S. Cation specificity of osmosensing by the betaine carrier BetP of *Corynebacterium glutamicum*. *FEBS Letters* **563**, 108–112 (2004).
18. Rübenhagen, R., Morbach, S. & Krämer, R. The osmoreactive betaine carrier BetP from *Corynebacterium glutamicum* is a sensor for cytoplasmic K⁺. *The EMBO Journal* **20**, 5412–20 (2001).
19. Özcan, N., Reinhard, K. & Morbach, S. Chill Activation of Compatible Solute Transporters in *Corynebacterium glutamicum* at the Level of Transport Activity. *Journal of Bacteriology* **187**, 4752–4759 (2005).
20. Özcan, N. *et al.* Osmolality, Temperature, and Membrane Lipid Composition Modulate the Activity of Betaine Transporter BetP in *Corynebacterium glutamicum*. *Journal of Bacteriology* **189**, 7485–7496 (2007).
21. Morbach, S. & Krämer, R. Structure and Function of the Betaine Uptake System BetP of *Corynebacterium glutamicum*: Strategies to Sense Osmotic and Chill Stress. *Journal of Molecular Microbiology and Biotechnology* **10**, 143–153 (2005).
22. Farwick, M., Siewe, R. & Krämer, R. Glycine betaine uptake after hyperosmotic shift in *Corynebacterium glutamicum*. *J. Bacteriology* **177**, 4690–4695 (1995).
23. Peter, H., Burkovski, A. & Kramer, R. Osmo-sensing by N- and C-terminal Extensions of the Glycine Betaine Uptake System BetP of *Corynebacterium glutamicum*. *The Journal of Biological Chemistry* **273**, 2567–2574 (1998).

24. Morbach, S. & Krämer, R. Impact of transport processes in the osmotic response of *Corynebacterium glutamicum*. *Journal of Biotechnology* **104**, 69–75 (2003).
25. Krämer, R. & Ziegler, C. Regulative interactions of the osmosensing C-terminal domain in the trimeric glycine betaine transporter BetP from *Corynebacterium glutamicum*. *Biological Chemistry* **390**, 685–691 (2009).
26. Perez, C., Khafizov, K., Forrest, L. R., Krämer, R. & Ziegler, C. The role of trimerization in the osmoregulated betaine transporter BetP. *EMBO Reports* **12**, 804–10 (2011).
27. Gärtner, R. M., Perez, C., Koshy, C. & Ziegler, C. Role of bundle helices in a regulatory crosstalk in the trimeric betaine transporter BetP. *Journal of Molecular Biology* **414**, 327–36 (2011).
28. Schiller, D., Rübenhagen, R., Krämer, R. & Morbach, S. The C-terminal domain of the betaine carrier BetP of *Corynebacterium glutamicum* is directly involved in sensing K^+ as an osmotic stimulus. *Biochemistry* **43**, 5583–91 (2004).
29. Ott, V., Koch, J., Späte, K., Morbach, S. & Krämer, R. Regulatory properties and interaction of the C- and N-terminal domains of BetP, an osmoregulated betaine transporter from *Corynebacterium glutamicum*. *Biochemistry* **47**, 12208–18 (2008).
30. Rübenhagen, R., Rönsch, H., Jung, H., Krämer, R. & Morbach, S. Osmosensor and Osmoregulator Properties of the Betaine Carrier BetP from *Corynebacterium glutamicum* in Proteoliposomes. *The Journal of Biological Chemistry* **275**, 735–741 (2000).
31. Schiller, D., Ott, V., Reinhard, K. & Morbach, S. Influence of Membrane Composition on Osmosensing by the Betaine Carrier BetP from *Corynebacterium glutamicum*. *Journal of Biological Chemistry* **281**, 7737–7746 (2006).
32. Peter, H., Burkovski, A. & Krämer, R. Isolation, characterization, and expression of the *Corynebacterium glutamicum* betP gene, encoding the transport system for the compatible solute glycine betaine. *Journal of Bacteriology* **178**, 5229–34 (1996).
33. Nicklisch, S. C. T. *et al.* Conformational changes of the betaine transporter BetP from *Corynebacterium glutamicum* studied by pulse EPR spectroscopy. *Biochimica et Biophysica Acta* **1818**, 359–66 (2012).

-
34. Perez, C., Khafizov, K., Forrest, L. R., Krämer, R. & Ziegler, C. Supplementary information_Alternating-access mechanism in conformationally asymmetric trimers of the betaine transporter BetP. *Nature* **490**, (2012).
 35. Khafizov, K. *et al.* Investigation of the sodium-binding sites in the sodium-coupled betaine transporter BetP. *Proceedings of the National Academy of Sciences of the United States of America* **109**, E3035–44 (2012).
 36. Ge, L., Perez, C., Waclawska, I., Ziegler, C. & Muller, D. J. Locating an extracellular K⁺-dependent interaction site that modulates betaine-binding of the Na⁺-coupled betaine symporter BetP. *Proceedings of the National Academy of Sciences of the United States of America* **108**, E890–8 (2011).
 37. Korkmaz, F., Ressler, S., Ziegler, C. & Mäntele, W. K⁽⁺⁾-induced conformational changes in the trimeric betaine transporter BetP monitored by ATR-FTIR spectroscopy. *Biochimica et Biophysica Acta* **1828**, 1181–1191 (2013).
 38. Mäntele, W. *Biophysik*. (Eugen Ulmer Verlag: Stuttgart, 2012).
 39. Schmidt, W. *Optical Spectroscopy in Chemistry and Life Sciences*. (WILEY-VCH Verlag GmbH & Co. KGaA, Weinheim: 2005).
 40. Siebert, F. & Hildebrandt, P. *Vibrational Spectroscopy in Life Science*. (WILEY-VCH Verlag GmbH & Co. KGaA, Weinheim: 2008).
 41. Barth, A. & Zscherp, C. What vibrations tell us about proteins. *Quarterly Reviews of Biophysics* **35**, 369–430 (2002).
 42. Tamm, L. K. & Tatulian, S. A. Infrared spectroscopy of proteins and peptides in lipid bilayers. *Quarterly Reviews of Biophysics* **30**, 365–429 (1997).
 43. Arrondo J.L.R. & Goni F.M. Structure and dynamics of membrane proteins as studied by infrared spectroscopy. *Progress in Biophysics and Molecular Biology* **72**, 367–405 (1999).
 44. Goormaghtigh, E., Raussens, V. & Ruyschaert, J. M. Attenuated total reflection infrared spectroscopy of proteins and lipids in biological membranes. *Biochimica et Biophysica Acta* **1422**, 105–185 (1999).

-
45. Fabian, H. & Mäntele, W. Infrared spectroscopy of proteins. *Handbook of Vibrational Spectroscopy* 1–27 (2002).doi:10.1002/0470027320
 46. Barth, A. Infrared spectroscopy of proteins. *Biochimica et Biophysica Acta* **1767**, 1073–101 (2007).
 47. Krimm, S. & Bandekar, J. Vibrational spectroscopy and conformation of peptides, polypeptides, and proteins. *Advanced Protein Chemistry* **38**, 181–367 (1986).
 48. Glasoe, P. K. & Long, F. A. Use of glass electrodes to measure acidities in deuterium oxide. *The Journal of Physical Chemistry* **64**, 188–189 (1960).
 49. Lumry, R., Smith, E. L. & Glantz, R. R. Kinetics of Carboxypeptidase Action. I. Effect of Various Extrinsic Factors on Kinetic Parameters. *Journal of the American Chemical Society* **73**, 4330–4340 (1951).
 50. Rigaud, J.-L. Membrane proteins: functional and structural studies using reconstituted proteoliposomes and 2-D crystals. *Brazilian Journal of Medical and Biological Research* **35**, 753–66 (2002).
 51. Ziegler, C. *et al.* Projection structure and oligomeric state of the osmoregulated sodium/glycine betaine symporter BetP of *Corynebacterium glutamicum*. *Journal of Molecular Biology* **337**, 1137–47 (2004).
 52. Tsai, C.-J., Ejsing, C. S., Shevchenko, A. & Ziegler, C. The role of lipids and salts in two-dimensional crystallization of the glycine–betaine transporter BetP from *Corynebacterium glutamicum*. *Journal of Structural Biology* **160**, 275–286 (2007).
 53. Tsai, C.-J. & Ziegler, C. Structure determination of secondary transport proteins by electron crystallography: two-dimensional crystallization of the betaine uptake system BetP. *Journal of Molecular Microbiology and Biotechnology* **10**, 197–207 (2005).
 54. Mantsch, H. H. & McElhaney, R. N. Phospholipid phase transitions in model and biological membranes as studied by infrared spectroscopy. *Chemistry and Physics of Lipids* **57**, 213–226 (1991).
 55. Casal, H. L. & Mantsch, H. H. Polymorphic phase behaviour of phospholipid membranes studied by infrared spectroscopy. *Biochimica et Biophysica Acta* **779**, 381–401 (1984).

-
56. Cameron, D. G., Casal, H. L. & Mantsch, H. H. Characterization of the pretransition in 1,2-dipalmitoyl-sn-glycero-3-phosphocholine by Fourier transform infrared spectroscopy. *Biochemistry* **19**, 3665–3672 (1980).
57. Lewis, R. N. A. H. & McElhaney, R. N. Membrane lipid phase transitions and phase organization studied by Fourier transform infrared spectroscopy. *Biochimica et Biophysica Acta* **1828**, 2347–2358 (2013).
58. Arrondo, J. L. R. & Goni, F. M. Infrared studies of protein-induced perturbation of lipids in lipoproteins and membranes. *Chemistry and Physics of Lipids* **96**, 53–68 (1998).
59. Sukumaran, S., Hauser, K., Rauscher, A. & Mäntele, W. Thermal stability of outer membrane protein porin from *Paracoccus denitrificans*: FT-IR as a spectroscopic tool to study lipid–protein interaction. *FEBS* **579**, 2546–2550 (2005).
60. Korkmaz, F., Köster, S., Yildiz, Ö. & Mäntele, W. The Role of Lipids for the Functional Integrity of Porin: An FTIR Study Using Lipid and Protein Reporter Groups. *Biochemistry* **47**, 12126–12134 (2008).
61. Balázs Szalontai Membrane protein dynamics: limited lipid control. *PMC Biophysics 2009* **2:1**, (2009).
62. Güler, G., Džafić, E., Vorob'ev, M. M., Vogel, V. & Mäntele, W. Real time observation of proteolysis with Fourier transform infrared (FT-IR) and UV-circular dichroism spectroscopy: watching a protease eat a protein. *Spectrochimica acta. Part A, Molecular and Biomolecular Spectroscopy* **79**, 104–111 (2011).
63. Stuart, B. H. *Infrared Spectroscopy: Fundamentals and Applications. Methods* **8**, 224 (John Wiley & Sons, Ltd: 2004).
64. S.Y., V. & F.G, P. Water (H₂O and D₂O) Molar Absorptivity in the 1000–4000 cm⁻¹ Range and Quantitative Infrared Spectroscopy of Aqueous Solutions. *Analytical Biochemistry* **248**, 234–245 (1997).
65. Oberg, K. A. & Fink, A. L. A new attenuated total reflectance Fourier transform infrared spectroscopy method for the study of proteins in solution. *Analytical Biochemistry* **256**, 92–106 (1998).

-
66. Dzafić, E., Klein, O., Screpanti, E., Hunte, C. & Mäntele, W. Flexibility and dynamics of NhaA Na⁺/H⁺-antiporter of *Escherichia coli* studied by Fourier transform infrared spectroscopy. *Spectrochimica acta. Part A, Molecular and Biomolecular Spectroscopy* **72**, 102–109 (2009).
67. Goormaghtigh, E. & Ruyschaert, J. M. Subtraction of atmospheric water contribution in Fourier transform infrared spectroscopy of biological membranes and proteins. *Spectrochimica acta. Part A, Molecular and Biomolecular Spectroscopy* **50**, 2137–2144 (1994).
68. Goormaghtigh, E., Cabiaux, V. & Ruyschaert, J. M. Determination of soluble and membrane protein structure by Fourier transform infrared spectroscopy. II. Experimental aspects, side chain structure, and H/D exchange. *Subcellular Biochemistry* **23**, 363–403 (1994).
69. Raussens, V., Ruyschaert, J.-M. & Goormaghtigh, E. Analysis of ¹H/²H exchange kinetics using model infrared spectra. *Applied Spectroscopy* **58**, 68–82 (2004).
70. Marcsisin, S. R. & Engen, J. R. Hydrogen exchange mass spectrometry: what is it and what can it tell us? *Analytical and Bioanalytical Chemistry* **397**, 967–972 (2010).
71. Scheirlinckx, F., Raussens, V., Ruyschaert, J.-M. & Goormaghtigh, E. Conformational changes in gastric H⁺/K⁺-ATPase monitored by difference Fourier-transform infrared spectroscopy and hydrogen/deuterium exchange. *The Biochemical Journal* **382**, 121–9 (2004).
72. Dzafić, E., Klein, O., Goswami, P., Kühlbrandt, W. & Mäntele, W. Infrared spectroscopic study of the structural and functional properties of the Na(+)/H(+) antiporter MjNhaP1 from *Methanococcus jannaschii*. *Biochimica et Biophysica Acta* **1787**, 730–7 (2009).
73. Vanderkooi, J. M., Dashnau, J. L. & Zelent, B. Temperature excursion infrared (TEIR) spectroscopy used to study hydrogen bonding between water and biomolecules. *Biochimica et Biophysica Acta* **1749**, 214–33 (2005).
74. Jiang, X. *et al.* Resolving voltage-dependent structural changes of a membrane photoreceptor by surface-enhanced IR difference spectroscopy. *Proceedings of the National Academy of Sciences of the United States of America* **105**, 12113–7 (2008).
75. Goormaghtigh, E., Cabiaux, V. & Ruyschaert, J. M. Determination of soluble and membrane protein structure by Fourier transform infrared spectroscopy. I. Assignments and model compounds. *Subcellular Biochemistry* **23**, 329–62 (1994).

-
76. Goormaghtigh, E., Cabiaux, V. & Ruyschaert, J. . M. Determination of soluble and membrane protein structure by Fourier transform infrared spectroscopy. III. Secondary structures. *Subcellular Biochemistry* **23**, 405–50 (1994).
 77. Susi, H. & Byler, D. M. Protein structure by Fourier transform infrared spectroscopy: second derivative spectra. *Biochemical and Biophysical Research Communications* **115**, 391–7 (1983).
 78. Byler, D. M. & Susi, H. Examination of the secondary structure of proteins by deconvolved FTIR spectra. *Biopolymers* **25**, 469–87 (1986).
 79. Kauppinen, Jyrki K. Moffatt, Douglas J. Mantsch, Henry H. Cameron, D. G. Fourier Self-Deconvolution: A Method for Resolving Intrinsically Overlapped Bands. *Applied Spectroscopy* **34**, 271–276 (1981).
 80. Kauppinen, J. K., Moffatt, D. J., Mantsch, H. H. & Cameron, D. G. Fourier transforms in the computation of self-deconvoluted and first-order derivative spectra of overlapped band contours. *Analytical Chemistry* **53**, 1454–1457 (1981).
 81. Marquardt, D. W. An Algorithm for Least-Squares Estimation of Nonlinear Parameters. *Journal of the Society for Industrial and Applied Mathematics* **11**, 431–441 (1963).
 82. Barth, A. The infrared absorption of amino acid side chains. *Progress in Biophysics & Molecular Biology* **74**, 141–173 (2000).
 83. Fabian, H. *et al.* Secondary structure of streptokinase in aqueous solution: A Fourier transform infrared spectroscopic study. *Biochemistry* **31**, 6532–6538 (1992).
 84. Chirgadze, Y. N., Fedorov, O. V & Trushina, N. P. Estimation of amino acid residue side-chain absorption in the infrared spectra of protein solutions in heavy water. *Biopolymers* **14**, 679–94 (1975).
 85. Venyaminov SYu & Kalnin, N. N. Quantitative IR spectrophotometry of peptide compounds in water (H₂O) solutions. I. Spectral parameters of amino acid residue absorption bands. *Biopolymers* **30**, 1243–57 (1990).
 86. De Jongh, H. H., Goormaghtigh, E. & Ruyschaert, J. M. Monitoring structural stability of trypsin inhibitor at the submolecular level by amide-proton exchange using Fourier transform infrared spectroscopy: A test case for more general application. *Biochemistry* **36**, 13593–602 (1997).

-
87. Vigano, C. *et al.* Hydrogen-deuterium exchange in membrane proteins monitored by IR spectroscopy: A new tool to resolve protein structure and dynamics. *Biopolymers* **74**, 19–26
88. Güldenhaupt, J. *et al.* Secondary structure of lipidated Ras bound to a lipid bilayer. *The FEBS journal* **275**, 5910–5918 (2008).
89. Prestrelski, S. J., Byler, D. M. & Liebman, M. N. Comparison of various molecular forms of bovine trypsin: Correlation of infrared spectra with x-ray crystal structures. *Biochemistry* **30**, 133–143 (1991).
90. Prestrelski, S. J., Byler, D. M. & Thompson, M. P. Effect of metal ion binding on the secondary structure of bovine α -lactalbumin as examined by infrared spectroscopy. *Biochemistry* **30**, 8797–8804 (1991).
91. Navarro, S., Borchman, D. & Bicknell-Brown, E. Lipid-protein ratios by infrared spectroscopy. *Analytical Biochemistry* **136**, 382–389 (1984).
92. Tsai, C.-J. *et al.* Structural asymmetry in a trimeric Na⁺/betaine symporter, BetP, from *Corynebacterium glutamicum*. *Journal of Molecular Biology* **407**, 368–81 (2011).
93. Rübenhagen, R., Rönsch, H., Jung, H., Krämer, R. & Morbach, S. Osmosensor and osmoregulator properties of the betaine carrier BetP from *Corynebacterium glutamicum* in proteoliposomes. *The Journal of Biological Chemistry* **275**, 735–41 (2000).
94. Dave, N. *et al.* Secondary structure components and properties of the melibiose permease from *Escherichia coli*: a fourier transform infrared spectroscopy analysis. *Biophysical Journal* **79**, 747–55 (2000).
95. Koshy, C. *et al.* Structural evidence for functional lipid interactions in the betaine transporter BetP. *The EMBO Journal* **32**, 3096–3105 (2013).
96. Fringeli, U. P. & Günthard, H. H. Hydration sites of egg phosphatidylcholine determined by means of modulated excitation infrared spectroscopy. *Biochimica et Biophysica Acta (BBA) - Lipids and Lipid Metabolism* **450**, 101–106 (1976).
97. Blume, A., Hübner, W. & Messner, G. Fourier transform infrared spectroscopy of ¹³C:O labeled phospholipids hydrogen bonding to carbonyl groups. *Biochemistry* **27**, 8239–8249 (1988).

98. Lewis, R. N., McElhaney, R. N., Pohle, W. & Mantsch, H. H. Components of the carbonyl stretching band in the infrared spectra of hydrated 1,2-diacylglycerolipid bilayers: a reevaluation. *Biophysical Journal* **67**, 2367–75 (1994).
99. Noda, I. Two-Dimensional Correlation Analysis Useful for Spectroscopy, Chromatography, and Other Analytical Measurements. *Analytical Sciences* **23**, 139–146 (2007).
100. Noda, I. & Ozaki, Y. *Two-dimensional Correlation Spectroscopy: Applications in Vibrational and Optical Spectroscopy*. (John Wiley & Sons Ltd, West Sussex PO19 8SQ, England: 2004).
101. De la Arada, I., Seiler, C. & Mäntele, W. Amyloid fibril formation from human and bovine serum albumin followed by quasi-simultaneous Fourier-transform infrared (FT-IR) spectroscopy and static light scattering (SLS). *European Biophysics Journal: EBJ* **41**, 931–8 (2012).

7. ACKNOWLEDGEMENTS

I would like to express my deep gratitude to my supervisor **Prof. Dr. Werner Mäntele**, Institute for Biophysics, Frankfurt am Main, Germany, for accepting me as a PhD student, for his continuous support, enthusiastic encouragement, for giving me the a great opportunity to work in your laboratory, and for being the excellent and enthusiastic mentor to me throughout this work.....

Also I would like to thank for providing a generous funding throughout my PhD. Finally, I would like to offer my special thanks for his endurance for my routine travels to Turkey to see my husband.

I would like to express my sincere appreciation to **Prof. Dr. Christine Ziegler**, her PhD student **Rebecca Gärtner** as well as to **Dr. Camilo Perez**, Department of Structural Biology, Max-Planck-Institute of Biophysics, Frankfurt, Germany, for kindly providing the BetP samples, for their help, and for their valuable and constructive suggestions and discussions during the planning and performing of this work.

I would like to give my heartfelt appreciation to all the members of **Institute for Biophysics** in Frankfurt for the all moments we shared together. My special thanks are extend to **Dr. Oliver Klein** for providing me the computer programmes, **Dr. Georg Wille** for helping me with chemicals and for the scientific discussions, **Hans-Werner Müller**, **Dr. Jürgen Maurer**, **Dr. Andreas Roth**, **Dr. Miquel Pleitez**, **Katharina Lommel**, **Annette Kopitz**, **Erhan Deniz** and **Ernst Winter** for all their help, support and for being always ready to help me. Thank you very much also for your friendship.

I would like to offer my special thanks to my office-mate **Dr. Vitali Vogel** for the all scientific or daily discussions and recommendations. I understand him right now better what he mined by saying “Alles wird besser sein!”..... He is really an elusive guide for me in the Institute. I wish to thank also **Lie Xie** for being a very kind office-mate and for providing a variety of tee.

I wish to acknowledge the help provided by **Dr. Filiz Korkmaz** whose BetP project I took over, from Atılım University, Faculty of Engineering, Physics Group, Ankara, Turkey. Also I thank to her

for the support, being always ready to help me and for our scientific discussions even over telephone.

I would like to give my heartfelt appreciation to my husband **Ahmet Güler**, who has accompanied me with his enduring love and unlimited patience. I could not manage and even venture this work at all without your support, encouragement, understanding and confidence. Thank you and I love you.... And our son **Arda Güler**, who was born in the beginning of my PhD and has grown up almost in the airplanes or among the books, papers or items. To watch his healthy development, and to play with him after the work are the only things that motivated me throughout this work. Thank you for joining to our small family.....

I would like to give my heartfelt appreciation to **my parents (Güler and Görücü Families)** for always being there for me and for your unconditional love, prayers and support. Particularly, I would like to acknowledge my Mothers, without whom my thesis would not have been possible at all, for child caring and for their uncountable travelling to Germany.

My sincere gratitude to **Oesterreicher Family** for their constant support and their home-made delicious cakes (Deutscher Kuchen). You did not allow me to feel alone in Frankfurt. Thank you very much for the all moments we shared together in Frankfurt.

My sincere thanks to my friends **Dr. Enela Džafić, Sevgi Öztürk, Mesut, İrem** and **Mahmut** for being always ready to help me and for all the very joyful moments we had together in Frankfurt. Thank you very much also for your unending friendship.

CURRICULUM VITAE

Personal Information

Surname, First Name	GÜLER, Günnur
Date of Birth	September 17, 1979
Place of Birth	Giessen, Germany
Marital Status	Married
Children	1 child
E-Mail	gunnur.guler@biophysik.uni-frankfurt.de; gunnurgorucu@gmail.com



Education

- **PhD degree.** Institute of Biophysics, Department of Physics, Goethe University, Frankfurt, Germany (10/2010–present).
 - **MSc degree.** Institute of Biophysics, Department of Physics, Goethe University, Frankfurt, Germany (09/2008–01/2010).
 - **BSc degree.** Department of Physics, Science Faculty, Izmir Institute of Technology, Izmir, Turkey (2004–2008).
 - English Preparatory School, Izmir Institute of Technology, Department of Foreign Languages, Izmir, Turkey (2003–2004).
 - Ege University, Atatürk Medical Technology Vocational Training School, Audiometry, Izmir, Turkey (2001–2003).
 - Dokuz Eylül University, Vocational School of Health Services, Nursing, Izmir, Turkey (1996–1998).
-

Work Experience

- Research and laboratory teaching assistant at Goethe University (09/2008–to date).
 - Nurse (government employee), Aegean Obstetrics and Gynecology Teaching and Research Hospital, Yenisehir, Izmir, Turkey (1998-2008).
-

Awards and Honors

- **PhD scholarship** by German Research Foundation Collaborative Research Center 807 “Transport and Communication across Biological Membranes (TRAM)”
 - Funding of travel expenses for the scientific purposes (being a student of “Integrated research training group” for **TRAM** PhD students).
 - A member of Goethe Graduate Academy (**GRADE**) during PhD
 - **MSc scholarship** by Goethe University, Frankfurt, Germany.
 - MSc degree with high honor and **excellent student** with a grade of 1.4 (1.0 is the highest grade). Institute of Biophysics, Goethe University, Frankfurt (2008-2010).
 - BSc degree with high honor, Izmir Institute of Technology, Science Faculty, Department of Physics, graduated **2nd rank** with a grade of 3.41(4.0 is the highest grade) (2004-2008).
 - Ege University, Atatürk Medical Technology Vocational Training School, Audiometry, graduated **summa cum laude (1st rank)** (2001-2003).
 - Ege University, Atatürk Medical Technology Vocational Training School, **3rd rank** among the all programs (2001-2003).
-

Attended Conferences/Projects

- **PhD thesis** (October 2010-present) “*Investigation of structural and functional properties of betaine transporter BetP from Corynebacterium glutamicum by using infrared spectroscopy*”. Goethe University, Institute of Biophysics, Department of Physics, Frankfurt, Germany.
 - **MSc thesis** (09/2008-01/2010) “*FT-IR and CD studies on Fragmentation of Proteins by Proteases*”. Goethe University, Institute of Biophysics, Department of Physics, Frankfurt, Germany.
 - **BSc project** (2006-2008) “*Quantum Tunneling and Synaptic Transfer*”. Izmir Institute of Technology, Science Faculty, Department of Physics (supported by TUBITAK: Turkish Scientific and Technological Research Council, Turkey).
 - Supervision of 3 international summer-internship students with their major projects in Goethe University, Institute of Biophysics, Department of Physics, Frankfurt, Germany.
-

Poster Presentations:

- “*Na⁺-coupled betaine symporter BetP from Corynebacterium glutamicum studied by Fourier transform infrared spectroscopy*”. Annual Meeting of the German Biophysical Society, Goettingen, Germany (23-26/09/2012).
- “*Betaine transporter BetP from Corynebacterium glutamicum in proteoliposomes studied by Fourier transform infrared spectroscopy: K⁺-stimulated activation and hydrogen/deuterium exchange*”. 3rd International Workshop on Molecular Approaches to Obesity and Diabetes with New Implications, Middle East Technical University, Ankara, Turkey (15-16/03/2012).
- “*FTIR and CD Spectroscopy Studies on Fragmentation of Proteins by Proteases*”, SFB-Internal PhD Symposium, Goethe University, Frankfurt, Germany (24-25/05/2011).

Participant:

- Minisymposium on “Bioanalytical Infrared Spectroscopy: *Oua vadis?*” Institute of Biophysics, Goethe University, Frankfurt, Germany (21/11/2012).
- Users meetings, Bruker Optics, Ettlingen, Germany (23/11/2010)
- Duru-Fest Workshop, Izmir Institute of Technology, Izmir, Turkey, 06/2006.

Oral Talks:

- “*Analysis of the molecular mechanisms of the activation of the betaine transporter BetP from Corynebacterium glutamicum by FT-IR spectroscopy*”. 31st EUCMOS, Cluj Napoca, Romania (26 - 31/08/2012).
 - “*Proteoliposomes of Betaine transporter BetP from Corynebacterium studied by Fourier transform infrared spectroscopy*”. SFB 807 Students’ Retreat, Marienburg, Zell/Mosel, Germany (4-6/06/2012).
 - “*Real time observation of proteolysis with Fourier transform infrared (FT-IR) and UV-circular dichroism spectroscopy: Watching a protease eat a protein*”. 14th ECSBM, Coimbra, Portugal (29/08 – 3/09/2011).
 - “*Space-time Curvature*”, III. Physics Students Meeting, Eskisehir, Turkey (05/2007).
 - “*Neuron Physiology and Synapses*”, II. Physics Students Meeting, Izmir, Turkey (05/2006).
-

Attended Workshops/Trainings

- Training laboratory course on “3D crystallization of proteins and X-ray analysis”, Department of Structural Biology, Max-Planck-Institute of Biophysics, Frankfurt, Germany (6-7/12/2012).
 - Transferable skills workshops for TRAM students offered by GRADE (since 10/2010):
 1. “Oral Scientific Presentation” (23/03/2012, by Dr. Med. Tanja Meyer-Traschan)
 2. “Scientific Paper Writing” (15-16/07/2011, by Dr. Volker Grimm)
-

-
3. “Networking: How to maintain contacts at conferences” (14/07/2011, by Dr. S. Löhken)
 4. “Basics of Scientific Work” (20-22/10/ 2011, by Dr. Uta Bronner)
- Voluntary attended interdisciplinary courses (summer-semester 2012):
 1. Biochemistry II: Protein function and structure (Prof. Dr. Robert Tampe)
 2. Quantum Molecular Dynamics (Prof. Dr. Eberhard Engel)
 3. Visual System-Neural Structure, Dynamics, and Function (Prof. Dr. Thomas Burwick)
 - PyMoL demo and Q/A session, Goethe University, Frankfurt, Germany (09/05/2012).
 - Basic Training and Course Modules of Undergraduate Course: “Electrical and photonic measurements for CCFL applications”, Material Physics, Science Engineering, Queen Mary Collage University of London, summer 2007.
-

Languages

- **Turkish** (Native)
 - Advanced **English** qualification with EF language schools in London, U.K (fluent)
 - Advanced **German** qualification with Frankfurt Goethe University, Germany (fluent)
-

ERKLÄRUNG

Ich versichere hiermit, dass ich die vorliegende Arbeit selbständig verfasst, keine anderen, als die angegebenen Hilfsmittel verwendet und sämtliche Stellen, die aus benutzten Werken im Wortlaut oder dem Sinne nach entnommen sind, mit Quellen- bzw. Herkunftsangaben kenntlich gemacht habe.

Frankfurt am Main, den.....

.....